KLAIPĖDA UNIVERSITY

Rasa IDZELYTĖ

ASSESSMENT AND IMPACT OF ICE COVER AND FUTURE PROJECTIONS FOR THE BALTIC CURONIAN LAGOON

DOCTORAL DISSERTATION

Natural sciences,
ecology and environmental sciences (N 012)

Klaipėda, 2021

Doctoral dissertation was prepared in the period 2016–2021 at Klaipėda University, based on the conferment a doctorate right which was granted for Klaipėda University by the order of the Minister of Education and Science (Republic of Lithuania) No. V-1019, signed on 8 June, 2011, by the order of the Minster of Education, Science and Sport (Republic of Lithuania) No. V-160, signed on 22 February, 2019.

Academic advisor

prof. dr. Georg UMGIESSER (Klaipėda University, Natural Sciences, Ecology and Environmental Sciences – N 012).

Research consultants:

dr. Igor KOZLOV (Klaipėda University, Natural Sciences, Physical Geography – N 006);
dr. Ričardas PAŠKAUSKAS (Nature Research Centre, Natural Sciences, Ecology and Environmental Sciences – N 012).

The doctoral dissertation is defended at the Board of Klaipėda University in Ecology and Environmental Sciences:

Chairman

prof. dr. Darius DAUNYS (Klaipėda University, Natural Sciences, Ecology and Environmental Sciences – N 012);

Members:

prof. dr. Kai Antero MYRBERG (Finnish Environment Institute, Finland, Natural Sciences, Physical Geography – N 006);
prof. dr. Inga DAILIDIENĖ (Klaipėda University, Natural Sciences, Physical Geography – N 006);
dr. Boris CHUBARENKO (P. P. Shirshov Institute of Oceanology of Russian Academy of Sciences, Russia, Natural Sciences, Physical Geography – N 006);
dr. Darius JAKIMAVIČIUS (Lithuanian Energy Institute, Technological Sciences, Environmental Engineering – T 004).

The dissertation will be defended in a public meeting of the Board in Ecology and Environmental Sciences, Klaipėda University, Marine Research Institute Conference Hall at 10 a. m. on 24th September, 2021.
Address: Universiteto alley 17, LT-92294, Klaipėda, Lithuania.

The doctoral dissertation was sent out on 24th August, 2021.
The doctoral dissertation is available for review at the Library of the Klaipėda University.

KLAIPĖDOS UNIVERSITETAS

Rasa IDZELYTĖ

KURŠIŲ MARIŲ LEDO DANGOS VERTINIMAS, POVEIKIS IR ATEITIES PROGNOZĖS

DAKTARO DISERTACIJA

GAMTOS MOKSLAI,
EKOLOGIJA IR APLINKOTYRA (N 012)

Klaipėda, 2021

Mokslo daktaro disertacija rengta 2016–2021 metais Klaipėdos universitete pagal Klaipėdos universitetui Lietuvos Respublikos švietimo ir mokslo ministro 2011 m. birželio 8 d. įsakymu Nr. V-1019 ir Lietuvos Respublikos švietimo, mokslo ir sporto ministro 2019 m. vasario 22 d. įsakymu Nr. V-160 suteiktą doktorantūros teisę.

Vadovas

prof. dr. Georg UMGIESSER (Klaipėdos universitetas, gamtos mokslai, ekologija ir aplinkotyra – N 012).

Moksliniai konsultantai:

dr. Igor KOZLOV (Klaipėdos universitetas, gamtos mokslai, fizinė geografija – N 006);

dr. Ričardas PAŠKAUSKAS (Klaipėdos universitetas, gamtos mokslai, ekologija ir aplinkotyra – N 012).

Daktaro disertacija ginama Klaipėdos universiteto Ekologijos ir aplinkotyros mokslo krypties taryboje:

Pirmininkas

prof. dr. Darius DAUNYS (Klaipėdos universitetas, gamtos mokslai, ekologija ir aplinkotyra – N 012);

Nariai:

prof. dr. Kai Antero MYRBERG (Suomijos aplinkos tyrimų institutas, Suomija, gamtos mokslai, fizinė geografija – N 006);

prof. dr. Inga DAILIDIENĖ (Klaipėdos universitetas, gamtos mokslai, fizinė geografija – N 006);

dr. Boris CHUBARENKO (Rusijos mokslų akademijos P. P. Širšovo okeanologijos institutas, Rusija, gamtos mokslai, fizinė geografija – N 006);

dr. Darius JAKIMAVIČIUS (Lietuvos energetikos institutas, technologijos mokslai, aplinkos inžinerija – T 004).

Daktaro disertacija bus ginama viešame Ekologijos ir aplinkotyros mokslo krypties tarybos posėdyje 2021 m. rugsėjo 24 d. 10 val. Klaipėdos universiteto Jūros tyrimų instituto konferencijų salėje.
Adresas: Universiteto al. 17, LT-92294, Klaipėda, Lietuva.

Daktaro disertacija išsiųsta 2021 m. rugpjūčio 24 d.
Disertaciją galima peržiūrėti Klaipėdos universiteto bibliotekoje.

Abstract

This study, for the first time, presents comprehensive analysis of ice cover phenology, thickness distribution, as well as impact on the aquatic environment of the largest lagoon in Europe – the Curonian Lagoon. Combination of advanced remote sensing imaging techniques, conventional *in situ* observations, and numerical modelling techniques enabled the exploration of new approaches in the monitoring and forecasting of the ice cover. Using satellite data in the numerical modeling framework SHYFEM revealed the importance of high resolution ice observations for describing the physical processes during the ice cover season, such as circulation, water exchange capabilities, saltwater intrusions, water residence time, and suspended sediment dynamics. The incorporation of an advanced sea ice thermodynamic model in the modelling framework SHYFEM, together with remote sensing and ground observations, serve as an important tool for the analysis and representation of ice thickness over the whole lagoon surface, testing the impact of different climate change scenarios on the ice cover, and further improve the numerical description of this freshwater lagoon.

Key words

Ice phenology, Satellite observations, Ice thickness, Thermodynamic ice model, Climate change

Reziumė

Šiuo tyrimu pirmą kartą pateikiama išsami Kuršių marių ledo dangos fenologijos, storio pasiskirstymo, taip pat poveikio povandeninei aplinkai analizė. Pažangių nuotolinių tyrimų, įprastų *in situ* stebėjimų bei skaitinio modeliavimo metodų derinys leidžia ištirti naujas ledo dangos stebėjimo ir prognozavimo galimybes. Palydovinių duomenų panaudojimas skaitinio modeliavimo sistemoje SHYFEM atskleidė didelės skiriamosios gebos ledo stebėjimų svarbą apibūdinant fizinius procesus ledo dangos sezono metu, tokius kaip cirkuliacija, vandens mainų pajėgumas, druskingo vandens prietaka, vandens užsilaikymo laikas ir suspenduotų nuosėdų dinamika. Pažangaus ledo termodinaminio modelio įtraukimas į modeliavimo sistemą SHYFEM kartu su nuotoliniais ir antžeminiais stebėjimais yra puikus įrankis analizuoti ir vaizduoti ledo storį visame Kuršių marių paviršiuje, tirti skirtingų klimato kaitos scenarijų įtaką ledo dangai bei patobulinti skaitinį šių gėlavandenių marių apibūdinimą.

Reikšmingi žodžiai

Ledo fenologija, Palydoviniai stebėjimai, Ledo storis, Termodinaminis ledo modelis, Klimato kaita

Contents

List of original publications

The material of this study was presented in 4 original publications, published in peer-reviewed scientific journals, referred in the text by their Roman numbers:

I. **Idzelytė R.**, Kozlov I.E., Umgiesser G. 2019. Remote Sensing of Ice Phenology and Dynamics of Europe's Largest Coastal Lagoon (The Curonian Lagoon). Remote Sensing, 11, 2059, doi: 10.3390/rs11172059.

II. Mėžinė J., Ferrarin C., Vaičiūtė D., **Idzelytė R.**, Zemlys P., Umgiesser G. 2019. Sediment Transport Mechanisms in a Lagoon with High River Discharge and Sediment Loading. Water, 11, 1970, doi: 10.3390/w11101970.

III. **Idzelytė R.**, Mėžinė J., Zemlys P., Umgiesser G. 2020 Study of ice cover impact on hydrodynamic processes in the Curonian Lagoon through numerical modeling. Oceanologia, 62, 428-442, doi: 10.1016/j.oceano.2020.04.006.

IV. **Idzelytė R.**, Umgiesser G. 2021. Application of an ice thermodynamic model to a shallow freshwater lagoon. Boreal Environment Research, 26, 6177, ISSN 1797-2469.

Author's contribution

I. Idzelytė contributed to the study design, performed the satellite data collection, preprocessing, postprocessing, and data analysis, wrote the manuscript draft.

II. Idzelytė prepared and structured satellite data for use in the numerical model, contributed to writing, reviewing and editing of the manuscript draft.

III. Idzelytė contributed to the study design, carried out modelling experiments, data preprocessing, postprocessing, and analysis, wrote the manuscript draft.

IV. Idzelytė translated model code from Matlab to Fortran programming language, adapted the ice model for coupling with hydrodynamic model SHYFEM, carried out model experiments, data analysis and postprocessing, wrote manuscript draft.

Abbreviations

Abbreviation	Explanation
CL	Curonian Lagoon
EOM	Earth Observation Mission
FF	Full Freezing
FO	Freeze Onset
ISD	Ice Season Duration
LOI	Last Observation of Ice
MO	Melt Onset
MODIS	Moderate resolution imaging spectroradiometer
NAO	North Atlantic Oscillation
NID	Number of ice days
RCP	Representative Concentration Pathways
RMSE	Root Mean Square Error
RS	Remote Sensing
SAR	Synthetic Aperture Radar
SHYFEM	Shallow water Hydrodynamic Finite Element Model
SSC	Suspended Sediment Concentration
WRT	Water Residence Time

1

Introduction

Ice phenology evolution in the scope of climate change and its implications to the society. Ice phenology is undergoing extreme changes during the past decades, which is evident in the Arctic (Post et al., 2019) as well as smaller waterbodies in the northern hemisphere, such as the Baltic Sea (Luomaranta et al., 2014) and the Curonian Lagoon (Jakimavičius et al., 2019). Ice season duration, thickness, coverage, and ice phenology parameters (freeze-up, break-up, melt-off) are the main elements that have been investigated in polar and temperate zones. One of the main factors driving the ice growth and decay patters is air temperature, which is evidently increasing globally (Hu et al., 2018), thus the loss of ice is a clear and early indicator of warming climate (Kumar et al., 2020; Woolway et al., 2020; Haustein et al., 2017). Although many of the ice studies are focusing on Polar Regions (Notz and Stroeve, 2018; Stroeve and Notz, 2015; Meier et al., 2014), research of ice in the smaller water bodies, such as lakes in the northern hemisphere, also show undergoing dramatic changes (Woolway et al., 2020). It is recognized that the ice cover season in the northern temperate lakes has shortened at a rate of 7 to 17 days per century (Sharma et al., 2019; EEA, 2017) with warmer air temperatures contributing to the later freeze-up and sooner melt-off, but rates of ice cover loss are not the same in all places (Sharma et al., 2019).

The overall ice cover phenology is closely linked to the ecosystem services, having many socio-economic impacts to the regional environment – particularly transportation,

shipping, fishing, tourism, and recreational activities. An important ice impact on many northern region communities and environments is the frequent ice jam events (Prowse et al., 2007). By blocking the discharging river water of reaching the nearby water bodies, the large surrounding areas can become flooded, altering the wildlife habitat, damaging the infrastructure, and disrupting the daily commute and way of life of the residents in the affected area (Kolerski, 2018). The shorelines of the big lakes and lagoons also suffer from massive ice block drift induced by high winds, damaging the infrastructure, cultural heritage sites, contributing to the coastal erosion. Accurate predictions of ice thermodynamic, dynamic, and other characteristics are crucial for designing the offshore and coastal structures, i.e., wind power stations, oil platforms, quays, breakwaters, etc. (Wu et al., 2020; Marchenko, 2018; Heinonen and Rissanen, 2017). While the ice cover tends to be more and more unstable due to the changing climate, the recreational activities on ice will likely disappear. The present-day situation of many water bodies subjected to the ice cover reveal that the winter leisure activities, such as ice fishing, are becoming more unsafe, occasionally also needing dangerous and costly rescue missions.

While the ice cover provides many negative environmental consequences, e.g., threats to good ecological status (anoxia risk, fish kills, changes in chemical and community composition), there are many new opportunities arising due to the shortening ice cover season, too. The above-mentioned ice jam events will probably become less frequent or not as extensive (Das et al., 2020). In the Arctic, the ice melting will open new passages for shipping, fishing, and natural resource extraction (Meier et al., 2014). However, these new opportunities might not all be so sustainable (Lindenschmidt et al., 2018). The topic of the changing ice phenology and its impact to the overall environment requires an interdisciplinary approach for evaluation and management of the opportunities and threats to socio-economic and ecological elements of the system (Das et al., 2018; Crépin et al., 2017).

Ice cover impact on the aquatic environment. The under-ice physical processes that many studies focus on are underwater light climate, temperature, salinity, and overall mixing capabilities. The onset of the ice cover highly diminishes the light penetration to the water column (Cooper et al., 2020). However, the scale of it depends on the ice type, with white ice blocking most of the light transmission or black ice nearly transparent to the incoming solar radiation. Although, if the snow cover is present on the top of ice the transmission highly decreases or becomes absent (Warren, 2019; Nicolaus et al., 2012; Perovich, 2003). The main temperature regulator in the surface layers of the water is incoming solar radiation. Temperature regulates the vertical mixing (Bengtsson, 2012), with a possible stratification in the deeper water bodies (Cahill et al., 2005). The heat exchange with the sediments is a slow process able of lasting the whole ice cover season (Golosov and Kirillin, 2010) and even suitable for use as a renewable heat source for low energy networks (Mäkiranta et al., 2018). Another point regarding sediments is their transport, which is strongly diminished with the ice

cover present on the water surface, due to the blocked wind stress and water exchange capabilities (Jiang et al., 2020; Chubarenko et al., 2019).

Water bodies connected to the sea, such as lagoons, can be prone to saltwater intrusions (Müller et al., 2018; Zemlys et al., 2013), which can become increasingly more frequent due to the decreasing ice season duration and water level rise (Vargas et al., 2017; Mimura, 2013). The most fundamental ice implication to physical processes is diminished water circulation due to the limited wind stress on the water surface by the ice cover (Danilov et al., 2015), especially when the ice is landfast. For bodies of water that are not only influenced by the seawater, but also affected by the freshwater inflow from the rivers, this input is also highly diminished, having only a local effect on the circulation (Kirillin et al., 2012), resulting in increased water residence time (Umgiesser et al., 2016). These physical processes (through various chemical processes) have strong impacts on aquatic ecosystem structure, productivity, and dynamics (Hampton et al., 2017).

The most important element regulating the chemical processes and biological activity in aquatic ecosystems is dissolved oxygen. Thick and opaque ice cover highly diminishes the natural aeration, even leading to anoxia risk and winter fish kills, especially in shallow water bodies (Granados et al., 2020; Fang and Stefan, 2012). With sufficient light in the surface water just under the ice cover, the aquatic plants produce oxygen through the process of photosynthesis (Obertegger et al., 2017; Yang et al., 2017; Hampton et al., 2015). However, as microorganisms continue to decompose material in the lower water column and in the sediments, they consume oxygen, and the dissolved oxygen is depleted without the ability to be replenished from the atmosphere (Lindenschmidt et al., 2018). Since the ice season duration is expected to shorten in the future, this will have a lower impact on dissolving oxygen from the atmosphere, although other risks might arise due to the increasing temperature and biological productivity (Winder and Sommer, 2012).

Ice cover impact on phytoplankton seasonal succession and community structure is extensively investigated in lake ecosystems (Öterler, 2017; Beall et al., 2016; Winder et al., 2012). The succession has been well described in many northern temperate lakes and is strongly linked with ice phenology records (Rühland et al., 2015; Prowse et al., 2011). The most observed effects of ice phenology changes is the intensity (Dong et al., 2020; Pełechata et al., 2015) and regime shifts of spring phytoplankton blooms (Hjerne et al., 2019; Alvarez-Fernandez et al., 2012; Kromkamp and Van Engeland, 2010; Adrian et al., 1999), with higher phytoplankton numbers recorded in the growing seasons after more severe winters and advanced maximal total algal biomass – after shorter milder winters. Due to the climate change the onset of the spring phytoplankton bloom will occur earlier, likewise altering the zooplankton community structure (Beaver et al., 2019; Grosbois et al., 2017). In some cases, understanding

winter conditions can help to foresee summer conditions (Warner et al., 2018; Hampton et al., 2017; Jahan and Choi, 2014).

Ice observations and their limitations. The conventional ice measurements taken *in situ* are usually spatially sparse, because travelling on ice can be very time consuming, dangerous, and costly (Block et al., 2019), thus it is not spatially representative. Additionally, the network of the ground observation stations is slowly decreasing due to the maintaining costs or budget cuts. The measurements are done using different tools and instruments, thus the internationally accepted standards and guidelines are needed to be implemented for the extended analysis of ice and snow cover changes worldwide (Jindrova et al., 2017).

Remote sensing (RS) methods in recent decades play an increasingly important role in monitoring the ice cover, being the only practical method to obtain consistent continuous records of ice with wide geographical extent (Du et al., 2019; Zhang and Pavelsky, 2019; Cui et al., 2018; Murfitt et al., 2018). There are different types of sensors operating in various spectral bands used for ice and snow cover observations; there is no all-purpose sensor and each of them has its advantages and disadvantages (Emery and Camps, 2017). The most suitable RS instrument for ice cover observations is Synthetic Aperture Radar (SAR), being able to operate under all-weather conditions and, most importantly, independently of daylight (Jawak et al., 2015). Its wide swaths and high spatial resolution makes this sensor suitable for regional and local ice cover observations (Murfitt and Duguay, 2020; Engram et al., 2018; Wang et al., 2018). RS sensing provides an important insight of ice formation and decay stages, evaluating the ice drift, type, concentration, etc. (Mäkynen et al., 2020; Aulicino et al., 2019; Sumata et al., 2015). To get the maximum benefit of the RS observations it has to be used in conjunction with *in situ* data, thus ground observations cannot be eliminated. Although RS is a very good approach for describing ice phenology over a wide area, the accurate ice thickness data cannot be directly retrieved from SAR images (Zakhvatkina et al., 2019), and temporal resolution of satellite data is still not high enough to capture the important ice parameters.

Numerical modelling of ice conditions. The solution for dealing with drawbacks of ice observation methods is numerical modelling. Incorporating *in situ* and RS observations into modelling can highly improve the predictive capabilities of the ice models for analyzing ice thickness and phenology (Allard et al., 2018; Karvonen et al., 2012). Modelling of the ice cover has become increasingly active since the second half of the last century (Hunke et al., 2011). The development of sophisticated sea-ice models is an ongoing process and with improved ice observation methods and climate change awareness, the ice modeling is advancing by encompassing better physics and resolution (Blockley et al., 2020; Roach et al., 2019; Hunke et al., 2011).

The main processes that are being modelled are ice thermodynamics and dynamics (Hu et al., 2018; Herman et al., 2011; Hunke et al., 2011). Initially, ice models were

based on regular computations grids due to the limited computing power (Losch et al., 2010; Vancoppenolle et al., 2009). Nowadays, the grid structure is more refined, described by unstructured meshes able of dealing with complex coastlines and bathymetry (Danilov et al., 2015; Wang et al., 2014; Gao et al., 2011; Timmermann et al., 2009), which are easier applicable for regional and local studies. The processes controlling the freshwater ice formation and growth are much less complicated than that of sea-ice (Wiese et al., 2015), e.g., freezing at a constant temperature, higher than the freezing point of sea-ice, thus ice is forming faster, further, the brine-pocket physics can be eliminated (Marchenko and Lishman, 2017).

Modelling not only allows forecasting of past, present, future states of ice and investigating its feedback to changing climate, but also inspecting the response of physical and ecological processes occurring during the ice cover period (Meier et al., 2014). The biological processes in the aquatic environment highly depend on the physical conditions, thus it is necessary to incorporate at least ice thickness computations in the coupled hydrodynamic and biogeochemical modelling frameworks (Ganju et al., 2016). Excluding ice from the advanced modelling frameworks could alter the results of ecological and hydrodynamic simulations and make them less reliable, as in some cases, understanding of winter ice dynamics and how the living organisms respond to the changes of the ice cover, can facilitate prediction of summer conditions (Hampton et al., 2017).

Ice studies in the Curonian Lagoon. Ice phenology records and the overall scale of the ice cover impact on the underwater environment are varying depending of the location of the water body, thus it is important to evaluate each domain separately. The Curonian Lagoon is subjected to freezing for several months during the winter period; it is beneficial to investigate the dynamics of ice cover properties. Considering the shallow nature of this waterbody, a smaller volume of water beneath the ice is present and the freezing occurs faster than in deeper waters, leading to a stronger impact on physical and ecological processes in it. Thus far, ice in the Curonian Lagoon was investigated only using the conventional *in situ* measurements, statistical modelling or analyzing its impact on other processes and regimes within it (Jakimavičius et al., 2019; Umgiesser et al., 2016; Rukšėnienė et al., 2015; Dailidienė, 2007), with one recent study employing RS products for ice thickness estimation (Kozlov et al., 2020). However, so far there have been no comprehensive studies combining ice cover extent, phenology, thickness, season duration, and their dynamics over the whole lagoon surface, derived through the application of advanced analytical methods – remote sensing and numerical modelling. The projections of forthcoming ice cover conditions, foreseen by the presented ice thermodynamic model and meteorological data from regional climate models, shows what to expect in the future under changing climate. Furthermore, an ice model integrated in the hydrodynamic modelling framework can be further used for coupling it with the ecological model for evaluating ice cover effect on the entire ecosystem of the Curonian Lagoon.

1.1. Aim and objectives

The aim of this study is to investigate ice cover phenology and dynamics in the Curonian Lagoon using remote sensing techniques and numerical modelling approaches in the scope of climate change and analyze ice cover impact on the hydrodynamic properties in the lagoon.

The following objectives were addressed:

1. To evaluate the dynamics of ice phenology, derive ice growth and decay patterns from satellite images, and assess ice season duration relationship with air temperature variability.
2. To apply satellite ice cover data in the numerical model and analyze the ice cover effect on the circulation, saltwater intrusions, water renewal capabilities, and suspended sediment transport.
3. To perform model computations of ice thickness, validate the obtained results with *in situ* data, integrate ice thermodynamic model in the hydrodynamic modelling framework SHYFEM for assessing the ice thickness distribution over the entire lagoon surface, and investigate the future projections of the climate change scenarios RCP4.5 and RCP8.5.

1.2. Novelty

This study, for the first time, presents the combined knowledge of the ice cover phenology in the Curonian Lagoon. It explores new approaches in the monitoring and forecasting of the ice cover by comparing conventional *in situ* observations with advanced remote sensing imaging techniques, and accentuates the benefits of the latter. The application of satellite data in the shallow water hydrodynamic finite element model (SHYFEM) shows the importance of high-resolution ice observations for adequately describing the physical processes during the ice season, which is considerably improved by this study. So far there have been no working high-resolution ice model applied to the Curonian Lagoon, which has been developed as a part of this research project. The incorporation of the advanced sea ice thermodynamic model in the modelling framework SHYFEM, in combination with *in situ* and remote sensing observations, serve as an important tool for analyzing different ice parameters and likewise improving the numerical description of this freshwater lagoon.

Summarizing, the novel aspects of this thesis deal with ice cover in the Curonian Lagoon with regard to 1) an advanced description of ice phenology and dynamics; 2) an evaluation of hydrodynamic properties under ice; 3) the establishment of ice thermodynamic model in the hydrodynamic modelling framework; 4) long-term projections of ice thickness. The created subroutines and code structure of the ice model provides a possibility for future coupling with other modules in the SHYFEM modelling framework.

1.3. Scientific and applied significance of the results

The results of this study broaden our knowledge of ice cover phenology and dynamics over the entire surface of the Curonian Lagoon, as well as the alteration of the hydrodynamic processes beneath ice. The assessment of remote sensing data demonstrated that in many cases it has a better performance over ground observations regarding ice phenology records over the whole lagoon surface, therefore it could be advocated for the use in the regional ice monitoring programs. The usage of satellite ice data in the hydrodynamic model provided a more advanced insight into the ice cover impact on physical processes, since RS data have a much wider coverage than *in situ* observations, providing an opportunity to study areas far from the coast as well. Numerical modelling of the ice itself allows predicting the evolution of ice thickness and distribution, as well as testing the impact of different scenarios of changes in atmosphere forcings on ice phenology in the scope of climate change. The proposed ice thermodynamic model showed to fit very well with the ground observation data of the Curonian Lagoon. Its further integration in the numerical modelling system SHYFEM enable us to not only thoroughly examine ice thickness over the whole area of the lagoon, but it will also be highly useful for other shallow lagoons or lakes in the northern region, where both the shallow nature and the possible ice cover have to be addressed. Through this research project, the created model setup and code base can be further integrated with an ecological model of the same SHYFEM modelling framework. All this will support a progress in describing and understanding the ecosystem of the Curonian Lagoon.

1.4. Scientific approval

Results of this study were presented in 3 international and 2 regional conferences:

1. Jūros ir krantų tyrimai, Klaipėda, Lithuania, May 2018.
2. 7th IEEE/OES Baltic Symposium: Clean and Safe Baltic Sea and Energy Security for the Baltic countries, Klaipėda, Lithuania, June 2018.
3. Jūros ir krantų tyrimai, Klaipėda, Lithuania, May 2019.
4. ESA Living Planet Symposium, Milan, Italy, May 2019.
5. AGILE Conference 2019, Limassol, Cyprus, June 2019.

2

Materials and methods

2.1. Study site

The Curonian Lagoon (Fig. 1) is a shallow (average depth – 3.8 m, greatest natural depth – 5.8 m) estuarine freshwater body; nevertheless, it is the largest coastal lagoon in Europe (area ~1600 km^2, volume 6.3 km^3) (Gasiūnaitė et al., 2008; Žaromskis, 1996). It is located in the southeastern corner of the Baltic Sea (between 54.9°N and 55.9°N), connected to it by a narrow artificially deepened (up to 15.5 m) Klaipėda Strait and separated from it by the sandy Curonian Spit. During the suitable wind regimes, northern part of the lagoon is prone to saline seawater intrusions (Zemlys et al., 2013). Saltwater flows along the western shoreline, due to the outflowing freshwater from Nemunas River, which is the largest river discharging in the lagoon, being the main water renewal source, especially in the northern part (Umgiesser et al., 2016). Every year all the discharging rivers deliver fresh water of nearly 4 times the lagoon volume (Dailidienė and Davulienė, 2008). Since the saltwater does not reach the southern part of the lagoon, it is considered freshwater.

Historical observational data analysis (Baukšys, 1978) showed that during the period of 1948–1972 the ice in the Curonian Lagoon would start to form in the beginning of December and disintegrate on average in the end of March, after 6–13 days the lagoon would be free of ice. Ice cover lasted on average for 110 days (ranging from 12 to 169 days), while ice thickness varied from 10 to 70 cm. Due to the ongo-

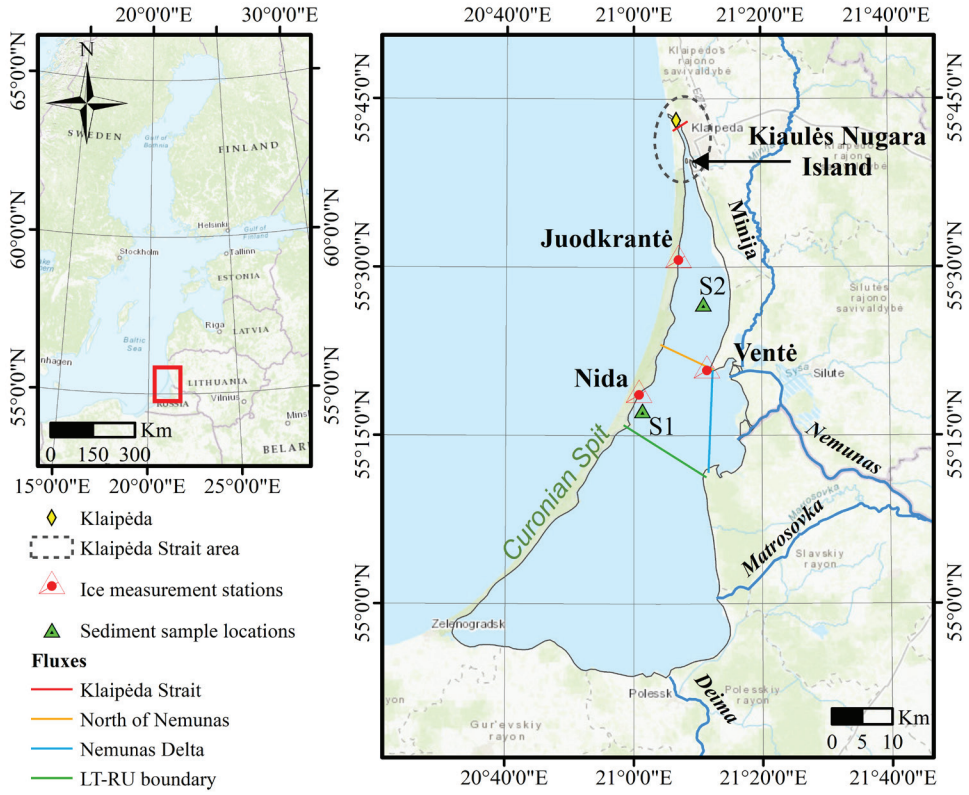

Figure 1. Location of the Curonian Lagoon (right) with respect to the Baltic Sea (left). The legend indicates the areas and points for the analysis. In the text, the northern part of the lagoon is considered as the area northward of the LithuanianRussian boundary, southern part – southward (green line), the Nemunas Delta area is eastward of Nemunas Delta cross section (blue line). Basemap source: ESRI.

ing climate change and the forecasts of increasing air temperature the ice parameters will likely change towards shorter duration and thinner ice. Indeed, the resent study of future projection of ice phenology and thickness in the lagoon using a statistical model (Jakimavičius et al., 2019) shows that in the near future (2021–2040) the average ice thickness will only be 13–15 cm and by the end of the century it will decline to 0–13 cm. The change can already be observed in the western part of the lagoon, where the ice season duration decreased by half, comparing the periods of 1961–1975 and 1991–2005 (Dailidienė, 2007; Jarmalavičius, 2007).

2.2. Data

2.2.1. Ice remote sensing data

Satellite data of C-band synthetic aperture radar (SAR) were acquired from three Earth observation missions (EOM): Envisat Advanced SAR (ASAR), RADARSAT-2, and Sentinel-1A and 1B (bottom row in Fig. 2). The analyzed period was from 2002 to 2017 (15 winters). Since the frequency of SAR images during some winters was insufficient for describing ice cover dynamics, the additional available cloud-free images from moderate resolution imaging spectroradiometer (MODIS, on board the Terra satellite) were used. Overall, 514 SAR and 101 MODIS images were obtained and processed (top and bottom rows in Fig. 2). The data of ASAR observations was acquired approximately every 3 days, with even occasional two images per day. RADARSAT-2 had the highest frequency – every 2 days, while the lowest was of Sentinel-1A and 1B – only 2–3 images per week.

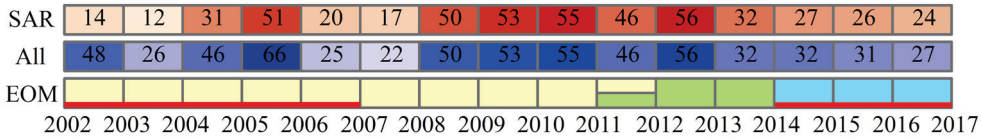

Figure 2. Representation of number of images and Earth observation missions (EOM) of which the satellite data were analyzed. Top (SAR) and middle (All) rows indicate number of SAR and SAR+MODIS images, respectively. Bottom row shows EOM with yellow colored boxes indicating ASAR, green – RADARSAT-2, and blue – Sentinel-1A and 1B, underlying red lines indicate MODIS data. Modified from Paper I.

Since water, ice, and snow cover on top of it have different strength of backscattered signal, the edge of the ice cover can be distinguished from the open water rather effectively (Muckenhuber et al., 2016; Dierking, 2013). While the Curonian Lagoon is not a particularly large waterbody, the visual identification of the ice edge was used in this study. SNAP EO processing software was applied for deriving an orthorectified subset of each SAR image in GeoTIFF format for further processing in the ArcGIS software (ArcMap). The manually digitized ice polygons were converted to a raster format and summed up by considering the time intervals between the consecutive satellite observations and measured air temperature. This way, for each winter spatially detailed maps of the ice season duration were acquired. Based on these maps, a maximum, D_{SAR}, and spatial-mean (averaged over the lagoon area), $\overline{D}_{SAR}$, were defined for each winter season, which were then then classified into three categories: short ($\overline{D}_{SAR} < 50$ days), intermediate (50 days $\leq \overline{D}_{SAR} \leq 100$ days), and long winters ($\overline{D}_{SAR} > 100$ days).

The dates of the ice freeze onset (FO), full freezing (FF), melt onset (MO), and last observation of ice (LOI) were defined by the dates of the acquired images having these ice formation and decay stages. Air temperature measurements were also taken into account for defining the FO and MO dates. The statistical significance of inter-annual variability linear trends of these characteristics was determined by the Mann-Kendall test (Käyhkö et al., 2015; Kendall and Gibbons, 1990) at a 0.05 significance level with a 95% confidence level.

T_a^{CN}

The correlation coefficient between the ISD and Hurrell's winter (December through March) NAO_{DJFM} index (provided by the Climate Analysis Section, NCAR, Boulder, USA) was calculated to determine the dependency of changes in the ISD on the intensity of the North Atlantic Oscillation (NAO). The dependency of ISD and cumulative negative air temperature (derived from coastal observations), T_a^{CN}, was analyzed to better understand ice cover properties in the Curonian Lagoon. Everything regarding the used data and applied processing methods are thoroughly described in Paper I.

The satellite data derived from this thesis were used in the numerical modelling framework SHYFEM for analyzing ice cover effect on physical processes, which are described in section 2.3.4 Simulation setup and scenarios section, as well as Papers II and III. Remote sensing data was also used for validating the modelled ice thickness extent.

2.2.2. Ice ground observations

The satellite images were validated with data from three coastal stations in Nida, Juodkrantė, and Ventė (Fig. 1). Ground data consists of daily observations of ice formation stages, coverage (on a scale from zero – no-ice to 10 – fully ice-covered), state, density, thickness, and drift, as well as air and water temperature, wind speed, and visibility. For Nida and Ventė, *in situ* data covers the whole study period (2002–2017), however, in Juodrantė the ice observation program was discontinued in 2012. The measurement data were provided by the Environmental Protection Agency (EPA) of Lithuania.

Ice cover extent derived from satellite images was validated by considering the ice concentration in circular buffers centered on the ground station points. The radius of each buffer was set to the visibility value recorded each day when the ice measurements were taken. Parts of the buffers were removed based on the overlap with the coast. All computations were done by running a custom python script using ArcPy module. The dates of the ice FO, FF, MO, and LOI of ice were defined also for *in situ* observations and compared to those of remote sensing data by computing the difference between them in days. The dates of *in situ* data were defined when a given ice stage was observed at least at one coastal station. ISD was also defined for the coastal observations, D_{st}.

The ice thickness records were used for ice thermodynamic model calibration. The results were evaluated by computing the average of RMSE and Pearson correlation coef-

ficient (R) between the modelled and observed values of the ice thickness of three points in the lagoon corresponding with the ice observation stations. The correlation coefficient is accompanied by the sample size (n) and significance p-value, computed with 95% confidence level. Ice season duration of the calibrated ice model was also compared with the observations from the coastal stations, based on the same FO and LOI dates.

2.2.3. Meteorological data

Meteorological forcings, i.e. cloud cover, downward shortwave radiation, precipitation, humidity, air temperature, atmospheric pressure, and wind speed, were obtained from the forecasts of operational numerical weather prediction model HIRLAM provided by the Lithuanian Hydrometeorological Service and operational forecasts from European Centre for Medium-Range Weather Forecasts (ECMWF, Table 1). As well as data from ERA5 – the fifth generation ECMWF reanalysis for the global climate and weather hourly data on single levels data (Hersbach et al. 2018) were used for ice thickness modelling. EPA of Lithuania provided the measurements of air temperature in all three stations (Nida, Juodkrantė, and Ventė, Fig. 1), and Lithuanian Hydrometeorological Service provided the precipitation measurement data in Nida, which were used to correct the bias in the climate data.

Table 1. Summary of the data sourced used in the numerical modelling framework SHYFEM.

Name	Period	Model abbreviation	Institution
Salinity, temperature, water level	2004–2006	MIKE21	Danish Hydraulic Institute
	2007–2009 2014–2016	HIROMB	Swedish Meteorological and Hydrological Institute
	2010–2013	MOM	Leibniz Institute for Baltic Sea Research in Warnemünde, Germany
River discharge	2004–2016		Lithuanian Hydrometeorological Service
Meteorological data	2009–2010	HIRLAM	Lithuanian Hydrometeorological Service
	2004–2008 2009–2016	0.1^{o}x0.1^{o} resolution	European Centre for Medium-Range Weather Forecasts
	2004–2017	ERA5	European Centre for Medium-Range Weather Forecasts reanalysis

2.2.4. Hydrological data

There are five open boundaries defined in the model study domain – one for the Baltic Sea, and four for the discharging rivers: Nemunas, Minija, Matrosovka, and Deima (Fig. 1). Salinity, temperature, and water level data for the Baltic Sea open boundary were acquired from the forecasts of the operational hydrodynamic models MIKE21 and High Resolution Operational Model for the Baltic Sea (HIROMB), as well as Modular Ocean Model (MOM). The Lithuanian Hydrometeorological Service under the Ministry of Environment provided daily river discharge data. The source of the data and periods are shown in Table 1.

2.2.5. Climate data

For the analysis of climate change impact on ice thickness in the Curonian Lagoon, a historical period (1986–2005) was compared to the future period (2006–2100) based on two Representative Concentration Pathway (RCP) scenarios: RCP4.5 and RCP8.5. Meteorological data for these projections was acquired from CORDEX (Coordinated Regional Downscaling Experiment) scenarios for Europe from the Rossby Centre regional climate model (RCA4), which consists of 5 sets of simulations (downscaling) driven by the five global climate models described in Table 2. The computations were done for three point locations corresponding with measurement stations.

Table 2. Summary of the sources of regional climate model data.

Model abbreviation	Model	Institution
ICHEC	EC-Earth	Irish Centre for High-End Computing
CNRM	CNRM-CM5	Centre National de Recherches Météorologiques
IPSL	IPSL-CM5A-MR	The Institut Pierre-Simon Laplace
MOHC	HadGEM2-ES	Met Office Hadley Centre
MPI	MPI-ESM-LR	Max Planck Institute for Meteorology

The air temperature data from climate models revealed some bias compared with the measurements, thus it had to be corrected. This was done by applying a basic bias-correction method by simply adding the difference between the observed ($\bar{T}_O$) and modelled ($\bar{T}_m$) average air temperature computed for the November-April period of 1993–2005 (Lenderink et al., 2007):

$$T_{BC}(t) = T_m(t) + (\bar{T}_O - \bar{T}_m) \quad (1)$$

Precipitation (Pr_{BC}) was corrected by multiplying the ratio between the observed ($\overline{Pr_O}$) and modelled ($\overline{Pr_m}$) values, computed for the same period as for air temperature corrections:

$$Pr_{BC}(t) = Pr_m(t)\,\frac{\overline{Pr_O}}{\overline{Pr_m}} \tag{2}$$

The trend significance of the air temperature and ice thickness was assessed using Mann-Kendall test at a significance level of 0.05 with a 95% confidence level, the tendency rate (for the period 2006–2100) was evaluated by taking the slope parameter from linear regression equation.

2.3. Numerical modelling

The processed remote sensing data was used in the finite element hydrodynamic model SHYFEM for analyzing the ice cover effect on physical processes and suspended sediment concentration in the Curonian Lagoon. Further, a separate enhanced sea ice thermodynamic model was tested for the Curonian Lagoon (CL) case and integrated in the same hydrodynamic model. Everything regarding the models, data, simulation setups, and applied processing methods are thoroughly described in Papers II–IV.

2.3.1. Hydrodynamic model

SHYFEM is an open source unstructured-grid finite-element hydrodynamic model for shallow water bodies. This model was developed at ISMAR-CNR (Institute of Marine Sciences – National Research Council, http://www.ismar.cnr.it/shyfem) in Venice, Italy, where it is operationally implemented for forecasting storm surges (Cavaleri et al., 2019; Zampato et al., 2016). The calibration and validation of the model was already done for the Curonian Lagoon (Zemlys et al., 2013; Ferrarin et al., 2008a) and model application for studying hydrodynamic processes was already successful for numerous lagoons throughout Europe including the CL (Maicu et al., 2018; Molinaroli et al., 2014; Umgiesser et al., 2014; Ferrarin et al., 2010).

The model solves 3D hydrodynamic equations, vertically integrated over each layer. The equations are integrated in time using a semi-implicit discretization scheme and spatial discretization is achieved using a partially modified finite element method (Umgiesser et al., 2004). The irregular triangular computation grid makes the model

suitable for applications to the waterbodies with complicated geometry and bathymetry (e.g., lagoons, coastal seas, estuaries, and lakes).

The satellite ice cover data in the model is interpolated to cover the whole ice season and represented by numbers between 0 – water and 1 – fully ice-covered, and with this value the wind drag coefficient is weighted. This way the momentum input through the surface is scaled by the area free of ice. The ice-ocean stress is not considered. Ice value is also used for albedo calculation for using the heat flux model. However, the model takes into account just a fraction of the ice cover, not the thickness or the snow cover on top of it. This might be a good approach for momentum, but less correct for light penetration.

The hydrodynamic model is able to provide 2D as well as 3D computations. A 3D setup was used for the application of remote sensing ice cover data for the analysis of circulation, saltwater intrusions from the Baltic Sea, water residence time in the lagoon, mass fluxes through sections shown in Fig. 1, and suspended sediment concentration (SSC) under the ice, while 2D setup was used for ice thermodynamic modelling.

2.3.2. Ice model

An enhanced sea-ice thermodynamic model ESIM2 by Tedesco et al. (2010) was used for studying the ice thickness and its integration in SHYFEM modelling system. The initial version of the model showed satisfying results for predicting the seasonal changes of the ice and snow thickness in the Baltic Sea. The ice model computes three layers of the snow, adopting a new parametrization for snow compaction using a "bucket model" for solid precipitation, two intermediate layers (meteoric ice – snow ice and superimposed ice), and two layer of sea ice.

The formation of the snow ice is initiated every time the ice draft exceeds the thickness of the ice, while the superimposed ice in the model is formed when the melted snow refreezes being in contact with the ice layer. Ice layer is divided in biologically active and biologically inactive parts for simulating salinity evolution in the sea-ice and being compatible with the biogeochemical flux model (Tedesco et al., 2010). The model also computes the temperature at the interface of each snow and ice layer, and at the surface. In previous model applications the oceanic heat flux was set to a constant value, however, here a bulk formulation by Omstedt and Wettlaufer (1992) is incorporated:

$$F_w = \rho_w C_p C_h \Delta U \left(T_\infty - T_f\right) \tag{3}$$

where ρ_w is water density, C_p – specific heat of water, C_h – heat transfer coefficient, ΔU – relative velocity between the ice drift and the current at a reference level, T_∞ – far field temperature (here it is called mixed layer temperature), and T_f – freezing temperature. The full description of ice thermodynamic model, its evolution, and applications can be found in Tedesco (2009), Tedesco et al. (2010, 2009).

The ice thermodynamic model was coupled with a hydrodynamic model to further enhance the SHYFEM modelling system. The main part of the SHYFEM code is composed in FORTRAN. The source code of the ice model, kindly provided by M. Vichi, is written in MATLAB, thus it had to be rewritten and restructured to fit the main modelling framework. The coupling was done by taking the salinity, water temperature, and depth of the mixed layer produced by SHYFEM and passing as inputs to the ice module. The varying salinity values were also used to adjust the freezing temperature. The output of the mixed layer temperature from the ice module is passed back to the hydrodynamic model.

2.3.3. Sediment model

The sediment transport rate model SEDTRANS05 was used for studying the sediment dynamics under the ice cover. This model also belongs to the same SHYFEM modelling framework, working on the same computational grid. At each model time step the erosion and accumulations rates are computed based on the wind induced waves and currents, likewise, the depth is updated based on the erosion and deposition for computing the hydrodynamics at the next time step. The velocity in the bottom layer computed by the hydrodynamic model is used for computing the bed shear stress.

The initial bottom sediment composition was derived from maps (Gelumbauskaitė et al., 1999; Gulbinskas and Žaromskis, 2002) and used in the model by constructing the nine-class regular sediment grid, ranging from clay to coarse sand and represented as a percentage of total suspended sediment concentration (SSC) for each class. The SSC at the open sea boundary was set to zero, due to the absence of data. A more thorough description of the model and its applications can be found in (Ferrarin et al., 2016, 2010b, 2008b; Neumeier et al., 2008) and Paper II.

2.3.4. Simulation setup and scenarios

Computation grid, corresponding to the Curonian Lagoon domain, consisted of 1309 nodes and 2027 triangular elements with a much finer resolution in the Klaipėda Strait area, and 10 sigma layers have been used for the vertical discretization. A part of the Baltic Sea is included for preventing the disturbances in computations of the exchanges through the Klaipėda Strait area. For the application of satellite ice cover

data in the hydrodynamic model SHYFEM, the Baltic Sea and Klaipėda Strait were considered ice-free. The simulation period was from 2004-01-01 to 2015-12-31 and the first year was discarded as model spin-up time. Three types of simulations have been carried out – without ice ("no-ice"), with satellite ice cover data ("real ice"), and with ice fully covering the lagoon for each ice season ("idealized ice", Table 3). Comparison of the simulation results of the latter two allows a better understanding of the ice cover role in the hydrodynamic processes.

Table 3. Summary of model simulations for the analysis of hydrodynamic properties under the ice cover.

Abbreviation	Description
No-ice	Ice cover artificially switched off in the model
Real ice	With ice cover data obtained from the satellite data
Idealized ice	The lagoon is completely covered by ice during the ice cover season, including the Klaipėda Strait area

For the analysis of ice cover impact on the circulation, salinity, and water residence time (WRT), the above mentioned simulation results were averaged over the meteorological seasons of the year: winter (December, January, February), spring (March, April, May), summer (June, July, August), and autumn (September, October, November), as well as over the ice cover seasons (each of them having different durations). The impact of ice was evaluated by computing the average difference of simulation results obtained with ice switched on and off in the model ("real ice" minus "no-ice" and "idealized ice" minus "no-ice"). The number of hours per year of salt concentration exceeding the 1 and 3 g kg^{-1} thresholds in Klaipėda Strait (marked yellow in Fig. 1) was identified by computing the salinity time series difference between the bottom and top layers of the water column. The number of days when the salt concentration exceeds the 2 g kg^{-1} threshold in Juodkrantė was computed from vertically averaged salinity time series. WRT was computed for the ice cover season and every meteorological season of the year defined above (Table 4). WRT was computed separately for northern and southern parts of the lagoon (separated by LT-RU boundary in Fig.1), and for the total lagoon area.

Table 4. Summary of Water Residence Time (WRT) computation periods in different model setup types described in Table 3.

Abbreviation	Computation period
WRT_{ice}^{real}	During the ice cover season in simulation with satellite (real) ice cover data
WRT_{ice}^{ideal}	During the ice cover season in simulation with idealized ice cover data
WRT_{ice}^{no-ice}	During the ice cover season in simulation without ice cover ("no-ice")
WRT_{season}^{real}	Every meteorological season in simulation with satellite (real) ice cover data
WRT_{season}^{no-ice}	Every meteorological season in simulation without ice cover ("no-ice")
WRT_{winter}^{real}	During winter (Dec, Jan, Feb) in simulation with satellite (real) ice cover data
WRT_{winter}^{no-ice}	During winter (Dec, Jan, Feb) in simulation without ice cover ("no-ice")

For the analysis of ice cover impact to the sediment distribution and transport a different grid was used, consisting of 2033 nodes and 3294 elements with five sigma layers for the vertical discretization. Two sets of short-term simulation runs (from 15 January 2014 until 7 March 2014) were computed ("real ice" and "no-ice"). The comparison of these simulation runs was done by computing the average suspended sediment concentration (SSC) values of the whole lagoon and by looking at the time series of SSC in the water column of two monitoring stations in the northern part of the CL (S1 and S2 in Fig. 1). The difference between simulation setup types is evaluated by applying t-Test with 0.05 significance level.

The ice thermodynamic model was calibrated for the period 2004–2017. For this, two types of simulation are presented: 1) with initial model set-up as described in Tedesco et al. (2010) (hereafter $Pres_{Orig}$), and 2) with increased densities of all snow types by 50 kg m^{-3} (hereafter $Pres_{\rho_s}$). The results were compared with *in situ* ice thickness observations in Nida, Juodkrantė, and Ventė (Fig. 1) by computing the average root-mean-square error (RMSE) and Pearson correlation coefficient (R). The correlation coefficient is accompanied by the sample size (n) and significance p value, computed with 95% confidence level.

In order to make future predictions of the ice cover thickness, the meteorological data from five regional climate models were chosen (Table 2) based on two climate change scenarios, termed Representative Concentration Pathways (RCP). The RCP4.5 and RCP8.5 were chosen for being the most realistic outcome. The simulations were carried out for two periods: 1) historical, and 2) future estimations, analysis for the future period was divided in near and far future (Table 5).

Table 5. Summary of simulations for climate change analysis. The data for the near and far future was extracted from RCP4.5 and RCP8.5 simulation results.

Name	Period	Description
Hist	1986-2005	Historical period
RCP4.5	2006-2100	Stabilization scenario
RCP8.5	2006-2100	"Business as usual" scenario
$RCP4.5_{near}$	2021-2040	RCP4.5 scenario in the near future
$RCP4.5_{far}$	2081-2100	RCP4.5 scenario in the far future
$RCP8.5_{near}$	2021-2040	RCP8.5 scenario in the near future
$RCP8.5_{far}$	2081-2100	RCP8.5 scenario in the far future

3

Results & Discussion

3.1. Ice cover phenology and dynamics

Ice cover phenology and dynamics is presented in this section. All the results and analysis are summarized with reference to Paper I, where a thorough explanation can be found.

3.1.1. Ice phenology based on remote sensing and *in situ* observations

Ice concentration derived from satellite images correspond very well to the one observed in the ground stations ($R = 0.92$, $n = 1014$, $p = 0$). Most of the remaining inconsistencies arise from the limitations of deriving ice type from RS. In reality, ice observations in the coastal stations can be of several types: slush, frazil, grease, broken, etc., and it will gradually receive lower observation values during the melting period (from 10 to zero). However, in this study the pixels in the satellite images are not categorized by the ice type, but rather a binomial classification is applied: ice-free (zero) or ice-covered (10), and in some cases the thin or low concentration ice cannot be detected in the RS images. Still, the chosen image processing method allowed investigating the spatial extent, seasonal and inter-annual variability of the ice cover properties in the Curonian Lagoon comprehensively.

The comparison of the dates of the freeze onset (FO), full freezing (FF), melt onset (MO), last observation of ice cover (LOI), and ice season duration (ISD) between satellite and *in situ* observations also showed some discrepancies (Fig. 3). The average difference of FO dates is only half a day, with ice formation being firstly observed at the coastal stations. The frequency of the RS images is not high enough to observe the rapid ice formation, nevertheless in 38% of the cases FO was observed in satellite images earlier than at the coastal stations. The similar average difference is observed in the FF case, however, here in 62% of the cases when FF is observed in the coastal stations, the satellite images still show open water regions further away from the coast.

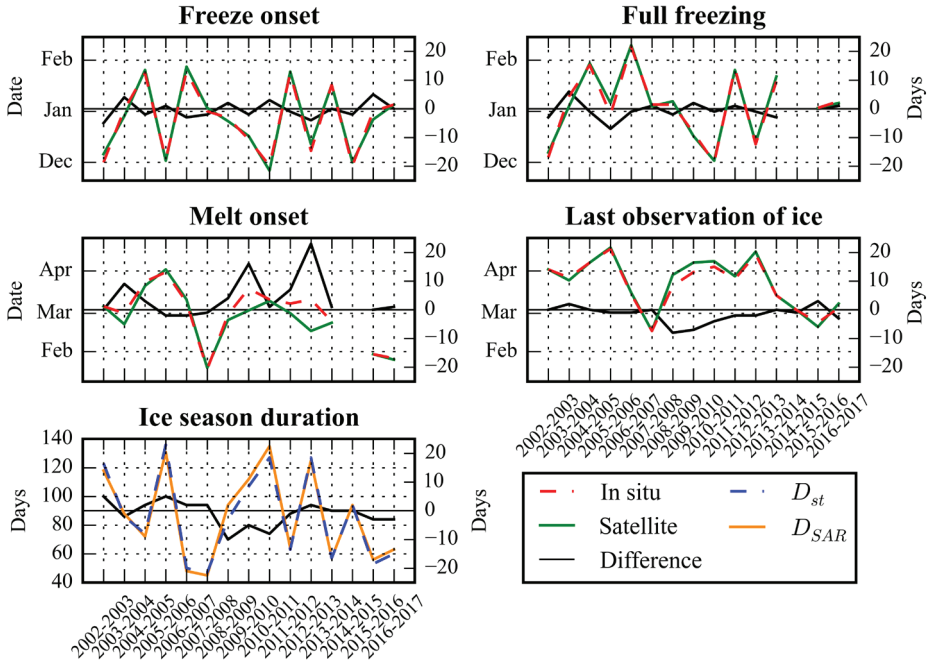

Figure 3. Dates of the freeze onset, full freezing, melt onset, last observation of ice, and ice season duration (D_{st} and D_{SAR}, e) derived from satellite images (green solid lines) and coastal observation (red dashed lines), and the difference between them (*in situ* minus satellite, black solid lines). Please pay attention to the winter of 2014–2015 in full freezing and melt onset graphs, where it was excluded from the analysis due to unstable ice cover conditions not allowing an identification of these dates from ground observations. Modified from Paper I.

The highest difference between RS and *in situ* observations is observed in defining the melt onset date. It is detected on average five days earlier in satellite images than at the coastal stations (75% of all cases), denoting the fact that the ice break-up first

occurs further away from the coastal stations, likewise, the last ice cover traces. LOI is on average two days later than it is recorded at the coast (so much as 82% of all the cases). These results clearly emphasize the role of RS for providing a high spatial overview of the ice cover on the entire lagoon surface for defining the key stages of ice cover formation and the overall ice season duration. The latter is shown to be longer by an average of four days in 57% of the cases.

The mean success rate of the satellite observations is 63% for all five parameters shown in Fig. 3. The comparison of freeze onset and last observation of ice dates derived from RS and coastal observations allows establishing a corrected ISD value (D_{corr}), taking the earlier FO dates frequently observed at the coastal stations and later the LOI dates usually recorded in the satellite images. The updated ISD in 73% of the cases is longer by up to 10 days than the one derived from *in situ* observations, thus it is the most adequate record to describe the overall period of the ice season.

3.1.2. Ice cover extent, its progression and decay

It takes on average six days (ranging from zero to 35 days) after the freeze onset for the Curonian Lagoon to be completely covered by ice. Satellite images often show a very rapid freezing – the first received image already displaying full freezing of the lagoon. This occurs during the periods of low negative air temperature. However, if the temperature is unstable during the freezing period, then ice formation can be traced in several consecutive satellite images. Ice formation starts all along the eastern and southern shoreline of the lagoon, as well as a slightly earlier freezing in the Nemunas Delta area (Fig. 4a). The latest ice formation occurs along the southern section of the Curonian Spit and over the deepest (natural depth of around 5 m) southwestern part of the lagoon.

All analyzed ice seasons in 2002–2017 display a full freezing of the lagoon, which lasts on average for 40 days (ranging from 10 to 90 days). Several melting events can occur in various parts of the lagoon between the full freezing and final melt onset dates (when the ice starts melting after the last full freezing period), due to the rise of air temperature above 0 °C. On average ice cover starts to decay at the end of February, while the whole melting period lasts on average for a month (ranging from 6 to 60 days). Ice usually starts to decompose in the northern part of the lagoon (Fig. 4b), due to the interaction with inflowing warmer water from the Baltic Sea and further spreads along the western coastline. The dominant factor shaping the ice retreat patterns is a prevailing wind direction. During the melting season, frequent westerly winds push the drifting ice towards the southeastern part of the lagoon and in the Nemunas Delta, thus ice can be observed to stay there the longest.

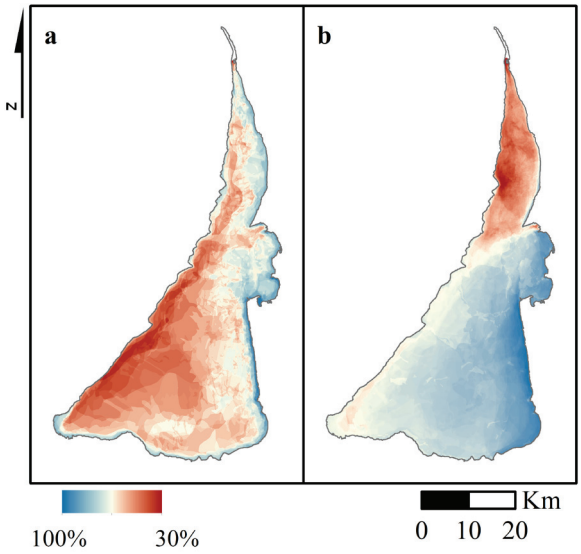

Figure 4. Distribution of ice cover extent during the freezing (a) and melting (b) periods. Colored maps depict the percentage of ice observations during these periods – blue color in (a) shows the initial ice formation areas, red color in (b) represents the initial ice melting areas. Redrawn from Paper I.

Out of all four ice cover formation and decay stages, only the dates of the final melt onset and last observation of ice have a clear decreasing pattern. This means that ice cover is starting to break up and dissolve earlier during the last years. However, only the trend of the melt onset dates is statistically significant ($p = 0.02$).

3.1.3. Variability of ice season duration

With this study of remote sensing ice cover data of the Curonian Lagoon, spatially detailed ice season duration (ISD) maps for the period of 2002–2017 are presented for the first time, displaying a very pronounced inter-annual variability. Here, in Fig. 5, the average ISD of all the analyzed ice cover seasons is demonstrated. The ice cover remains longest in the southeastern limnic part of the lagoon and along the eastern shore, as well as Nemunas Delta area (15-year average ISD is 75–85 days), opposed to the ISD in the western and southwestern parts of the lagoon (average ISD is 65–70 days). However, the shortest ISD is observed in the northern part of the lagoon (average ISD is <65 days), due to the turbid nature of this area – inflowing saline water from the Baltic Sea and outflowing fresh Nemunas River water. The overall 15-year spatially-averaged average ISD is 71±32 days.

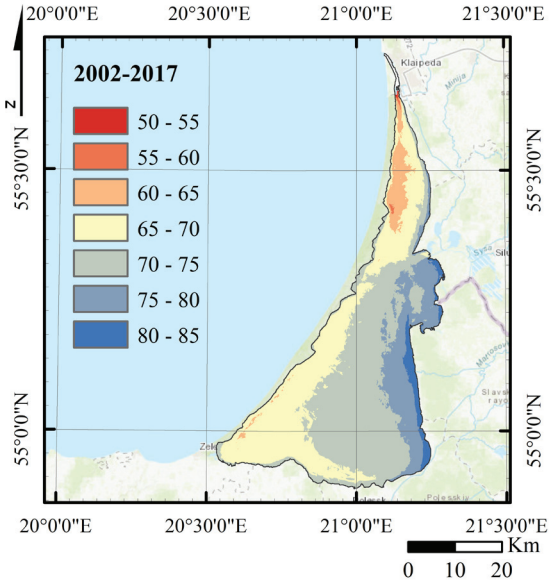

Figure 5. Average ice season duration in the Curonian Lagoon for the period of 2002–2017, derived from remote sensing data. Basemap source: ESRI. Redrawn from Paper I.

Fig. 6 shows the inter-annual variability and decreasing trends of various ISD types. The average ISD value derived from the coastal records D_{st} = 86 ±30 days, while corrected ISD, D_{corr}, is slightly longer – 89±31 days. The corrected ISD is observed to decrease at a rate of 1.6 days year^{-1} during 2002–2017. However, these two ISD definitions lack the spatial properties offered by remote sensing. The spatial-mean ISD, $\overline{D}_{SAR}$, provides a better representation of the spatial variability of the ice cover conditions in the Curonian Lagoon. $\overline{D}_{SAR}$ is lower than other ISDs, because of the changing ice cover properties in the CL, e.g., the multiple melting and refreezing periods during the ice season, having a more pronounced decreasing trend than other ISDs with a shortening rate of 2.3 days year^{-1}. Similar results of shortening ice cover season were reported for the Baltic Sea over the past century (Haapala et al., 2015). The inter-annual variability of the ISD in the CL correlates very well with similar results obtained for the Gulf of Riga (Siitam et al., 2017) along the coast of Latvia (Kļaviņš et al., 2016), and the Vistula Lagoon (Chubarenko et al., 2019).

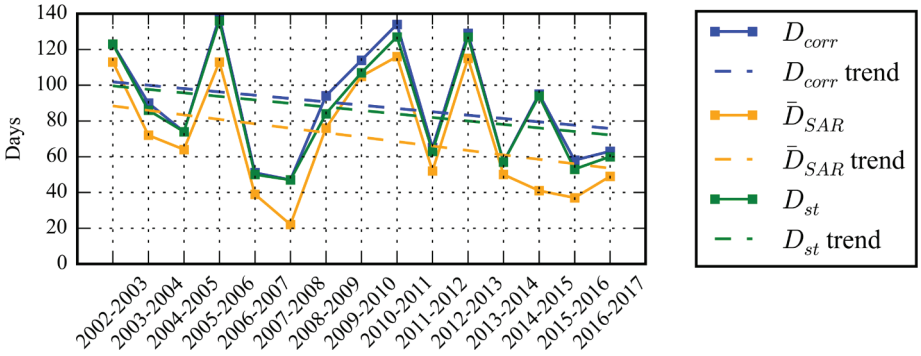

Figure 6. The variability of ice season duration (ISD) derived from satellite data (spatial-mean, $\bar{D}_{SAR}$) and ground observations (D_{st}), as well as overall corrected ISD (D_{corr}) over the period 2002–2017. Redrawn from Paper I.

All 15 ice cover seasons can be classified in three categories based on their spatial-mean ISD ($\bar{D}_{SAR}$): short, intermediate and long (Table 6). Ice formation during the short winters starts nearly a month later than that of long winters. The ice cover extent during the short winters is not steady with prevailing melting events. Furthermore, short winter are not only short in their ISD, but they are also characterized having a very short period of the ice cover extent above 80% of total lagoon area compared to intermediate and long winters. The longest ISD over the study period was observed in 2005–2006 (138 days) and 2010–2011 (134 days), while the shortest in 2006–2007 (51 days) and 2007–2008 (47 days). It has to be noted that on 18 September 2007 the first registered minimum ice extent in the Arctic Ocean was observed (Comiso et al., 2008). The second minimum ice extent in the Arctic (Petty et al., 2018) likewise correlates with a shorter ice seasons in the CL in 2015–2016 (2016–2017) lasting 58 (63) days. It is believed that the decreasing Arctic sea ice cover could weaken the Atlantic Meridional Overturning Circulation leading to harsher winters and a stormier weather in Europe (Sévellec et al., 2017; Francis and Skific, 2015), however the impact on the colder European weather is still questionable (Screen, 2017).

Table 6. Classification of ice cover seasons based on their spatialmean ice season duration ($\overline{D}_{SAR}$).

Name	Condition	List of winters
Short	$\overline{D}_{SAR} < 50$ days	2006–2007, 2007–2008, 2014–2015, 2015–2016, 2016–2017
Intermediate	$50 \leq \overline{D}_{SAR} \leq 100$ days	2003–2004, 2004–2005, 2008–2009, 2011–2012, 2013–2014
Long	$\overline{D}_{SAR} > 100$ days	2002–2003, 2005–2006, 2009–2010, 2010–2011, 2012–2013

In turn, the regional climate fluctuations over the Curonian Lagoon are known to be related to the North Atlantic Oscillation (Dailidienė et al., 2012). The correlation between the NAO winter index (NAO_{DJFM}) and ISD derived from the coastal records (D_{st}) is negative and strong with R = -0.71 (p = 0.003, here and further in this section n = 15, Fig. 7a). Similar relationship is observed between NAO_{DJFM} and D_{corr} (R = -0.73, p = 0.002). Although, much better results are obtained when considering the correlation between NAO_{DJFM} and spatial-mean ISD, $\overline{D}_{SAR}$ (R = -0.83, p = 0.0001), indicating the richness of remote sensing data for better understanding the basis of ongoing ISD changes in the Curonian Lagoon. Further, the ISD shows a clear dependency on locally measured cumulative negative air temperature, T_a^{CN} (Fig. 7b), having a clear tendency to increase resulting in warmer and shorter winters in the CL. The correlation between T_a^{CN} and D_{st} along with D_{corr} is negative and strong R = -0.81 (p = 0.0002). However, the best results are achieved when comparing T_a^{CN} with spatially-rich $\overline{D}_{SAR}$ (R = -0.92, p = 0.000002).

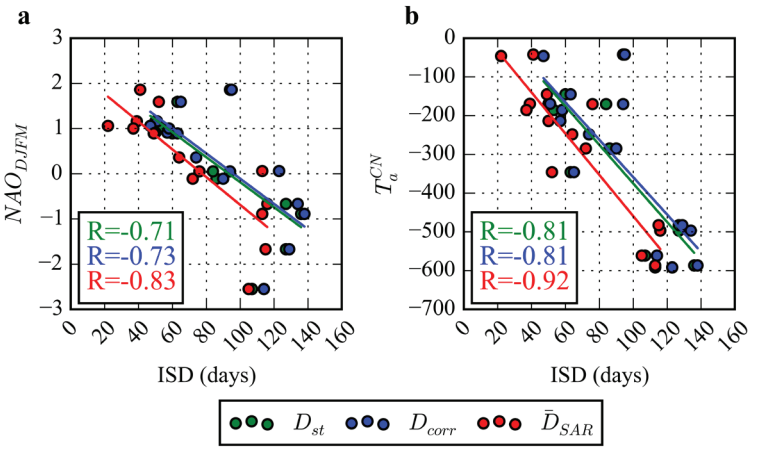

Figure 7. Scatterplots of the ice season duration (ISD) values derived from the coastal records (D_{st}), corrected values based on coastal and satellite data (D_{corr}), and spatially-averaged satellite data ($\overline{D}_{SAR}$) compared to the NAO winter index (a) and cumulative negative air temperature (b). Redrawn from Paper I.

3.2. Ice impact on water column characteristics

In this section ice cover effect on the aquatic environment is presented. The analysis of under-ice circulation, saltwater intrusions, water residence time, and suspended sediments is thoroughly presented in Paper II and III.

3.2.1. Circulation and fluxes

Water circulation in the Curonian Lagoon has different patterns throughout the meteorological seasons of the year. The highest current speed throughout the year is recorded in the northern part of the CL, where the outflow from the Nemunas River travels northward to the Klaipėda Strait. In the southern part, the current speed notably decreases during the ice cover season, due to this area being sheltered from wind induced movement for a longer period compared to the northern part.

Since the ice season duration (ISD) usually does not correspond to the winter season months, it is more accurate to analyze the residual currents averaged only over the ice cover seasons. Under the real ice cover a two-gyre systems in the southern part of the lagoon can be observed, which is similar to the results averaged over the winter season. However, they are less pronounced and there is a third anticlockwise gyre next to them, as well as only one gyre in the middle of the lagoon (Fig. 8a). Considering the no-ice model setup (Fig. 8b), there are four gyre systems in the lagoon – two anticlockwise along the eastern shoreline, one clockwise in the middle, and a small anticlockwise gyre in the southeastern part of the lagoon. The distribution of the gyres slightly differs from similar study done by Umgiesser et al. (2016), where they used spatially unrepresentative ice data interpolated from coastal stations and limited to 4 years of observations.

The difference of real ice and no-ice simulation results show that circulation under the ice cover becomes weaker by up to 0.03 m s^{-1} (Fig. 8c). When considering the idealized ice cover case (lagoon completely covered by ice during the whole ISD), the water flows slower along the western and slightly faster along the eastern shoreline in the northern part of the lagoon, compared to the flow during the real ice cover season (see Fig. 3 in Paper III).

Out of four sections for the computations of water fluxes (colored lines in Fig. 1), it is clearly seen that the ice cover has a higher impact on the water fluxes in the Nemunas delta area and through the Lithuanian-Russian border, where the difference of real ice and no-ice simulation results is nearly twice higher than in the Klaipėda Strait and north of Nemunas sections. The comparison of idealized ice and real ice cover seasons show that the prolonged full ice cover (idealized ice) also has greater impact in this area (see Fig. 4 in Paper III), because the water mass exiting the Nemunas Delta becomes more steady, not cycling between the delta and the lagoon as much compared to the ice-free simulation, thus less water is diverted to the south.

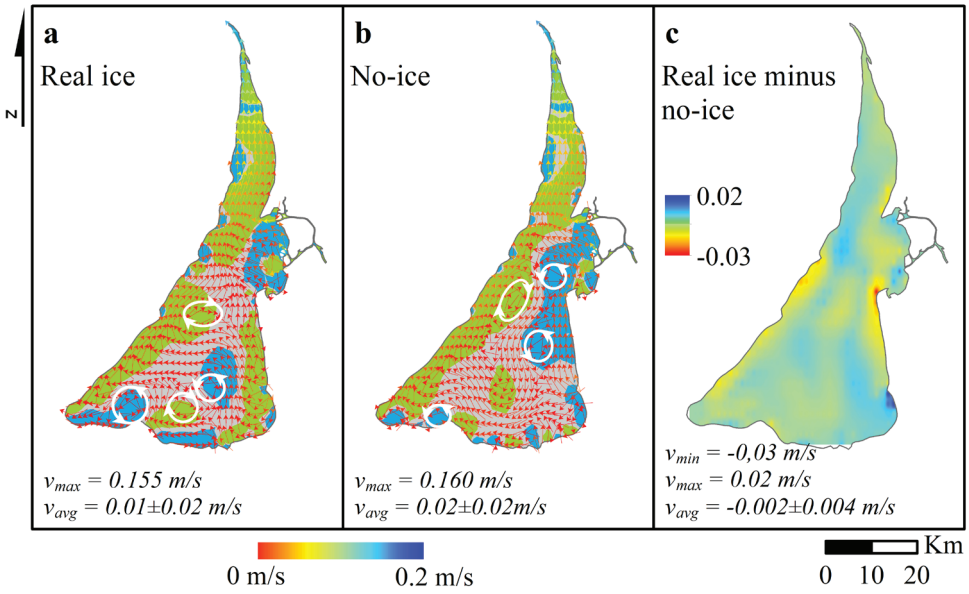

Figure 8. Water circulation (vectors are colored by the current speed in m s^{-1}) averaged over ice cover seasons in simulation with "real ice" (a) and "no-ice" model set-up (b), as well as the current speed difference in m/s between simulations: "real ice" minus "no-ice" (c). White circles with arrows in a and b show gyre systems and their direction, colors in these maps show positive (blue), negative (green) and neutral (gray) vorticity. The numbers indicate the minimum (v_{min}), maximum (v_{max}), and average (v_{avg}) velocity of the residual currents. Modified from Paper III.

3.2.2. Saltwater intrusions

The salinity concentration is highest in the northern part of the lagoon, which is prone to saltwater intrusions from the Baltic Sea during the northerly wind events. Simulation results show, that in Klaipėda Strait the salinity difference between bottom and top layers of the water column exceeds the 1 g kg^{-1} threshold on average for 130±47 hours $year^{-1}$ when considering real ice cover in model computations, while for "no-ice" computations it is on average for 114±35 hours $year^{-1}$ ($p = 0.04$). In Juodkrantė, which is approximatelly 15 km soutward from Kiaulės Nugara Island, salinity averaged over the water column exceeds the 2 g kg^{-1} threshold on average nearly 90±17 days $year^{-1}$ when the real ice cover is considered in the model computations, which is on average 13.9±7.3 days less than "no-ice" simulation results ($p = 0.0002$). When the lagoon is completely covered by ice during the whole ISD ("idealized ice"), it is on average 16.3±7.2 days less than no-ice computations ($p < 0.001$). This clearly shows the importance of full ice cover on decreasing the salinity concentration in the very northern part of the Curonian Lagoon.

The highest maximum salt concentration is observed during the autumn season while the lowest – in spring. Salinity during spring and summer is very similar (spatial-mean of 0.23±0.23 and 0.26±0.38 g kg^{-1}, respectively), likewise during autumn and winter season when ice cover is not taken into account in model computations (spatial-mean of 0.41±0.62 and 0.32±0.34 g kg^{-1}, respectively). However, model computations using real ice cover data show that spatial-mean salinity averaged over winter season is only 0.31±0.29 g kg^{-1}, with the main difference, compared to no-ice computations, occurring in the northern part of the lagoon, while salinity difference in the southern part is negligible.

Salinity during the real and idealized ice cover season does not show a very high difference (spatial-mean of 0.31±0.29 and 0.27±0.26 g kg^{-1}, respectively, p = 0). The spatially averaged salinity of the differences between simulations with real ice cover and without it (Fig. 9) show that under the real ice cover salinity can decrease by up to 1.02 g kg^{-1}. During the idealized ice cover season, salinity under the ice can decrease by up to 1.18 g kg^{-1}. This shows the importance of ice presence and the duration of its full cover for decreasing the intensity of saltwater intrusions from the Baltic Sea into the Curonian Lagoon.

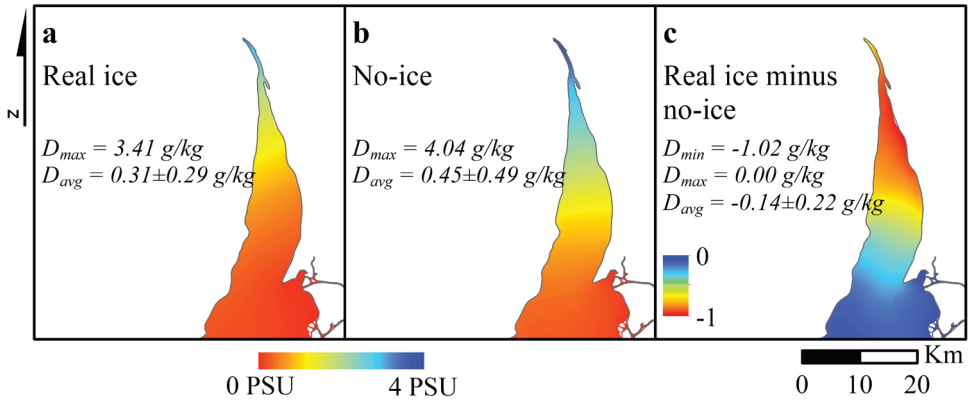

Figure 9. Salinity averaged over ice cover seasons in simulation with "real ice" (a) and "no-ice" model setup (b), as well as the difference between simulations: "real ice" minus "no-ice" (c). The numbers indicate the minimum (D_{min}), maximum (D_{max}), and average (D_{avg}) of salinity over the total lagoon area. Modified from Paper III.

3.2.3. Water residence time

In the northern part of the CL (northward of LT-RU boundary in Fig.1) average water residence time is around 55 days, and in the southern (southward of LT-RU boundary in Fig.1) – 150 days under the real ice cover (WRT_{ice}^{real}, Table 7), which

are ~1.5 days (p = 0.13) and ~ 24 days (p = 0.003) longer than it would be if the ice cover would not be present (WRT_{ice}^{no-ice}). Considering the WRT during the idealized ice cover season (WRT_{ice}^{ideal}), in the southern part it increases by ~63 days (p = 0.008), while in the northern part – it is lower by 3 days (p = 0.005), comparing with WRT_{ice}^{real} (WRT_{ice}^{no-ice}), due to the decreased exchanges between the northern and southern part of the CL. The WRT results averaged over the winter season with ice cover (WRT_{winter}^{real}) is very similar to the value of WRT_{ice}^{no-ice} in the northern part of the lagoon, due to the variability of the ice season duration (ISD) in this area, although it is not statistically significant (p = 0.44). The overall WRT in the CL (averaged over all meteorological seasons through all 11-year simulation period, WRT_{season}^{real}) is around 130 days under the ice cover, which is a ~1.5 days longer compared to the theoretical period without ice (WRT_{season}^{no-ice}, p = 0.07).

Table 7. Averaged water residence time (WRT) computed for the northern (WRT_{north}), southern (WRT_{south}) parts and for the total (WRT_{total}) lagoon area. Subscript indicates different WRT computation periods (ice – ice cover season, winter – Dec, Jan, Feb, and season – every meteorological season), superscript indicates the model setup type (real – satellite ice cover data, ideal – idealized ice cover data, no-ice – without ice). Redrawn from Paper III.

Simulation	WRT_{north} (days)	WRT_{south} (days)	WRT_{total} (days)
WRT_{ice}^{real}	55.48±13.72	150.54±41.10	113.79±28.68
WRT_{ice}^{ideal}	50.01±13.16	190.10±97.92	124.22±43.85
WRT_{ice}^{no-ice}	53.09±14.53	126.52±28.79	99.67±23.97
WRT_{ice}^{real} *correlation with ISD:*	*0.71*	*0.79*	*0.84*
WRT_{winter}^{real}	53.81±9.94	152.47±50.16	112.15±26.33
WRT_{winter}^{no-ice}	56.44±7.60	135.62±33.91	106.43±22.20
WRT_{winter}^{real} *correlation with ISD:*	*0.09*	*0.79*	*0.75*
WRT_{season}^{real}	66.66±18.93	170.53±52.67	129.96±36.09
WRT_{season}^{no-ice}	67.24±18.39	166.60±52.07	128.58±36.49

The correlation coefficient between ISD and different WRT computation periods ranges from 0.71 to 0.84 (n = 12, p ranging from 0.001 to 0.01), indicating the significance of the ice cover impact on the WRT. Although, only WRT_{winter}^{real} does not

show any relation to the ISD in the northern part of the lagoon, as mentioned before due to ice cover being more dynamic in this area during the winter season. The WRT increase is particularly apparent after the long and severe winters in the southern part of the lagoon, where the ice stays the longest.

WRT slightly varies during the ice-free meteorological seasons, although the overall pattern is the same – high WRT values in the southern part of the lagoon, especially in the southwestern section of it where the data of the inflowing smaller rivers is not available for using in the modelling studies. The highest WRT of the ice-free period is observed in summer, due to the decreased wind speed and water inflow from the rivers, and lowest during spring. The longest WRT is observed during the ice cover season – the average WRT is nearly twice as long as it would be if the ice would not be present (Fig. 10). The average WRT distribution derived from "no-ice" simulation is similar to the one of spring season (p = 0). The difference between simulations with and without ice also shows higher values in the southeastern corner of the lagoon and in Nemunas Delta (areas next to the main river outlets), compared to the results using the real ice cover data, meaning that under the ice water is renewing faster. The comparison of the results from "real ice" and "idealized ice" model setups shows that the prolonged full ice cover has a much higher impact on the WRT in the southwestern part of the CL.

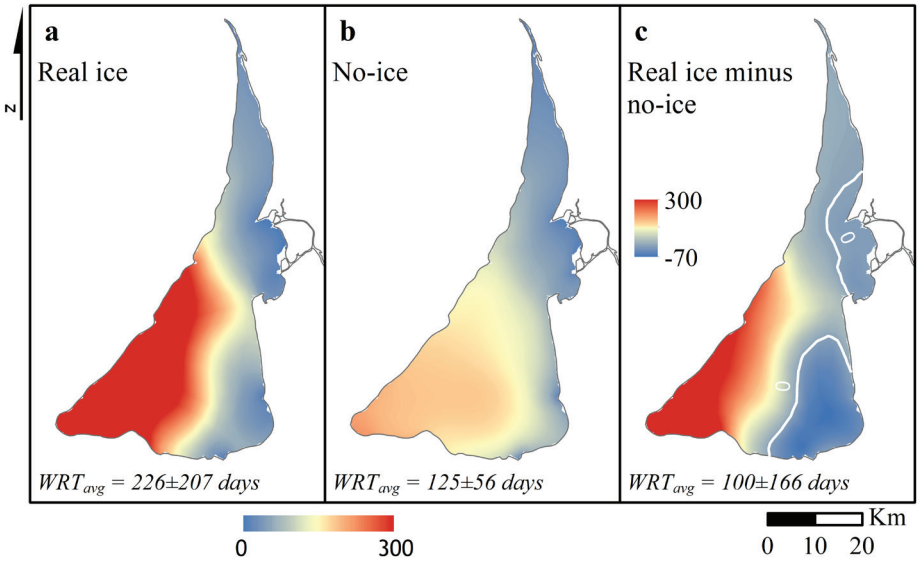

Figure 10. Water residence time (WRT, in days) averaged over ice cover seasons in the simulation with "real ice" (a), and "no-ice" model set-up (b), as well as the difference between the simulations: "real ice" minus "no-ice" (c). The numbers indicate the spatial average (WRT_{avg}) of WRT. Contour lines indicate the zero-value threshold (no difference). Modified from Paper III.

3.2.4. Suspended sediments

Ice cover takes a very important part regulating the sediment dynamics in the Curonian Lagoon. The comparison of two simulations – with ice cover and without it – shows that average suspended sediment concentration (SSC) differs from 1.5±1.8 mg L^{-1} to 2.8±2.7 mg L^{-1} ($p = 0.002$), respectively, with a significant increase observed during the strong wind events, when the absent ice cover caused the increased bed shear stress boosting the SSC in the water column. The SSC time series showed that the influence of ice cover in the deeper and muddier northern point of the lagoon (S1 in Fig. 1) is observed only with the very high eastern, south-eastern, or southern winds (>10 m s^{-1}). The shallower and sandier point (S2 in Fig. 1) time series showed that ice cover starts to impact the SSC already with winds of >6 m s^{-1}, blowing from south-west to north-west. This shows the importance of ice for water exchange capabilities causing the increase of SSC in the water column. However, this can change due to the forecasted extreme alteration of the ice cover phenology (Jakimavičius et al., 2019; Haapala et al., 2015), together with the projected increase of winter sediment load from the Nemunas River (Čerkasova, 2019). For more detailed description of the results see section 5.4.1 in Paper II.

3.3. Ice thickness

This section combines the results and analysis from Paper IV regarding the ice thermodynamic model calibration, validation, and its application for the climate change impact analysis, as well as some new unpublished material of ice model applications – coupling with the numerical modelling framework SHYFEM in section 3.3.2. A thorough explanation of subsections 3.3.1 and 3.3.3 is given in the Paper IV.

3.3.1. Ice thermodynamic model calibration and validation

Out of several simulation runs, ice model setup with increased snow density values ($Pres_{\rho_s}$) gave better ice thickness results having higher correlation coefficient value (Table 8). However, the fitness of model results highly depends on the accuracy of forcing data, e.g., ERA5 reanalysis datasets gave better results than using meteorological data described in Table 1. The snow thickness correlation with the observations was strong in Nida and Juodkrantė, while in Ventė it was moderate. A study by (Cheng et al., 2008) demonstrated that an increased model vertical resolution can lead to improved results, however, the authors also found that the accuracy of forcing data was much more important than the vertical resolution. This was also true for the study presented in this dissertation – the applied ice thermodynamic model's ability to accurately simulate snow thickness increased with higher resolution of meteorological

forcing data. The model application with local weather observations produced much better results. More detailed explanation of the results can be found in Paper IV.

Table 8. Ice and snow thickness calibration statistics, based on the model set-up types: $Pres_{Orig}$ – original setup from Tedesco et al. (2010), and $Pres_{\rho_s}$ – increased densities of all snow types by 50 kg m^{-3}. RMSE is in meters. Redrawn from Paper IV. Correlation coefficient significance of all stations is p = 0. Sample size is n.

		Nida (n = 383)		Juodkrantė (n = 436)		Ventė (n = 388)	
		$Pres_{Orig}$	$Pres_{\rho_s}$	$Pres_{Orig}$	$Pres_{\rho_s}$	$Pres_{Orig}$	$Pres_{\rho_s}$
Ice	R	0.89	0.92	0.95	0.96	0.87	0.89
	RMSE	0.08	0.07	0.06	0.04	0.06	0.06
Snow	R	0.69	0.73	0.62	0.63	0.56	0.56
	RMSE	0.05	0.05	0.07	0.07	0.04	0.04

Overall, the model describes the ice thickness evolution rather well (Fig. 11), although ice season duration was highly overestimated (on average by 1 month). This was due to the short sporadic freezing events in the beginning of the ice season an occasionally after continuous ice season in the modelling results, which were not recorded in observation data. After elimination of these freezing events, the ISD values become much more similar to observation data (three station mean R=0.98, compared to R=0.78, of uncorrected ice seasons, n = 33, p = 0).

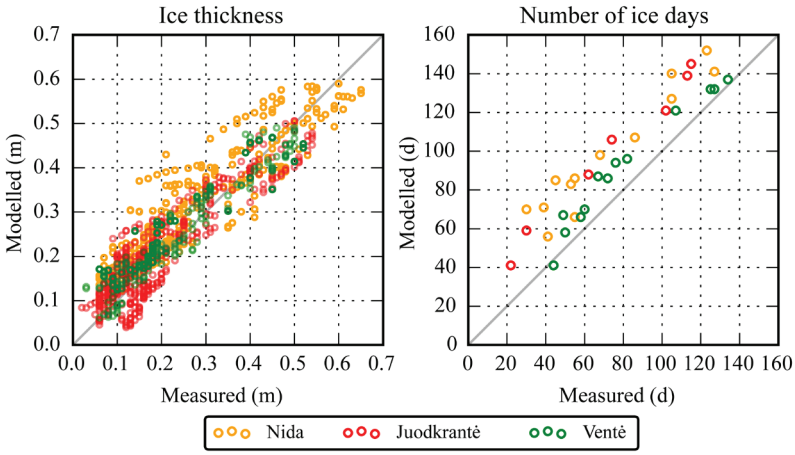

Figure 11. Scatterplots of measured and modelled ice thickness and ice season duration in Nida, Juodkrantė, and Ventė for the period of 2004–2017. Redrawn from Paper IV.

3.3.2. Ice thickness distribution

As described in the previous section, ice thickness evolution is simulated very well, although the lack of the dynamical component in the ice modelling becomes apparent when looking at the results of the coupled ice and hydrodynamic model simulations. During the beginning and ending of the ice season, when the ice is very thin and easily transferrable by the wind, the ice model is not capable to reproduce the real conditions as seen in remote sensing images (Fig. 12). The ice thermodynamic model results depict the setting of a fictional situation – without wind stress on the surface, allowing for the ice to continuously grow and thicken. In this way, it takes more time to melt during the occasional temperature increases during the ice cover period. In 2005–2006 a melt-off in the beginning of the ice season was observed. Although it was too thick to completely disappear from the modelling results, the overall thickness highly decreased.

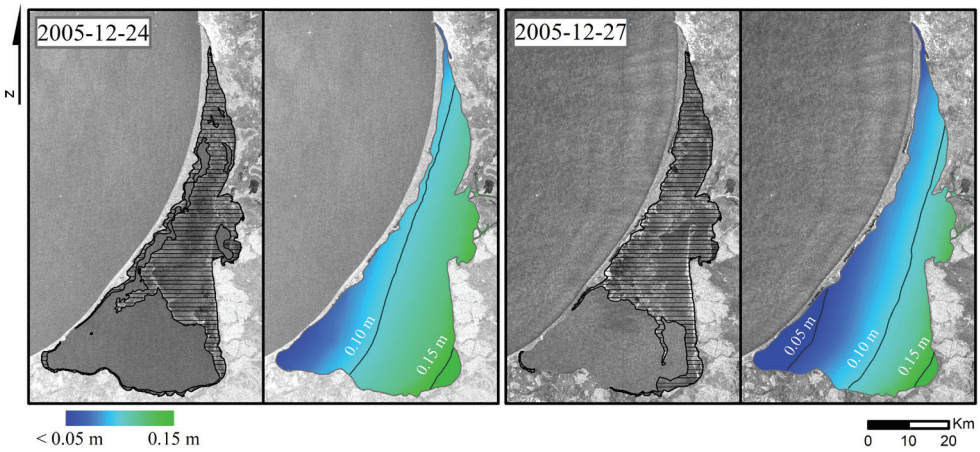

Figure 12. Ice thickness distribution during the freezing period on 24 and 27 December, 2005. Satellite data and modeling results. Ice cover from Envisat Advanced SAR images is displayed in horizontal hatch pattern. Unpublished results.

It is clear, that during unstable air temperature (fluctuating around the freezing temperature) during the freezing period, predictions of the ice thickness are unreliable using only the ice thermodynamic model. However, in the northern part, where the water is more saline due to the saltwater intrusions, it affects the distribution of thin ice (up to 5 cm), due to altered freezing temperature.

When air temperature is continuously low, i.e., during the winter of 2013–2014 (Fig. 13), allowing fast and full freezing of the lagoon, the thicker ice forms along

the eastern and southern parts of the lagoon. Ice in the western shoreline is thinner (as seen in profile graphs in Fig. 13), presumably due to the slightly warmer air temperature, wind blowing from the Baltic Sea. The difference between the most eastern and western values is ~4 cm. The north-south profile line indicates a thinner ice in the middle of the lagoon, with thicker ice forming in the southern part of the CL.

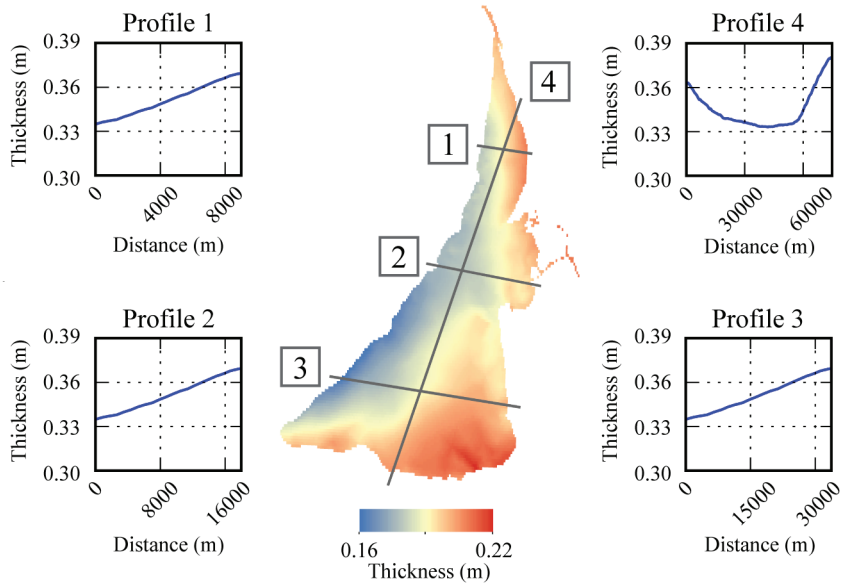

Figure 13. Four ice thickness profile lines (shown in graphs) and average ice thickness (coloured map) during 2013–2014. Profile lines are plotted for the 2014-02-07 snapshot, when the total ice thickness maximum of this ice season was reached; W-E profile lines (distance) go from west to east, N-S profiles – from north to south. Unpublished results.

In the future, ice cover characteristics are likely to change, as it is described in the next section of this dissertation – leading to shorter ice seasons with much thinner ice. Thus, it might become difficult to simulate ice thickness distribution based solely on the thermodynamic model setup, without inclusion of the dynamic processes in the sea ice modelling.

3.3.3. Ice thickness future projections

The five model mean/max ice thickness of 9±3/20 cm during the historical period will likely decrease to 6±3/15 cm and 6±2/16 cm in the near future (~30/25% and ~30/20% less compared with the historical period) under RCP4.5 and RCP8.5

scenarios, respectively. In the far future the average ice thickness is likely to be 4±1/9 cm and 1±1/4 cm (~60/55% and 85/80% less compared with the historical period) under RCP4.5 and RCP8.5 scenarios, respectively (Fig. 14). The percentage of change for $RCP4.5_{far}$ is similar to that from the study of applying statistical methods (Jakimavičius et al., 2019), although the authors projected that under $RCP8.5_{far}$ ice would form once every five years reaching 4–11 cm thickness.

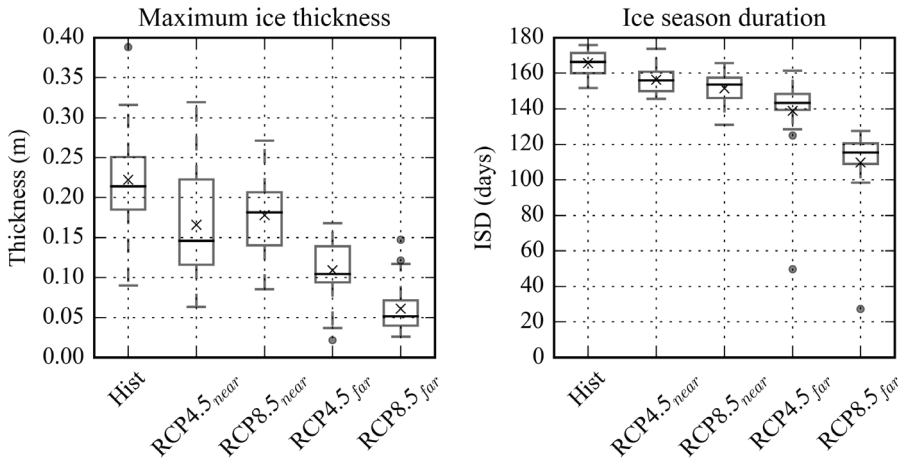

Figure 14. Five model (ICHEC, CNRM, IPSL, MOHC, and MPI) mean maximum ice thickness (left) and ice season duration (right), during the historical (Hist, 1986–2100), near (2021–2040) and far (2081–2100) future periods under RCP4.5 and RCP8.5 scenarios. Circles denote the outliers, black line indicates the median, and symbol "x" is the mean. Adapted from Paper IV.

The number of ice days (Fig. 14) is likely to decrease by ~15% in the near future under both RCP scenarios, compared with the historical period, while in the far future this change is much higher – 30% under RCP4.5 and 57% under RCP8.5. That is on average 110±9 days in the near future and 92±11 days in $RCP4.5_{far}$ and 56±13 days in $RCP8.5_{far}$, compared with 130±11 days during the historical period. However, these values have to be taken cautiously, because the ice model overestimates the ISD, thus it is more likely that these numbers are lower. These numbers differ from those in Jakimavičius et al. (2019) study, although they also used data from the Klaipėda Strait, where the ice is usually very thin, not land locked, and lasts for a shorter period, due to the more saline water and intensive shipping.

The trend analysis showed that the maximum ice thickness will decrease at a rate of 0.11–0.18 cm year^{-1} under RCP4.5 and 0.11–0.30 cm year^{-1} under RCP8.5 scenarios, while the statistical data of trends in the Baltic sea, the area outside the Bay of

Bothnia, project that the mean annual maximum ice thickness will decrease at a rate of 0.1–0.34 and 0.08–0.76 cm $year^{-1}$ under RCP4.5 and RCP8.5, respectively, with higher values northward (Luomaranta et al., 2014). In this study the ISD is projected to decrease at a rate of ~0.41 days $year^{-1}$ under RCP4.5, and ~0.83 days $year^{-1}$ under RCP8.5 scenario.

4

Conclusions

1. Multi-mission remote sensing data of spatially detailed ice cover conditions in the Curonian Lagoon revealed a good performance in defining the key ice phenology elements regarding the whole lagoon surface (mean success rate of the satellite observations is 63%) and could be advocated for its exploitation in regional ice monitoring programs.

2. The initial ice formation in the Curonian Lagoon starts along the eastern and southern shoreline with slightly earlier freezing observed in the Nemunas Delta area. Ice formation is latest in the deepest southwestern part of the lagoon. Occasional melting events can occur during the full freezing period before the final melt onset, due to the air temperature increase above the freezing threshold. Ice cover starts to decompose in the northern part of the lagoon continuing along the western coastline and slowly retreating towards the eastern shoreline due to the prevailing westerly winds.

3. High-resolution ice season duration (ISD) maps reveal a high inter-annual variability, however on average ice resides the longest in the limnic southern, south-eastern part of the Curonian Lagoon, especially along the eastern coast (including Nemunas Delta). The shortest ice season is observed in the northern part of the lagoon, due to the turbid nature of this area and saltwater intrusions. The ice season duration over the 2002–2017 period is 86 days, based on the ground observations. Combining the benefits of satellite and *in situ* data, a corrected ice season duration record was presented,

increasing the average ISD up to 89 days. Although, the best parameter to describe the ice season variability in the whole lagoon domain is the spatial-mean ISD, being much lower – 71 days on average. The ice season duration is shortening at a rate of 1.6–2.3 days year^{-1} during this period. While the dates of the freeze onset and full freezing have not changed much, the timing of final melt onset and last observation of ice display a clear decreasing trend, leading toward an earlier ice break-up and melt-off.

4. The ice season duration is closely linked to the predominant air temperature, which is increasing and leading to warmer and shorter winters in the Curonian Lagoon. The cumulative negative air temperature has a very close relationship to the spatial-mean ISD (R=-0.92), revealing the benefit of satellite data, compared to spatially constrained *in situ* observations (R=-0.81). Since the regional air temperature fluctuations are closely linked to the North Atlantic Oscillation (NAO), the variability of spatial-mean ISD is much closer related to the NAO winter index records (R=0.83) than that of coastal records (R=0.71) or corrected ISD (R=0.73).

5. Numerical modelling studies revealed that ice cover changes the formation and location of gyre systems in the Curonian Lagoon. Water exchange capabilities also decrease due to the diminished circulation under the ice, especially in the cross section in the middle of the lagoon where the suppressed wind forcing has a bigger impact on the water movement. Ice cover decreases the salinity in the northern part of the lagoon, as well as the time and distance of saltwater intrusions by nearly 14 days year^{-1}. Water residence time increases prominently after long ice cover periods, especially further away from the river outlets and in southern part of the lagoon, where wind also plays a major role for water renewal. Ice cover significantly decreases the average suspended sediment concentration (SSC). This is especially prominent during the strong wind events, due to the increased bed shear stress. If the ice would not be present in the CL, the waves induced by strong winds and increased water exchange capabilities would lead to a higher SSC in the water column.

6. The proposed ice thermodynamic model gives satisfactory results for simulating ice thickness evolution in the Curonian Lagoon (three station mean R=0.92, RMSE=6 cm). Although the model's capability to produce good results highly depends on the accuracy of the forcing data, it is suitable for further applications. However, the overall number of ice days is overestimated by on average 1 month, due to the sporadic short freezing event produced by the model, which were not recorded in coastal stations. Thus, this parameter has to be taken into account cautiously. Additionally, the coupled ice and hydrodynamic modelling system is not fully able to represent the real ice cover distribution as seen in the remote sensing images. During thin ice formation or decay events, the wind forcing plays a significant role in distributing the ice. Using only ice thermodynamics in the modelling framework will not be enough to simulate ice thickness distribution, especially under changing climate and projected ice thinning.

7. The future projection of the ice thickness in the scope of climate change estimate that compared to the historical period, the maximum ice thickness could decrease by 20–25% in the near future, while in the far future it could decrease by up to 55% under RCP4.5 and 80% under RCP8.5 scenario. The mean number of ice days could decrease by 15% in the near future, while by the end of the century it could decrease by 30% under RCP4.5 or 57% under RCP8.5 scenario. The projected decreasing trend of ice thickness and phenology records will not only affect the underwater environment, but also fisheries, and recreational activities in the Curonian Lagoon.

Acknowledgements

The biggest thank you goes to my supervisor and friend Georg Umgiesser. I will be eternally grateful for the opportunity to learn from you, for all the lessons and support in difficult times, for pushing me further. I was very lucky to work with you, Georg. This dissertation is for you, thank you. All seriousness aside, your cooking lessons did not go to waste, they are laid out in my secret recipe book: *carbonara*, *spaghetti alle vongole, alla puttanesca, orata*, and many more… It will be passed through generations as "Georg's special". Thank you for all the 6 months in Italy (or more, I lost the count, it is like home now), for the wonderful (nearly fulfilled) list of the must-see places and must-taste dishes, for pushing me to explore and experience all the adventures, I would not have done all of this without your encouragement.

Another person I would like to thank is my advisor Igor Kozlov. Thank you for the introduction to the research work. This completely "green" young (forever) scientist is now able to write articles. My wonderful debut in this field would not be so wonderful without your guidance. It was a challenging start, needing a lot of patience and dedication. I really learned that, and now life and work is much easier, thank you! It was worth reaching article version 9756834657.

Next on the plate is the modelling group. Firstly, thank you Vitalijus Denisovas who introduced me to this company and indirectly helped find my passion, career. I am one of the many people that will be forever grateful to you for my start in life. Thank you to

Petras Zemlys for the emotional and scientific support, patience and writing, programming lessons. Thank you to Natalja Čerkasova for the support and lessons on how to do nice presentations and how not to present unnecessary information, but I am full of unnecessary information so I am still learning the last one… Thank you to Ali Ertürk for your time, 5 am in the hotel lobby after an entertaining evening, programming lessons, beer lessons, for everything… You are the only person that I have seen turning water into wine in real life, that says a lot. And an enormous thank you goes to Jovita Mėžinė – in a way you made this dissertation possible, at the end of this journey my life would have been much more stressful without your brilliance.

Thank you to the houseparty squad – Georg, Ali, Natalja, Ričardas, and Oleg. You were the spritz in my quarantine, working in the isolation would be unbearable without evenings together on skype. Thank you again to Ričardas Paškauskas, our collaboration was cut short, but hopefully it will not be forgotten and we can pick up where we left off. Thank you to my former colleagues in the port authority (especially Ligita), I grew up and started blooming with you, one of the happiest days of my life were spent with you, you were the sunshine during the most cloudy days, I will always remember the flying bag of candy behind my window. Thank you to my family who made it possible for me to concentrate on my degrees. Thank you to my friends for staying with me during these busy years, I promise I will be more available now, we can start travelling and partying! Thank you to everyone who read this big piece of work, especially to Darius Daunys and Kai Myrberg for the review and suggestions that made it better.

I am not a person of many words, it is difficult to express my gratitude, but these thank yous come from the best, most sincere part of my heart. Thank you once again. The PhD project is over, let us party!

Cheers,
Rasa

References

Adrian, R., Walz, N., Hintze, T., Hoeg, S., Rusche, R., 1999. Effects of ice duration on plankton succession during spring in a shallow polymictic lake. Freshw. Biol. 41, 621–634. https://doi.org/10.1046/j.1365-2427.1999.00411.x

Allard, R.A., Farrell, S.L., Hebert, D.A., Johnston, W.F., Li, L., Kurtz, N.T., Phelps, M.W., Posey, P.G., Tilling, R., Ridout, A., Wallcraft, A.J., 2018. Utilizing CryoSat-2 sea ice thickness to initialize a coupled ice-ocean modeling system. Adv. Sp. Res. 62, 1265–1280. https://doi.org/10.1016/j.asr.2017.12.030

Alvarez-Fernandez, S., Lindeboom, H., Meesters, E., 2012. Temporal changes in plankton of the North Sea: community shifts and environmental drivers. Mar. Ecol. Prog. Ser. 462, 21–38. https://doi.org/10.3354/meps09817

Aulicino, G., Wadhams, P., Parmiggiani, F., 2019. SAR Pancake Ice Thickness Retrieval in the Terra Nova Bay (Antarctica) during the PIPERS Expedition in Winter 2017. Remote Sens. 11, 2510. https://doi.org/10.3390/rs11212510

Baukšys, J., 1978. Ice regime, in: Rainys, A. (Ed.), The Curonian Lagoon. Vilnius, pp. 34–49.

Beall, B.F.N., Twiss, M.R., Smith, D.E., Oyserman, B.O., Rozmarynowycz, M.J., Binding, C.E., Bourbonniere, R.A., Bullerjahn, G.S., Palmer, M.E., Reavie, E.D., Waters, L.M.K., Woityra, L.W.C., McKay, R.M.L., 2016. Ice cover extent drives phytoplankton and bacterial community structure in a large north-temperate lake:

implications for a warming climate. Environ. Microbiol. 18, 1704–1719. https://doi.org/10.1111/1462-2920.12819

Beaver, J.R., Arp, C.D., Tausz, C.E., Jones, B.M., Whitman, M.S., Renicker, T.R., Samples, E.E., Ordosch, D.M., Scotese, K.C., 2019. Potential shifts in zooplankton community structure in response to changing ice regimes and hydrologic connectivity. Arctic, Antarct. Alp. Res. 51, 327–345. https://doi.org/10.1080/15230430.2019.1643210

Bengtsson, L., 2012. Ice Covered Lakes, in: Bengtsson, L., Herschy, R.W., Fairbridge, R.W. (Eds.), Encyclopedia of Lakes and Reservoirs. Springer Netherlands, Dordrecht, pp. 357–360. https://doi.org/10.1007/978-1-4020-4410-6_10

Block, B.D., Denfeld, B.A., Stockwell, J.D., Flaim, G., Grossart, H.P.F., Knoll, L.B., Maier, D.B., North, R.L., Rautio, M., Rusak, J.A., Sadro, S., Weyhenmeyer, G.A., Bramburger, A.J., Branstrator, D.K., Salonen, K., Hampton, S.E., 2019. The unique methodological challenges of winter limnology. Limnol. Oceanogr. Methods 17, 42–57. https://doi.org/10.1002/lom3.10295

Blockley, E., Vancoppenolle, M., Hunke, E., Bitz, C., Feltham, D., Lemieux, J.-F., Losch, M., Maisonnave, E., Notz, D., Rampal, P., Tietsche, S., Tremblay, B., Turner, A., Massonnet, F., Ólason, E., Roberts, A., Aksenov, Y., Fichefet, T., Garric, G., Iovino, D., Madec, G., Rousset, C., Salas y Melia, D., Schroeder, D., 2020. The Future of Sea Ice Modeling: Where Do We Go from Here? Bull. Am. Meteorol. Soc. 101, E1304–E1311. https://doi.org/10.1175/BAMS-D-20-0073.1

Cahill, K.L., Gunn, J.M., Futter, M.N., 2005. Modelling ice cover, timing of spring stratification, and end-of-season mixing depth in small Precambrian Shield lakes. Can. J. Fish. Aquat. Sci. 62, 2134–2142. https://doi.org/10.1139/f05-127

Cavaleri, L., Bajo, M., Barbariol, F., Bastianini, M., Benetazzo, A., Bertotti, L., Chiggiato, J., Davolio, S., Ferrarin, C., Magnusson, L., Papa, A., Pezzutto, P., Pomaro, A., Umgiesser, G., 2019. The October 29, 2018 storm in Northern Italy – An exceptional event and its modeling. Prog. Oceanogr. 178, 102178. https://doi.org/10.1016/j.pocean.2019.102178

Čerkasova, N., 2019. Nemunas River Watershed Input to the Curonian Lagoon: Discharge, Microbiological Pollution, Nutrient and Sediment Loads under Changing Climate. Ph.D. Thesis, Klaipėda University, Klaipėda, Lithuania.

Cheng, B., Zhang, Z., Vihma, T., Johansson, M., Bian, L., Li, Z., Wu, H., 2008. Model experiments on snow and ice thermodynamics in the Arctic Ocean with CHINARE 2003 data. J. Geophys. Res. 113, C09020. https://doi.org/10.1029/2007JC004654

Chubarenko, B., Chechko, V., Kileso, A., Krek, E., Topchaya, V., 2019. Hydrological and sedimentation conditions in a non-tidal lagoon during ice coverage – The example of Vistula Lagoon in the Baltic Sea. Estuar. Coast. Shelf Sci. 216, 38–53. https://doi.org/10.1016/j.ecss.2017.12.018

Comiso, J.C., Parkinson, C.L., Gersten, R., Stock, L., 2008. Accelerated decline in the Arctic sea ice cover. Geophys. Res. Lett. 35, L01703. https://doi.org/10.1029/2007GL031972

Cooper, M.G., Smith, L.C., Rennermalm, A.K., Tedesco, M., Muthyala, R., Leidman, S.Z., Moustafa, S.E., Fayne, J. V., 2020. First spectral measurements of light attenuation in Greenland Ice Sheet bare ice suggest shallower subsurface radiative heating and ICESat-2 penetration depth in the ablation zone. Cryosph. Discuss. https://doi.org/10.5194/tc-2020-53

Crépin, A.-S., Gren, Å., Engström, G., Ospina, D., 2017. Operationalising a social–ecological system perspective on the Arctic Ocean. Ambio 46, 475–485. https://doi.org/10.1007/s13280-017-0960-4

Cui, Y., Chen, X., Gao, J., Yan, B., Tang, G., Hong, Y., 2018. Global water cycle and remote sensing big data: overview, challenge, and opportunities. Big Earth Data 2, 282–297. https://doi.org/10.1080/20964471.2018.1548052

Dailidienė, I., 2007. Hidroklimatinių sąlygų kaitos ypatumai Baltijos jūros Lietuvos priekrantėje ir Kuršių mariose. Klaipėda University.

Dailidienė, I., Davulienė, L., 2008. Salinity trend and variation in the Baltic Sea near the Lithuanian coast and in the Curonian Lagoon in 1984-2005. J. Mar. Syst. 74, 20–29. https://doi.org/10.1016/j.jmarsys.2008.01.014

Dailidienė, I., Davulienė, L., Kelpšaitė, L., Razinkovas, A., 2012. Analysis of the Climate Change in Lithuanian Coastal Areas of the Baltic Sea. J. Coast. Res. 28, 557–569. https://doi.org/10.2112/JCOASTRES-D-10-00077.1

Danilov, S., Wang, Q., Timmermann, R., Iakovlev, N., Sidorenko, D., Kimmritz, M., Jung, T., Schröter, J., 2015. Finite-Element Sea Ice Model (FESIM), version 2. Geosci. Model Dev. 8, 1747–1761. https://doi.org/10.5194/gmd-8-1747-2015

Das, A., Reed, M., Lindenschmidt, K.-E., 2018. Sustainable Ice-Jam Flood Management for Socio-Economic and Socio-Ecological Systems. Water 10, 135. https://doi.org/10.3390/w10020135

Das, A., Rokaya, P., Lindenschmidt, K.-E., 2020. Ice-Jam Flood Risk Assessment and Hazard Mapping under Future Climate. J. Water Resour. Plan. Manag. 146, 04020029. https://doi.org/10.1061/(ASCE)WR.1943-5452.0001178

Dierking, W., 2013. Sea Ice Monitoring by Synthetic Aperture Radar. Oceanography 26, 101–111. https://doi.org/10.5670/oceanog.2013.33

Dong, K., Kvile, Ø., Stenseth, N., Stige, L., 2020. Associations among temperature, sea ice and phytoplankton bloom dynamics in the Barents Sea. Mar. Ecol. Prog. Ser. 635, 25–36. https://doi.org/10.3354/meps13218

Du, J., Watts, J.D., Jiang, L., Lu, H., Cheng, X., Duguay, C., Farina, M., Qiu, Y., Kim, Y., Kimball, J.S., Tarolli, P., 2019. Remote Sensing of Environmental Changes in Cold Regions: Methods, Achievements and Challenges. Remote Sens. 11, 1952. https://doi.org/10.3390/rs11161952

EEA, 2017. Climate change, impacts and vulnerability in Europe 2016. An indicator-based report. Luxembourg: Publications Office of the European Union. https://doi.org/10.2800/534806

Emery, W., Camps, A., 2017. Introduction to Satellite Remote Sensing. Elsevier. https://doi.org/10.1016/C2015-0-04517-8

Engram, M., Arp, C.D., Jones, B.M., Ajadi, O.A., Meyer, F.J., 2018. Analyzing floating and bedfast lake ice regimes across Arctic Alaska using 25 years of space-borne SAR imagery. Remote Sens. Environ. 209, 660–676. https://doi.org/10.1016/j.rse.2018.02.022

Fang, X., Stefan, H.G., 2012. Impacts of Climatic Changes on Water Quality and Fish Habitat in Aquatic Systems, in: Handbook of Climate Change Mitigation. Springer US, New York, NY, pp. 531–569. https://doi.org/10.1007/978-1-4419-7991-9_16

Ferrarin, C., Cucco, A., Umgiesser, G., Bellafiore, D., Amos, C.L., 2010. Modelling fluxes of water and sediment between Venice Lagoon and the sea. Cont. Shelf Res. 30, 904–914. https://doi.org/10.1016/j.csr.2009.08.014

Ferrarin, C., Razinkovas, A., Gulbinskas, S., Umgiesser, G., Bliudžiute, L., 2008a. Hydraulic regime-based zonation scheme of the Curonian Lagoon. Hydrobiologia 611, 133–146. https://doi.org/10.1007/s10750-008-9454-5

Ferrarin, C., Umgiesser, G., Cucco, A., Hsu, T.-W., Roland, A., Amos, C.L., 2008b. Development and validation of a finite element morphological model for shallow water basins. Coast. Eng. 55, 716–731. https://doi.org/10.1016/j.coastaleng.2008.02.016

Ferrarin, C., Umgiesser, G., Roland, A., Bajo, M., De Pascalis, F., Ghezzo, M., Scroccaro, I., 2016. Sediment dynamics and budget in a microtidal lagoon — A numerical investigation. Mar. Geol. 381, 163–174. https://doi.org/10.1016/j.margeo.2016.09.006

Francis, J., Skific, N., 2015. Evidence linking rapid Arctic warming to mid-latitude weather patterns. Philos. Trans. R. Soc. A Math. Phys. Eng. Sci. 373, 20140170. https://doi.org/10.1098/rsta.2014.0170

Ganju, N.K., Brush, M.J., Rashleigh, B., Aretxabaleta, A.L., del Barrio, P., Grear, J.S., Harris, L.A., Lake, S.J., McCardell, G., O'Donnell, J., Ralston, D.K., Signell, R.P., Testa, J.M., Vaudrey, J.M.P., 2016. Progress and Challenges in Coupled Hydrodynamic-Ecological Estuarine Modeling. Estuaries and Coasts 39, 311–332. https://doi.org/10.1007/s12237-015-0011-y

Gao, G., Chen, C., Qi, J., Beardsley, R.C., 2011. An unstructured-grid, finite-volume sea ice model: Development, validation, and application. J. Geophys. Res. 116, C00D04. https://doi.org/10.1029/2010JC006688

Gasiūnaitė, Z.R., Daunys, D., Olenin, S., Razinkovas, A., 2008. The Curonian Lagoon, in: Schiewer, U. (Ed.), Ecology of Baltic Coastal Waters. Springer, Berlin/Heidelberg, Germany, pp. 197–215. https://doi.org/10.1007/978-3-540-73524-3_9

Gelumbauskaitė, L.Y., Grigelis, A., Cato, I., Repečka, M., Kjellin, B., 1999. Bottom Topography and Sediment Maps of the Central Baltic Sea: Scale 1: 500,000. A Short Description. [WWW Document]. LGT Ser. Mar. Geol. Maps No. 1/SGU Ser. Geol. Maps Ba No. 54. URL https://www.dmu.dk/1_Viden/2_Miljoe-tilstand/3_vand/4_Charm/charm_res/data/WP1/Deliverable9/charm_all maps.htm (accessed 9.20.18).

Golosov, S., Kirillin, G., 2010. A parameterized model of heat storage by lake sediments. Environ. Model. Softw. 25, 793–801. https://doi.org/10.1016/j.envsoft.2010.01.002

Granados, I., Toro, M., Giralt, S., Camacho, A., Montes, C., 2020. Water column changes under ice during different winters in a mid-latitude Mediterranean high mountain lake. Aquat. Sci. 82, 30. https://doi.org/10.1007/s00027-020-0699-z

Grosbois, G., Mariash, H., Schneider, T., Rautio, M., 2017. Under-ice availability of phytoplankton lipids is key to freshwater zooplankton winter survival. Sci. Rep. 7, 11543. https://doi.org/10.1038/s41598-017-10956-0

Gulbinskas, S., Žaromskis, R., 2002. The Curonian Lagoon Map for Fishery M 1:50 000. Lithuanian Deparment of Fisheries, Vilnius, Lithuania.

Haapala, J.J., Ronkainen, I., Schmelzer, N., Sztobryn, M., 2015. Recent Change—Sea Ice, in: The BACC II Author Team (Ed.), Second Assessment of Climate Change for the Baltic Sea Basin, Regional Climate Studies. Springer International Publishing, Cham, pp. 145–153. https://doi.org/10.1007/978-3-319-16006-1_8

Hampton, S.E., Galloway, A.W.E., Powers, S.M., Ozersky, T., Woo, K.H., Batt, R.D., Labou, S.G., O'Reilly, C.M., Sharma, S., Lottig, N.R., Stanley, E.H., North, R.L., Stockwell, J.D., Adrian, R., Weyhenmeyer, G.A., Arvola, L., Baulch, H.M., Bertani, I., Bowman, L.L., Carey, C.C., Catalan, J., Colom-Montero, W., Domine, L.M., Felip, M., Granados, I., Gries, C., Grossart, H.P., Haberman, J., Haldna, M., Hayden, B., Higgins, S.N., Jolley, J.C., Kahilainen, K.K., Kaup, E., Kehoe, M.J., MacIntyre, S., Mackay, A.W., Mariash, H.L., McKay, R.M., Nixdorf, B., Nõges, P., Nõges, T., Palmer, M., Pierson, D.C., Post, D.M., Pruett, M.J., Rautio, M., Read, J.S., Roberts, S.L., Rücker, J., Sadro, S., Silow, E.A., Smith, D.E., Sterner, R.W., Swann, G.E.A., Timofeyev, M.A., Toro, M., Twiss, M.R., Vogt, R.J., Watson, S.B., Whiteford, E.J., Xenopoulos, M.A., 2017. Ecology under lake ice. Ecol. Lett. 20, 98–111. https://doi.org/10.1111/ele.12699

Hampton, S.E., Moore, M. V., Ozersky, T., Stanley, E.H., Polashenski, C.M., Galloway, A.W.E., 2015. Heating up a cold subject: prospects for under-ice plankton research in lakes. J. Plankton Res. 37, 277–284. https://doi.org/10.1093/plankt/fbv002

Haustein, K., Allen, M.R., Forster, P.M., Otto, F.E.L., Mitchell, D.M., Matthews, H.D., Frame, D.J., 2017. A real-time Global Warming Index. Sci. Rep. 7, 15417. https://doi.org/10.1038/s41598-017-14828-5

Heinonen, J., Rissanen, S., 2017. Coupled-crushing analysis of a sea ice-wind turbine interaction – feasibility study of FAST simulation software. Ships Offshore Struct. 12, 1056–1063. https://doi.org/10.1080/17445302.2017.1308782

Herman, A., Jedrasik, J., Kowalewski, M., 2011. Numerical modelling of thermodynamics and dynamics of sea ice in the Baltic Sea. Ocean Sci. 7, 257–276. https://doi.org/10.5194/os-7-257-2011

Hersbach H., Bell B., Berrisford P., Biavati G., Horányi A., Muñoz Sabater J., Nicolas J., Peubey C., Radu R., Rozum I., Schepers D., Simmons A., Soci C., Dee D., Thépaut J-N. 2018. ERA5 hourly data on single levels from 1979 to present. Copernicus Climate Change Service (C3S) Climate Data Store (CDS). (Accessed on < 15-Nov-2020 >), doi: 10.24381/cds.adbb2d47.

Hjerne, O., Hajdu, S., Larsson, U., Downing, A.S., Winder, M., 2019. Climate Driven Changes in Timing, Composition and Magnitude of the Baltic Sea Phytoplankton Spring Bloom. Front. Mar. Sci. 6. https://doi.org/10.3389/fmars.2019.00482

Hu, X., Cai, M., Yang, S., Sejas, S.A., 2018. Air temperature feedback and its contribution to global warming. Sci. China Earth Sci. 61, 1491–1509. https://doi.org/10.1007/s11430-017-9226-6

Hu, X., Sun, J., Chan, T.O., Myers, P.G., 2018. Thermodynamic and dynamic ice thickness contributions in the Canadian Arctic Archipelago in NEMO-LIM2 numerical simulations. Cryosph. 12, 1233–1247. https://doi.org/10.5194/tc-12-1233-2018

Hunke, E.C., Lipscomb, W.H., Turner, A.K., 2011. Sea-ice models for climate study: Retrospective and new directions. J. Glaciol. 56, 1162–1172. https://doi.org/10.3189/002214311796406095

Jahan, R., Choi, J.K., 2014. Climate Regime Shift and Phytoplankton Phenology in a Macrotidal Estuary: Long-Term Surveys in Gyeonggi Bay, Korea. Estuaries and Coasts 37, 1169–1187. https://doi.org/10.1007/s12237-013-9760-7

Jakimavičius, D., Šarauskienė, D., Kriaučiūnienė, J., 2019. Influence of climate change on the ice conditions of the Curonian Lagoon. Oceanologia 62, 164–172. https://doi.org/10.1016/j.oceano.2019.10.003

Jarmalavičius, D., 2007. Jūrinis krantas, in: Bukantis, A., Šinkūnas, P., Taločkaitė, E. (Eds.), Klimato Kaita: Prisitaikymas Prie Jos Poveikio Lietuvos Pajūryje. Vilniaus Universiteto Leidykla, Vilnius, pp. 25–31.

Jawak, S.D., Bidawe, T.G., Luis, A.J., 2015. A Review on Applications of Imaging Synthetic Aperture Radar with a Special Focus on Cryospheric Studies. Adv. Remote Sens. 04, 163–175. https://doi.org/10.4236/ars.2015.42014

Jiang, M., Pang, C., Liu, Z., Jiang, J., 2020. Impact of Sea Ice on the Hydrodynamics and Suspended Sediment Concentration in the Coastal Waters of Qinhuangdao, China. Water 12, 611. https://doi.org/10.3390/w12020611

Jindrova, M., Llinàs, J.B., Torres, A.Z., 2017. Copernicus Land Monitoring Services. Task 3: Continuation of snow&ice task. D 3.2: Summary Report to Support EEA.

Karvonen, J., Cheng, B., Vihma, T., Arkett, M., Carrieres, T., 2012. A method for sea ice thickness and concentration analysis based on SAR data and a thermodynamic model. Cryosph. 6, 1507–1526. https://doi.org/10.5194/tc-6-1507-2012

Käyhkö, J., Apsite, E., Bolek, A., Filatov, N., Kondratyev, S., Korhonen, J., Kriaučiūnienė, J., Lindström, G., Nazarova, L., Pyrh, A., Sztobryn, M., 2015. Recent Change—River Run-off and Ice Cover, in: The BACC II Author Team (Ed.),

Second Assessment of Climate Change for the Baltic Sea Basin. Springer, Cham, Germany, pp. 99–116. https://doi.org/10.1007/978-3-319-16006-1_5

Kendall, M.G., Gibbons, J.D., 1990. Rank Correlation Methods. Edward Arnold, London, UK.

Kirillin, G., Leppäranta, M., Terzhevik, A., Granin, N., Bernhardt, J., Engelhardt, C., Efremova, T., Golosov, S., Palshin, N., Sherstyankin, P., Zdorovennova, G., Zdorovennov, R., 2012. Physics of seasonally ice-covered lakes: a review. Aquat. Sci. 74, 659–682. https://doi.org/10.1007/s00027-012-0279-y

Kļaviņš, M., Avotniece, Z., Rodinovs, V., 2016. Dynamics and Impacting Factors of Ice Regimes in Latvia Inland and Coastal Waters. Proc. Latv. Acad. Sci. Sect. B. Nat. Exact, Appl. Sci. 70, 400–408. https://doi.org/10.1515/prolas-2016-0059

Kolerski, T., 2018. Mathematical Modeling of Ice Dynamics as a Decision Support Tool in River Engineering. Water 10, 1241. https://doi.org/10.3390/w10091241

Kozlov, I.E., Krek, E. V., Kostianoy, A.G., Dailidienė, I., 2020. Remote Sensing of Ice Conditions in the Southeastern Baltic Sea and in the Curonian Lagoon and Validation of SAR-Based Ice Thickness Products. Remote Sens. 12, 3754. https://doi.org/10.3390/rs12223754

Kromkamp, J.C., Van Engeland, T., 2010. Changes in Phytoplankton Biomass in the Western Scheldt Estuary During the Period 1978–2006. Estuaries and Coasts 33, 270–285. https://doi.org/10.1007/s12237-009-9215-3

Kumar, A., Yadav, J., Mohan, R., 2020. Global warming leading to alarming recession of the Arctic sea-ice cover: Insights from remote sensing observations and model reanalysis. Heliyon 6, e04355. https://doi.org/10.1016/j.heliyon.2020.e04355

Lenderink, G., Buishand, A., Van Deursen, W., 2007. Estimates of future discharges of the river Rhine using two scenario methodologies: Direct versus delta approach. Hydrol. Earth Syst. Sci. 11, 1145–1159. https://doi.org/10.5194/hess-11-1145-2007

Lindenschmidt, K.-E., Baulch, H., Cavaliere, E., 2018. River and Lake Ice Processes—Impacts of Freshwater Ice on Aquatic Ecosystems in a Changing Globe. Water 10, 1586. https://doi.org/10.3390/w10111586

Losch, M., Menemenlis, D., Campin, J.-M., Heimbach, P., Hill, C., 2010. On the formulation of sea-ice models. Part 1: Effects of different solver implementations and parameterizations. Ocean Model. 33, 129–144. https://doi.org/10.1016/j.ocemod.2009.12.008

Luomaranta, A., Ruosteenoja, K., Jylhä, K., Gregow, H., Haapala, J., Laaksonen, A., 2014. Multimodel estimates of the changes in the Baltic Sea ice cover during the present century. Tellus A Dyn. Meteorol. Oceanogr. 66, 22617. https://doi.org/10.3402/tellusa.v66.22617

Maicu, F., De Pascalis, F., Ferrarin, C., Umgiesser, G., 2018. Hydrodynamics of the Po River-Delta-Sea System. J. Geophys. Res. Ocean. 123, 6349–6372. https://doi.org/10.1029/2017JC013601

Mäkiranta, A., Martinkauppi, B., Hiltunen, E., Lieskoski, M., 2018. Seabed Sediment as an Annually Renewable Heat Source. Appl. Sci. 8, 290. https://doi.org/10.3390/app8020290

Mäkynen, M., Haapala, J., Aulicino, G., Balan-Sarojini, B., Balmaseda, M., Gegiuc, A., Girard-Ardhuin, F., Hendricks, S., Heygster, G., Istomina, L., Kaleschke, L., Karvonen, J., Krumpen, T., Lensu, M., Mayer, M., Parmiggiani, F., Ricker, R., Rinne, E., Schmitt, A., Similä, M., Tietsche, S., Tonboe, R., Wadhams, P., Winstrup, M., Zuo, H., 2020. Satellite Observations for Detecting and Forecasting Sea-Ice Conditions: A Summary of Advances Made in the SPICES Project by the EU's Horizon 2020 Programme. Remote Sens. 12, 1214. https://doi.org/10.3390/rs12071214

Marchenko, A., 2018. Thermo-mechanical loads of confined sea ice on structures. Philos. Trans. R. Soc. A Math. Phys. Eng. Sci. 376, 20170341. https://doi.org/10.1098/rsta.2017.0341

Marchenko, A., Lishman, B., 2017. The influence of closed brine pockets and permeable brine channels on the thermo-elastic properties of saline ice. Philos. Trans. R. Soc. A Math. Phys. Eng. Sci. 375, 20150351. https://doi.org/10.1098/rsta.2015.0351

Meier, W.N., Hovelsrud, G.K., van Oort, B.E.H., Key, J.R., Kovacs, K.M., Michel, C., Haas, C., Granskog, M.A., Gerland, S., Perovich, D.K., Makshtas, A., Reist, J.D., 2014. Arctic sea ice in transformation: A review of recent observed changes and impacts on biology and human activity. Rev. Geophys. 52, 185–217. https://doi.org/10.1002/2013RG000431

Mimura, N., 2013. Sea-level rise caused by climate change and its implications for society. Proc. Japan Acad. Ser. B 89, 281–301. https://doi.org/10.2183/pjab.89.281

Molinaroli, E., Sarretta, A., Ferrarin, C., Masiero, E., Specchiulli, A., Guerzoni, S., 2014. Sediment grain size and hydrodynamics in Mediterranean coastal lagoons: Integrated classification of abiotic parameters. J. Earth Syst. Sci. 123, 1097–1114. https://doi.org/10.1007/s12040-014-0445-9

Muckenhuber, S., Nilsen, F., Korosov, A., Sandven, S., 2016. Sea ice cover in Isfjorden and Hornsund, Svalbard (2000–2014) from remote sensing data. Cryosph. 10, 149–158. https://doi.org/10.5194/tc-10-149-2016

Müller, S., Jessen, S., Duque, C., Sebök, E., Neilson, B., Engesgaard, P., 2018. Assessing seasonal flow dynamics at a lagoon saltwater–freshwater interface using a dual tracer approach. J. Hydrol. Reg. Stud. 17, 24–35. https://doi.org/10.1016/j.ejrh.2018.03.005

Murfitt, J., Brown, L., Howell, S., 2018. Evaluating RADARSAT-2 for the Monitoring of Lake Ice Phenology Events in Mid-Latitudes. Remote Sens. 10, 1641. https://doi.org/10.3390/rs10101641

Murfitt, J., Duguay, C.R., 2020. Assessing the Performance of Methods for Monitoring Ice Phenology of the World's Largest High Arctic Lake Using High-Density Time Series Analysis of Sentinel-1 Data. Remote Sens. 12, 382. https://doi.org/10.3390/rs12030382

Neumeier, U., Ferrarin, C., Amos, C.L., Umgiesser, G., Li, M.Z., 2008. Sedtrans05: An improved sediment-transport model for continental shelves and coastal waters with a new algorithm for cohesive sediments. Comput. Geosci. 34, 1223–1242. https://doi.org/10.1016/j.cageo.2008.02.007

Nicolaus, M., Katlein, C., Maslanik, J., Hendricks, S., 2012. Changes in Arctic sea ice result in increasing light transmittance and absorption. Geophys. Res. Lett. 39, 2012GL053738. https://doi.org/10.1029/2012GL053738

Notz, D., Stroeve, J., 2018. The Trajectory Towards a Seasonally Ice-Free Arctic Ocean. Curr. Clim. Chang. Reports 4, 407–416. https://doi.org/10.1007/s40641-018-0113-2

Obertegger, U., Obrador, B., Flaim, G., 2017. Dissolved oxygen dynamics under ice: Three winters of high-frequency data from Lake Tovel, Italy. Water Resour. Res. 53, 7234–7246. https://doi.org/10.1002/2017WR020599

Omstedt, A., Wettlaufer, J.S., 1992. Ice growth and oceanic heat flux: Models and measurements. J. Geophys. Res. Ocean. 97, 9383–9390. https://doi.org/10.1029/92JC00815

Öterler, B., 2017. Winter Phytoplankton Composition Occurring in a Temporarily Ice-Covered Lake: a Case Study. Polish J. Environ. Stud. 26, 2677–2688. https://doi.org/10.15244/pjoes/74015

Pełechata, A., Pełechaty, M., Pukacz, A., 2015. Winter temperature and shifts in phytoplankton assemblages in a small Chara-lake. Aquat. Bot. 124, 10–18. https://doi.org/10.1016/j.aquabot.2015.03.001

Perovich, D.K., 2003. Complex yet translucent: the optical properties of sea ice. Phys. B Condens. Matter 338, 107–114. https://doi.org/10.1016/S0921-4526(03)00470-8

Petty, A.A., Stroeve, J.C., Holland, P.R., Boisvert, L.N., Bliss, A.C., Kimura, N., Meier, W.N., 2018. The Arctic sea ice cover of 2016: a year of record-low highs and higher-than-expected lows. Cryosph. 12, 433–452. https://doi.org/10.5194/tc-12-433-2018

Post, E., Alley, R.B., Christensen, T.R., Macias-Fauria, M., Forbes, B.C., Gooseff, M.N., Iler, A., Kerby, J.T., Laidre, K.L., Mann, M.E., Olofsson, J., Stroeve, J.C., Ulmer, F., Virginia, R.A., Wang, M., 2019. The polar regions in a 2°C warmer world. Sci. Adv. 5, eaaw9883. https://doi.org/10.1126/sciadv.aaw9883

Prowse, T., Alfredsen, K., Beltaos, S., Bonsal, B.R., Bowden, W.B., Duguay, C.R., Korhola, A., McNamara, J., Vincent, W.F., Vuglinsky, V., Walter Anthony, K.M., Weyhenmeyer, G.A., 2011. Effects of Changes in Arctic Lake and River Ice. Ambio 40, 63–74. https://doi.org/10.1007/s13280-011-0217-6

Prowse, T.D., Bonsal, B.R., Duguay, C.R., Lacroix, M.P., 2007. River-ice break-up/freeze-up: a review of climatic drivers, historical trends and future predictions. Ann. Glaciol. 46, 443–451. https://doi.org/10.3189/172756407782871431

Roach, L.A., Bitz, C.M., Horvat, C., Dean, S.M., 2019. Advances in Modeling Interactions Between Sea Ice and Ocean Surface Waves. J. Adv. Model. Earth Syst. 11, 4167–4181. https://doi.org/10.1029/2019MS001836

Rühland, K.M., Paterson, A.M., Smol, J.P., 2015. Lake diatom responses to warming: reviewing the evidence. J. Paleolimnol. 54, 1–35. https://doi.org/10.1007/s10933-015-9837-3

Rukšėnienė, V., Dailidienė, I., Myrberg, K., Dučinskas, K., 2015. Simple approach for statistical modelling of ice phenomena in the curonian lagoon, the south-eastern baltic sea. Baltica 28, 11–18. https://doi.org/10.5200/baltica.2015.28.02

Screen, J.A., 2017. The missing Northern European winter cooling response to Arctic sea ice loss. Nat. Commun. 8, 14603. https://doi.org/10.1038/ncomms14603

Sévellec, F., Fedorov, A. V., Liu, W., 2017. Arctic sea-ice decline weakens the Atlantic Meridional Overturning Circulation. Nat. Clim. Chang. 7, 604–610. https://doi.org/10.1038/nclimate3353

Sharma, S., Blagrave, K., Magnuson, J.J., O'Reilly, C.M., Oliver, S., Batt, R.D., Magee, M.R., Straile, D., Weyhenmeyer, G.A., Winslow, L., Woolway, R.I., 2019. Widespread loss of lake ice around the Northern Hemisphere in a warming world. Nat. Clim. Chang. 9, 227–231. https://doi.org/10.1038/s41558-018-0393-5

Siitam, L., Sipelgas, L., Pärn, O., Uiboupin, R., 2017. Statistical characterization of the sea ice extent during different winter scenarios in the Gulf of Riga (Baltic Sea) using optical remote-sensing imagery. Int. J. Remote Sens. 38, 617–638. https://doi.org/10.1080/01431161.2016.1268734

Stroeve, J., Notz, D., 2015. Insights on past and future sea-ice evolution from combining observations and models. Glob. Planet. Change 135, 119–132. https://doi.org/10.1016/j.gloplacha.2015.10.011

Sumata, H., Kwok, R., Gerdes, R., Kauker, F., Karcher, M., 2015. Uncertainty of Arctic summer ice drift assessed by high-resolution SAR data. J. Geophys. Res. Ocean. 120, 5285–5301. https://doi.org/10.1002/2015JC010810

Tedesco, L., 2009. Modelling coupled physical-biogeochemical processes in ice-covered oceans. University of Bologna.

Tedesco, L., Vichi, M., Haapala, J., Stipa, T., 2010. A dynamic Biologically Active Layer for numerical studies of the sea ice ecosystem. Ocean Model. 35, 89–104. https://doi.org/10.1016/j.ocemod.2010.06.008

Tedesco, L., Vichi, M., Haapala, J., Stipa, T., 2009. An enhanced sea-ice thermodynamic model applied to the Baltic Sea. Boreal Environ. Res. 14, 68–80.

Timmermann, R., Danilov, S., Schröter, J., Böning, C., Sidorenko, D., Rollenhagen, K., 2009. Ocean circulation and sea ice distribution in a finite element global sea ice–ocean model. Ocean Model. 27, 114–129. https://doi.org/10.1016/j.ocemod.2008.10.009

Umgiesser, G., Canu, D.M., Cucco, A., Solidoro, C., 2004. A finite element model for the Venice Lagoon. Development, set up, calibration and validation. J. Mar. Syst. 51, 123–145. https://doi.org/10.1016/j.jmarsys.2004.05.009

Umgiesser, G., Ferrarin, C., Cucco, A., De Pascalis, F., Bellafiore, D., Ghezzo, M., Bajo, M., 2014. Comparative hydrodynamics of 10 Mediterranean lagoons by means of numerical modeling. J. Geophys. Res. Ocean. 119, 2212–2226. https://doi.org/10.1002/2013JC009512

Umgiesser, G., Zemlys, P., Erturk, A., Razinkovas-Baziukas, A., Mezine, J., Ferrarin, C., 2016. Seasonal renewal time variability in the Curonian Lagoon caused by atmospheric and hydrographical forcing. Ocean Sci. 12, 391–402. https://doi.org/10.5194/os-12-391-2016

Vancoppenolle, M., Fichefet, T., Goosse, H., Bouillon, S., Madec, G., Maqueda, M.A.M., 2009. Simulating the mass balance and salinity of Arctic and Antarctic sea ice. 1. Model description and validation. Ocean Model. 27, 33–53. https://doi.org/10.1016/j.ocemod.2008.10.005

Vargas, C.I.C., Vaz, N., Dias, J.M., 2017. An evaluation of climate change effects in estuarine salinity patterns: Application to Ria de Aveiro shallow water system. Estuar. Coast. Shelf Sci. 189, 33–45. https://doi.org/10.1016/j.ecss.2017.03.001

Wang, J., Duguay, C., Clausi, D., Pinard, V., Howell, S., 2018. Semi-Automated Classification of Lake Ice Cover Using Dual Polarization RADARSAT-2 Imagery. Remote Sens. 10, 1727. https://doi.org/10.3390/rs10111727

Wang, Q., Danilov, S., Sidorenko, D., Timmermann, R., Wekerle, C., Wang, X., Jung, T., Schröter, J., 2014. The Finite Element Sea Ice-Ocean Model (FESOM) v.1.4: formulation of an ocean general circulation model. Geosci. Model Dev. 7, 663–693. https://doi.org/10.5194/gmd-7-663-2014

Warner, K., Fowler, R., Northington, R., Malik, H., McCue, J., Saros, J., 2018. How Does Changing Ice-Out Affect Arctic versus Boreal Lakes? A Comparison Using Two Years with Ice-Out that Differed by More Than Three Weeks. Water 10, 78. https://doi.org/10.3390/w10010078

Warren, S.G., 2019. Optical properties of ice and snow. Philos. Trans. R. Soc. A Math. Phys. Eng. Sci. 377, 20180161. https://doi.org/10.1098/rsta.2018.0161

Wiese, M., Griewank, P., Notz, D., 2015. On the thermodynamics of melting sea ice versus melting freshwater ice. Ann. Glaciol. 56, 191–199. https://doi.org/10.3189/2015AoG69A874

Winder, M., Berger, S.A., Lewandowska, A., Aberle, N., Lengfellner, K., Sommer, U., Diehl, S., 2012. Spring phenological responses of marine and freshwater plankton to changing temperature and light conditions. Mar. Biol. 159, 2491–2501. https://doi.org/10.1007/s00227-012-1964-z

Winder, M., Sommer, U., 2012. Phytoplankton response to a changing climate. Hydrobiologia 698, 5–16. https://doi.org/10.1007/s10750-012-1149-2

Woolway, R.I., Kraemer, B.M., Lenters, J.D., Merchant, C.J., O'Reilly, C.M., Sharma, S., 2020. Global lake responses to climate change. Nat. Rev. Earth Environ. 1, 388–403. https://doi.org/10.1038/s43017-020-0067-5

Wu, T., Qiu, W., Wu, G., 2020. Fatigue Damage Evaluation of Pile-Supported Bridges under Stochastic Ice Loads. Adv. Civ. Eng. 2020, 1–14. https://doi.org/10.1155/2020/1853963

Yang, B., Young, J., Brown, L., Wells, M., 2017. High-Frequency Observations of Temperature and Dissolved Oxygen Reveal Under-Ice Convection in a Large Lake. Geophys. Res. Lett. 44, 12,218-12,226. https://doi.org/10.1002/2017GL075373

Zakhvatkina, N., Smirnov, V., Bychkova, I., 2019. Satellite SAR Data-based Sea Ice Classification: An Overview. Geosciences 9, 152. https://doi.org/10.3390/geosciences9040152

Zampato, L., Bajo, M., Canestrelli, P., Umgiesser, G., 2016. Storm surge modelling in Venice: two years of operational results. J. Oper. Oceanogr. 9, s46–s57. https://doi.org/10.1080/1755876X.2015.1118804

Žaromskis, R., 1996. Oceans, Seas, Estuaries. Debesija, Vilnius.

Zemlys, P., Ferrarin, C., Umgiesser, G., Gulbinskas, S., Bellafiore, D., 2013. Investigation of saline water intrusions into the Curonian Lagoon (Lithuania) and two-layer flow in the Klaipeda Strait using finite element hydrodynamic model. Ocean Sci. 9, 573–584. https://doi.org/10.5194/os-9-573-2013

Zhang, S., Pavelsky, T.M., 2019. Remote Sensing of Lake Ice Phenology across a Range of Lakes Sizes, ME, USA. Remote Sens. 11, 1718. https://doi.org/10.3390/rs11141718

Summary in Lithuanian

ĮVADAS

Temos aktualumas

Ledo danga blokuodama į vandenį prasiskverbiančią šviesą, natūralų aeravimą ir vandens cirkuliaciją per įvairius cheminius procesus modifikuoja visą vandens telkinio ekosistemą, jos struktūrą, produktyvumą ir dinamiką (Hampton ir kt., 2017). Užšalimo pradžia, trukmė ir ledo storis daro didelį socioekonominį poveikį, t. y. riboja laivybą, eismą, žvejybą, rekreacinę veiklą ir kt. Tikslios ledo storio, dreifo ir kitų savybių prognozės yra labai svarbios projektuojant saugius molus, jūroje esančius vėjo jėgainių parkus, planuojant saugias operacijas, poveikio vertinimus ir kt. (Heinonen ir Rissanen, 2017; Marchenko, 2018; Wu ir kt., 2020). Ledo stebėjimai, atlikti *in situ*, paprastai yra erdviškai nereprezentatyvūs – matavimai yra atliekami keliose pavienėse pozicijose, nes keliavimas ledu yra neretai daug laiko reikalaujantis, pavojingas ir brangus procesas (Block ir kt., 2019). Pastaraisiais dešimtmečiais nuotolinio stebėjimo metodai vaidina vis svarbesnį vaidmenį stebint ledo dangą ir yra vienintelis praktiškas metodas, leidžiantis gauti nuoseklų tęstinį didelės geografinės apimties ledo dangos registrą (Cui ir kt., 2018; Du ir kt., 2019; Murfitt ir kt., 2018; Zhang ir

Pavelsky, 2019). Nors nuotoliniai tyrimai ir yra labai geras metodas apibūdinant ledo fenologiją plačiu mastu, tokio tipo duomenų skiriamoji geba vis dar nėra pakankamai didelė, kad būtų galima užfiksuoti svarbius ledo parametrus, tokius kaip užšalimo, tirpimo pradžia ar ledo storis (Zakhvatkina ir kt., 2019). Šis trūkumas gali būti išspręstas skaitiniu modeliavimu.

Antžeminių ir nuotolinių stebėjimų derinimas su modeliavimu gali labai pagerinti ledo modelių prognozavimo galimybes analizuojant ledo storį ir fenologiją (Allard ir kt., 2018; Karvonen ir kt., 2012). Skaitinis modeliavimas leidžia ne tik prognozuoti buvusias, dabartines bei būsimas ledo būsenas atsiliepiant į kintantį klimatą, bet ir tirti fizinius ir ekologinius procesus, vykstančius ledo dangos laikotarpiu (Meier ir kt., 2014). Ledo dangos neįtraukimas į pažangias modeliavimo sistemas gali pakeisti ekologinių ir hidrodinaminių modelių rezultatus ir padaryti juos mažiau patikimus, nes kai kuriais atvejais supratimas apie ledo dinamiką žiemos periodu ir tai, kaip gyvas organizmas reaguoja į ledo dangos pokyčius, gali palengvinti vasaros sąlygų prognozavimą (Hampton ir kt., 2017).

Tobulėjant ledo stebėjimo metodams, skaitinio modeliavimo galimybėms bei augant supratimui apie klimato ir aplinkos pokyčius, ledo sąlygų tyrimai tampa vis aktyvesni. Nors dauguma ledo tyrimų yra sutelkti į poliarinius regionus (Meier ir kt., 2014; Notz ir Stroeve, 2018), nes ilgalaikiai jo pokyčiai yra globalios klimato kaitos indeksas (Haustein ir kt., 2017; Kumar ir kt., 2020; Woolway ir kt., 2020), vietinio masto ledo parametrų tyrimai spartėja (Woolway ir kt., 2020). Šiaurės pusrutulyje esančių ežerų ledo fenologiniai duomenys taip pat jau rodo dramatiškus šiltėjančio klimato požymius, tačiau ledo dangos tirpimo greičio rodikliai ne visose vietose yra vienodi (EEA, 2017; Sharma ir kt., 2019).

Kadangi žiemos laikotarpiu Kuršių marios užšąla keletai mėnesių, naudinga ištirti ledo dangos savybių dinamiką. Atsižvelgiant į tai, kad marios yra seklus vandens telkinys ir vandens tūris po ledu yra mažas, užšalimas įvyksta greičiau nei gilesniuose vandenyse, o tai daro didesnį poveikį mariose vykstantiems fiziniams ir ekologiniams procesams. Iki šiol ledas Kuršių mariose buvo tiriamas tik naudojant įprastus *in situ* matavimus, statistinį modeliavimą arba analizuojant jo poveikį kitiems marių procesams (Dailidienė, 2007; Jakimavičius ir kt., 2019; Rukšėnienė ir kt., 2015; Umgiesser ir kt., 2016). Tačiau vis dar nebuvo atlikti išsamūs tyrimai, susijusę su ledo dangos apimties, fenologijos, storio, sezono trukmės dinamika, taikant pažangius analitinius metodus – nuotolinius tyrimus ir skaitinį modeliavimą. Būsimų ledo dangos sąlygų prognozės, apskaičiuotos naudojant pateiktą ledo termodinaminį modelį, naudojant meteorologinius duomenis iš regioninių klimato modelių rodo, ko tikėtis ateityje keičiantis klimatui. Be to, hidrodinaminio modeliavimo sistemoje integruotas ledo modelis gali būti toliau naudojamas kartu su ekologiniu modeliu, siekiant įvertinti ledo dangos poveikį visai Kuršių marių ekosistemai.

Tyrimo tikslas ir pagrindiniai uždaviniai

Šio tyrimo tikslas yra ištirti Kuršių marių ledo dangos fenologiją ir dinamiką klimato kaitos kontekste, naudojant nuotolinių stebėjimų ir skaitinio modeliavimo metodus, ir išanalizuoti ledo dangos poveikį marių hidrodinaminėms savybėms.

Pagrindiniai uždaviniai:

1. įvertinti ledo fenologijos dinamiką ir iš palydovo vaizdų nustatyti ledo augimo ir irimo dėsningumus bei įvertinti nuotolinio stebėjimo duomenų panaudojamumą regioniniam ledo dangos stebėjimui,
2. pritaikyti palydovinius ledo dangos duomenis skaitiniame modelyje ir išanalizuoti ledo dangos poveikį cirkuliacijai, druskingo vandens prietakai, vandens užsilaikymo galimybėms ir suspenduotų nuosėdų koncentracijai,
3. atlikti ledo storio modelinius skaičiavimus, patvirtinti gautus rezultatus *in situ* duomenimis ir ištirti būsimas klimato kaitos scenarijų RCP4.5 ir RCP8.5 prognozes,
4. integruoti ledo termodinaminį modelį į hidrodinaminio modeliavimo sistemą SHYFEM ir įvertinti ledo storio pasiskirstymą visame Kuršių marių paviršiuje.

Darbo naujumas

Šis tyrimas pirmą kartą pateikia jungtines žinias apie Kuršių marių ledo dangos fenologiją. Joje nagrinėjami nauji ledo dangos stebėjimo ir prognozavimo metodai, lyginant su įprastais *in situ* matavimais ir pažangiais nuotolinio stebėjimo metodais, bei pabrėžiami pastarųjų privalumai. Palydovinių duomenų panaudojimas seklių vandenų baigtinių elementų hidrodinaminiame modelyje (SHYFEM) rodo didelės skiriamosios gebos ledo stebėjimų svarbą tinkamai apibūdinant fizinius procesus ledo sezono metu. Iki šiol Kuršių marioms nebuvo taikomas veikiantis ledo skaitinis modelis, tai taip pat buvo atlikta šio tyrimo metu. Pažangaus ledo termodinaminio modelio įtraukimas į modeliavimo sistemą SHYFEM kartu su *in situ* ir nuotolinio stebėjimo duomenimis yra puiki priemonė ledo termodinamikai analizuoti visame marių paviršiuje bei patobulinanti skaitinį šių gėlavandenių marių aprašymą.

Apibendrinant galima teigti, kad nauji šio darbo aspektai yra susiję su 1) išplėstiniu Kuršių ledo fenologijos ir dinamikos aprašymu; 2) hidrodinaminių savybių vertinimu po ledu; 3) ledo termodinaminio modelio integravimu į hidrodinaminio modeliavimo sistemą; 4) ilgalaikėmis ledo storio prognozėmis. Sukurtos ledo modelio paprogramės ir kodo struktūra suteikia galimybę ateityje jį susieti su kitais modeliais SHYFEM modeliavimo sistemoje.

Rezultatų mokslinė ir praktinė reikšmė

Šio tyrimo rezultatai papildė mūsų žinias apie ledo dangos fenologiją ir dinamiką visame Kuršių marių paviršiuje, taip pat fizinių procesų pokyčius po ledu. Atlikus palydovinių duomenų vertinimą paaiškėjo, kad daugeliu atvejų jie yra geresni, palyginti su antžeminiais stebėjimais, nustatant ledo parametrus visame marių paviršiuje. Palydovinių ledo duomenų panaudojimas hidrodinaminiame modelyje suteikė galimybę giliau pažvelgti į ledo dangos poveikį fiziniams procesams Kuršių mariose. Skaitinis paties ledo modeliavimas leidžia prognozuoti marių ledo storio ir paviršiaus padengimo ledu raidą, taip pat išbandyti skirtingų klimato kaitos scenarijų įtaką ledo fenologijai. Pasiūlytas ledo termodinaminis modelis labai gerai sutampa su Kuršių marių antžeminių ir nuotolinių stebėjimų duomenims. Tolesnė šio modelio integracija į skaitinio modeliavimo sistemą SHYFEM leidžia mums ne tik nuodugniai ištirti ledo storį visame tyrimų rajone, bet ir bus labai naudinga modelio pritaikymui kitiems sekliems vandens telkianiams, kuriems būdinga ledo danga. Šio darbo metu sukurta ledo modelio programinė integracija su hidrodinaminiu modeliu (paprogramės ir kodo struktūra) gali būti toliau vystoma susiejant jį su kitais SHYFEM modeliavimo sistemos modeliais. Visa tai bus geras žingsnis į priekį apibūdinant Kuršių marių ekosistemą.

Rezultatų aprobavimas

Šio tyrimo rezultatai buvo pristatyti 3 tarptautinėse ir 2 regioninėse konferencijose:

„Jūros ir krantų tyrimai“, Klaipėda, Lietuva, 2018 m. gegužės mėn.
7-ajame IEEE/OES Baltijos šalių simpoziume „Švari ir saugi Baltijos jūra ir energetinis saugumas Baltijos šalims“, Klaipėda, Lietuva, 2018 m. birželio mėn.
„Jūros ir krantų tyrimai“, Klaipėda, Lietuva, 2019 m. gegužė.
ESA „Living Planet“ simpoziume, Milanas, Italija, 2019 m. gegužės mėn.
AGILE konferencijoje 2019 m., Limasolis, Kipras, 2019 m. birželio mėn.

Šios disertacijos rezultatai buvo paskelbti mokslinėse publikacijose:

Idzelytė R., Kozlov I.E., Umgiesser G. 2019. Remote Sensing of Ice Phenology and Dynamics of Europe’s Largest Coastal Lagoon (The Curonian Lagoon). Remote Sensing, 11, 2059, doi: 10.3390/rs11172059.

Mėžinė J., Ferrarin C., Vaičiūtė D., **Idzelytė R.**, Zemlys P., Umgiesser G. 2019. Sediment Transport Mechanisms in a Lagoon with High River Discharge and Sediment Loading. Water, 11, 1970, doi: 10.3390/w11101970.

Idzelytė R., Mėžinė J., Zemlys P., Umgiesser G. 2020 Study of ice cover impact on hydrodynamic processes in the Curonian Lagoon through numerical modeling. Oceanologia, 62, 428-442, doi: 10.1016/j.oceano.2020.04.006.

Idzelytė R., Umgiesser G. 2020. Application of an Ice Thermodynamic Model to a Shallow Freshwater Lagoon. Boreal Environment Research, 26, 6177, ISSN 1797-2469.

TYRIMŲ MEDŽIAGA IR METODAI

Tyrimų rajonas

Šiame darbe analizuojama tyrimo sritis yra pietrytinėje Baltijos jūros dalyje esančios Kuršių marios. Nors ir esantis seklus gėlavandenis vandens telkinys (vidutinis gylis – 3,8 m, didžiausias natūralus gylis – 5,8 m), marios yra didžiausia lagūna visoje Europoje (plotas ~ 1600 km^2, tūris 6,3 km^3) (Gasiūnaitė ir kt., 2008; Žaromskis, 1996). Kuršių marios yra sujungtos su jūra siauru Klaipėdos sąsiauriu ir esant tinkamam vėjo režimui šiaurinė marių dalis pasižymi druskingo vandens prietaka (Zemlys ir kt., 2013), kuris teka palei vakarinę kranto liniją dėl dominuojančio gėlo vandens nuotekio iš Nemuno, kuris yra pagrindinis marių vandens atsinaujinimo šaltinis (Umgiesser ir kt., 2016).

Istoriniai ledo stebėjimo duomenys rodo, kad 1948–1972 m. ledo sezono trukmė buvo vidutiniškai 110 dienų (svyruojant nuo 12 iki 169 dienų), o ledo storis svyravo nuo 10 iki 70 cm (Baukšys, 1978). Dėl vykstančių klimato pokyčių ir oro temperatūros kilimo prognozių ledo dangos storis ir fenologijos parametrai greičiausiai pasikeis pesimistinės pusės link (Jakimavičius ir kt., 2019). Pokytis jau pastebimas vakarinėje marių dalyje, kur ledo sezono trukmė sumažėjo perpus, lyginant 1961–1975 ir 1991–2005 m. laikotarpius (Dailidienė, 2007; Jarmalavičius, 2007).

Duomenų rinkmenos

Palydoviniai ledo stebėjimai. Palydoviniai C dažnių juostos sintetinės apertūros radaro (angl. Synthetic Aperture Radar, SAR) duomenys buvo gauti iš trijų Žemės stebėjimo misijų: Envisat Advanced SAR (ASAR), RADARSAT-2 ir Sentinel-1A ir 1B (apatinė eilutė, 2 pav.). Analizuojamas 15 žiemų laikotarpis nuo 2002 iki 2017 m. SAR duomenys buvo papildyti debesų neturinčiomis vidutinės skiriamosios gebos vaizdavimo spektroradiometro (MODIS, Terra) nuotraukomis. Iš viso buvo gauti ir apdoroti 514 SAR ir 101 MODIS vaizdai (viršutinė ir apatinė eilutės, 2 pav.). Šiame tyrime buvo naudojamas vizualus ledo krašto identifikavimas naudojant SNAP ir ArcGIS programine įrangą. Ledo sezono trukmė buvo apskaičiuota susumuojant iš kiekvienos palydovinės nuotraukos nuskaitmenintam ledo plotui priskyrus jo galiojimo reikšmę,

paremtą dienų skirtumu tarp gautų nuotraukų ir oro temperatūra. Remiantis šiais duomenimis išskirti du ledo sezono trukmės parametrai: maksimalus (D_{SAR}) ir vidutinis erdvinis ($\overline{D}_{SAR}$). Pastarasis buvo suskirstytas į tris kategorijos: trumpas ($\overline{D}_{SAR} < 50$ d.), vidutinis (50 d. $\leq \overline{D}_{SAR} \leq 100$ d.) ir ilgas ($\overline{D}_{SAR} > 100$ d.). Iš palydovinių nuotraukų taip pat buvo nustatytos pirminio ir visiško užšalimo, paskutinio tirpimo bei paskutinės ledo dienos datos. Šių parametrų kintamumo tendencijos įvertintos naudojant Manno–Kendallo testą 0,05 reikšmingumo lygyje su 95% patikimumo lygiu.

Norint nustatyti ledo sezono trukmės priklausomybę nuo Šiaurės Atlanto svyravimų intensyvumo (angl. North Atlantic Oscilation, NAO), apskaičiuotas koreliacijos koeficientas tarp ledo trukmės ir Hurrello žiemos (nuo gruodžio iki kovo mėn., NAO_{DJFM}) indekso, kurį pateikė Klimato analizės skyrius, NCAR, Boulder, JAV. Tuo pačiu įvertintas ir ledo sezono trukmės ryšys su sumine neigiama oro temperatūra, išmatuota Kuršių mariose. Palydoviniai ledo duomenys taip pat panaudoti vizualiai ledo modelio rezultatų validacijai.

Antžeminiai ledo matavimai. Ledo duomenis iš Nidos, Juodkrantės ir Ventės matavimo stočių pateikė Lietuvos aplinkos apsaugos agentūros jūrinių tyrimų departamentas. Nidos ir Ventės duomenys apima visą tyrimo laikotarpį (2002–2017 m.), tačiau Juodrantėje ledo stebėjimo programa buvo nutraukta nuo 2012 m. Duomenis sudaro ledo rūšys ir formos, ledų kiekis balais (skalėje nuo nulio – be ledo, iki 10 – visiškai padengta ledu), būklė, tankis, storis ir dreifas bei oro ir vandens temperatūra, vėjo greitis ir matomumas, iš kurių nustatytos pirminio ir visiško užšalimo, paskutinio tirpimo bei paskutinės ledo dienos datos, kartu nustatant ledo sezono ilgį (D_{st}). Ši informacija lyginta su palydoviniais duomenimis, skaičiuojant dienų skirtumą tarp šių datų. Ledų kiekis lygintas su ledo koncentracija palydovinėse nuotraukose apibrėžtame plote, kuris atitinka buferinę zoną aplink matavimo stotis (spindulys – kintantis pagal išmatuotą kiekvienos dienos matomumą). Ledo storio matavimai naudoti termodinaminio modelio kalibracijai.

Meteorologiniai duomenys. Debesuotumo, trumpųjų bangų spinduliuotės, kritulių, drėgmės, oro temperatūros, atmosferos slėgio ir vėjo greičio duomenys buvo gauti iš Lietuvos hidrometeorologijos tarnybos (operatyvinio skaitinio oro prognozavimo modelio HIRLAM) ir Europos vidutinio nuotolio orų prognozių centro (1 lentelė).

Hidrologiniai duomenys. Baltijos jūros druskingumo, temperatūros ir vandens lygio duomenys gauti iš operatyvinio hidrodinaminių modelio MIKE21 ir didelės skiriamosios gebos Baltijos jūros operatyvinio modelio (HIROMB) bei modulinio vandenyno modelio (MOM) prognozių (1 lentelė). Lietuvos hidrometeorologijos tarnyba prie Aplinkos ministerijos pateikė kasdienius upių nuotėkio duomenis.

Klimato duomenys. Analizuojant klimato kaitos poveikį ledo storiui Kuršių mariose, istorinis laikotarpis (1986–2005) buvo lyginamas su būsimuoju laikotarpiu (2006–2100), remiantis dviem tipinių koncentracijų kelių (angl. Representative Concentration Pathway, RCP) scenarijais: RCP4.5 ir RCP8. 5. Šių prognozių meteorologiniai duomenys gauti iš CORDEX (angl. Coordinated Regional Downscaling Experiment) scena-

rijų Europai iš Rossby centro regioninio klimato modelio (RCA4), kurį sudaro penki modeliavimo rinkiniai, pagrįsti penkiais pasauliniais klimato modeliais (2 lentelė). Šių modelių oro temperatūros duomenys buvo pataisyti pridėjus vidutinį skirtumą tarp stebėtos ir modeliuotos lapkričio–balandžio mėn. oro temperatūros, apskaičiuotos 1993–2005 m. laikotarpiui. Oro temperatūros ir ledo storio tendencijos įvertintos naudojant Manno–Kendallo testą 0,05 reikšmingumo lygyje su 95% patikimumo lygiu.

Matematinis modeliavimas

Hidrodinaminis modelis. Tyrimui buvo naudojamas atviro kodo baigtinių elementų hidrodinaminis modelis sekliems vandens telkiniams SHYFEM. Modelis sprendžia 3D hidrodinamines lygtis, vertikaliai integruotas kiekviename sluoksnyje. Lygtys integruojamos laike naudojant pusiau neišreikštinę diskretizavimo schemą, o erdvinė diskretizacija pasiekiama naudojant iš dalies modifikuotą baigtinių elementų metodą (Umgiesser ir kt., 2004). Netaisyklingų trikampių skaičiavimo tinklelis leidžia modelį pritaikyti sudėtingos geometrijos ir batimetrijos vandens telkiniams. Šiame modelyje palydovinio ledo dangos duomenys yra interpoliuojami, kad apimtų visą ledo sezoną, ir pateikiami skaičiais tarp 0 – vanduo ir 1 – visiškai padengta ledu, ir šia verte pasveriamas vėjo pasipriešinimo koeficientas, taip sumažinant judesio kiekio impulsą į vandens paviršių. Ledo vertė taip pat naudojama skaičiuojant albedą. Modelyje atsižvelgiama tik į ledo dangos dalį, o ne į jos storį ar sniego dangą. Modelio 3D konfigūracija buvo naudojama palydovinių ledo dangos duomenų pritaikymui analizuojant hidrodinaminius procesus ir nuosėdų pernešimą po ledu, o 2D – ledo dangos storio visame marių paviršiuje modeliavimui.

Ledo modelis. Patobulintas ledo termodinaminis modelis ESIM2 (Tedesco ir kt., 2010) buvo naudojami ledo storio tyrimams ir ledo modelio integravimui į SHYFEM modeliavimo sistemą. Modelyje skaičiuojami trys sniego sluoksniai (iškritęs sniegas surenkamas į „virtualių kibirą“, o kai jis prisipildo, ištuštinamas ir sniegas sutankinamas), du tarpiniai sluoksniai (užšalęs ištirpęs sniegas ir ledas, susidarantis užšąlant vandens prisotintam sniegui) bei du sluoksniai ledo (biologiškai aktyvus ir biologiškai neaktyvus). Šioje studijoje analizuojamas bendras ledo storis susumuojant tarpinių ir ledo sluoksnių storius, taip pat modelis papildytas šilumos srauto iš vandens Omstedto ir Wettlauferio (1992) lygtimi. Modelis taip pat apskaičiuoja temperatūrą kiekvieno sniego ir ledo sluoksnio sąsajoje bei paviršiuje. Integracija į hirodnaminį modelį SHYFEM atlikta nustatant abipusį ryši tarp modelių skaičuojamos vandens temperatūros bei hidrodinaminio modelio druskingumas naudojamas apskaičiuoti užšalimo temperatūrą.

Sedimentų modelis. Nuosėdų pernašos modelis SEDTRANS05 (priklausantis tai pačiai SHYFEM modeliavimo sistemai) buvo naudojamas tiriant ledo įtaką suspenduotų nuosėdų koncentracijai. Kiekviename modelio laiko žingsnyje erozijos ir akumuliacijos

greičiai apskaičiuojami remiantis vėjo sukeltomis bangomis ir srovėmis, taip pat atnaujinamas gylis hidrodinaminių procesų reikšmių skaičiavimui sekančiame modelio laiko žingsnyje. Priedugnio vandens sluoksnio greitis, apskaičiuotas hidrodinaminio modelio, naudojamas apskaičiuojant dugno šlyties jėgą. Pradinė dugno nuosėdų struktūra buvo gauta iš (Gelumbauskaitės ir kt., 1999; Gulbinskas ir Žaromskis, 2002) žemėlapių ir panaudota modelyje sukonstravus devynių klasių taisyklingą nuosėdų tinklelį, kiekvienai klasei priskiriant suspenduotų nuosėdų koncentracijos procentą.

Modeliavimo nustatymai ir scenarijai. Ledo dangos poveikiui hidrodinaminiams procesams analizuoti naudojamas skaičiavimo tinklelis, atitinkantis Kuršių marių teritoriją, susideda iš 1309 mazgų ir 2027 trikampių elementų, o vertikaliai diskretizacijai panaudota 10 sigma sluoksnių. Dalis Baltijos jūros yra taip pat įtraukta į skaičiavimo tinkelį tam, kad būtų išvengta trikdžių skaičiuojant vandens mainus per Klaipėdos sąsiaurį. Taikant palydovinius ledo dangos duomenis hidrodinaminiame modelyje, Baltijos jūra ir Klaipėdos sąsiauris buvo laikomi be ledo. Modeliavimo laikotarpis buvo nuo 2004-01-01 iki 2015-12-31. Atlikti trijų tipų modeliavimai: be ledo, su palydoviniais ledo dangos duomenimis ir su idealizuota ledo danga, kai marių paviršius yra visiškai padengtas ledu viso ledo sezono laikotarpiu (3 lentelė). Cirkuliacijos, druskingumo ir vandens užsilaikymo duomenys buvo suvidurkinti pagal kalendorinius sezonus bei ledo sezono laikotarpiu (kiekvienais metais skirtingas). Ledo įtakai įvertinti skaičiuojamas vidutinis skirtumas tarp modelio skaičiavimų naudojant ledo duomenis ir ne. Taip pat skaičiuotas valandų skaičius per metus, kai druskos koncentracijos skirtumas tarp paviršinio ir priedugnio vandens sluoksnių viršijo 1 ir 3 g kg^{-1} ribas Klaipėdos sąsiauryje (1 pav., pažymėta geltona spalva), bei dienų skaičius, kai vertikaliai suvidurkinta druskos koncentracija viršija 2 g kg^{-1} ribą Juodkrantėje. Vandens užsilaikymo laikas buvo atskirai apskaičiuotas šiauriniam, pietiniam ir visam marių plotui.

Ledo dangos poveikis suspenduotų nuosėdų koncentracijai analizuojamas naudojant 2033 mazgų ir 3294 elementų skaičiavimo tinklelį su penkiais sigma sluoksniais vertikaliai diskretizacijai. Skaičiavimo laikotarpis nuo 2014-01-15 iki 2014-03-07, skaičiavimus atliekant panaudojus ledo palydovinius duomenis ir ne. Šių skaičiavimų palyginimas buvo atliktas apskaičiuojant visų marių vidutinę suspenduotų nuosėdų koncentraciją ir žvelgiant į koncentracijos vandens storymėje laiko eilutes dviejose stebėjimo stotyse šiaurinėje marių dalyje (1 pav., S1 ir S2).

Ledo termodinaminis modelis buvo sukalibruotas 2004–2017 m. laikotarpiui, skaičiavimams naudojant modelio nustatymus iš Tedesco ir kt. (2010) () ir padidinus visų sniego tipų tankį 50 kg m^{-3} ($Pres_{\rho_s}$). Rezultatai buvo palyginti su ledo storio matavimais Nidoje, Juodkrantėje ir Ventėje (1 pav.), apskaičiuojant šaknį iš vidutinės kvadratinės paklaidos (RMSE) ir Pirsono koreliacijos koeficientą (R).

Ateities ledo storio prognozėms naudoti RCP4.5 ir RCP8.5 scenarijais paremti penkių klimato modelių duomenys. Rezultatai suskirstyti į istorinį periodą (1986–

2005) bei artimą (2021–2040) ir tolimą ateitį (2081–2100), skaičiuojant pasirinktų modelių vidutines ledo storio, sezono ilgio ir oro temperatūros lapkričio–balandžio mėnesiais reikšmes (5 lentelė).

REZULTATAI IR DISKUSIJA

Ledo fenologija ir dinamika

Palydoviniai ledo stebėjimų lyginimas su in situ. Ledo dangos koncentracija, gauta iš palydovinių vaizdų, puikiai sutampa su antžeminiais stebėjimais (R = 0,92), likę neatitikimai atsiranda dėl palydovinėse nuotraukose sunkiai atpažįstamų plono ir mažos koncentracijos ledo. Skirtumas tarp užšalimo pradžios datų, nustatytų iš palydovinių nuotraukų ir pakrantės stočių, yra tik 0,5 dienos, pirmiau pastebint pakrantės stotyse. Nors nuotolinių vaizdų dažnis nėra pakankamai didelis, kad būtų galima pastebėti greitą ledo formavimąsi, vis dėlto 38% atvejų jis buvo pastebėtas palydovinėse nuotraukose anksčiau nei pakrantės stotyse. Panašus vidutinis skirtumas pastebimas visiško užšalimo metu, tik čia 62% atvejų, kai jis jau užfiksuotas stebėjimų stotyse, palydovinės nuotraukose vis dar matomi atviro vandens plotai toliau nuo pakrantės. Didžiausias skirtumas tarp nuotolinių ir *in situ* stebėjimų yra apibrėžiant paskutinio tirpimo datą, kai palydovinėse nuotraukose jis aptinkamas vidutiniškai 5 dienomis anksčiau nei pakrantės stotyse (75% visų atvejų). Paskutinė ledo diena fiksuojama vidutiniškai 2 dienomis vėliau nei pakrantėje (net 82% visų atvejų). Sujungę nuotolinių ir antžeminių stebėjimų ledo foromavimosi ir ištirpimo datas gauname pataisytą ledo sezono trukmę (D_{corr}), kuri 73% atvejų yra iki 10 dienų ilgesnė, nei gauta iš *in situ* stebėjimų.

Ledo dangos plotas, jo augimas ir irimas. Po ledo formavimosi pradžios praeina vidutiniškai 6 dienos (nuo 0 iki 35 dienų), kol Kuršių marios pilnai pasidengia ledu, priklausomai nuo vyraujančios neigiamos oro temperatūros. Ledo formavimasis prasideda išilgai marių rytinės ir pietinės pakrantės, taip pat šiek tiek anksčiau užšąla Nemuno deltos teritorija (4a pav.). Vėliausiai ledas formuojasi palei pietinę Kuršių nerijos atkarpą ir virš giliausios pietvakarinės marių dalies. 2002–2017 m. kiekvieną žiemą pastebimas visiškas marių užšalimas, trunkantis vidutiniškai 40 dienų (nuo 10 iki 90 dienų). Tarp visiško užšalimo ir paskutinio tirpimo datų pastebimi keletas ledo tirpimo atvejų dėl pakilusios, teigiamos oro temperatūros. Vidutiniškai ledo danga pradeda nykti vasario pabaigoje, o visas tirpimo laikotarpis vidutiniškai trunka mėnesį (nuo 6 iki 60 dienų). Tirpimas prasideda šiaurinėje marių dalyje, kur yra aktyvesnė vandens cirkuliacija ir druskingo vandens prietaka iš Baltijos jūros, ir tęsiasi pagal vakarinę pakrantę. Vyraujanti vėjo kryptis yra pagrindinis faktorius reguliuojantis ledo atsitraukimo dėsningumus. Dažniausiai vakarų vėjai dreifuojantį ledą stumia rytinės,

pietrytinės marių dalies link. Ledo danga per pastaruosius metus pradeda irti ir nutirpti vis anksčiau, tačiau statistiškai reikšminga yra tik paskutinio tirpimo datų ankstėjimo tendencija (p = 0,02).

Ledo sezono ilgis. Šio tyrimo metu pirmą kartą pristatyti detalūs ledo sezono trukmės žemėlapiai. Vidutinė 15-os sezonų ledo danga ilgiausiai matoma marių pietrytinėje limniškoje dalyje ir palei rytinę pakrantę, taip pat Nemuno deltos rajone (75–85 dienos), trumpiau – vakarinėje ir pietvakarinėje marių dalyje (65–70 dienų), o trumpiausias – šiaurinėje dalyje (<65 dienos), dėl aktyvios hidrodinamikos ir sūraus vandens prietakos. Vidutinė 15-os metų erdvinė ledo sezono trukmė yra 71 diena, matavimų stotyse ji yra 86 dienos, o pataisytoji ledo sezono tukmė – 89 dienos. Pastaroji trumpėja apie 1,6 dienos per metus 2002–2017 m. periodu. Erdvinis ledo sezono ilgis geriau atspindi ledo dangos sąlygų Kuršių mariose erdvinį kintamumą, jis taip pat turi ryškesnę trumpėjimo tendenciją (2,3 dienos per metus). Panašūs ledo dangos sezono sutrumpėjimo rezultatai buvo užfiksuoti ir per pastarąjį šimtmetį Baltijos jūroje (Haapala ir kt., 2015). Ledo sezono daugiametis kintamumas turi panašias tendencijas kaip ir Rygos įlankoje (Siitam ir kt., 2017) Latvijos priekrantėje (Kļaviņš ir kt., 2016) ir Aistmarėse (Chubarenko ir kt., 2019). Ledo sezonus suskirsčius į trumpus, vidutinius ir ilgus, pastebėta, kad ledo formavimasis trumpomis žiemomis prasideda beveik mėnesiu vėliau nei ilgomis, bei periodas, kai ledas marių paviršių dengia >80%, yra trumpesnis.

Regioniniai klimato svyravimai virš Kuršių marių yra susiję su Šiaurės Atlanto svyravimais (Dailidienė ir kt., 2012). Pastebėta stipri koreliacija tarp NAO_{DJFM} ir ledo sezono trukmės (-0,71, -0.73 ir -0,83 atitinkamai lyginant su D_{st}, D_{corr} ir $\overline{D}_{SAR}$). Be to, ledo trukmė rodo aiškią priklausomybę nuo lokaliai išmatuotos suminės neigiamos oro temperatūros (R = -0.81 lyginant su D_{st} ir D_{corr} bei R = -0.92 lyginant su $\overline{D}_{SAR}$), kuri tendencingai kyla vedant prie šiltesnių ir trumpesnių žiemų. Kaip pastebite, geriausi rezultatai gaunami atsižvelgiant į vidutinį erdvinį ledo sezono ilgį, įrodant nuotolinių stebėjimų privalumus ledo dangos sezono trukmės svyravimų supratimui.

Ledo poveikis

Cirkuliacija ir vandens srautai. Didžiausias vandens srovės greitis pastebimas šiaurinėje marių dalyje, kur Nemuno vanduo teka link Klaipėdos sąsiaurio. Pietinėje dalyje po ledo danga srovių greitis pastebimai sumažėja, nes vėjas yra pagrindinis jų generatorius. Srovės suvidurkintos kiekvienam kalendoriniam sezonui rodo skirtingus sūkurių išsidėstymus, bėgant sezonams pasislenkant į skirtingas marių vietas ir formuojantis naujoms sūkurinėms sistemoms. Po ledu sūkuriai yra labiau susispaudę pietinėje marių dalyje, jei ledo dangos nebūtų, dauguma jų būtų marių viduryje. Sistemų pasiskirstymas šiek tiek skiriasi nuo panašaus tyrimo, kurį atliko Umgiesser ir

kt. (2016), kur jie naudojo 4 metų teritoriškai nereprezentatyvius ledo duomenis iš pakrančių stočių. Analizuojant idealizuotos ledo dangos atvejį (kai viso ledo sezono metu marios yra visiškai padengtos ledu), vanduo teka lėčiau palei vakarinę ir šiek tiek greičiau palei rytinę kranto liniją šiaurinėje marių dalyje, lyginant su tekėjimu po tikrąja ledo danga. Iš keturių pasirinktų sekcijų (1 pav., spalvotos linijos) aiškiausiai matoma, kad ledo danga daro didesnę įtaką vandens srautams Nemuno deltos rajone ir per Lietuvos–Rusijos sieną, kur skirtumas tarp modeliavimo rezultatų su ledu ir be jo yra beveik dvigubai didesnis nei Klaipėdos sąsiauryje ir į šiaurę nuo Nemuno. Užsitęsusi pilna ledo danga (idealizuotas ledas) taip pat turi didžiausią įtaką šioje srityje, nes vandens masė, išeinanti iš Nemuno deltos, yra pastovesnė, necirkuliuoja tarp deltos ir marių palyginti su modeliavimu be ledo, todėl mažiau vandens nukreipiama į pietus.

Sūraus vandens prietaka. Druskingumo koncentracija yra didžiausia marių šiaurinėje dalyje, kur dėl šiaurinių vėjų yra būdinga sūraus vandens prietaka iš Baltijos jūros, pietinėje dalyje druskos koncentracija yra itin maža ir nereikšminga. Didžiausia druskos koncentracija yra rudens sezono metu, o mažiausia – pavasarį. Druskingumas pavasarį ir vasarą yra labai panašus (erdvinis vidurkis atitinkamai 0,23 ir 0,26 g kg^{-1}), o tikrojo ir idealizuoto ledo dangos sezono metu neparodo labai didelio skirtumo (erdvinis vidurkis atitinkamai 0,31 ir 0,27 g kg^{-1}). Tačiau tikros ledo dangos metu druskingumas gali sumažėti iki 1,02 g kg^{-1}, o idealizuoto – iki 1,18 g kg^{-1}. Tai parodo pilnos ledo dangos ir jos trukmės svarbą mažinant druskingo Baltijos jūros vandens prietakos intensyvumą į Kuršių marias.

Modeliavimo rezultatai rodo, kad Klaipėdos sąsiauryje druskingumo skirtumas tarp vandens priedugnio ir paviršiaus viršija 1 g kg^{-1} ribą vidutiniškai 130 valandų per metus, kai modelio skaičiavimuose naudojama tikra ledo danga, o jei ledas skaičiavimuose nenaudojamas, tai šis skirtumas yra vidutiniškai 114 valandų per metus. Juodkrantėje vidutinis vandens stulpo druskingumas viršija 2 g kg^{-1} ribą vidutiniškai beveik 90 dienų per metus, kai modelio skaičiavimuose atsižvelgiama į tikrąją ledo dangą, tačiau į ją neatsižvelgus šis periodas pailgėja vidutiniškai 13,9 dienomis.

Vandens užsilaikymo laikas. Šiaurinėje marių dalyje vidutinis vandens užsilaikymo laikas (VUL) yra apie 55 dienos, o pietuose – 150 dienų po tikra ledo danga, o tai yra ~ 1,5 dienos ir ~ 24 dienomis ilgiau nei visiškai nebūnant ledo. Žvelgiant į VUL idealizuotos ledo dangos atveju, pietinėje dalyje jis padidėja ~40 dienų (~63 dienos), lyginant su tikrojo ledo (be ledo) modelio rezultatais, tačiau šiaurinėje marių dalyje jis yra 5 dienomis (2 dienomis) mažesnis, dėl sumažėjusių vandens mainų tarp šiaurinės ir pietinės marių dalies. Bendras VUL po ledo danga Kuršių mariose per 11 metų modeliavimo laikotarpį yra apie 130 dienų, tai yra ~ 1,5 dienos ilgesnis, palyginti su teoriniu laikotarpiu be ledo (7 lentelė). Koreliacijos koeficientas tarp ledo sezono ilgio ir skirtingų vandens užsilaikymo skaičiavimo laikotarpių yra nuo 0,71 iki 0,84. Ledo dangos poveikio reikšmingumas vandens atsinaujinimui akyvaizdus, ypač po ilgų ir atšiaurių žiemų pietinėje marių dalyje, kur ledas išlieka ilgiausiai. Meteorologiniais

sezonais VUL šiek tiek skiriasi: ilgiausias – vasarą, dėl sumažėjusio vėjo greičio ir vandens srautų iš upių, o trumpiausias – pavasarį, tačiau bendra schema yra ta pati – didelės laiko vertės pietinėje marių dalyje, ypač pietvakarinėje jos pusėje, kur mažesnių upių nuotėkio duomenys nebuvo prieinami modeliavimo studijoms. Ilgiausias laikas stebimas ledo dangos sezono metu – vidutiniškai beveik dvigubai ilgesnis nei nesant ledui (10 pav.).

Suspenduotos nuosėdos. Dviejų modeliavimų rezultatų – su ledo danga ir be jos – palyginimas rodo, kad vidutinė suspenduotų nuosėdų koncentracija skiriasi atitinkamai nuo 1,5 ± 1,8 mg L^{-1} iki 2,8 ± 2,7 mg L^{-1}, o reikšmingas padidėjimas pastebėtas stiprių vėjų metu. Laiko eilutės rodo, kad ledo dangos įtaka gilesniame ir dumblėtame šiauriniame marių taške (1 pav., S1) pastebima tik esant labai stipriam rytų, pietryčių ar pietų vėjui (> 10 m s^{-1}), o seklesniame ir smėlingame taške (1 pav, S2) – jau esant > 6 m s^{-1} vėjui, pučiančiam iš pietvakarių į šiaurės vakarus. Tai rodo ledo svarbą blokuojant stiprių vėjų sukeltas bangas ir vandens mainų galimybes, dėl kurių vandens stulpe padidėja suspenduotų nuosėdų koncentracija.

Ledo storis

Ledo modelio kalibracija ir validacija. Skirtingi modelių nustatymo tipai parodė, kad $Pres_{\rho_s}$ duoda geresnius ledo storio prognozių rezultatus. Ledo termodinaminis modelis gana gerai apibūdina ledo storio raidą (11 pav.), trijų stočių vidutinis koreliacijos koeficientas yra 0.92 (8 lentelė). Priešinga situacija yra su ledo sezono trukme. Ledo modelis pervertina sezono trukmę vidutiniškai 1 mėn. dėl modelyje skaičiuojamo labai plono ledo, kuris realybėje yra labai judrus ir gali būti lengvai pernešamas vėjo tolėliau nuo matavimo stočių. Deja, modelio našumas tinkamai įvertinti sniego storio dinamiką nebuvo toks aukštas (R = 0,64), lyginant su ledo storiu.

Ledo storio pasiskirstymas marių plote. Dinaminio komponento trūkumas ledo modelyje tampa labai akyvaizdus atliekant skaičiavimus su integruotu ledo modeliu į hidrodinaminį modelį. Ledo sezono pradžioje ir pabaigoje, kai ledas yra labai plonas ir lengvai pernešamas vėjo, ledo modelis negali atkurti realių sąlygų, matomų nuotolinio stebėjimo vaizduose (12 pav.). Tačiau, kai oro temperatūra yra nuolat žema (13 pav.), leidžianti marioms greitai ir visiškai pasidengti ledu, ledo modelis yra tinkamas anlizuoti ledo storio kintamumą visame Kuršių marių paviršiuje. Tokiu atveju jis susidaro storesnis palei rytinę ir pietinę marių dalis. Ledas vakarų pakrantėje yra plonesnis (kaip matyti profilių grafikuose 13 pav.) dėl šiek tiek šiltesnės oro temperatūros, atkeliaujančios nuo Baltijos jūros pusės.

Ledo storio ateities prognozės. Modelio rezultatai rodo, kad vidutinis/maksimalus 9/20 cm ledo storis istoriniu laikotarpiu artimiausiu metu greičiausiai sumažės iki 6/15 cm ir 6/16 cm, o tai yra 30/25% ir 30/20% mažiau pagal ir scenarijus atitin-

kamai. Tolimoje ateityje vidutinis ledo storis tikėtina pasieks 4/9 cm ir 1/4 cm, o tai yra 60/55% ir 85/80% mažiau pagal $RCP4.5_{far}$ ir $RCP8.5_{far}$ scenarijus atitinkamai (14 pav.). Ledo sezono trukmė tikėtina sumažės ~15% artimoje ateityje pagal abu scenarijus lyginant su istoriniu periodu, t.y. nuo vidutiniškai 110 dienų artimiausioje ateityje ir 92 dienų (56 dienų) tolimesnėje ateityje pagal RCP4.5 (RCP8.5). Tačiau šias vertes reikia vertinti atsargiai, nes ledo modelis pervertina sezono trukmę, todėl labiau tikėtina, kad šie įverčiai bus bent ~30 dienų mažesni.

IŠVADOS

1. Pristatytas pirmasis išsamus erdvinis ledo dangos sąlygų pasiskirstymas Kuršių mariose tiriant nuotolinių tyrimų duomenis, davusius gerus rezultatus nustatant pagrindinius ledo fenologijos reiškinius (vidutinis palydovinių stebėjimų pranašumo rodiklis yra 63%), taip išryškinant šių duomenų naudojimo galimybę regioninėse ledo stebėjimo programose.

2. Ledas pradeda formuotis palei rytinę ir pietinę Kuršių marių kranto liniją, šiek tiek anksčiau pradedant šalti Nemuno deltos teritorijoje. Pastebėta, kad ledas vėliausiai susidaro giliausioje pietvakarinėje marių dalyje. Dėl oro temperatūros pakilimo kartais gali pasitaikyti keletas tirpimo reiškinių nuo pirmojo pastebėto visiško marių užšalimo iki paskutinio tirpimo užfiksavimo. Ledo danga pradeda irti šiaurinėje marių dalyje, tęsiasi palei vakarinę pakrantę ir dėl vyraujančių vakarinių vėjų lėtai traukiasi rytinės pakrantės link.

3. Didelės skiriamosios gebos ledo sezono trukmės žemėlapiai rodo didelį kintamumą per 15 metų laikotarpį, tačiau vidutiniškai ledas ilgiausiai užsilieka limniškoje pietinėje, pietrytinėje Kuršių marių dalyje, ypač palei rytinę pakrantę (įskaitant Nemuno deltą). Trumpiausias ledo sezonas pastebimas šiaurinėje marių dalyje dėl aktyvios vandens pernašos šioje vietoje ir druskingo vandens prietakos iš Baltijos jūros. Remiantis antžeminiais stebėjimais, vidutinė 15 metų ledo sezono trukmė yra 86 dienos. Derinant palydovinių ir *in situ* duomenų pranašumus, buvo pateikta pataisyta ledo sezono trukmė, padidinanti vidutinę sezono trukmę iki 89 dienų. Nors geriausias parametras, apibūdinantis ledo sezono kintamumą visoje marių teritorijoje, yra vidutinė erdvinė ledo sezono trukmė, kuri yra daug mažesnė – vidutiniškai 71 diena. Ledo sezono trukmė trumpėja 1,6–2,3 dienomis per metus, analizuojant 2002–2017 m. laikotarpį. Nors užšalimo pradžios ir visiško užšalimo datos mažai pasikeitė, paskutinio ledo tirpimo ir stebėjimo datos rodo aiškią ankstėjimo tendenciją – ledas anksčiau suskyla ir ištirpsta.

4. Ledo sezono trukmė yra glaudžiai susijusi su vyraujančia oro temperatūra, kuri kyla ir linksta į šiltesnes ir trumpesnes žiemas. Suminė neigiama oro temperatūra turi labai glaudų ryšį su vidutine erdvine ledo sezono trukme (R = -0,92), atskleidžiant

palydovinių duomenų privalumus lyginant su erdviškai apribotais *in situ* stebėjimais (R = -0,81). Kadangi regioninio klimato svyravimai yra glaudžiai susiję su Šiaurės Atlanto svyravimais (NAO), vidutinės erdvinės ledo sezono trukmės kintamumas yra daug artimesnis NAO žiemos indekso įrašams (R = 0,83) nei priekrančių stebėjimų (R = 0,71) arba *in situ* ir palydovinių duomenų kombinacijos (R = 0,73).

5. Skaitinio modeliavimo tyrimai atskleidė, kad ledo danga keičia vandens sūkurinių sistemų formavimąsi ir vietą Kuršių mariose. Vandens mainų galimybės taip pat sumažėja dėl sumažėjusios cirkuliacijos po ledu, ypač išilgai marių vidurio, kur slopinamas vėjo poveikis daro didesnę įtaką vandens judėjimui. Ledo danga sumažina druskingumą šiaurinėje marių dalyje, taip pat druskingo vandens prietakos atstumą ir laiką beveik 14 dienų per metus. Vandens užsilaikymo laikas pastebimai ilgėja po ilgų ledo dangos periodų. Tai ypač pastebima toliau nuo upių ištakų ir pietinėje marių dalyje, kur vėjas taip pat vaidina svarbų vaidmenį atnaujinant vandenį. Ledo danga ženkliai sumažina vidutinę suspenduotų nuosėdų koncentraciją. Tai ypač akivaizdu stiprių vėjų metu padidėjus dugno šlyties jėgoms. Jei ledo mariose nebūtų, bangos, kurias sukelia stiprus vėjas, ir padidėjusios vandens mainų galimybės, sukeltų aukštesnę suspenduotų nuosėdų koncentraciją vandens stulpe.

6. Pasiūlytas ledo termodinaminis modelis duoda patenkinamus ledo storio raidos Kuršių mariose rezultatus (vidurtinis R = 0,86, RMSE = 9 cm). Nors modelio rezultatų tikslumas priklauso nuo įvesties duomenų tikslumo, jis yra tinkamas kitoms modelio pritaikymo reikmėms. Tačiau bendra ledo sezono trukmė pervertinama vidutiniškai vienu mėnesiu dėl modelio rezultatuose matomo trumpų užšalimo epizodų, kurie nebuvo užfiksuoti pakrančių stotyse. Taigi į šį parametrą reikia atsižvelgti atsargiai. Be to, sujungta ledo ir hidrodinaminio modeliavimo sistema negali visiškai atspindėti tikrojo ledo dangos pasiskirstymo, kaip matyti nuotolinio stebėjimo vaizduose. Plono ledo susidarymo ar tirpimo metu vėjas turi ryškų vaidmenį lemiantį ledo pasiskirstymą. Kintant klimatui ir numatomam ledo plonėjimui, nepakaks imituoti ledo storio pasiskirstymą naudojant tik ledo termodinamiką modeliavimo sistemoje.

7. Ateities ledo storio prognozė, remiantis klimato kaitos scenarijais, rodo, kad maksimalus ledo storis (sezono ilgis) artimiausiu metu sumažės (sutrumpės) 20–25% (15%) artimoje ateityje ir 55–80% (30–57%) tolimoje ateityje, lyginant su istoriniu laikotarpiu. Numatoma ledo storio ir fenologinių parametrų mažėjimo tendencija paveiks ne tik vandens ekosistemą, bet ir žuvininkystę bei rekreacinę veiklą Kuršių mariose.

PUBLICATIONS

PAPER I

remote sensing

MDPI

Article

Remote Sensing of Ice Phenology and Dynamics of Europe's Largest Coastal Lagoon (The Curonian Lagoon)

Rasa Idzelytė [1,*], Igor E. Kozlov [1,2,3] and Georg Umgiesser [1,4]

1 Marine Research Institute, Klaipeda University, Universiteto ave. 17, LT-92294 Klaipeda, Lithuania
2 Satellite Oceanography Laboratory, Russian State Hydrometeorological University, Malookhtinsky Prosp., 98, 195196 Saint Petersburg, Russia
3 Natural Sciences Department, Klaipeda University, Herkaus Manto str. 84, LT-92294 Klaipeda, Lithuania
4 ISMAR-CNR, Institute of Marine Sciences, Arsenale—Tesa 104, Castello 2737/F, 30122 Venezia, Italy
* Correspondence: rasa.idzelyte@apc.ku.lt; Tel.: +370-6234-0360

Received: 8 July 2019; Accepted: 30 August 2019; Published: 2 September 2019

Abstract: A first-ever spatially detailed record of ice cover conditions in the Curonian Lagoon (CL), Europe's largest coastal lagoon located in the southeastern Baltic Sea, is presented. The multi-mission synthetic aperture radar (SAR) measurements acquired in 2002–2017 by Envisat ASAR, RADARSAT-2, Sentinel-1 A/B, and supplemented by the cloud-free moderate imaging spectroradiometer (MODIS) data, are used to document the ice cover properties in the CL. As shown, satellite observations reveal a better performance over in situ records in defining the key stages of ice formation and decay in the CL. Using advantages of both data sources, an updated ice season duration (ISD) record is obtained to adequately describe the ice cover season in the CL. High-resolution ISD maps provide important spatial details of ice growth and decay in the CL. As found, ice cover resides longest in the south-eastern CL and along the eastern coast, including the Nemunas Delta, while the shortest ice season is observed in the northern CL. During the melting season, the ice melt pattern is clearly shaped by the direction of prevailing winds, and ice drift velocities obtained from a limited number of observations range within 0.03–0.14 m/s. The pronounced shortening of the ice season duration in the CL is observed at a rate of 1.6–2.3 days year^{-1} during 2002–2017, which is much higher than reported for the nearby Baltic Sea regions. While the timing of the freeze onset and full freezing has not changed much, the dates of the final melt onset and last observation of ice have a clear decreasing pattern toward an earlier ice break-up and complete melt-off due to an increase of air temperature strongly linked to the North Atlantic Oscillation (NAO). Notably, the correlation between the ISD, air temperature, and winter NAO index is substantially higher when considering the lagoon-averaged ISD values derived from satellite observations compared to those derived from coastal records. The latter clearly demonstrated the richness of the satellite observations that should definitely be exploited in regional ice monitoring programs.

Keywords: ice cover; remote sensing; synthetic aperture radar (SAR); mapping; ice drift; Curonian Lagoon; NAO; climate change

1. Introduction

Ice cover is a natural barrier between the water and atmosphere. It is of great importance to the hydrodynamic and biogeochemical processes in all seasonally ice-covered water bodies as it significantly alters the sea level oscillations, transfer of momentum and heat, and gas exchange with the atmosphere. In the shallow coastal waters, like semi-enclosed bays or estuarine lagoons, ice

formation occurs very rapidly and any small changes in the ice regime clearly reflect the changes in the regional climate.

Nowadays, many studies of ice conditions are focused on polar oceans because long-term changes in the Arctic and Antarctic sea ice play an important role in the global climate [1,2]. Nonetheless, ice phenology records from lakes in the Northern Hemisphere also show a dramatic evidence of the warming climate and more frequent extreme events. However, rates of ice cover loss are not the same in all places [3,4] with the shift in timing of the ice freeze-up and break-up, and shortening of the ice season serving as key indicators of ongoing changes [5].

In the Baltic Sea, the ice cover phenology is also an important aspect for marine traffic, which makes investigation of the current and future trends of sea ice conditions very important for the economies of its nine surrounding countries [6–8]. The annual ice cover extent in the Baltic Sea is highly variable and there are numerous studies describing its characteristics [9–11]. Some of these works make use of the satellite remote sensing, in particular measurements taken by synthetic aperture radars (SARs), to infer various aspects of the sea ice regime over the Baltic Sea, including the retrieval of different sea ice types [12], operational SAR-based monitoring of the ice drift [13], estimates of ice concentration and thickness [14,15], degree of ice ridging [16], etc. Indeed, SAR appears to be the most suitable remote sensing instrument for this purpose [17], as it is able to operate under all weather conditions independently of daylight, has a high spatial resolution order of 10–100 m, and swath widths of 100–500 km, large enough to observe regional and local variations of the ice cover state [18].

The Curonian Lagoon is the largest coastal lagoon in Europe with high nutrient loadings from the surrounding rivers [19], thus it is a highly eutrophic water body. Not mentioning the obvious ice cover implications on the hydrodynamic processes (water residence time [20], mixing, etc.), it has a considerable impact on the ecological status of the entire lagoon. For example, a shorter ice season duration (ISD) can lead to earlier spring phytoplankton blooms [21,22] and, hence, induce the dissolved oxygen (DO) depletion. In turn, a longer ISD can lead to lowering the under-ice DO concentration due to the decay of the organic matter [23]. The ice season duration plays a major role in the tourism sector too. During wintertime, the Curonian Lagoon becomes famous for ice fishing, being, however, a dangerous leisure, since strong winds can break off the ice fields and drift them away from the shore together with the fishermen. With the changing climate resulting in warmer weather and more unstable ice cover, such incidents might increase in the future and require detailed information on the ice cover to plan rapid rescue missions.

In the south-eastern Baltic (SEB), where the Curonian Lagoon (CL) is located, spaceborne SAR observations have been already used before to study the coastal upwelling and its environmental implications [24,25], monitoring of cyanobacteria blooms [26], and short-term mapping of ice conditions for planning potential zebra mussel farms [27]. However, the comprehensive use of spaceborne SAR data for detailed analysis of ice conditions in the Curonian Lagoon and the SEB is still lacking. The attention of local researches was primarily focused on studying the ice phenology in rivers and lakes [28,29], and observations and prediction of ice jams in the larger rivers [30,31]. Existing studies of ice conditions in the SEB and in the CL are not comprehensive, because they still rely on conventional in situ records based, for the most part, on the spatially-limited visual observations made at several coastal stations [32–34]. Some other studies [20,35] have considered the recent changes in the CL hydrology and water renewal with only modest links to its ice regime. Lastly, the authors of [34] used different statistical models in the attempt to predict the ice cover formation in the CL based on observational data. They concluded that the available in situ measurements are sparse and irregular, and do not describe the ice conditions over the entire lagoon, pointing out that an additional spatially-detailed information about the ice regime is critical to solve this task.

The aim of this study is, therefore, to use high-resolution multi-mission SAR observations, supplemented with cloud-free visible-band MODIS data, to reveal, for the first time, detailed spatial and temporal characteristics of ice cover properties in the Curonian Lagoon during a 15-year period in 2002–2017.

Remote Sens. **2019**, *11*, 2059

2. Study Area

The Curonian Lagoon (Figure 1) is a large estuarine coastal freshwater body with an area of approximately 1586 km^2 and a volume of 6.3 km^3. The lagoon is relatively shallow with a mean depth of approximately 3.8 m, the greatest natural depth of 5.8 m, and artificially deepened in the Klaipėda Strait (the only lagoon outlet) to a depth of up to 16 m [36,37]. It is an open system, influenced by the saline water from the Baltic Sea and discharge of the fresh water from the Nemunas River and other smaller rivers. Every year the rivers carry the amount of fresh water about four times the lagoon volume, thus it is the main water renewal source for the lagoon [20]. The southern and central parts of the lagoon are considered to be fresh since the average annual water salinity is less than 0.5‰. The Klaipėda Strait located in the northern CL has an annual average water salinity of around 3‰–5.5‰ due to the water intrusion from the Baltic Sea having an average salinity of 7‰, and decreases toward the south [38].

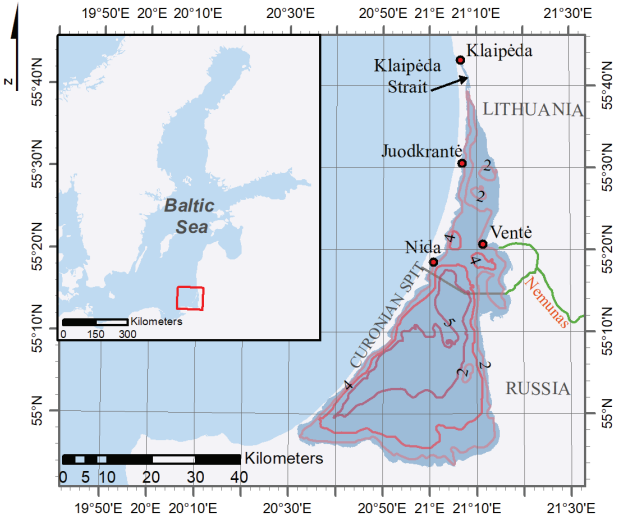

Figure 1. Location of the study area–the Curonian Lagoon, with respect to the Baltic Sea. The red frame in the smaller map shows the location of the lagoon in the southeastern part of the Baltic Sea, while the red points indicate the locations of the coastal stations. The contour lines inside the lagoon indicate the bathymetry.

A historical study of ice observational data done by [32] shows that a 10–70 cm thick ice cover is forming every year in the lagoon. As described, the ice cover usually forms in the beginning of December, and the lagoon is completely frozen about 12 days after the freeze onset. The northern part of the lagoon usually freezes later due to the influence of saline seawater and inflow from the Nemunas River basin. In spring, the ice break-up starts on average in the end of March in the northern part of the lagoon, and in the Nemunas Delta. The ice completely melts within 6–13 days after the melt onset. The average length of the ice season is reported to be 110 days (minimum—12 days, maximum—169 days) with the ice cover thickness varying throughout the winter season. The ice cover usually forms and disintegrates two or more times during the season [39].

Due to the climate change and projected air temperature increase, winters are expected to get warmer thus the ice cover period in the lagoon will get shorter leading to the increased probability of thaws and even more unstable ice cover [5,40]. This can already be observed in Nida (a station in the western part of the lagoon), where the number of days with ice phenomena decreased by 50%,

comparing the periods of 1961–1975 and 1991–2005 [33,41]. However, this and the above-mentioned historical studies are based on solely point-wise observational data, lacking the overall view of the entire lagoon surface.

3. Materials and Methods

3.1. Satellite Data

In this study, the ice cover in the Curonian Lagoon is investigated in the period between 2002 and 2017 (15 winters in total). Satellite data were the C-band (~5.6 cm) synthetic aperture radar measurements from three Earth observation missions: Envisat Advanced SAR (ASAR), RADARSAT-2, and Sentinel-1A and 1B. ASAR operating in a wide swath mode has a 400 km by 400 km image with a spatial resolution of 150 m by 150 m, at a VV or HH polarization. After 10 years of service, Envisat finished its mission on 8 April 2012. As a result, there was a two-year gap in the SAR data prior to the planned launch of the Sentinel-1A on 3 April 2014. Fortunately, the Earth observation (EO) data from commercial satellite missions was made available during that period under the COPERNICUS program of the European Union and European Space Agency (ESA). The data used for this period was taken from the DWH_MG1_CORE_11 dataset and consisted of observations from the RADARSAT-2 mission, operating in a ScanSAR Wide Beam mode with a 500 km swath size, a dual polarization (HH and HV), and a spatial resolution of 100 m by 100 m. The Sentinel-1A and 1B operating in an interferometric wide swath and extra-wide swath modes provide higher resolution (see Table 1) dual polarized images with a swath width of 250 km and 400 km, respectively. The revisit time for each of the above satellites is 12 days. The Sentinel-1B was launched almost two years later after the Sentinel-1A. With both satellites operating, the repeat cycle over the study site is six days. In this study, we also make use of the visible band 250 m resolution imagery from the moderate resolution imaging spectroradiometer (MODIS) on board the Terra satellite. These data were used to determine the ice extent in the Curonian Lagoon for the cloud-free days when the frequency of available SAR images was low. The summary of the actual satellite data analyzed in this study is given in Table 2.

Table 1. The list and technical characteristics of Earth observation (EO) missions used for the analysis of the ice cover in the Curonian Lagoon. Colors mark specific data sets used during the study period and shown at the bottom of the table, the underlying red lines indicate the available moderate resolution imaging spectroradiometer (MODIS) images.

Mission	Image Mode	Resolution (m)	Pixel Spacing (m)	Swath Width (km)	Data Coverage
Envisat Advanced SAR (ASAR)	Wide swath mode (WSM)	150 × 150	75 × 75	400	2002–2012 April
RADARSAT-2	ScanSAR	100 × 100	50 × 50	500	2012–2014 April
Sentinel-1A	Interferometric Wide swath (IW High) Extra-Wide swath (EW Medium)	5 × 20, 93 × 87	10 × 10, 40 × 40	250 400	November 2014–2017
Sentinel-1B	Interferometric Wide swath (IW High) Extra-Wide swath (EW Medium)	5 × 20, 93 × 87	10 × 10, 40 × 40	250 400	December 2016–2017
MODIS		250 × 250	250	2330	2002–2007, 2014–2017

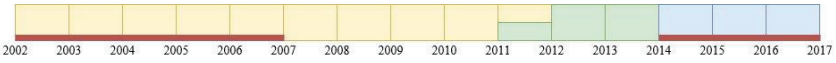

Overall, 514 SAR images were processed during the study (see Table 2). This number consists of both full and partial views of the Curonian Lagoon. The mean frequency of the ASAR observations

was about 1–3 images per week with an average interval between the consecutive images of three days. Yet, sometimes two ASAR images were available per day. The frequency of the RADARSAT-2 observations was higher with the average interval equal to two days–the highest frequency among all single SAR sensors. The dataset of winter 2011–2012 consists of both ASAR and RADARSAT-2 images (Table 1) resulting in the increased number of observations with the shortest interval between the images equal to 1.4 days. In contrast, the frequency of the Sentinel-1A was only 1–2.5 images per week with an average interval of 2.8 days similar to the ASAR. Combined with the Sentinel–1B, it increased up to 2–3 images per week with an average interval of 2.6 days for the winter 2016–2017. Despite only 2–3 SAR images per week were available on average, this was still enough to observe the ice cover dynamics in the CL quite well. However, when the data gap between the SAR images was more than three days, the cloud-free visible-band MODIS images were additionally considered (overall 101 images, Table 2).

Table 2. Summary of the processed satellite data and ice season duration (ISD). D_{SAR} is a maximum value of the ISD, $\overline{D}_{SAR}$ —spatial-mean ISD, D_{st} —maximum value of the ISD observed at the coastal stations, and D_{corr} is a corrected ISD, T_a^{CN} is a cumulative negative air temperature.

Year	Image Count (+MODIS)	SAR Images per Week (with MODIS)	D_{SAR} [days]	$\overline{D}_{SAR}$ [days]	D_{st} [days]	D_{corr} [days]	T_a^{CN} [°C]
2002–2003	14(+ 34)	0–2(1–5)	118	113	123	123	−591.9
2003–2004	12(+ 14)	0–3(0–5)	88	72	86	90	−284.7
2004–2005	31(+ 15)	1–3(2–8)	72	64	74	74	−248.4
2005–2006	51(+ 15)	1–3(1–7)	138	113	136	138	−586.8
2006–2007	20(+ 5)	1–4(2–4)	48	39	50	51	−169.4
2007–2008	17(+ 5)	2–3	45	22	47	47	−46.0
2008–2009	50	1–3	94	76	84	94	−170.3
2009–2010	53	2–3	112	105	107	114	−561.7
2010–2011	55	1–3	134	116	127	134	−497.0
2011–2012	46	2–4	64	52	63	65	−346.0
2012–2013	56	1–3	125	115	127	129	−483.1
2013–2014	32	2–3	57	50	57	57	−214.0
2014–2015	27(+ 5)	1–2(1–4)	93	41	94	95	−42.5
2015–2016	26(+ 5)	1–2(1–5)	55	37	53	58	−185.5
2016–2017	24(+ 3)	2–3(2–4)	63	49	60	63	−145.0

3.2. Ground Observations

The ice thickness and ice cover area in the Curonian Lagoon are being measured since the second half of the 20th century. Since 1992, the lagoon is monitored by the Marine Research Department of the Environment Protection Agency of Lithuania, and since 1993 the observations are carried out only in the economic zone of Lithuania [42]. Up to 2011 there were four ground stations in the Curonian Lagoon (in the Klaipėda Strait, Juodkrantė, Nida, and Ventė, see Figure 1) that measured the ice formation stages, coverage, state, density, thickness, and drift. The observations were taken once per day using a scale from zero (no ice) to 10 (fully ice-covered). Currently, the ice thickness measurements are carried out only at two stations in Ventė and Nida. The data on the ice properties and air temperature used in this work were provided by the Marine Research Department of the Environmental Protection Agency of Lithuania.

3.3. Methods of Data Analysis

SAR is an active microwave device, which emits its own microwave signal and then records the amplitude and phase of the return signal scattered back from the ice or sea surface. The level of the backscatter depends on the surface roughness, dielectric properties of the medium, and the incidence angle of the radar signal. An object with a higher surface roughness produces a stronger radar backscatter and appears bright in the SAR images and vice versa. The strength of the backscatter is also governed by the media dielectric constant. Water has higher dielectric constant compared to ice, and most of the radar signal is reflected at the very water surface. For the ice, radio waves can penetrate to some depth depending on the radar frequency, incidence angle, temperature, and conductivity that, in turn, depends on salinity [43]. The low salinity ice, i.e., freshwater or multiyear ice, has a larger penetration depth of the radar signal resulting in a volume scattering and an overall higher backscatter as compared to the new or first year ice that has higher salinity and lower porosity.

Although the sea ice, snow cover on top of it, and open water, all have different levels of signal backscatter, the ice edge can still be distinguished from the open water rather effectively [18,44]. The main factor influencing the determination of the ice edge in the SAR images is wind. During the freezing/melting periods, the ice can appear as very dark slick-like zones due to the grease ice dampening the short wind waves. Further, the ice edge can be compact or diffused depending on the wind direction. When considering matured ice, the level of the backscatter highly depends on the wind speed. If the wind is low, the ice will have a stronger backscatter (especially if it has a rough surface). When the wind is moderate to high, the open water zones will be covered by intensive wave breaking in addition to the resonant scattering from the Bragg waves, making the backscatter similar to or higher than that of ice. Nevertheless, it is still possible to distinguish the two using an experienced specialist [43].

Since the ice cover extent can be identified in the SAR data visually [45] and the Curonian Lagoon is not a very large water body, we use a visual identification of the ice-open water boundary in this work. Firstly, the subset of every image taken over the lagoon area was created to minimize the computational loads. Then, for every SAR image, the range-Doppler terrain correction was applied. The received outcome of the SAR and MODIS images was exported to the GeoTIFF format for further processing in the ArcGIS software, where ice polygons were manually digitized. Next, the ice polygons for a given winter season were converted to a raster format and summed up using the cell statistics function of the ArcGIS software by considering the time intervals between the consecutive satellite observations. As a result, spatially detailed maps of the ice season duration (ISD) were obtained for every winter season during the study period. Based on these spatial ISD maps, a maximum value of the ice season duration, D_{SAR}, and a spatial-mean (averaged over the lagoon area), $\overline{D}_{SAR}$, were defined for every winter season. The analyzed 15 winter seasons were then classified into three categories using the spatially-mean ISD values: Short ($\overline{D}_{SAR} < 50$ days), intermediate (50 days $\leq \overline{D}_{SAR} \leq 100$ days), and long winters ($\overline{D}_{SAR} > 100$ days).

In addition to ISD, the dates of the ice freeze onset (FO), full freezing (FF), melt onset (MO), and last observation of ice (LOI) were defined. An inter-annual variability of these characteristics was then analyzed with the statistical significance of linear trends determined by the Mann–Kendall test (also called Kendall's tau; [46–48]) at a 0.05 significance level with a 95% confidence level. This nonparametric test is insensitive to outliers contrary to the parametric test [49]. In the test, the null hypothesis is tested, which states that there is no trend in the data series, and the alternative hypothesis, that the trend exists. The trend significance was calculated in Excel using the XLSTAT statistical software (www.xlstat.com). As has been already proven in the literature, the Mann–Kendall test is an appropriate method to test the significance of trends in the 'ice freeze/melt onset, ice thickness, season duration, and air temperature [49–53].

In order to determine the dependency of changes in the ice season duration on the intensity of the North Atlantic Oscillation (NAO), the correlation coefficient between the ice cover duration and

Hurrell's winter (December through March) NAO_{DJFM} index was calculated. The NAO data were obtained from the Climate Analysis Section, NCAR, Boulder, USA [54].

For the comparison of the ice cover extent detected from the satellite data and measured in situ we used observations from the three coastal stations in Nida, Ventė, and Juodkrantė until 2011, and from Nida and Ventė onwards. Measurements from the Port of Klaipėda located in Klaipėda Strait (see Figure 1) were not included, since the full ice cover is not forming in this area due to higher water depths, inflow of warmer and more saline water from the Baltic Sea, and active ship navigation. Satellite data were compared against the ground observations by considering the ice concentration in circular buffers centered around the ground station. The radius of each buffer was set to the visibility value recorded on each day during the time when the ice observations were taken. Since the stations are located onshore, a part of each buffer contained land that was removed during the analysis. The calculations were done by running the custom python script in the ArcGIS software.

For the observational records from coastal stations, the dates of FO, FF, MO, LOI, as well as ISD (D_{st}) were also derived. The dates of FO, MO, and LOI were defined when a given ice stage was observed at least at one coastal station. Exceptions were the sporadic days of short ice formation before the continuous ice cover season when defining the FO date. The FF date was defined when the ice cover was observed at all stations. These values were then compared to those obtained from the satellite data, and the difference between them was evaluated in a number of days.

The air temperature measurements were taken at the same time the ice observations were done in the coastal stations. A correlation between the ISDs derived from the satellite data and cumulative negative air temperature, hereinafter T_a^{CN}, derived from the coastal records is then used to better understand the ice cover properties in the Curonian Lagoon.

4. Results

In this section we first present the results of the comparison of satellite observations with the in situ records made at the coastal stations. Next, a general description of the ice cover conditions in 2002–2017 is provided with an emphasis on the most important features observed during the various winter seasons. Lastly, a detailed description of the spatial ice cover properties, some peculiarities of the ice formation and decay during the freezing and melting seasons, as well as the ice season duration in the Curonian Lagoon is presented and discussed.

4.1. Satellite versus Coastal Observations

Comparison of the remotely sensed ice cover extent in the circular buffers around the coastal stations with that defined from the in situ observations shows a great similarity between these two properties with a correlation coefficient of R = 0.92. However, some inconsistencies arise during the melting period due to the limited visibility of coastal observations and a much wider spatial coverage of the satellite sensors, providing a better view of the ice cover extent over the Curonian Lagoon. Further, ice can be observed in several types at the coastal stations: Slush, frazil, grease, broken, fast ice, etc. However, in this study, all these ice types are not distinguished from the satellite images, but are considered either as an ice-free (zero) or fully ice-covered (10) pixels. Moreover, the ground observations consist of two different values for the landfast ice and drifting ice fields both scaled from zero to 10. During the melting period, the ice types will gradually receive lower ice type values, contrary to processing of the satellite images, where the ice pixels over the specified buffer area would get just a constant value equal to the pixel full of ice. In some cases, when the ice cover is thin or has a low concentration it cannot be effectively detected in the SAR images. While there are methods to retrieve the ice concentration [14,55] and different ice types [56–58] from the SAR images, they were not applied here, as our main purpose is primarily to examine the spatial extent and interannual variability of the ice season duration in the Curonian Lagoon. Given that each of the methods has its own pros and cons, it seems to be very practical to assess the performance of satellite retrievals compared to standard coastal observations in defining the timing of key stages of the ice formation in the Curonian Lagoon.

The dates of the freeze onset (FO), full freezing (FF), melt onset (MO), last observation of ice cover (LOI), and ice season duration (ISD) were compared between the coastal records (T_c) and satellite observations (T_{sat}) for every winter season, and the time difference (in the amount of days) between them (T_d) was defined as $T_d = T_c - T_{sat}$ and plotted in Figure 2. Below we also present a measure of a 'success rate' of satellite observations (SSR) defined here as a ratio of the number of times the FO, MO (FF, LOI, ISD) dates were observed earlier (later/longer for ISD) in the satellite data compared to the ground stations, and a total number of all non-zero differences (Table 3). Here, we assume that positive (negative) differences for the FO, MO (FF, LOI, ISD) dates shown in Figure 2 and Table 3 mean that satellite observations have a better performance over the in situ records. The winter of 2014–2015 was excluded from the FF and MO analysis, because these dates could not be identified from the in situ data due to the very unstable ice cover conditions during that year.

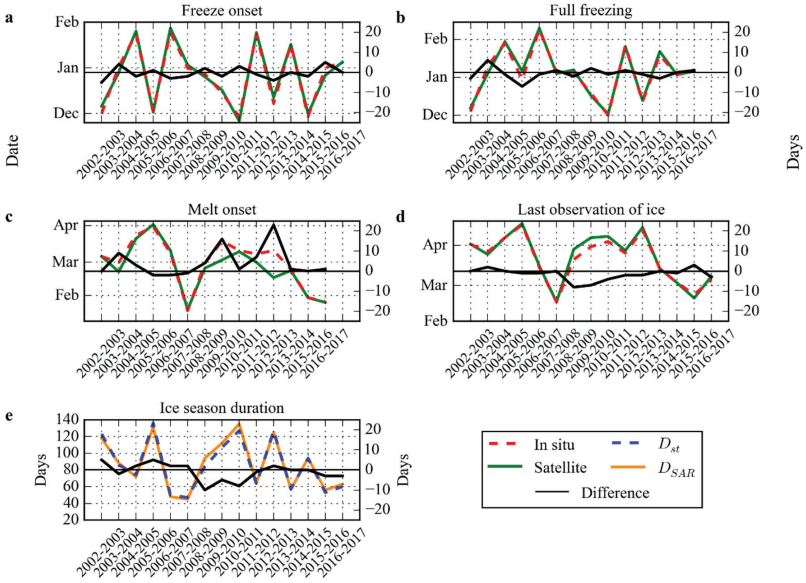

Figure 2. Intercomparison of the (**a**) freeze onset (FO), (**b**) full freezing (FF), (**c**) melt onset (MO), (**d**) last observation of ice cover (LOI) dates, and (**e**) ice season duration (D_{st} and D_{SAR}) derived from the satellite observations (solid lines) and in situ records (dashed lines), and the time difference between them (black solid line).

The mean FO date for the period of 2002–2017 as derived from the satellite observations is 27 December, being one day later than that derived from the coastal records, 26 December. The mean time difference in defining the FO between the coastal records and satellite observations is just half a day, and the sum of all differences during 2002–2017 is $\sum T_d^{FO} = -6$ days (Table 3), meaning that the very first signatures of the ice formation are more often observed at the coastal stations and a little later in the satellite images. This is often caused by a fast ice freezing in the CL occurring within just 1–2 days and a relatively low frequency of satellite observations during the FO phase. Nevertheless, satellite observations allowed defining the FO date earlier than at the coastal stations in 38% of the cases (see Figure 2a and Table 3).

For the FF date, the performance of satellite observations is somewhat better than that of the in situ records (Figure 2b). The mean FF date observed in the satellite images is 4 January, the same as for the coastal stations (Table 3). The mean time difference between the ground observations and satellite

data for the FF date is −0.62 days and the sum of all differences is also negative, $\sum T_d^{FF} = -8$ days, i.e., in 62% of the cases FF is recorded at the coastal stations when the open water regions still exist in the lagoon and are clearly seen in the satellite data.

Table 3. Statistics in defining the timing of the key stages of the ice formation in the Curonian Lagoon from the satellite observations and coastal records.

	FO	FF	MO	LOI	ISD
Date from in situ	26 December	4 January	1 March	21 March	86
Date from satellite data	27 December	4 January	24 February	23 March	87
Average difference (days)	−0.46	−0.62	5	−2.18	−1.29
Sum of all differences (days)	−6	−8	60	−24	−18
Max difference (days)	−5/5	−7	23	−8	−10
Satellite success rate (SSR)	**38%**	**62%**	**75%**	**82%**	**57%**
	Mean SSR				**63%**

The largest differences (up to 23 days) between the satellite and coastal observations are found when defining the melt onset date (Figure 2c). Here, the satellite data are three times more effective than the coastal records (SSR = 75%) with the MO usually detected five days earlier than at the coastal stations (Table 3). The sum of all the differences $\sum T_d^{MO} = 60$ days, which results from the ice break-up first occurring far away from the coastal stations and, hence, not recorded there. The average MO date is observed in the satellite images on 24 February, while at the coastal stations it is recorded on 1 March. The maximum difference when defining the MO date was observed in the winter of 2012–2013, when the satellite detected the melt onset in the northern part of the lagoon 23 days prior to its detection from the coast (Figure 2). This example illustrates quite well the spatial capability of the satellite data to cover the entire lagoon at once.

The satellite observations also show that the last ice traces survive on average two days longer than it is recorded at the coastal stations, i.e., the average satellite LOI date is 23 March, while the coastal records indicate it a day earlier on 21 March (Table 3). The sum of all the differences $\sum T_d^{LOI} = -24$ days, meaning that quite often there is still some ice left in the lagoon and not detected at the coastal stations. The satellite success rate for deriving the LOI date is 82% (Table 3), clearly emphasizing the role of the satellite observations to provide an unabridged record of the ice season duration.

When considering the ISD, satellite data show a four-day (mean value) longer ice season in 57% of the cases (eight out of 14 non-zero differences), which is thanks to their wide coverage and ability to observe the ice cover far from the coastal stations, especially during the melting season. The difference in the ISD between the coastal and satellite observations varies from year to year (Figure 2e) with $\sum T_d^{ISD} = -18$ days, meaning that the longer ISDs derived from the satellite data clearly dominate in the record with the average difference equal to 1.29 days (Table 3).

To summarize, the mean success rate of the satellite observations is 63% for all five parameters listed in Table 3. Apart from the FO dates, satellite data have a better performance over the in situ records in defining the key stages of the ice formation in the Curonian Lagoon and should be definitely exploited in the ice monitoring programs. A comparison between the coastal and satellite observations for the FO and LOI dates allows using the advantages of both data sources and establishing a corrected ISD value, D_{corr} (Table 2), that includes the earlier FO dates typically observed at the coastal stations and later the LOI dates usually registered from the satellite observations. As obtained, the updated ISD record is longer than the original in situ-based by 1–10 days in 73% of the cases with the average difference of three days. D_{corr} is then the most adequate record to describe the overall length of the ice cover season in the CL, but it does not account for the spatial ice cover inhomogeneities occurring during a particular winter. The ISD of such kind obtained from averaging the spatial ice cover maps derived from the satellite observations for a given winter season will be presented in Section 4.3 below.

4.2. Ice Cover Conditions in The Curonian Lagoon During 2002–2017

In this section, we will shortly describe some peculiar features of ice cover conditions in the Curonian Lagoon between 2002 and 2017. Although the Klaipėda Strait is considered to be ice free in this study, this area is covered by ice for some short periods, e.g., when the drifting ice is flowing out from the lagoon to the Baltic Sea (Figure 3).

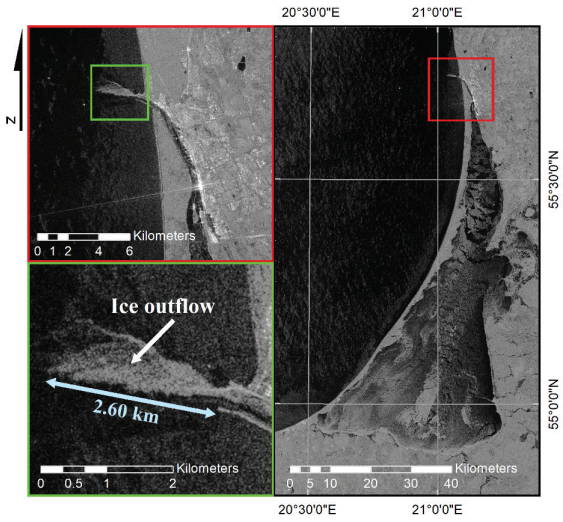

Figure 3. Sentinel-1B image of ice outflow from the Curonian Lagoon to the Baltic Sea (taken on the January 6 2017). The light blue arrow indicates the magnitude of the ice outflow from the port gates.

The SAR dataset of winter of 2002–2003 is relatively sparse. The first image received on 7 December shows the lagoon completely covered by ice, and this state lasts for nearly three months until 18 March 2003, when the ice cover starts to retreat along the eastern shoreline in the northern part of the lagoon. However, the gap between the SAR image of 18 March and a previous one is almost one month, and the date of the melting onset cannot be evaluated properly from the SAR images alone. Fortunately, there were a few cloud-free MODIS images during this period that show a start of the ice melt in the north-western part of the lagoon led by prevailing northwesterly wind of 4–5 m/s (Figure 4). Coastal records show that the winter of 2002–2003 is characterized by low air temperatures dropping down to −25.7 °C, and the cumulative negative air temperature has a record lowest value, $T_a^{CN} = -591.9$ °C. The ice season duration for the winter of 2002–2003 is also one of the longest during the study period—123 days (Table 2). It is much shorter for the next winter of 2003–2004—90 days, as it started 20 days later and the T_a^{CN} is twice as small than that of the previous winter (Table 2).

The winter of 2004–2005 has a better data coverage with a high number of full views of the lagoon. The ice formation starts quite late on 27 January 2005 and is observed all over the lagoon apart from its southwestern part. The final melting stage occurs very rapidly—the southern part of the lagoon is fully ice-covered on 4 April, while it becomes almost entirely ice-free on 7 April apart from a few drifting ice floes. The 4th of April is notable of having two consecutive SAR images acquired nearly 12 h apart showing clear signatures of the two drifting ice floes (Figures 5a,b, and 6a). The linear distances between the polygon centroids of these ice floes are 5730 m (A1-B1) and 2590 m (A2-B2) that translates to the ice drift velocities of 0.14 m/s and 0.06 m/s, correspondingly. The smaller ice floe (A2, shown in yellow in Figure 6a) drifts westward along the wind direction together with a freshwater outflow current from the Nemunas River. Its movement is accompanied by a slight clockwise rotation

and breakage of its upper right corner when passing the Ventė Cape (Figure 5b). The larger ice floe (A1 shown in red in Figure 6a) is also directed along the freshwater current that goes northward in this location, and thaws along its northern border while flowing northeast (Figure 5b).

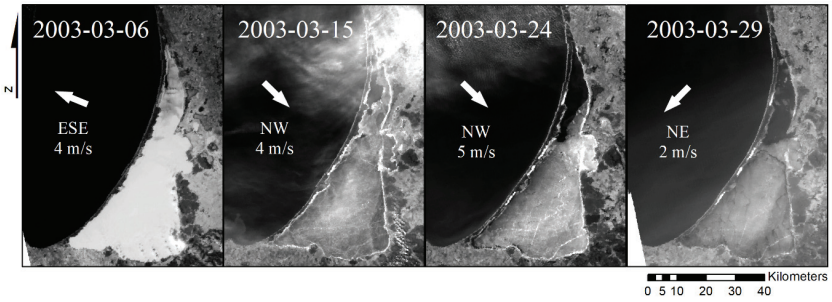

Figure 4. MODIS images of the ice cover retreat in the northern Curonian Lagoon during the winter of 2002–2003. Labels and arrows indicate the wind speed and direction.

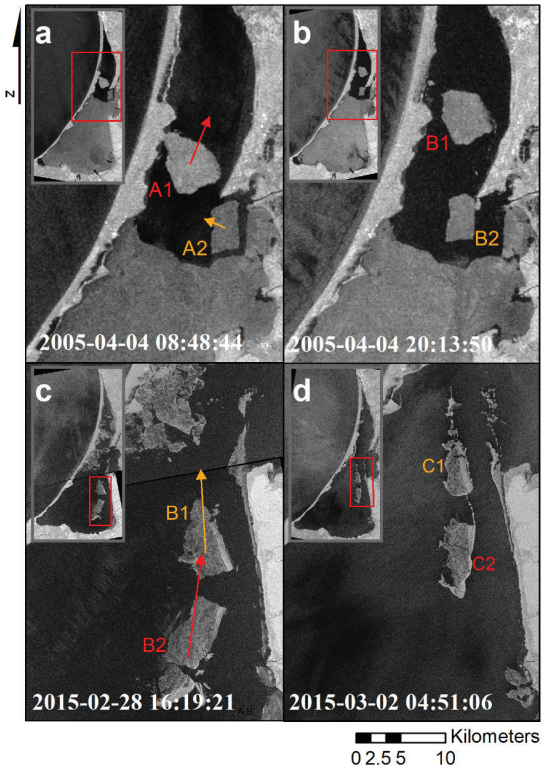

Figure 5. Examples of the ice drift in the Curonian Lagoon observed in the SAR images. Envisat ASAR images of the two ice floes in the Lithuanian part of the Curonian Lagoon taken on 4 April 2005 at 8:48:44 UTC (**a**) and at 20:13:50 UTC (**b**). Sentinel-1A images of the ice floes in the Russian part of the lagoon acquired on 28 February 2015 at 16:19:21 UTC (**c**) and 2 March at 04:51:06 UTC (**d**).

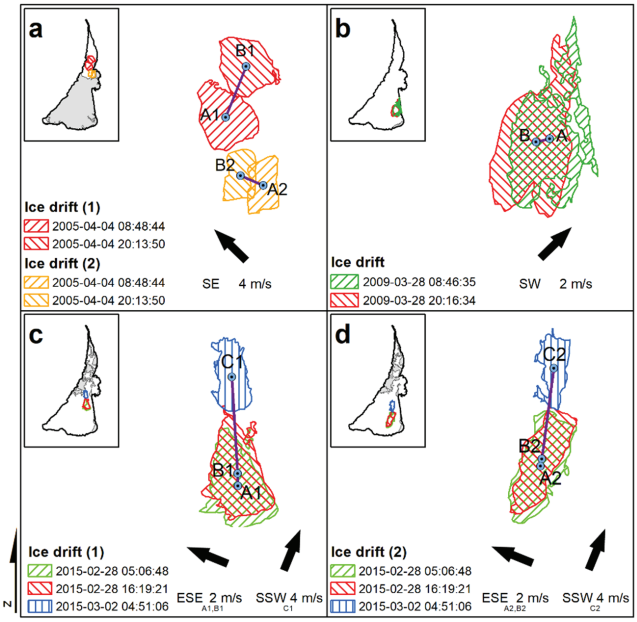

Figure 6. SAR-derived parameters of the ice drift in the Curonian Lagoon. (**a**) Drift of two ice floes observed on 4 April 2005; (**b**) drift of an ice floe on 28 March 2009; (**c**) drift of the first ice floe on 28 February and 2 March 2015; (**d**) drift of the second ice floe on 28 February and 2 March 2015. Labeled points indicate the polygon centroids, lines represent the linear distance between them, and the arrows indicate an average wind speed and direction.

The ice season duration for the winter of 2005–2006 is the longest throughout the study period, D_{corr} = 138 days, while the spatially-mean ISD is somewhat smaller, $\overline{D}_{SAR}$ = 113 days, which accounts for multiple melting periods during the season. The cumulative negative air temperature for this season is the second lowest with $T_a^{CN} = -586.8$ °C.

The ISD values in 2006–2007 and 2007–2008 are the shortest during the entire study period, lasting for 51 and 47 days, respectively (Table 2). Nonetheless, the full ice cover is still able to form during such a relatively short period. The winter of 2007–2008 has a very pronounced decrease of air temperature in the beginning of the season when T_a drops from 1 °C down to −11.8 °C between 29 December 2007 and 5 January 2008 (Figure 7). Full freezing of the lagoon is recorded on 4 January 2008, while in a few days the air temperature rises again above zero. The ice break-up and final melting starts on 20 January 2008 lasting for 28 days out of 47 days of the total ice season duration. The last ice traces are observed on 15 February 2008. The cumulative negative air temperature for this season is only $T_a^{CN} = -46$ °C, while the spatially-mean ice season duration, $\overline{D}_{SAR}$, is only 22 days—record low values over the entire study period.

The duration of the ice cover period during the winter of 2008–2009 increases two times as compared to the previous season due to longer periods of negative air temperatures, $T_a^{CN} = -170.3$. The freeze-up starts on the eastern side and eventually covers the entire lagoon. The melting starts from the northern part, spreading to the south-west. In the last two SAR images taken on the 28 March with the time difference of 11.5 h, the drifting ice floe can be observed (Figure 6b). The linear distance between the polygon centroids is 1140 m that equals to the mean ice drift velocity of 0.03 m/s. The observed temporal changes of the ice extent during this season correspond quite well to the air temperature variations measured at the coastal stations.

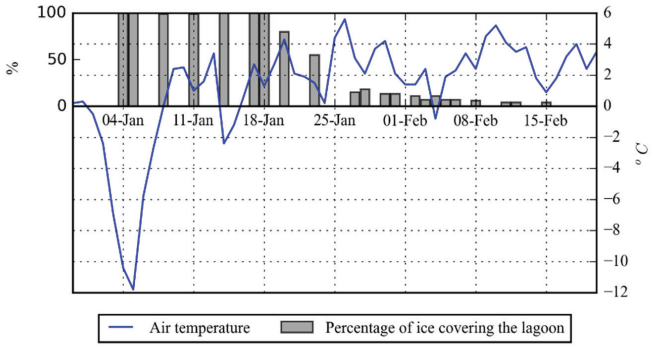

Figure 7. Variations of the average air temperature (blue line) and percentage of the ice cover (gray bars) in the Curonian Lagoon during the shortest winter season of 2007–2008.

The winter seasons of 2009–2010 and 2010–2011 are remarkable for having long ice season duration values, 114 and 134 days (Table 2). The winter of 2010–2011 also has the earliest start of the ice season dated on 26 November 2010. The thermal conditions between these two winters are somewhat similar, yet the winter of 2009–2010 is slightly colder than that of 2010–2011 with the T_a^{CN} values of −561.7 °C and −497.0 °C, respectively.

The ice season duration in 2011–2012 is more than twice shorter than that of the previous winter (65 days) and has a very late start at the end of January 2011. Nevertheless, the lagoon has frozen quite rapidly and remained such for more than a month due to the very low air temperatures dropping down to −23 °C (T_a^{CN} = −346.02 °C). The high temporal resolution of the SAR images of the lagoon allows observing how graciously the ice retreats from the western shoreline to the eastern one, and then finally disappears in the southeastern corner (Figure 8). As one may note, the ice melt direction and its overall pattern are clearly shaped by the direction of the prevailing moderate-to-strong westerly and northwesterly winds. The duration of the melting period is similar to the previous years and lasts about 28 days.

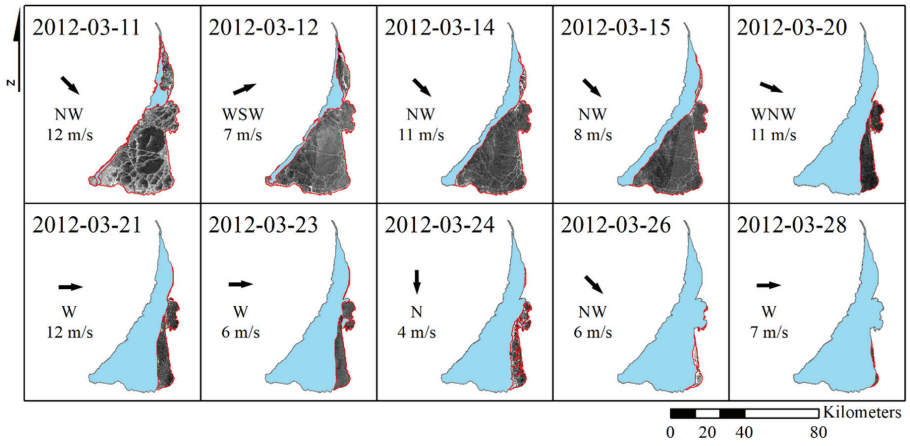

Figure 8. The ice cover retreat in the Curonian Lagoon in the winter of 2011–2012 under the prevalence of northwesterly winds. The red color indicates the ice cover boundary, the blue color shows water, the labels and arrows show the wind speed and direction.

The consecutive winter (2012–2013) is nearly twice longer and has multiple freezing and melting periods. The final melting duration lasts for more than 50 days, while the overall ISD is one of the longest, 129 days (Table 2). In 2013–2014 ice covers the lagoon for about one month only. The ice melt starts from the eastern shoreline in the northern part of the lagoon. The observed melting pattern matches exactly one of the prevailing winds. As seen in Figure 9, the moderate easterly wind acting for about two weeks after the melt onset makes the melting pattern spread first along the north-eastern coast and finally opening the entire northern part two weeks later. Once the wind changes to the NW direction, the ice cover starts melting in the southern part and accumulates in the central eastern part of the lagoon, where it stays longest until the final retreat. The total duration of the ice season was 57 days (Table 2), i.e., about two months shorter than during the previous season.

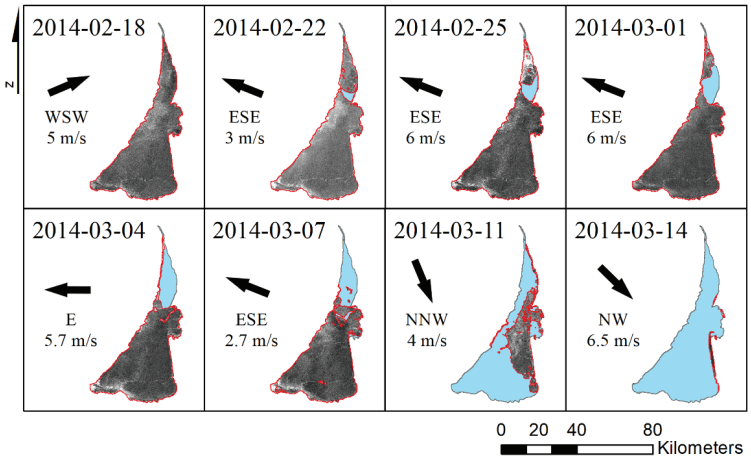

Figure 9. The ice cover retreat in the Curonian Lagoon in the winter of 2013–2014 under the prevalence of easterly and northerly winds. The red color indicates the ice cover boundary, the blue color shows water, the labels and arrows show the wind speed and direction.

The ice season of 2014–2015 starts with nearly full freezing of the entire lagoon on 1 December 2014. However, on the SAR image acquired ten days later southern and southeastern parts of the lagoon are seen ice-free, and the lagoon is never again fully covered by ice during this season. The Sentinel-1A dataset for this winter season is rather sparse, but still capable of capturing a very unstable ice formation with multiple partial freezing of the lagoon. A very uncommon feature is that the southern part is ice-free most of the time, while the northern part is mostly ice-covered This winter season was very warm, relative to others, with the record high value of the cumulative negative temperature T_a^{CN} = −42.5 °C. However, there were still a few days with the air temperature dropping down to about −10.1 °C. The ice season lasted for 95 days. The high-resolution Sentinel-1A images provide a very detailed view of the drift and degradation of two large ice floes moving northward at the end of the ice season (Figure 5c,d). Consecutive SAR images acquired on 28 February 2015 with an 11 h time difference show the linear distances between the polygon centroids are 1060 m and 840 m, equal to the ice drift velocities of 0.03 m/s and 0.02 m/s (Figure 6c,d). Another image acquired 36.5 h later shows these floes being twice smaller and travelled 8340 m and 10780 m further northward with a mean speed of 0.06 m/s and 0.08 m/s, respectively.

The winter seasons of 2015–2016 and 2016–2017 are quite similar in all aspects. They are rather short, about 60 days long (Table 2). The melting duration lasts for nearly a month, starting in the north, while the melting patterns follow those of preceding winters—ice remains longest along the eastern

shoreline. The cumulative negative air temperature values for both seasons were not exceeding −200 °C.

4.3. Spatial Properties of Ice Cover Extent in The Curonian Lagoon

The analysis of satellite data presented above allowed, for the first time, to build up the spatially detailed ice season duration maps of the Curonian Lagoon for 2002–2017 (Figures 10 and 11). Note that all the maps in Figures 10 and 11 also contain the spatially-mean ice season duration value, $\overline{D}_{SAR}$. The latter is usually lower than an overall ice season duration, D_{SAR}, because of the changing ice cover properties (e.g., the multiple melting periods) during a single winter season over the different locations of the CL. Figure 10 shows a yearly-mean ice season duration map obtained by averaging all the satellite-derived ISD maps from the fifteen winter seasons in 2002–2017 (Figure 11).

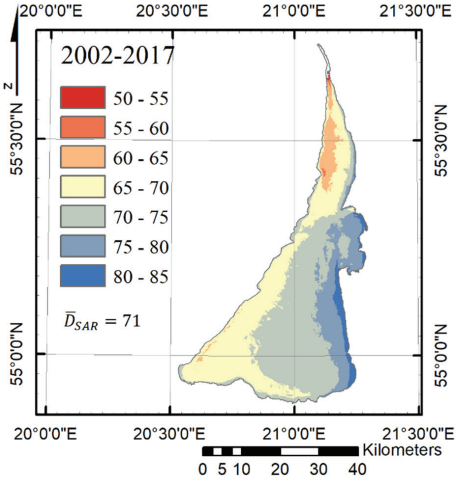

Figure 10. Yearly-mean ice season duration in the Curonian Lagoon as derived from the satellite data in 2002–2017.

As seen from Figure 10, the ice cover resides longest in the southeastern limnic part of the lagoon and along the eastern coast. The yearly-mean ice season duration reaches 75–85 days per winter season in these regions. Such high ISD values are also observed in the Nemunas Delta. In contrast, about ten days shorter the ice season duration (65–70 days) is observed in the western and southwestern parts of the lagoon (see Section 4.4. Freezing and Melting Seasons). Yet, the shortest ice season is clearly observed in the northern (transit) part of the lagoon where $\overline{D}_{SAR}$ values are below 65 days. Here, the ice breaks and melts faster due to an interaction of ice cover with the warmer and saltier waters coming from the Baltic Sea, and movement of the riverine waters passing northward. The lagoon-averaged multi-year $\overline{D}_{SAR}$ value is 71 days. As shown below, this value is not a constant and has a very pronounced interannual variability.

Figure 11 shows the ice season duration maps for every winter season in 2002–2017. To repeat shortly, the longest (shortest) ice season duration is observed in 2005–2006 (2007–2008). One can note that most often the lagoon is partitioned into two main parts in terms of the ice season duration. There are six winter seasons with a clear south–north asymmetry of this parameter in 2002–2003, 2004–2005, 2008–2009, 2009–2010, 2012–2013, and 2013–2014 with the northern part having a shorter ice season duration, and longer D_{SAR} over the southern part. Yet, there are also another six years when this asymmetry has an east-west orientation (2003–2004, 2006–2007, 2007–2008, 2010–2011, 2011–2012, and 2016–2017) with a much longer ice season observed along the eastern coast of the

lagoon. The most rarely occurring situation (2005–2006, 2014–2015, and 2015–2016) is when D_{SAR} is low in the southwestern part of the lagoon and higher over the rest of it, including its northern part, usually having a shorter ice season. As seen, the noted reversal in the spatial properties of the ice season duration is observed mostly during the last years, and, perhaps, is attributed to the changes in the predominant wind conditions during the melting season.

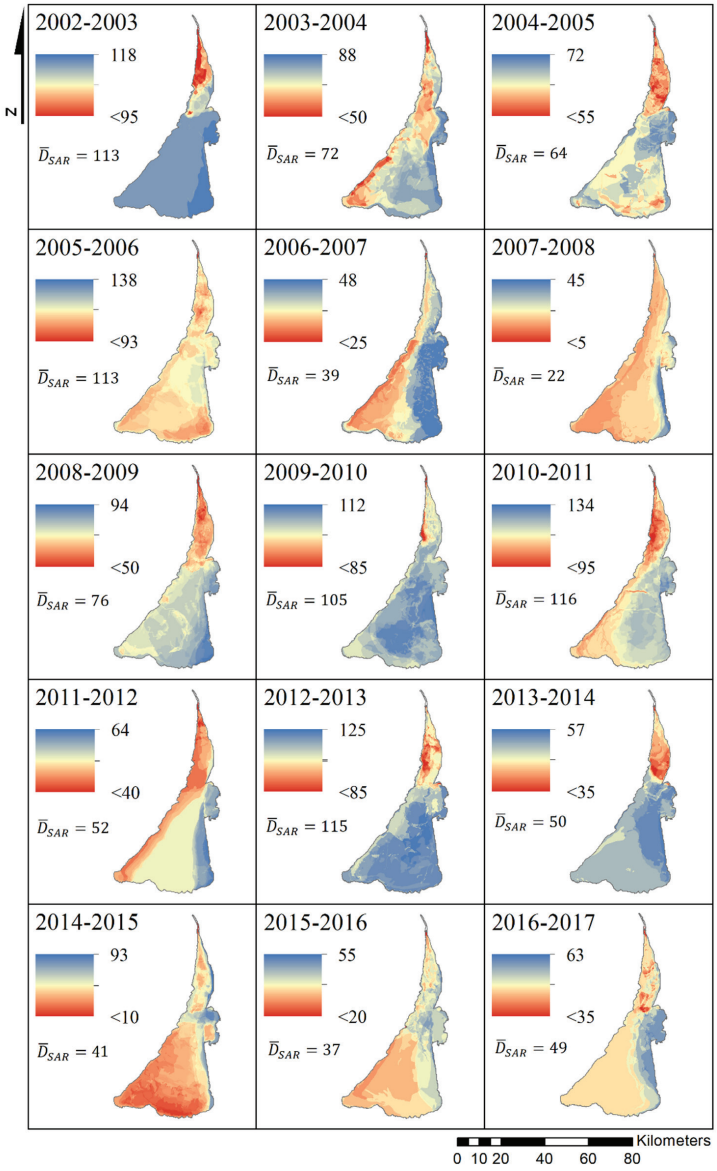

Figure 11. Yearly maps of the ice season duration in the Curonian Lagoon obtained from satellite data in 2002–2017.

In general, Figure 11 clearly exhibits a pronounced shortening of the ice season duration in the CL during the last years. This is shown and explained in more details below in Section 4.4. Freezing and Melting, Figure 14. One may also note that starting from 2014 the ice cover season becomes much shorter over the southern part of the lagoon reaching only 20–50 days compared to 60–80 days as observed before.

All fifteen winter seasons can be divided into three categories based on their $\overline{D}_{SAR}$ values (listed in Table 2): Short winters with $\overline{D}_{SAR} < 50$ days (2006–2007, 2007–2008, 2014–2015, 2015–2016, and 2016–2017), intermediate winters with $50 \leq \overline{D}_{SAR} \leq 100$ days (2003–2004, 2004–2005, 2008–2009, 2011–2012, and 2013–2014), and long winters with $\overline{D}_{SAR} > 100$ days (2002–2003, 2005–2006, 2009–2010, 2010–2011, and 2012–2013). Notably, the interannual variability of the ice season duration in the Curonian Lagoon correlates very well with similar results obtained for the Gulf of Riga [59].

The time variability of the ice cover extent averaged over a 10-day period for the three winter categories defined above are shown in Figure 12. As seen, the ice formation usually starts in the beginning of January during the short winters, while for the intermediate winters it starts a bit earlier—in late December. During the long winters, the ice season usually starts in late November to early December. Figure 12 also shows that the ice extent is not steady during the season. This is especially prominent during the short winters, when a noticeable drop down to 50% of the ice extent is seen in the middle of February. Moreover, the short winters are not only shorter, but they also have a very short period of the ice cover extent above 80% (of the total lagoon area) observed in January. Later on, the ice cover is constantly decreasing until the full decay in late March. For the intermediate (long) winters, the lagoon becomes ice-free by the middle (end) of April.

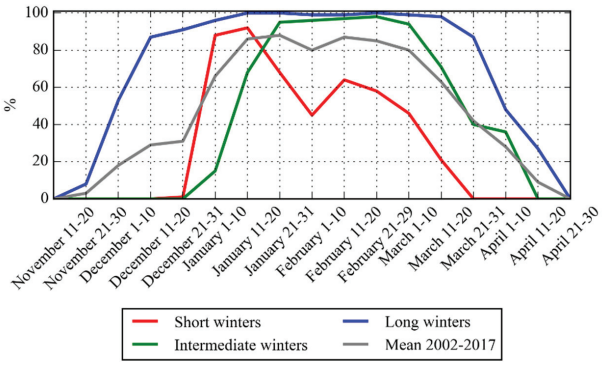

Figure 12. The 10-day averaged percentage of the ice cover extent in the Curonian Lagoon for the three winter categories.

4.4. Freezing and Melting Seasons

The ice cover in the Curonian Lagoon starts to form on average on 27 December. The earliest date of the freeze onset (FO) was recorded on 26 November 2010, and the latest—on 28 January 2007. The lagoon is fully covered by ice on average six days after the FO (ranging from zero to 35 days). The satellite images, however, show that the freezing usually starts very quickly with the first received image being fully or nearly fully covered by ice. The fast freezing occurs during the periods of the low negative air temperature. If the negative air temperature is unstable, the formation of the ice cover might be not very fast and, therefore, traceable in several consecutive images.

Figure 13a provides a generalized view of the spatial behavior of the ice cover during the ice growth period. As seen, the ice cover starts to form all along the eastern shore of the lagoon with a slightly earlier occurrence in its southern part and in the Nemunas Delta. Note also an early ice formation in the very southwestern corner of the lagoon. For the northern part of the CL, the ice forms

earlier along the eastern coast. The latest ice formation is observed along the southern part of the Curonian Spit and over the deepest southwestern limnological part of the CL having a mean depth of about 5 m.

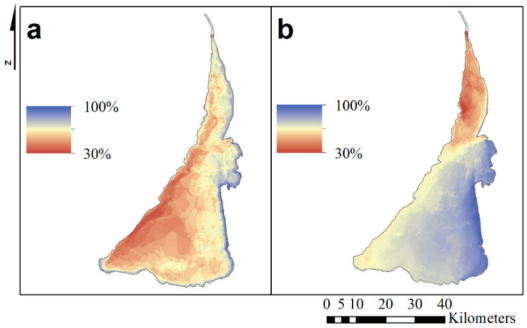

Figure 13. The spatial variations of the ice cover extent during (**a**) ice formation and (**b**) ice melting periods. The colors represent the percentage of ice observations during these periods, i.e., blue color in (**a**) shows the areas where the ice starts to form first, while the red color in (**b**) shows the areas where the ice melts first.

All analyzed winter seasons exhibit a full freezing (FF) of the lagoon, which usually occurs very fast, in a matter of days. On average, the lagoon is fully ice covered on 4 January, while the earliest (latest) day of the FF observed in the satellite images was 2 December 2010 (10 February 2007). During the period between the FF and final MO, several melting episodes can occur in different parts of the lagoon due to the short-term air temperature rise above 0 °C. The ice cover regime of the CL was exceptionally unstable during the winter of 2014–2015 when it had several occasions of a strong melt off followed by a nearly fully restored ice cover over the entire lagoon. The average period of the full ice cover in the CL is 40 days, ranging from around 10 to 90 days.

The final melt onset in the CL, counted after the date when the lagoon is fully ice-covered for the last time during the given winter season, is observed on average on 24 February. The earliest date of the final MO is recorded on 20 January 2008, and the latest—on 2 April 2006. The average period of the ice cover decay usually takes about a month (ranging from six to around 60 days) after the final MO. As clearly seen in Figure 13b), the melting season usually starts in the northern part of the lagoon, where it is connected to and interacts with the warmer water of the Baltic Sea, and continues along the western coast. In general, prevailing winds appear to be the dominant factor shaping the ice cover retreat patterns (see Figures 8 and 9 for reference). The ice cover stays longest in the southeastern part of the lagoon and in the Nemunas Delta owing to the westerly winds typically prevailing during the melting season and pushing the drifting ice towards these areas. The last traces of the ice cover in the lagoon are observed on average on 23 March, while the earliest and the latest dates of the last observation of ice (LOI) were recorded on 16 February 2008 and 18 April 2006, correspondingly.

Figure 14 shows an interannual variability of the several key parameters describing the timing of the ice cover properties in the Curonian Lagoon. As seen, the fluctuations of the FO inferred from the satellite data does not show any significant trend ($p = 0.84$). The FF date possesses some slight decrease over time but it also does not show a significant trend ($p = 0.55$). In turn, the dates of the final MO and LOI have a clear decreasing pattern, meaning an earlier ice break-up and decay observed during the last years, however, only the final MO has a significant decreasing trend ($p = 0.02$). One may also note a rapid drop both in the MO and LOI values observed in the winter of 2007–2008.

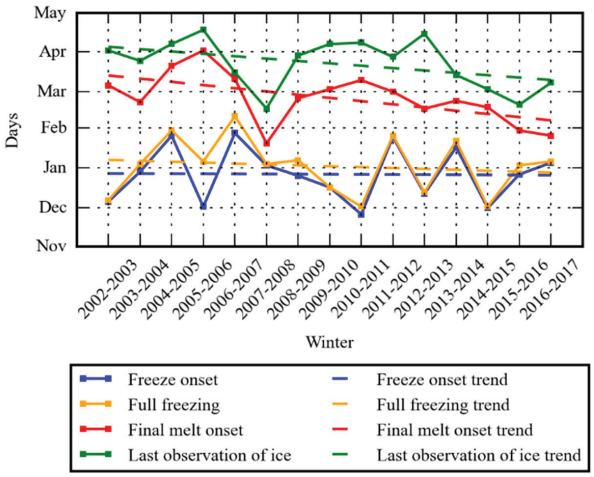

Figure 14. The interannual variability of the ice freeze onset, full freezing, final melt onset, and last observation of ice dates determined from the satellite data (solid lines) and their trends (dashed lines).

4.5. Ice Season Duration

Figure 15a shows an interannual variability of various ISD types over the Curonian Lagoon obtained both from the satellite data and coastal records between 2002 and 2017. As seen, all the ISD types possess a very significant interannual variability and a clear mark of a decrease over the years. The shortening of the ice season duration in the CL assessed from the corrected ISD record, D_{corr}, is observed at a rate of 1.6 days year^{-1} during the last 15 years.

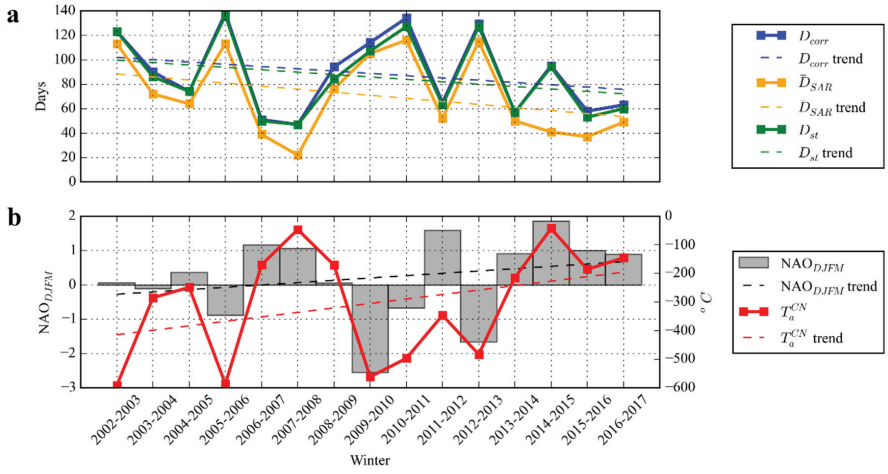

Figure 15. The interannual variability of the various ice season duration types (**a**), NAO winter index, and cumulative negative air temperature during the 15 winter seasons (**b**) in 2002–2017.

The mean value of D_{SAR} (not plotted in Figure 15a) is 87 days, similar to the average ISD value evaluated from the coastal records, D_{st} = 86 days. D_{corr} is slightly longer than D_{st} and D_{SAR}, with the mean value of 89 days (Table 2). However, all these ISD types lack spatial details of the ice season

duration offered by the satellite data. Instead, $\overline{D}_{SAR}$ should better represent the spatial variability of ice cover conditions in the CL. It has a lower mean value of 71 days, and a more pronounced decreasing trend than the other ISDs (Figure 15a) with a shortening rate of 2.3 days year^{-1}.

According to D_{corr}, the longest ice season was observed during the winter of 2005–2006 lasting up to 138 days ($\overline{D}_{SAR}$ = 113 days, see Table 2). However, this winter had a week-long ice-free period in the beginning of the season resulting in 131 days of the ice-cover in the lagoon. In turn, the longest period of continuous ice cover in the CL was observed in 2010–2011 and lasted up to 134 days ($\overline{D}_{SAR}$ = 116). The shortest ice season durations in the Curonian Lagoon were observed in 2006–2007 and 2007–2008 having only 51 and 47 days of the ice cover presence, respectively.

The regional climate fluctuations over the study site are known to be related to the North Atlantic Oscillation [60,61]. There were many studies aimed at displaying its effect on the variability of the ice cover in the Baltic Sea [62–64]. The comparison between the three ISD types in the Curonian Lagoon, winter NAO index (NAO_{DJFM}), and cumulative negative air temperature (T_a^{CN}) during 2002–2017 is further shown in Figure 15. One can clearly see a very good agreement between all these properties. During a negative NAO phase, the ice cover duration is markedly longer and T_a^{CN} is notably lower (Figure 15b). The situation is opposite during a positive NAO phase, when all the ISDs are distinctly shorter than their average values, and the level of T_a^{CN} is high. However, please note that D_{corr} and D_{st} do not correlate very well with the NAO index on the right side of the graph (starting from 2013), especially for the winter of 2014–2015. As already mentioned, the latter was exceptionally warm and had an unstable ice cover formation.

The correlation between the ISD derived from the coastal records (D_{st}) and NAO_{DJFM} is negative and strong with R = −0.71 (Figure 16). This is very similar to the results of a long-term (1961–2005) study by [60] showing a negative correlation of R = −0.69 between the ice season length observed at the stations and NAO index. The corrected ISD (D_{corr}) obtained from the joint use of the satellite and coastal observations, as well as D_{SAR}, have a slightly higher negative correlation with NAO_{DJFM}, R = −0.73. However, much better results are obtained when considering the correlation between NAO_{DJFM} and $\overline{D}_{SAR}$ that account for varying ice cover properties in the CL. The resulting correlation is more pronounced with R = −0.83, denoting the richness of the satellite data for better understanding the causes of ongoing changes in the ice cover extent over the Curonian Lagoon. In general, one can clearly see a very good agreement between all these properties, while somewhat a higher correlation between the NAO and ISD is observed during the positive NAO phase (see Figure 16 for details).

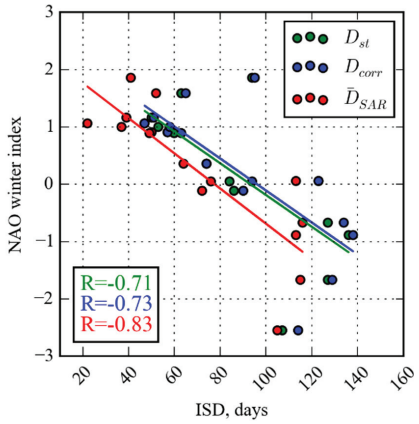

Figure 16. Scatterplots of the ice season duration values derived from the coastal records (D_{st}, green points), joint use of the coastal and satellite data (D_{corr}, blue points), and spatially-averaged satellite data (D_{SAR}, red points) compard to the NAO winter index.

So far, from Figure 15a one can clearly see that the ice season duration is becoming shorter in the CL. Similar results were reported over the past century for the Baltic Sea ([9] and references therein). In the Baltic Sea, ISD is highly variable and depends on the region, with the longest one observed in the Bothnian Bay and decreasing southward [9]. Studies of the ice regime of the Gulf of Riga and along the coast of Latvia [59,65] gave results very similar to our study. The severity of winters in 2002–2003, 2005–2006, 2009–2010, and 2010–2011, and milder winters observed in 2006–2007 and 2007–2008 over these regions correspond well with our results. A similar variability of the ice season duration was also described over the nearby Vistula Lagoon [66] located southwestward from the CL.

Analysis of the air temperature time series for every winter season shows that the ISD clearly depends on the cumulative negative air temperature (T_a^{CN}) for a given winter season. As seen in Figure 15b, the values of the locally measured air temperature have a clear tendency to increase over the last decade resulting in warmer and shorter winters in the Curonian Lagoon. Notably, the air temperature over the entire Baltic Sea area is also increasing and the major trends are observed in spring and winter south of 60 °N (the Curonian Lagoon is located between 54.9 °N and 55.7 °N) [67]. Figure 17 further shows the scatterplots between T_a^{CN} and the three ISD types—D_{st}, D_{corr}, $\overline{D}_{SAR}$. As seen, the correlation between T_a^{CN} and D_{st} (as well as D_{corr}) is strong and negative, R = −0.81 (Figure 17b). Here, one should keep in mind that the in situ records are spatially constrained, while the satellite-derived estimates have a much better spatial representation of the ice cover conditions over the entire Curonian Lagoon. Indeed, the best results are obtained when considering the spatially-rich estimate of the ice season duration, $\overline{D}_{SAR}$. In this case the correlation between T_a^{CN} and $\overline{D}_{SAR}$ is highest with R = −0.92 (Figure 17c). The dependency between T_a^{CN} and $\overline{D}_{SAR}$ can then be approximated by a regression function:

$$\overline{D}_{SAR} = 0.16\, T_a^{CN} + 22.83 \text{ (days)}, \quad (1)$$

which could be used elsewhere for predicting the spatial-mean ice season duration $\overline{D}_{SAR}$ in the Curonian Lagoon from the coastal records of T_a^{CN}.

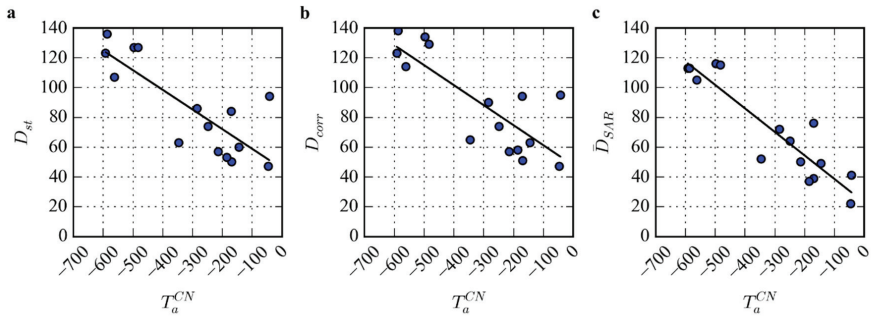

Figure 17. Scatterplots of the cumulative negative air temperature compared to the ice season duration (ISD) obtained from the coastal observations (**a**), maximum (**b**) and spatial-mean (**c**) ISD from the satellite data.

5. Discussion

Until now, there were not many investigations of the ice conditions in the Curonian Lagoon, the large seasonally ice-covered coastal lagoon located in the SE Baltic Sea. The previous knowledge based entirely on in situ records was obviously lacking the spatial information of the ice cover extent in the lagoon due to a limited number of measurement stations. In this work, the use of high-resolution spaceborne C-band SAR observations combined with the visible-band MODIS data has enabled to effectively solve this task.

Here, we used a visual identification of the ice cover extent in satellite images. We should acknowledge that the human supervised method could potentially contain various biases, which could be diminished upon further automatization of the method. The automated SAR algorithm, enabling to distinguish the various ice types, would certainly help to make more consistent comparisons with the in situ data. Nonetheless, our method allowed examining the spatial extent, seasonal and interannual variability of the ice cover properties in the Curonian Lagoon in detail.

According to [68], the ice cover extent is one of the most important freshwater ice variables, which is not easily studied because the freezing and melting can be rapid events requiring a high temporal and spatial resolution to represent them with a sufficient precision. Indeed, a detailed comparison between the satellite observations and coastal records shows that the temporal resolution of the satellite data was not high enough to fully resolve the freeze onset in the Curonian Lagoon. Moreover, in some cases the thin ice forms can be well–seen in the MODIS/in situ observations, but may not be detected by SAR. The FO was defined earlier in the satellite observations than at the coastal stations only in 38% of the cases. However, the temporal resolution of different SAR sensors was not similar–the highest frequency of image acquisitions over the CL was that of RADARSAT-2 (two days), while the combination of the Sentinel-1 A/B performed only a little bit better (2.6 days) than the ASAR alone (three days). Nevertheless, we believe that a relatively low performance of the SAR data during the FO phase will improve in the future with the launch of new non-commercial SAR missions. Additional analysis of the MODIS data has also improved the overall frequency of satellite observations despite the frequent cloud cover over the study region in winter.

Yet, all other important ice formation/decay stages, including the full freezing, melt onset, and last observation of ice are better captured from the space. The most critical differences were found for the identification of the melt onset date and the end of the ice season, where the satellite observations were much more effective due to their spatial capability to cover the entire lagoon at once and observe the ice conditions far away from the coastal stations.

As found, the longest ice seasons were observed during the winter of 2005–2006 (138 days) and 2010–2011 (134 days). The shortest ISDs were observed in 2006–2007 and 2007–2008 having only 51 and 47 days of the ice cover presence, respectively. Notably, the year of 2007 is well known for being the first registered minimum ice extent in the Arctic Ocean observed on 18 September 2007 [69]. The correlation between the ISD in the Curonian Lagoon and the ice extent in the Arctic Ocean is also observed for the year of 2016, when the second minimum ice extent was recorded in the Arctic [70] and only 58 (63) days of the ice cover were registered in the lagoon in winter of 2015–2016 (2016–2017). It also seems to work for the record-low Arctic ice extent observed on 17 September 2012. The duration of the ice season in the Curonian Lagoon during the preceding winter of 2011–2012 was also low, 65 days. It is believed that the loss of the Arctic sea ice could weaken the Atlantic Meridional Overturning Circulation and this could lead to harsher winters and a stormier weather in Europe [71,72]. Our record suggests that a shorter winter season is usually observed before and/or after the minimum September sea ice extent in the Arctic Ocean. However, the influence of the decreasing Arctic sea ice cover on the colder European weather is still questionable [73].

In turn, the North Atlantic Oscillation is a very important phenomenon affecting the variations of the climate in Europe [61]. For example, [65] showed that processes over the North Atlantic are the driving force for the sea ice regime along the nearby coast of Latvia. Our results also show a strong negative correlation between the ISD and winter NAO index. During the negative NAO phase, the ice season duration in the Curonian Lagoon is prominently longer with lower air temperatures, and vice versa. As further shown, the ice season duration in the CL clearly depends on the cumulative negative air temperature for a given winter season that have a clear tendency to increase over the last decade resulting in warmer and shorter winters in the Curonian Lagoon.

Notably, the correlation coefficients between the ISD and NAO index ($R = -0.83$), as well as the ISD and air temperature ($R = -0.92$) are substantially higher when considering the lagoon-averaged ISD values derived from the satellite observations compared to those derived from the spatially constrained

coastal records. This proves the merit of the satellite data for better understanding the causes and consequences of ongoing changes in the ice cover extent in the Curonian Lagoon. As suggested, such a high correlation between the ISD and air temperature may be used for the prediction of the lagoon-averaged ISD values from the coastal air temperature records.

6. Conclusions

Here, we present the first detailed record of spatial and temporal ice cover properties in the Curonian Lagoon over 15 winter seasons from 2002–2017 based on the analysis of the multi-mission satellite data. As observed, the ice cover starts to form along the eastern shore of the CL, in particular in its south-eastern part and in the Nemunas Delta. Later on, ice forms along the southern and in the deepest southwestern parts. The ice cover usually lasts from 10 to 90 days (40 days on average). Multiple melting occurrences may take place in different parts of the lagoon before the final melt onset.

The ice cover resides longest in the south-eastern limnic part of the lagoon and along the eastern coast owing to the westerly winds prevailing during the melting season and pushing the drifting ice toward these areas. Surprisingly, a long ice season is also observed in the Nemunas Delta, where one might expect a shorter ice season due to the destroying effect of the river discharge on the ice cover. The shortest ice season is clearly observed in the northern (transit) part of the lagoon where ice breaks and melts faster due to an interaction with the warmer Baltic Sea water and the movement of the riverine water passing northward. The lagoon-averaged multi-year ice season duration is 71 day.

As further shown, the ice cover decay usually lasts for a month and starts in the northern CL. It continues along the western coast and gradually moves to the eastern and south-eastern shores. Our analysis of a limited number of consecutive SAR image pairs during the melting season shows ice drift velocities of 0.03–0.14 m/s with a drift direction mostly coinciding with the background currents and wind.

Analysis of the interannual variability of various ice season duration types in the Curonian Lagoon derived from the satellite and coastal data shows a clear mark of the decrease over the years, which is mostly attributed to an earlier ice melting. The shortening of the ice season duration in the CL assessed from the updated ISD record amounts to a rate of 1.6 days year^{-1} during the last 15 years, while the lagoon-averaged ISD shows an even stronger tendency of 2.3 days year^{-1}. These values are much higher than 0.64 days year^{-1} as reported by [60] along the Lithuanian Baltic Sea coast for the period of 1960–2006, by [65] along the Latvian coast (0.3 days year^{-1}) and in the Gulf of Riga (0.05 days year^{-1}), or 0.6 days year^{-1} as reported by [74] for the eastern Gulf of Finland. While the length of our record is shorter than those mentioned above and the ISD trends reported here were not significant, it seems feasible to expect that a semi-enclosed coastal lagoon may experience more pronounced ice regime changes than other parts of the larger Baltic Sea, especially during the recent years.

The overall results obtained in this study clearly show the high potential of the satellite observations, particularly spaceborne SAR measurements, to reveal critical spatio-temporal information of ice cover variability and dynamics over the largest coastal lagoon of the Baltic Sea that should be definitely exploited in regional ice monitoring programs.

Author Contributions: Conceptualization, G.U. and I.E.K.; Formal analysis, R.I.; Investigation, R.I. and I.E.K.; Methodology, R.I. and I.E.K.; Supervision, G.U. and I.E.K.; Visualization, R.I.; Writing—original draft preparation: R.I.; Writing—review and editing, I.E.K. and G.U.; Funding acquisition, I.E.K.

Funding: The support from the Russian Science Foundation grant #17-77-30019 is acknowledged.

Acknowledgments: The authors would like to thank the Marine Research Department of the Environment Protection Agency of Lithuania for providing the data of the ice cover observations from coastal stations. Envisat ASAR images used in this work were available from the European Space Agency within the CAT-1 Project C1F.29721. RADARSAT-2 SAR data were kindly provided by ESA within the DWH_MG1_CORE_11 dataset. RADARSAT is an official trademark from the Canadian Space Agency.

Conflicts of Interest: The authors declare no conflict of interest.

References

1. Belchansky, G.I. *Arctic Ecological Research from Microwave Satellite Observations*; CRC Press: Boca Raton, FL, USA, 2004.
2. Meier, W.N.; Hovelsrud, G.K.; van Oort, B.E.H.; Key, J.R.; Kovacs, K.M.; Michel, C.; Haas, C.; Granskog, M.A.; Gerland, S.; Perovich, D.K.; et al. Arctic sea ice in transformation: A review of recent observed changes and impacts on biology and human activity. *Rev. Geophys.* **2014**, *51*, 185–217. [CrossRef]
3. Benson, J.B.; Magnuson, J.J.; Jensen, O.P.; Card, V.M.; Hodgins, G.; Korhonen, J.; Livingstone, D.M.; Stewart, K.M.; Weyhenmeyer, G.A.; Granin, N.G. Extreme events, trends, and variability in Northern Hemisphere lake-ice phenology (1855–2005). *Clim. Chang.* **2012**, *112*, 299–323. [CrossRef]
4. Weyhenmeyer, G.A.; Livingstone, D.M.; Meilis, M.; Jensen, O.; Benson, B.; Magnuson, J.J. Large geographical differences in the sensitivity of ice-covered lakes and rivers in the Northern Hemisphere to temperature changes. *Glob. Chang. Biol.* **2010**, *17*, 268–275. [CrossRef]
5. EEA (European Environment Agency) Report. *Climate Change, Impacts and Vulnerability in Europe 2016*; An Indicator-Based Report. No 1/2017; Publications Office of the European Union: Luxembourg, 2017, 2017. [CrossRef]
6. Höglund, A.; Pemberton, P.; Hordoir, R.; Schimanke, S. Ice conditions for maritime traffic in the Baltic Sea in future climate. *Boreal Environ. Res.* **2017**, *22*, 245–265.
7. Löptien, U.; Axell, L. Ice and AIS: Ship speed data and sea ice forecasts in the Baltic Sea. *Cryosphere* **2014**, *8*, 2409–2418. [CrossRef]
8. Krämer, I.; Borenäs, K.; Daschkeit, A.; Filies, C.; Haller, I.; Janßen, H.; Karstens, S.; Kūle, L.; Lapinskis, J.; Varjopuro, R. *Climate Change Impacts on Infrastructure in the Baltic Sea Region*; Baltadapt Report # 5; Danish Meteorological Institute: Copenhagen, Denmark, 2012.
9. Haapala, J.J.; Ronkainen, I.; Schmelzer, N.; Sztobryn, M. Recent Change—Sea Ice. In *Second Assessment of Climate Change for the Baltic Sea Basin. Regional Climate Studies*; Bolle, H.J., Menenti, M., Ichtiaque Rasool, S., Eds.; Springer: Cham, Germany, 2015; pp. 145–153.
10. Vihma, T.; Haapala, J. Geophysics of sea ice in the Baltic Sea: A review. *Prog. Oceanogr.* **2009**, *80*, 129–148. [CrossRef]
11. Granskog, M.; Kaartokallio, H.; Kuosa, H.; Thomas, D.N.; Vainio, J. Sea ice in the Baltic Sea—A review. *Estuar. Coast. Shelf Sci.* **2006**, *70*, 145–160. [CrossRef]
12. Askne, J.; Dierking, W. Sea Ice Monitoring in the Arctic and Baltic Sea Using SAR. In *Remote Sensing of the European Seas*; Barale, V., Gade, M., Eds.; Springer: Dordrecht, The Netherlands, 2008; pp. 383–398.
13. Karvonen, J. Operational SAR-based sea ice drift monitoring over the Baltic Sea. *Ocean Sci.* **2012**, *8*, 473–483. [CrossRef]
14. Karvonen, J. Evaluation of the operational SAR based Baltic Sea ice concentration products. *Adv. Space Res.* **2015**, *56*, 119–132. [CrossRef]
15. Similä, M.; Karvonen, J.; Haas, C. Inferring the degree of ice field deformation in the Baltic Sea using Envisat ASAR images. In *Advances in SAR Oceanography from Envisat and ERS Missions, Proceedings of SEASAR 2006, Frascati, Italy, 23–26 January 2006*; Lacoste, H., Ouwehand, L., Eds.; ESA Publications Division, ESTEC: Noordwijk, The Netherlands, 2006.
16. Gegiuc, A.; Similä, M.; Karvonen, J.; Lensu, M.; Mäkynen, M.; Vainio, J. Estimation of degree of sea ice ridging based on dual-polarized C-band SAR data. *Cryosphere* **2018**, *12*, 343–364. [CrossRef]
17. Jawak, S.D.; Bidawe, T.G.; Luis, A.J. A Review on Applications of Imaging Synthetic Aperture Radar with a Special Focus on Cryospheric Studies. *Adv. Remote Sens.* **2015**, *4*, 163–175. [CrossRef]
18. Dierking, W. Sea ice monitoring by synthetic aperture radar. *Oceanography* **2013**, *26*, 100–111. [CrossRef]
19. Vybernaite-Lubiene, I.; Zilius, M.; Saltyte-Vaisiauske, L.; Bartoli, M. Recent Trends (2012–2016) of N, Si, and P Export from the Nemunas RiverWatershed: Loads, Unbalanced Stoichiometry, and Threats for Downstream Aquatic Ecosystems. *Water* **2018**, *10*, 1178. [CrossRef]
20. Umgiesser, G.; Zemlys, P.; Ertürk, A.; Razinkovas-Baziukas, A.; Mėžinė, J.; Ferrarin, C. Seasonal renewal time variability in the Curonian Lagoon caused by atmospheric and hydrographical forcing. *Ocean Sci.* **2016**, *12*, 391–402. [CrossRef]
21. Adrian, R.; Walz, N.; Hintze, T.; Hoeg, S.; Rusche, R. Effects of ice duration on plankton succession during spring in a shallow polymictic lake. *Freshw. Biol.* **1999**, *41*, 621–632. [CrossRef]

22. Pełechata, A.; Pełechaty, M.; Pukacz, A. Winter temperature and shifts in phytoplankton assemblages in a small Chara-lake. *Aquat. Bot.* **2015**, *124*, 10–18. [CrossRef]
23. Vybernaite-Lubiene, I.; Zilius, M.; Giordani, G.; Petkuviene, J.; Vaiciute, D.; Bukaveckas, P.A.; Bartoli, M. Effect of algal blooms on retention of N, Si and P in Europe's largest coastal lagoon. *Estuar. Coast. Shelf Sci.* **2017**, *194*, 217–228. [CrossRef]
24. Kozlov, I.E.; Kudryavtsev, V.N.; Johannessen, J.A.; Chapron, B.; Dailidienė, I.; Myasoedov, A.G. ASAR imaging for coastal upwelling in the Baltic Sea. *Adv. Space Res.* **2012**, *50*, 1125–1137. [CrossRef]
25. Dabuleviciene, T.; Kozlov, I.E.; Vaiciute, D.; Dailidiene, I. Remote Sensing of Coastal Upwelling in the South-Eastern Baltic Sea: Statistical Properties and Implications for the Coastal Environment. *Remote Sens.* **2018**, *10*, 1752:1–1752:24. [CrossRef]
26. Adamo, M.; Matta, E.; Bresciani, M.; De Carolis, G.; Vaičiūte, D.; Giardino, C.; Pasquariello, G. On the synergistic use of SAR and optical imagery to monitor cyanobacteria blooms: The Curonian Lagoon case study. *Eur. J. Remote Sens.* **2013**, *46*, 789–805. [CrossRef]
27. Bagdanavičiūtė, I.; Umgiesser, G.; Vaičiūtė, D.; Bresciani, M.; Kozlov, I.; Zaiko, A. GIS-based multi-criteria site selection for zebra mussel cultivation: Addressing end-of-pipe remediation of a eutrophic coastal lagoon ecosystem. *Sci. Total Environ.* **2018**, *634*, 990–1003. [CrossRef] [PubMed]
28. Šarauskienė, D.; Jurgelėnaitė, A. Impact of Climate Change on River Ice Phenology in Lithuania. *Environ. Res. Eng. Manag.* **2008**, *46*, 13–22.
29. Kilkus, K.; Vilkelytė, D. Ledo dangos storio Lietuvos ežeruose daugiametė kaita. *GEOGRAFIJA* **2010**, *46*, 1–6.
30. Glavickas, T.; Stonevičius, E. Ledo sangrūdų paplitimo Lietuvos upėse ir jų poveikio upių vandens lygiui vertinimas. *GEOGRAFIJA* **2012**, *48*, 119–131. [CrossRef]
31. Petkevičius, D. The Ice Jam Modelling for Neris River Reach in Kaunas City. Master's Thesis, Aleksandras Stulginskis University, Kaunas, Lithuania, 2016.
32. Baušys, J. Ledo Režimas. In *Kuršių Marios II*; Rainys, A., Ed.; Mokslas: Vilnius, Lithuania, 1978; pp. 34–49.
33. Jarmalavičius, D. Lietuvos Jūrinis Krantas. In *Klimato Kaita: Prisitaikymas Prie Jos Poveikio Lietuvos Pajūryje*; Bukantis, A., Šinkūnas, P., Taločkaitė, E., Eds.; Vilniaus Universiteto Leidykla: Vilnius, Lithuania, 2007; pp. 25–31.
34. Rukšėnienė, V.; Dailidienė, I.; Myrberg, K.; Dučinskas, K. A simple approach for statistical modelling of ice phenomena in the Curonian Lagoon, the south-eastern Baltic Sea. *BALTICA* **2015**, *28*, 11–18. [CrossRef]
35. Dailidienė, I. Kuršių marių hidrologinio režimo pokyčiai. *GEOGRAFIJA* **2007**, *43*, 36–43.
36. Balevičienė, J.; Balevičius, A.; Stanevičius, V.; Vaitkus, G.; Gurova, E. *Kuršių Marių Pakrantės Augmenijos Pjovimo, Siekiant iš Marių Pašalinti Dalį Biogeninių Medžiagų*; Galimybių Studija: Vilnius, Lithuania, 2007.
37. Gasiūnaitė, Z.R.; Daunys, D.; Olenin, S.; Razinkovas, A. The Curonian Lagoon. In *Ecology of Baltic Coastal Waters*; Schiewer, U., Ed.; Springer: Berlin/Heidelberg, Germany, 2008; pp. 197–215.
38. Zemlys, P.; Ferrarin, C.; Umgiesser, G.; Gulbinskas, S.; Bellafiore, D. Investigation of saline water intrusions into the Curonian Lagoon (Lithuania) and two-layer flow in the Klaipėda Strait using finite element hydrodynamic model. *Ocean Sci.* **2013**, *9*, 573–584. [CrossRef]
39. Žilinskas, G.; Jarmalavičius, D.; Pupienis, D.; Gulbinas, Z.; Korotkich, P.; Palčiauskaitė, R.; Pileckas, M.; Raščius, G. *Kuršių Marių Krantų Apsaugos ir Naudojimo Studija*; VšĮ Gamtos paveldo fondas: Vilnius, Lithuania, 2012.
40. Van der Schrier, G.; van den Besselaar, E.J.M.; Klein Tank, A.M.G.; Verver, G. Monitoring European average temperature based on the E-OBS gridded data set. *J. Geophys. Res. Atmos.* **2013**, *118*, 5120–5135. [CrossRef]
41. Dailidienė, I. Hidroklimatinių Sąlygų Kaitos Ypatumai Baltijos Jūros Lietuvos Priekrantėje ir Kuršių Mariose. Ph.D. Thesis, Klaipėda University, Klaipėda, Lithuania, 2007.
42. Ministry of Environment of the Republic of Lithuania. *State Environmental Monitoring Program*; Public Information and Publishing Unit of the Ministry of the Environment of the Republic of Lithuania: Vilnius, Lithuania, 1998.
43. Jackson, C.R.; Apel, J.R. *Synthetic Aperture Radar Marine User's Manual*; U.S. Department of Commerce: Washington, DC, USA, 2004.
44. Johannessen, O.M.; Alexandrov, V.Y.; Frolov, I.Y.; Bobylev, L.P.; Sandven, S.; Pettersson, L.H.; Kloster, K.; Babich, N.G.; Mironov, Y.U.; Smirnov, V.G. *Remote Sensing of Sea Ice in the Northern Sea Route: Studies and Applications*; Springer: Chichester, UK, 2007.

45. Muckenhuber, S.; Nilsen, F.; Korosov, A.; Sandven, S. Sea ice cover in Isfjorden and Hornsund, Svalbard (2000–2014) from remote sensing data. *Cryosphere* **2016**, *10*, 149–158. [CrossRef]
46. Mann, H.B. Nonparametric tests against trend. *Econometrica* **1945**, *13*, 245–259. [CrossRef]
47. Kendall, M.G. *Rank Correlation Methods*, 4th ed.; Charles Griffin: London, UK, 1975.
48. Kendall, M.G.; Gibbons, J.D. *Rank Correlation Methods*; Edward Arnold: London, UK, 1990.
49. Gough, W.A.; Cornwell, A.R.; Tsuji, L.J.S. Trends in Seasonal Sea Ice Duration in Southwestern Hudson Bay. *Arctic* **2004**, *57*, 299–305. [CrossRef]
50. Gagnon, A.S.; Gough, W.A. East–west asymmetry in long-term trends of landfast ice thickness in the Hudson Bay region, Canada. *Clim. Res.* **2006**, *32*, 177–186. [CrossRef]
51. Duguay, C.R.; Prowse, T.D.; Bonsal, B.R.; Brown, R.D.; Lacroix, M.P.; Menard, P. Recent trends in Canadian lake ice cover. *Hydrol. Process.* **2006**, *20*, 781–801. [CrossRef]
52. Solvang, T. Historical Trends in Lake and River Ice Cover in Norway. Masters's Thesis, University of Oslo, Oslo, Norway, 2013.
53. Käyhkö, J.; Apsite, E.; Bolek, A.; Filatov, N.; Kondratyev, S.; Korhonen, J.; Kriaučiūnienė, J.; Lindström, G.; Nazarova, L.; Pyrh, A.; et al. Recent Change—River Run-off and Ice Cover. In *Second Assessment of Climate Change for the Baltic Sea Basin*; The BACC II Author Team, Ed.; Springer: Cham, Germany, 2015; pp. 99–116.
54. Research Staff (Ed.) The Climate Data Guide: Hurrell North Atlantic Oscillation (NAO) Index (PC-based). National Center for Atmospheric. Available online: https://climatedataguide.ucar.edu/climate-data/hurrell-north-atlantic-oscillation-nao-index-pc-based (accessed on 24 March 2018).
55. Karvonen, J.; Cheng, B.; Vihma, T.; Arkett, M.; Carrieres, T. A method for sea ice thickness and concentration analysis based on SAR data and a thermodynamic model. *Cryosphere* **2012**, *6*, 1507–1526. [CrossRef]
56. Fetterer, F.; Gineris, D.; Kwok, R. Sea ice type maps from Alaska Synthetic Aperture Radar Facility imagery: An assessment. *J. Geophys. Res.* **1994**, *99*, 22443–22458. [CrossRef]
57. Subashini, P.; Krishnaveni, M.; Ane, B.K.; Roller, D. SVM-Based Classification for Identification of Ice Types in SAR Images Using Color Perception Phenomena. In *Innovations in Bio-Inspired Computing and Applications*; Abraham, A., Krömer, P., Snášel, V., Eds.; Springer: Cham, Germany, 2014; pp. 285–293.
58. Zakhvatkina, N.Y.; Alexandrov, V.Y.; Johannessen, O.M.; Sandven, S.; Frolov, I.Y. Classification of Sea Ice Types in ENVISAT Synthetic Aperture Radar Images. *IEEE Trans. Geosci. Remote Sens.* **2013**, *51*, 2587–2600. [CrossRef]
59. Siitam, L.; Sipelgas, L.; Pärn, O.; Uiboupin, R. Statistical characterization of the sea ice extent during different winter scenarios in the Gulf of Riga (Baltic Sea) using optical remote-sensing imagery. *Int. J. Remote Sens.* **2017**, *38*, 617–638. [CrossRef]
60. Dailidienė, I.; Davulienė, L.; Kelpšaitė, L.; Razinkovas, A. Analysis of the Climate Change in Lithuanian Coastal Areas of the Baltic Sea. *J. Coast. Res.* **2012**, *28*, 557–569. [CrossRef]
61. Hanna, E.; Cropper, T.E. North Atlantic Oscillation. In *Oxford Research Encyclopedia of Climate Science*; Oxford University Press: New York, NY, USA, 2017. [CrossRef]
62. Karpechko, A.Y.; Peterson, K.A.; Scaife, A.A.; Vainio, J.; Gregow, H. Skilful seasonal predictions of Baltic Sea ice cover. *Environ. Res. Lett.* **2015**, *10*, 044007. [CrossRef]
63. Omstedt, A.; Elken, J.; Lehmann, A.; Leppäranta, M.; Meier, H.E.M.; Myrberg, K.; Rutgersson, A. Progress in physical oceanography of the Baltic Sea during the 2003–2014 period. *Prog. Oceanogr.* **2014**, *128*, 139–171. [CrossRef]
64. Girjatowicz, J.P. The Relationships between the North Atlantic Oscillation and Southern Baltic Coast Ice Conditions. *J. Coast. Res.* **2005**, *21*, 281–291. [CrossRef]
65. Kļaviņš, M.; Avotniece, Z.; Rodinovs, V. Dynamics and impacting factors of ice regimes in Latvia inland and coastal waters. *Proc. Latv. Acad. Sci.* **2016**, *70*, 400–408. [CrossRef]
66. Chubarenko, B.; Chechko, V.; Kileso, A.; Krek, E.; Topchaya, V. Hydrological and sedimentation conditions in a non-tidal lagoon during ice coverage—The example of Vistula Lagoon in the Baltic Sea. *Estuar. Coast. Shelf Sci.* **2019**, *216*, 38–53. [CrossRef]
67. Rutgersson, A.; Jaagus, J.; Schenk, F.; Stendel, M.; Barring, L.; Briede, A.; Claremar, B.; Hanssen-Bauer, I.; Holopainen, J.; Moberg, A.; et al. Recent Change—Atmosphere. In *Second Assessment of Climate Change for the Baltic Sea Basin*; The BACC II Author Team, Ed.; Springer: Cham, Germany, 2015; pp. 69–97.
68. Rees, W.G. *Remote Sensing of Snow and Ice*; CRC Press: Boca Raton, FL, USA, 2006.

69. Comiso, J.C.; Parkinson, C.L.; Gersten, R.; Stock, L. Accelerated decline in the Arctic sea ice cover. *Geophys. Res. Lett.* **2008**, *35*, L01703:1–L01703:6. [CrossRef]
70. Petty, A.A.; Stroeve, J.C.; Holland, P.R.; Boisvert, L.N.; Bliss, A.C.; Kimura, N.; Meier, W.N. The Arctic sea ice cover of 2016: A year of record-low highs and higher-than-expected lows. *Cryosphere* **2018**, *12*, 433–452. [CrossRef]
71. Francis, J.; Skific, N. Evidence linking rapid Arctic warming to mid-latitude weather patterns. *Philos. Trans. R. Soc. A* **2015**, *373*, 20140170:1–20140170:12. [CrossRef] [PubMed]
72. Sevellec, F.; Fedorov, A.V.; Liu, W. Arctic sea ice decline weakens the Atlantic meridional overturning circulation. *Nat. Clim. Chang.* **2017**, *7*, 604–610. [CrossRef]
73. Screen, J.A. The missing Northern European winter cooling response to Arctic sea ice loss. *Nat. Commun.* **2017**, *8*, 14603:1–14603:9. [CrossRef]
74. Ronkainen, I. Long-Term Changes in Baltic Sea Ice Conditions. Master's Thesis, University of Helsinki, Helsinki, Finland, 2013.

PAPER II

water

MDPI

Article

Sediment Transport Mechanisms in a Lagoon with High River Discharge and Sediment Loading

Jovita Mėžinė [1,*], Christian Ferrarin [2], Diana Vaičiūtė [1], Rasa Idzelytė [1], Petras Zemlys [1] and Georg Umgiesser [1,2]

[1] Marine Research Institute, Klaipėda University, Universiteto alley 17, 92294 Klaipėda, Lithuania; diana.vaiciute@jmtc.ku.lt (D.V.); rasa.idzelyte@apc.ku.lt (R.I.); petras.zemlys@apc.ku.lt (P.Z.); georg.umgiesser@ismar.cnr.it (G.U.)

[2] CNR—National Research Council of Italy, ISMAR—Institute of Marine Sciences, Venice, Castello 2737/f, 30122 Venice, Italy; c.ferrarin@ismar.cnr.it

* Correspondence: jovita.mezine@apc.ku.lt

Received: 21 August 2019; Accepted: 17 September 2019; Published: 21 September 2019

Abstract: The aim of this study was to investigate the sediment dynamics in the largest lagoon in Europe (Curonian Lagoon, Lithuania) through the analysis of in situ data and the application of a sediment transport model. This approach allowed to identify the propagation pathway of the riverine suspended sediments, to map erosion-accumulation zones in the lagoon and calculate the sediment budget over a 13-year-long simulation. Sampled suspended sediment concentration data are important for understanding the characteristics of the riverine and lagoon sediments, and show that the suspended organic matter plays a crucial role on the sediment dynamics for this coastal system. The numerical experiments carried out to study sediment dynamics gave satisfactory results and the possibility to get a holistic view of the system. The applied sediment transport model with a new formula for settling velocity was used to estimate the patterns of the suspended sediments and the seasonal and spatial sediment distribution in the whole river–lagoon–sea system. The numerical model also allowed understanding the sensitivity of the system to strong wind events and the presence of ice. The results reveal that during extreme storm events, more than 11.4×10^6 kg of sediments are washed out of the system. Scenarios without ice cover indicate that the lagoon would have much higher suspended sediment concentrations in the winter season comparing with the present situation with ice. The results of an analysis of a long-term (13 years) simulation demonstrate that on average, 62% of the riverine sediments are trapped inside the lagoon, with a marked spatially varying distribution of accumulation zones.

Keywords: sediment transport; numerical modeling; SHYFEM; Curonian Lagoon

1. Introduction

Sediment transport is an important process for all aquatic environments, especially lagoons where the amount and transport directions of the suspended matter have a direct effect on the water turbidity and can cause changes in primary production or other ecological processes in the system [1]. Lagoons are the most productive water bodies in coastal environments, but are vulnerable to human activity, sensitive to climate change [2], and must be monitored and managed for saving the good environmental status. The processes in such complex systems at the land–sea transitional zone are extremely dynamic and require a holistic approach in which the river–lagoon–sea continuum should be considered [3]. Sediments have a crucial role in shaping the landscape in areas where the river enters the sea. Deficiency of sediments reaching the sea may cause coastal erosion, with the consequent loss of land and tidal wetlands, resulting in the necessity of coast protections and saltmarsh or beach nourishment strategies.

Moreover, human intervention sometimes alters the coastline, giving rise to often unintentional changes in the unknown sediment transport pathways and coastal morphodynamics [4,5].

Sediment transport is a process of sediment erosion, transportation, and deposition due to currents and waves. These mechanisms can be influenced by physical, chemical, and biological processes that complicate the system and increase the difficulties to describe the sediment dynamics [1]. In shallow systems, many studies have identified wave energy as the main driver for sediment resuspension [6–9], though it can be influenced by other parameters as well (e.g., grain sizes, erosion and settling rates, biological material). Research on sediment transport mechanisms is essential for pollutant and bacteria dynamics [10], and biogeochemical processes as well [11]. The sediment balance in a semi-enclosed coastal basin is the result of a complex interaction of the above-mentioned processes occurring inside the basin, and is also regulated by the interactions between the tidal motion at the inlets and the longshore transport (see [12], and references therein). Main variables that describe the sediment transport mechanisms are the distribution of suspended sediment concentration, erosion-accumulation zones, bottom shear stress, and grain size distribution. It is difficult to obtain all these parameters from in situ measurements due to temporal and spatial heterogeneity. Therefore, numerical models can be powerful tools to estimate the sediment transport mechanisms in complex systems such as lagoons.

On the southern and southeastern Baltic Sea coast, large coastal water bodies such as bays and lagoons are common. Some of the lagoons are separated by sandy strips (Curonian and Vistula lagoons) and have one or more connections to the Baltic Sea (Darss-Zingst and Szczecin (Oder) lagoons). The Szczecin Lagoon and Curonian Lagoon are dominated by the discharge of the Odra (Oder) River and the Nemunas (Neman) River, respectively. It is important to mention that all of these lagoons are transboundary areas and monitoring programs are carried out by each state independently. There are not many studies done on the sediment dynamics in this region, especially in the past years. A few studies were carried out in the Kaliningrad bay in the Vistula Lagoon [13–15], based on field measurements and investigation on the total suspended sediment concentrations under the ice. The Kaliningrad bay is a similar waterbody to the Curonian Lagoon, which has a strong input from the Pregolya River with salinity close to the river mouth of about 2.

The sediment transport in the Curonian Lagoon, the largest freshwater lagoon in Europe, is still very little explored. Previous studies [16–18] were mostly focused on experimental methods to investigate sediment properties, but not the transport mechanisms in the lagoon. These studies provided only a very general understanding of the sediment dynamics in the system and its influence on the ecological processes. The mean sedimentation rate of about 3.2 mm y^{-1}, and for areas deeper than 3 m a higher sedimentation rate up to 3.6 mm y^{-1}, were estimated by [19]. A detailed study on the Curonian Lagoon bottom sediment distribution is presented in [20].

The modeling studies for the Curonian Lagoon were mostly focused on hydrodynamics. The horizontal and vertical circulation patterns were studied in [21] and [22], and the water renewal time in [23]. For sediment dynamics investigations, the numerical models were applied only in a few studies. The first time the SHYFEM modeling system for sedimentation processes was applied was by [24], when the two-dimensional hydrodynamic model coupled with the spectral wave model was used to investigate the variability of the combined (current and wave) bed shear stress. More detailed studies of the sediment transport for Klaipeda strait, which is the harbor area and connects the Curonian Lagoon with the Baltic Sea, using the DHI 2-D numerical modeling system MIKE-2 were carried out by [25] and by [26]. Nevertheless, these studies are not sufficient to accomplish a holistic view of the sediment transport and morphological changes in the system.

This study aims to identify the propagation of the suspended sediments from the Nemunas River to the lagoon, to map the erosion-accumulation zones in the lagoon due to the sediment dynamics and calculate the sediment budget changes over a 13-year-long simulation. The obtained information about possible pathways of the sediments will be useful not only for the comprehension of the current sedimentation status, but also for future studies of the sediment influence on ecological and other processes.

2. Study Site

The Curonian Lagoon (Figure 1) is a shallow water body placed in the southeastern coasts of the Baltic Sea, separated from the sea by the Curonian Spit and connected to the open sea through only one narrow inlet in the north (Klaipėda Strait). The Klaipėda Strait is a harbor area where the depths vary from 8 to 14.5 m. The total lagoon surface area is about 1584 km^2 (with 413 km^2 in Lithuania), the volume 6.3 km^3, the maximum length 93 km, the maximum width 46 km (in the southern part), and the mean water depth 3.8 m [27].

It is a heavily eutrophic lagoon, with cyanobacteria blooms in the late summer [28,29]. The shallow and weakly stratified lagoon is very turbid due to local winds and intensive primary production [16]. The Secchi disk depth varies from 0.3 to 2.2 m [30].

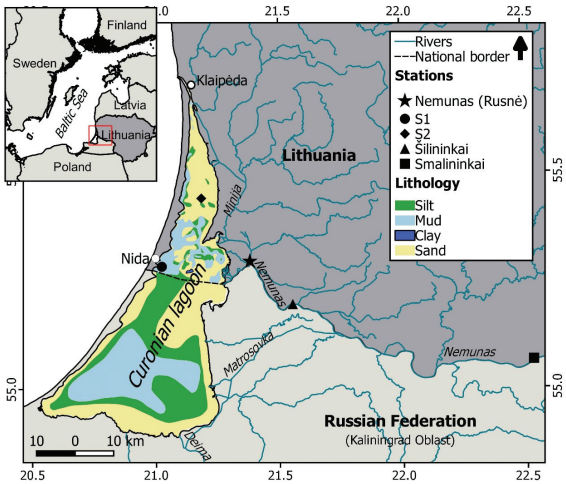

Figure 1. The study site with the calibration stations and bottom sediments in the Curonian Lagoon (the bottom sediment data acquired after [31,32]).

The Curonian Lagoon is a terrestrial runoff-dominated system, with its hydrology strongly related to the discharge of its catchment area. The main rivers which enter the lagoon are Nemunas (Neman), Minija, Deima, and Danė. The total drainage area of the Curonian Lagoon is 100,458 km^2 and covers four countries: Belarus (48%), Lithuania (46%), and 6% lies in Kaliningrad Oblast of Russia and Poland together [33]. The catchment area of Nemunas river only is 98,200 km^2 (47.5% in Lithuania) and on average brings about 21.8 km^3 of water per year to the lagoon (~700 m^3 s^{-1} calculated for the monitoring station Smalininkai, about 112 km from the river mouth) [34]. The Nemunas River enters the lagoon in the middle of the eastern coast and, every year, carries a big amount of fresh water that exceeds the water volume of the lagoon itself by about 3.6 times. Therefore, the southern and central parts of the lagoon are freshwater (average annual water salinity is 0.08), while the northern part is oligohaline (average annual water salinity is 2.45), with irregular salinity fluctuations of up to 7 due to the Baltic Sea water intrusions [35]. Previous studies [21] have shown that this lagoon could formally be divided in two sub-basins—a northern area influenced by both the freshwater flow and the lagoon–sea exchange, and a southern basin where hydrodynamics is mostly influenced by the wind.

The bottom of the Lithuanian part of the Curonian Lagoon is covered by medium sand (0.5–0.25 mm), fine sand (0.25–0.1 mm), coarse silt (0.1–0.05 mm), and fine silty mud (0.05–0.01 mm) [20]. In the northern part of the lagoon, the sandy sediments dominate. In the west, near the shore part of the lagoon, the medium sand has been accumulated as a result of aeolian activity (from wind-blown dunes),

whereas the central and eastern parts are dominated by the Nemunas drift material (fine sand) [20]. The dominant sediment fraction size in the Klaipeda Strait is 0.05–0.01 mm [36]. The southern part of the lagoon is covered mainly with silty and muddy sediments.

Different estimates exist about the source of the material input into the lagoon. According to [18], 87.4% of the total amount of all incoming terrigenous material comes from the rivers, 1.6% comes from the atmosphere and the sea, and 11% from the bottom and shore erosion and aeolian processes. The authors of [17] found that 59.3% of the total amount of incoming material comes from the rivers, 17.8% comes from the atmosphere and the sea, and 14.5% comes from other sources. Part of the incoming dragged and suspended sedimentary matter mostly deposits in the southern part of the lagoon, whereas another part is carried through the narrow Klaipėda Strait into the Baltic Sea [37].

3. Materials and Methods

3.1. In Situ Suspended Sediment Concentration (SSC) Data Collection

Several field campaigns for data sampling were carried out in 2014–2015 in the Curonian Lagoon. For the total suspended solids (TSS) and suspended sediment concentration (SSC), water samples were taken once or twice per month in the Nemunas River (Rusnė village) and a few times per season at station S1 near Nida and station S2 in the Northern part of the lagoon (see Figure 1). The selected stations represent the sites of the Curonian Lagoon with different sediment properties (Table 1). Station S1 is 3.35 m deep with a bottom covered by muddy sediments (percentage of mud 77%), while station S2 has a depth of 1.9 m and is mostly covered by the fine sand sediments (percentage of mud 1.6%). In total, 24 samples for Nemunas river station, 25 samples for the S1 station. and 20 for the S2 station were taken, covering all seasons, including the flood period.

Table 1. The main characteristics of the monitoring stations.

Station	Location	Depth, m	Median Bottom Grain Size, μm	Percentage of Mud, %	Number of Samples
S1	55.286017 N 21.021400 E	3.35	35	77	25
S2	55.444483 N 21.182733 E	1.90	210	1.6	20
Nemunas	55.298228 N 21.380543 E	2.00	350	1.8	24

Depending on the season, from 20 to 40 L of water was transported to the laboratory for further investigation. From 300 to 1500 mL of sample was filtered in triplicate through combusted (4 h at 550 °C) and pre-weighed Whatman GF/F (47 mm in diameter, pore size of 0.7 μm) glass fiber filters (tare weight). After filtration, samples were dried at 60 °C until they reached a stable weight. The TSS concentration was determined gravimetrically by the difference between dry weight and tare weight [38]. The inorganic part of the sample was determined after the 4-h filter muffling at the temperature of 550 °C in the NOBERTHERM muffler furnace. The SSC was determined gravimetrically by the difference between muffled filter weight and tare weight.

The rest of water sample was used for the analysis of suspended particles. Water tanks were left for 4 days until suspensions settled down. The suspensions were concentrated to a 1 L glass. Suspensions were centrifuged and concentrated to 2 × 50 mL tubes for grain size analysis. Two types of analysis were done: i) Grain size analysis of total suspension composition (not used in this article), and ii) grain size analysis without organic material. To eliminate the organic matter from the sample, 30% H_2O_2 was added to the concentrated material and boiled until 80 °C. The granulometric analysis was done from the liquid/wet sample by laser diffraction method using laser particle analyzer Analyzette 22 MicroTec

Plus, Fritsch (FRITCH GmbH, Idar-Oberstein, Germany) (measuring range 0.08–2000 µm). These results were used to calculate the percentage of concentration for each grain class used in the model.

Chlorophyll *a* concentration (Chl-*a*) was analyzed spectrophotometrically using a dual-beam SHIMADZU UV-2600 UV/VIS spectrophotometer (SHIMADZU, Tokyo, Japan) [39,40]. Prior to the analysis, water samples were filtered through GF/F glass fiber filters (Whatman, diameter 0.47 mm, pore size 0.7 µm) and extracted with 90% acetone for 24 h at 4 °C. Phytoplankton community composition was qualitatively assessed with a multi-spectral fluoroprobe (FluoroProbe II, bbe Moldaenke GmbH, Schwentinental, Germany). The probe measures fluorescence emitted by Chl-*a* following excitation of photosynthetic accessory pigments specific to each 'color' phytoplankton group, allowing estimation of the proportional contribution of cyanobacteria, green algae, cryptophytes, and diatoms plus dinoflagellates. These contributions are expressed as mg m^{-3} of Chl-*a*, following factory calibration of the Chl-*a* fluorescence yield against Chl-*a* concentrations [41]. These assessments do not take into account the environmentally variable production rates of accessory pigments, diurnal variation in fluorescence yield due to non-photochemical quenching, or state transitions in cyanobacteria, and are therefore only considered as qualitative estimates of the cyanobacteria percentage from the total abundance of phytoplankton.

A second dataset was collected in August and September 2016 over the Lithuanian part of the Curonian Lagoon during five different sampling campaigns. In total, 25 samples from 15 stations with suspended sediment concentration data were collected (yellow dots in Figure 2C). Samples were analyzed with the methodology described above.

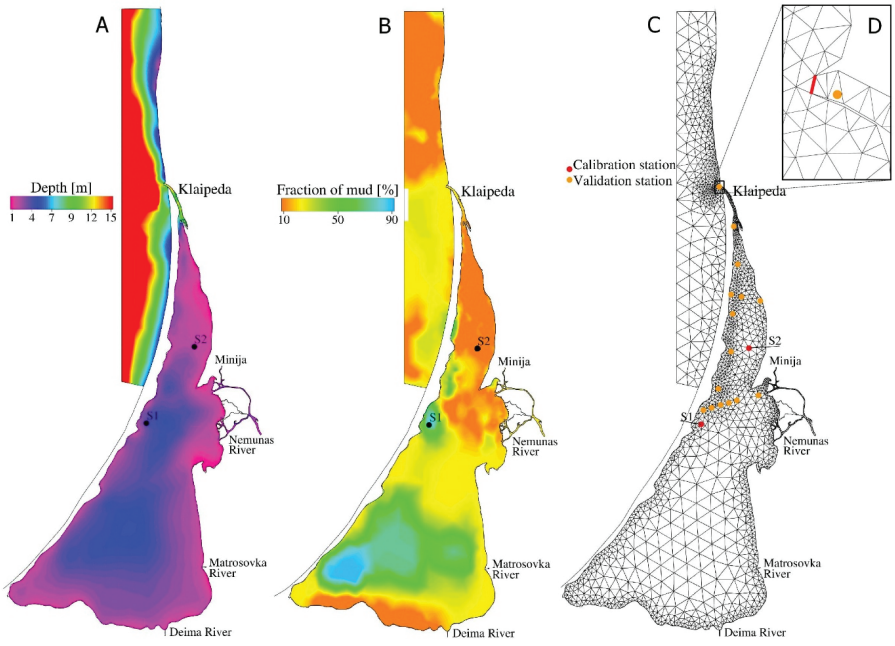

Figure 2. (**A**) Initial bathymetry; (**B**) initial bottom sediment composition; (**C**) computational grid with validation stations and calibration stations (S1 and S2); (**D**) the flux section for the sediment budget calculation.

3.2. The Modeling System

To investigate the estuarine systems as a river–sea continuum, a framework of open source numerical models (SHYFEM, http://www.ismar.cnr.it/shyfem) was applied to the domain that represents the Curonian Lagoon, the Nemunas Delta, and coastal area of the Baltic Sea. In this study, the three-dimensional (3D) hydrodynamic model, a transport and diffusion model, a wind wave model, and a sediment transport model (including a bed model) were used. SHYFEM has been successfully applied to many coastal environments such as river deltas, lagoons, and seas [3,22,42]. The standard model equations for hydrodynamic and sediment transport used herein have been previously published in [43] and [44], respectively.

The hydrodynamic part of the model have been applied to the Curonian Lagoon in previous studies. The reader can refer to [21,22] and [23] for further details on model equations, set-up, and validation for the Curonian Lagoon. The presence of ice cover has been accounted for by weighting the wind drag coefficient by the fractional ice concentration. This corresponds to scaling the momentum input through the surface by the area free of ice. The ice concentration is a value between 0 (ice free) and 1 (fully ice covered) and can be a fractional number. Where ice concentration equals 1, the momentum transfer to the sea is inhibited. No ice–ocean stress was considered in this study. Ice concentration was also used to properly calculate the albedo to be used in the heat flux model [23].

The sediment transport model SEDTRANS05 [44] was applied to study sediment dynamics in the lagoon. This sediment transport model has been successfully applied for investigating the sediment dynamics in the Venice Lagoon [45,46] and the Marano-Grado Lagoon [47]. The model computes erosion and accumulation rates for each time step according to wind waves and currents. A parametric wave module was used here to calculate the wave height and period from wind speed, fetch, and depth using an empirical shallow water equation [48].

The morphological behavior of estuaries and coastal areas often depend on non-cohesive, as well as cohesive, sediments. The sediment bed model uses a three-dimensional grid underneath the hydrodynamic grid. Sediment within each class is exchanged between the bed and the overlying water column through erosion and deposition. In the model, the bed is divided into many homogeneous layers that are characterized, as well as mixed layers, with its own grain size distribution, dry bulk density, and critical stress for erosion values. The linear relationship is assumed between two levels. Based on laboratory and field experiments, several researchers have identified a transition from non-cohesive to cohesive behavior of bottom sediments at increasing mud content in a sand bed [49]. A sand bed with small amounts of mud shows increased resistance against erosion. When the amount of mud (sum of fraction of sediment classes below 63 μm) is above a predetermined threshold (set in this study to 15%, [50]), the sediment behaves as cohesive and the cohesive sediment algorithm is used to compute the eroded mass. Otherwise, the sediment behaves as non-cohesive and the multiple sand grain size classes are considered to behave independently. An explicit combined-flow ripple predictor is included in the model to provide time-dependent bed roughness prediction [51]. The model assumes that total bed roughness is composed of grain roughness, bedform (ripple) roughness, as well as bedload roughness when sediment is in transport. For non-cohesive sediments, the friction factor and the bed roughness is computed from the grain size and the predicted bedform (ripple), while for cohesive sediments, the default values of 0.0022 for friction factor and 0.0002 m for bed roughness proposed by [52] is used. Bed roughness effects on boundary layer parameters are included in the computation of friction factor and effective bed shear stress. The model takes into account time and spatial dependent sediment distribution, bed armoring that gives bed evolution, and sediment grain size distribution changes for each time step. The updated water depth was used further in the hydrodynamics computation.

3.3. Model Set-up

The simulations were carried out using a grid with variable size elements (Figure 2). The numerical grid consisted of 2033 nodes and 3294 elements, with the finer elements in the Nemunas Delta, western

part of the lagoon, and the Klaipeda Strait. The spatial resolution varies from 100 m in the areas where hydrodynamic processes are more active to 3 km in the southern part of the lagoon and open sea. The model was applied in its 3D version, where the water column was discretized into five terrain-following sigma layers.

The open sea boundary water temperature (°C), salinity, and water levels (m) were obtained from three different sources. For the years 2004–2006, the boundary data were taken from the operational hydrodynamic model MIKE21 provided by the Danish Hydraulic Institute (DHI). For the years 2007–2009 and 2014–2016, the data were obtained from the operational hydrodynamic model HIROMB [53] provided by the Swedish Meteorological and Hydrological Institute by a spatial interpolation of 1 nautical mile. For the years 2010–2013, the data were taken from the model MOM (Modular Ocean Model) provided by the Leibniz Institute for Baltic Sea Research in Warnemünde, Germany.

The meteorological forcing of rain (mm day^{-1}), solar radiation (W m^{-2}), air temperature (°C), humidity (%), cloud cover (0—clear sky, 1—sky completely cloudy), 10 m high wind velocity in x and y directions (m s^{-1}), and atmospheric pressure (Pa) were used as surface forcing. For the years 2009–2010, the meteorological forcing fields were provided by the Lithuanian Hydrometeorological Service under the Ministry of Environment from the operational meteorological model HIRLAM (http://www.hirlam.org). For the other years (2004–2008 and 2011–2015), the meteorological data from European Centre for Medium-Range Weather Forecasts (ECMWF, http://www.ecmwf.int) were used. The modeled and measured air temperature and wind speed for station S1 are shown in Figures 3B and 3C, respectively. The statistical analysis shows a substantial relationship between measured and modeled air temperature data (R^2 = 0.97). The analysis of wind data is more complicated. Results show that the ECMWF model overestimates wind speed close to the Curonian Spit by 30%, but in Klaipėda station, the R^2 between measured and modeled values was equal to 0.75.

Daily discharge data (m^3 s^{-1}) for the rivers were provided by the Lithuanian Hydrometeorological Service under the Ministry of Environment. The Nemunas River discharge was measured for the Smalininkai monitoring station about 90 km from the model boundary. Therefore, the Nemunas River discharge for the open boundary conditions near Šilininkai (see Figure 1) was considered as the discharge sum from the Nemunas near Smalininkai, Šešupė, Jūra, and Šešuvis rivers, minus Gilija branch discharge (Gilija discharge is accounted for as a separate river input in the model, assumed to be 29% of Nemunas discharge near Smalininkai) [34]. The time necessary for the water to reach Šilininkai, starting from Smalininkai, was calculated from flow velocity obtained from the Manning equation [54]. It is known that during the spring, flood water coming from the Smalininkai station overflows before reaching the model boundary [55]. The real riverbed becomes wider compared with the riverbed in the model grid, because the model does not simulate the overflow of the water. Therefore, the calculated Nemunas River discharge was limited to 1300 m^3 s^{-1} to avoid the overestimation of the current speed in the riverbed. In order to conserve the total discharged water volume, the flood period was extended from two weeks to one month, depending on the water amount. The final river discharge for the model boundary is presented in Figure 3E.

The satellite ice cover data (Figure 3B) were acquired from the synthetic aperture radar (SAR) measurements from three Earth observation missions: Envisat ASAR, RADARSAT-2, and Sentinel-1A and 1B, complemented by cloud-free Moderate Imaging Spectroradiometer (MODIS) images. For the period 2004–2015, in total, 475 SAR and 64 MODIS images were processed by manually digitizing ice polygons using ArcGIS software, which were then validated with ground observations, showing that satellite data in many cases has better performance than in situ data for defining the key stages of ice cover formation and decay [56]. These polygon datasets were converted to regular grid points and then used to spatially interpolate onto the finite element grid. The ice cover presence in the model input file is set to a value of 0 (no ice) or 1 (ice cover). In all simulations, the Baltic Sea was considered as an ice free area.

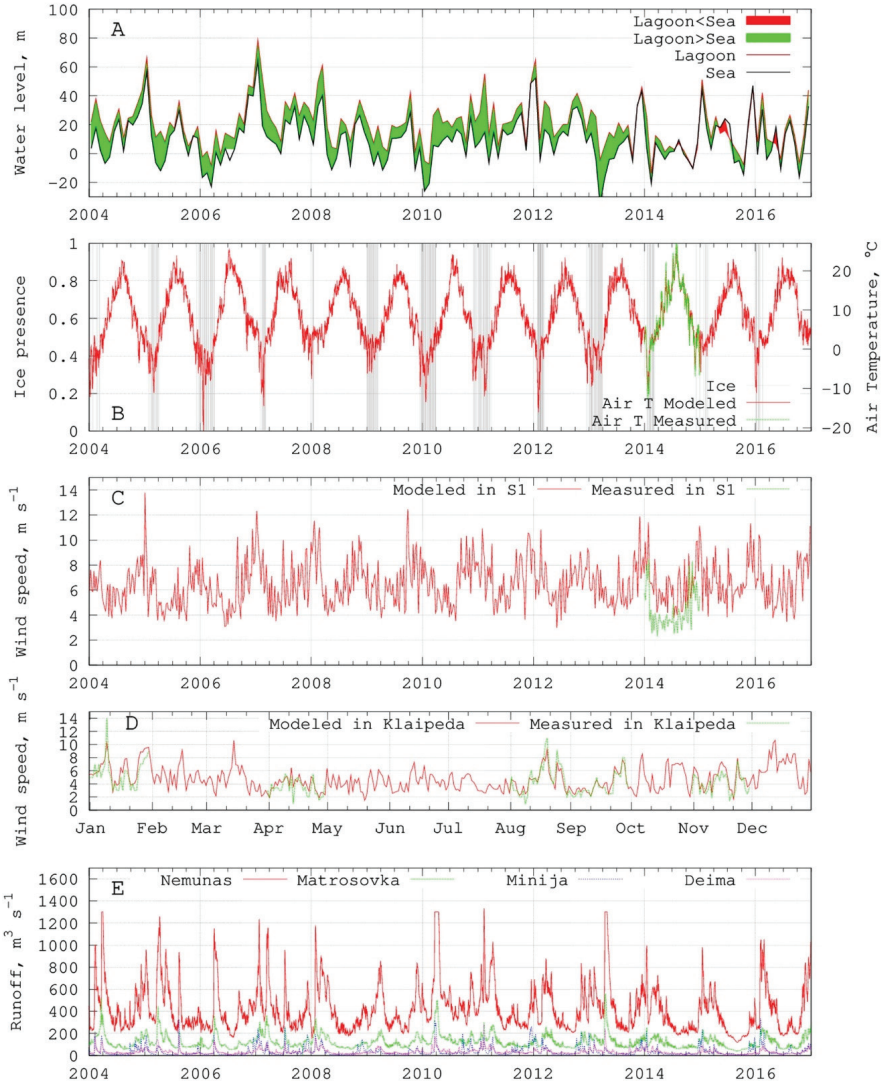

Figure 3. Time series of (**A**) differences between measured water levels in the Klaipeda Strait and Nida; (**B**) measured/modeled (ECMWF) air temperature in Nida and ice cover (grey band) presence in the lagoon from satellite data; (**C**) measured/modeled (ECMWF) weekly averaged wind speed for S1; (**D**) daily measured/modeled only for the year 2014 (ECMWF) wind speed in Klaipeda; (**E**) fresh water discharge into the lagoon.

The suspended sediment concentration data from the Nemunas River available for one year (see Section 4.1) were used for regression analyses to estimate the relationship between water discharge and suspended sediment concentration. The power law formula suggested by [57], called the sediment rating curve, to predict the suspended sediment concentration for intervals without samples according

to water river discharge was used for that purpose. This relationship was used to produce the continuous input data for all model simulation periods. The open boundary data for the suspended sediment concentrations coming from Matrosovka and Deima rivers were obtained from the study of [17]. The average SSC values for different seasons were calculated close to the river mouths that were used as an open river boundary for the sediment model. The daily SSC open boundary data are presented in the model as a matrix of sediment class concentrations.

The initial bottom sediment compositions for this study were compiled from two data sources: (i) a map of [31] for the southern part of the lagoon and the sea, and (ii) a map of [32] for the northern part of the Curonian Lagoon. As an input file for the initial bottom sediments, the regular grid was constructed with nine sediment classes (clay: <0.002 mm and 0.002–0.005 mm; fine silt: 0.005–0.01 mm; coarse silt: 0.01–0.063 mm; very fine sand: 0.063–0.1 mm; fine sand: 0.1–0.25 mm; medium sand: 0.25–0.5 mm; coarse sand: 0.5–1.0 mm; and very coarse sand: 1.0–2.0 mm) that were considered ranging from clay to coarse sand. The initial bottom sediment composition in the model was divided into nine sediment classes, which were presented as a percentage of total suspended sediment concentration for each class. The initial percentage distribution of mud fraction and the computational grid is shown in Figure 2. The critical shear velocity for erosion of non-cohesive sediment that initiates the sediment transport as bedload and in suspension was computed following the Van Rijn method [50]. The initial critical shear stress value of 0.3 N m^{-2} for erosion of cohesive sediments was calculated from the measured wet bulk density in the S1 monitoring station according to the proposed formula by [58].

Table 2 summarizes the dataset used in the model applications.

Table 2. The summary of the model set up data.

Data	Period	Description
Open sea boundary	2004–2006	DHI model MIKE 21
	2007–2010	SMHI model HIROMB
	2011–2013	IOW model MOM
	2014–2016	SMHI model HIROMB
Meteo forcing	2004–2008	ECMWF model data
	2009–2010	Lithuanian hydrometeorological service model HIRLAM
	2011–2016	ECMWF model data
River discharges	2004–2016	Lithuanian hydrometeorological service
Ice coverage	2004–2016	Satellite data provided by KU MRI
Initial bottom sediment composition	-	Gelumbauskaitė et al. [31] and Gulbinskas and Žaromskis [32]

The following numerical simulations were carried out in this study (Table 3):

- CAL: Simulation for model calibration for the period from 1 January 2013 until the end of 2015. Only the results for the year 2014–2015 were analyzed. The year 2013 was used as a spin up period.
- VAL: Simulation for model validation for the period 1 January 2015 until the end of 2016. The year 2015 was used as a spin up period.
- NoICE: Three-year-long simulation for analysis of ice influence on the sediment transport mechanisms in the Curonian Lagoon. Simulation period and set-up are the same as simulation CAL, but without ice cover data.
- LONG: Long-term simulation (13 years) for analysis of the sediment transport mechanisms in the Curonian Lagoon. Simulation period 2004–2016.

Table 3. Summary of numerical experiments carried out in this study.

Name	Period	Description
CAL	2013–2015	Simulation for sediment model calibration (also used for sensitivity tests)
VAL	2015–2016	Simulation for model validation
NoICE	2013–2015	As CAL, but without ice cover data
LONG	2004–2016	13-year simulation

4. Results

4.1. In Situ Suspended Sediment Observations

The observations of the monitoring stations are presented in Figure 4. The analysis of measured suspended sediment (SSC, mg L^{-1}) showed that in spring, summer, and autumn at the Nemunas station, the concentration varies from 4 to 13 mg L^{-1} with the maximum values (>20 mg L^{-1}) at the end of winter, beginning of spring, when the river flooding season starts. The flood season starts when the ice and snow cover melts and shows the highest values of total suspended solids (TSS) as well.

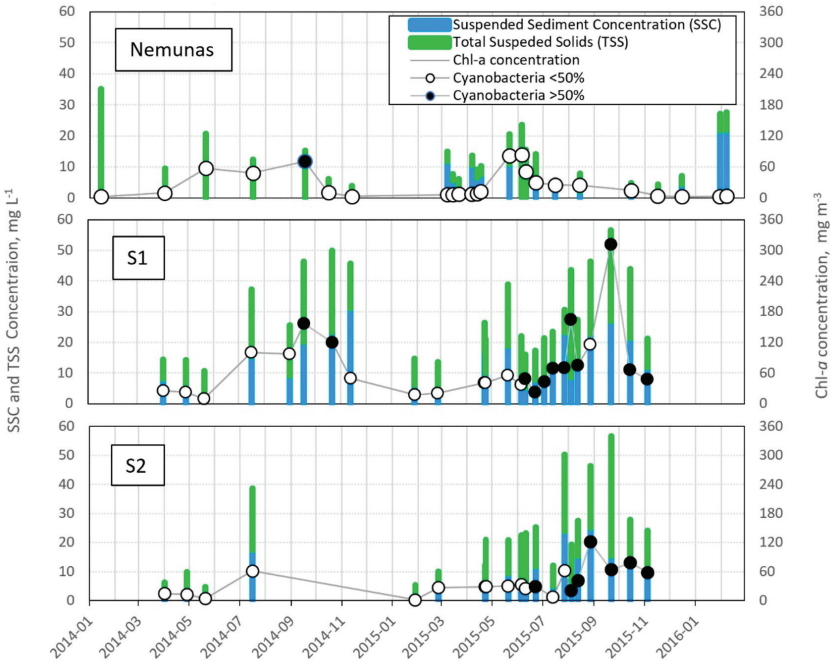

Figure 4. The time series of total (TSS), mineral sediment (SSC), and Chl-*a* concentrations and percentage of the cyanobacteria from the total phytoplankton community for monitoring stations Nemunas, S1, and S2. Columns without SSC values indicate field campaigns where only TSS were measured.

The highest concentrations values off TSS = 57 mg L^{-1} and SSC = 31 mg L^{-1} were found in summer and autumn during the algal bloom, when chlorophyll-*a* concentration peaked up to 300 mg m^{-3}. As is typical for the Curonian Lagoon in summer and autumn, the phytoplankton community was dominated by blue–green algae (cyanobacteria).

In general, the measured SSC varied form very low values (1–2 mg L^{-1}) to 30 mg L^{-1}. The TSS varied from 11 to 57 mg L^{-1}. It is important to mention that the sampling campaigns in the lagoon were planned when the weather conditions were calm and did not show the possible highest concentrations due to wind waves that could have a strong influence for the resuspension and sediment transport. Therefore, more observations are needed for better understanding of the system dynamics.

The results of the regression analysis for the relationship between SSC and water discharge based on the data sampled in 2015 are shown in Figure 5. On the model boundary, the averaged recalculated Nemunas River discharges in 2015 was 320 ± 171.3 m^3 s^{-1}, while the average discharge for the all of modeling period was 424.4 ± 217.4 m^3 s^{-1}.The power law function is a sediment rating curve that was used to estimate the missing SSC data for the river open boundary conditions.

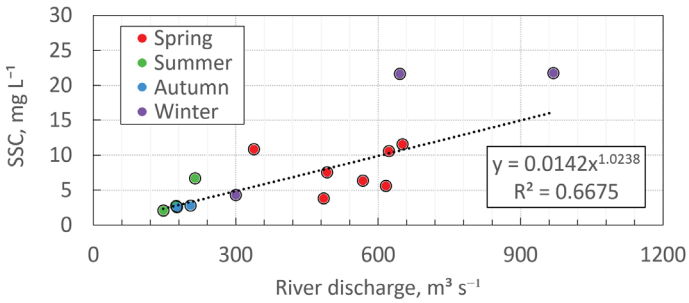

Figure 5. Relationship between SSC and Nemunas River discharge.

4.2. Model Calibration and Validation

The sediment transport model has several parameters that can be varied during the calibration process. Default model parameter values were obtained for the Venice Lagoon and could not be directly used for this study site [44,46]. The Van Rijn method for prediction of the non-cohesive sediment transport was chosen for the Curonian Lagoon. The initial critical shear stress value for erosion was set to 0.3 N m^{-2} according to the method mentioned above. The density for the freshly deposited mud was set to 775 kg m^{-3}.

The model performance quality criteria for calibration and validation were expressed in terms of the relative discrepancy defined as the ratio between measured and modeled SSC values (Figures 6 and 7). The model performance quality index was calculated as a percentage of points falling into the range of 0.5–2 (further called double relative discrepancy interval) of all values. It was assumed that the model performance quality is satisfactory if the model performance quality index exceeds 50% [44,59]. It means that predicted values should not be less than half or more than twice the observed values.

The first simulation for the period 2013–2015 was carried out with the real forcing data and sediment transport model parameters mentioned above. The measured and modeled SSC values in the water surface were compared in two Curonian Lagoon stations (S1 and S2) with different characteristics. Analysis of the results showed that the sediment model performance quality index was only 12.5% in station S1 (RMSE = 0.013 kg m^3) and 15% in station S2 (RMSE = 0.009 kg m^3). The highest discrepancies were observed in the summer and autumn seasons. Unsatisfactory calibration results obliged to analyze the processes that could influence the sediment transport mechanisms in the Curonian Lagoon in more details.

As highlighted above, SSC observations showed that in the lagoon, higher values were found during the summer–autumn period. Indeed, in late summer and beginning of autumn, modeled SSC values were lower compared with the measurements. The authors of [60] found that in the Curonian Lagoon, the settling velocities of total suspended solids (TSS) decrease in the summer months when positively buoyant cyanobacteria are present. Their calculated settling velocity for TSS in the summer

was about 0.3 m day^{-1} and the TSS concentrations in the lagoon correlated with Chl-*a* concentrations. There was no relationship found between river discharge and Chl-*a* that indicated the autochthonous origin of the suspended material. Also, it is known that diatoms and cyanobacteria scums can act as a trap for sediments because of the adhesive surface of their biofilms [61]. In Figure 4, it is shown that in the summer and autumn seasons, cyanobacteria were dominating in the Curonian Lagoon and especially in S1 station, where concentrations were very high. According to [62], one of the factors controlling the phytoplankton blooms is water temperature. Based on these studies a new formula (1) for fine sediment settling velocities as a function of water temperature was introduced into the model. The following new settling velocity equation was used for water temperature higher than 8 °C:

$$wws_b = a \times T + b, \quad (1)$$

where wws_b is the settling velocity in m day^{-1}, T the water temperature in °C. After calibration, the values $a = -0.03443$ and $b = 1.251117$ were used and, with the introduction of these changes, the model performance increased to 40% (RMSE = 11.5 mg L^{-1}) in station S1 (Figure 6A,B) and to 60% (RMSE = 5.7 mg L^{-1}) in station S2 (Figure 6C,D).

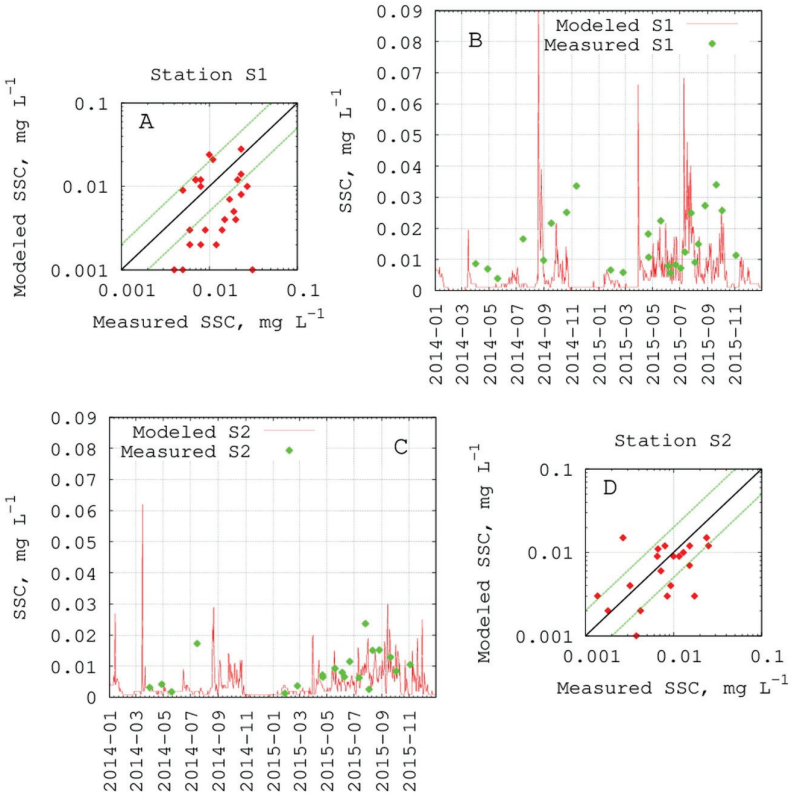

Figure 6. Comparison of the predicted and observed values after sediment model calibration for station S2 (**A**,**B**) and S1 (**C**,**D**). Scatterplots (**B**,**D**) are made using a logarithmic scale, where the solid line indicates absolute agreement with the measurements; the green lines correspond to the endpoints of double relative discrepancy intervals.

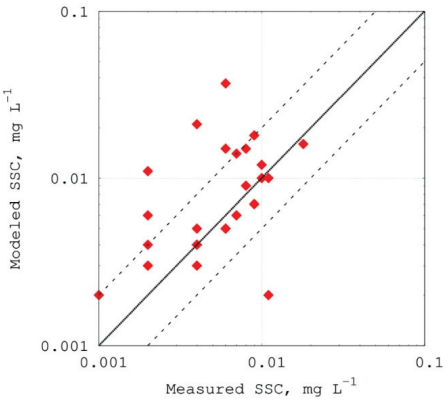

Figure 7. Scatterplot of the sediment transport model validation plotted on a logarithmic scale. Solid line indicates absolute agreement with the measurements, dashed lines corresponds to the endpoints of double relative discrepancy intervals. Data are sampled in 15 different places during August–September, 2016.

The results of the second simulation for the period 2015–2016 (VAL) were used for the model validation. The measured data for the end of August and first days of September in 2016, from the second dataset, were used (yellow dots in Figure 2C). Validation results show that modeled SSC values were in a good agreement with the measured data, with a model performance quality index (as defined above) of 72% (Figure 7).

4.3. Long-Term Simulation Results

Long-term simulation results gave us the possibility to analyze general sedimentation dynamics of the Curonian Lagoon, focusing on the suspended sediments distribution in the water column and erosion-accumulation zones. The year of 2004 was eliminated from the analysis as a spin up time, and 12 years of data were analyzed. The transition between smooth and rough hydrodynamic conditions of the flow near the bed depends on the friction velocity and the bottom roughness. According to the general characteristics of the seabed composition and the prevailing circulation dynamics, smooth turbulent flow predominates in the central and southern parts of the basin (muddy sediments, stagnant flow condition, accumulation zone), while transitional to rough conditions are expected to characterize the northern lagoon (sandy bottom, active flow conditions, erosion zone).

The averaged seasonal suspended sediment concentrations are shown in Figure 8. It can be seen that the lowest SSC values are found in the winter season, with an average value of 3 ± 1 mg L^{-1}. In spring, the highest SSC values were in the Nemunas Delta (average 23 ± 10 mg L^{-1}) and the Lithuanian part of the lagoon (average 12 ± 6 mg L^{-1}). The average spring concentration for all of the lagoon were 6 ± 6 mg L^{-1}. In the summer, the concentrations varied from 40 mg L^{-1} on the eastern coasts to 10 mg L^{-1} in the western part of the lagoon, with an average value of 19 ± 18 mg L^{-1} for all of lagoon. The SSC values in the autumn were more homogeneous, with the average concentration of 20 mg L^{-1} in the southern part and lower concentration on the eastern coast. The average autumn season value was 19 ± 15 mg L^{-1}.

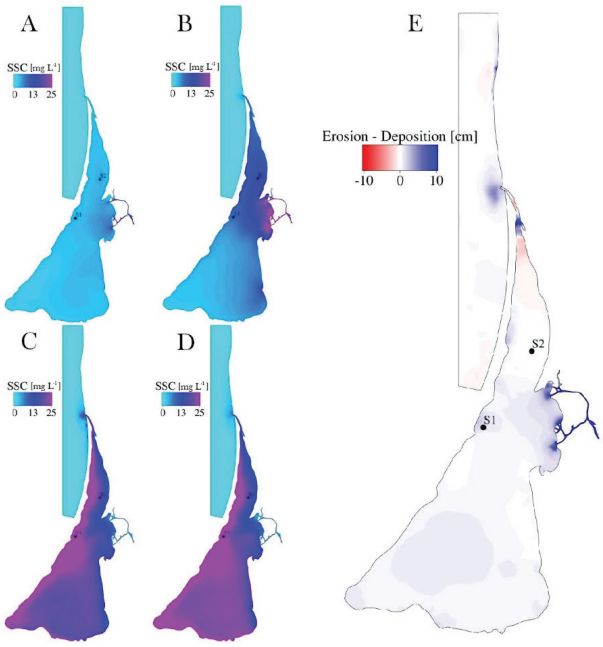

Figure 8. Seasonal distribution of SSC in the water column (**A**) winter, (**B**) spring, (**C**) summer, (**D**) autumn. (**E**) Erosion–deposition patterns after 12 years.

The erosion-accumulation zones after 12 years are presented in Figure 8E. Results show that the lagoon functions as a sediment sink with accumulation zones in the southern and central part of the lagoon and erosion zones in the north. On average, after 12 years, the southern and central parts became 6 mm shallower compared to the initial model bathymetry. Maximum (>+700 mm) bathymetry changes were in the Nemunas Delta. In the north, the averaged erosion was 3 mm after the whole simulation period.

The long-term simulation let us calculate the sediment budget for the Curonian Lagoon. It is important to remember that a value of zero for the SSC concentration was assumed on the model open sea boundary, because of the absence of measured suspended sediment data. The amount of sediments outgoing from the lagoon to the sea was calculated on the section shown in Figure 2D in Klaipeda harbor. The sediment input was considered as a sum of the sediments in the river mouths, directed into the lagoon, and the input of sediments from the sea on the Klaipeda harbor gates. Results show that there was no trend for the sediment input from the rivers to the system. It differed each year and depended on the rivers' discharges (Figure 9). The highest sediment input occurred in spring with the river flood period. The biggest calculated amount of riverine sediments was for the years 2010 and 2013, and was equal to 1.192×10^9 kg and 1.275×10^9 kg respectively. The average annual amount of sediment coming to the system was equal to $4.844 \times 10^8 \pm 3.780 \times 10^8$ kg y^{-1}. The computed sediment transport to the sea never exceeded the sediment input and had a strong correlation with the sediment input ($R^2 = 0.77$). The average annual amount of sediments flushed out of the system was equal to $1.858 \times 10^8 \pm 1.782 \times 10^8$ kg y^{-1}. On average, about 62% of the riverine sediments was trapped in the lagoon.

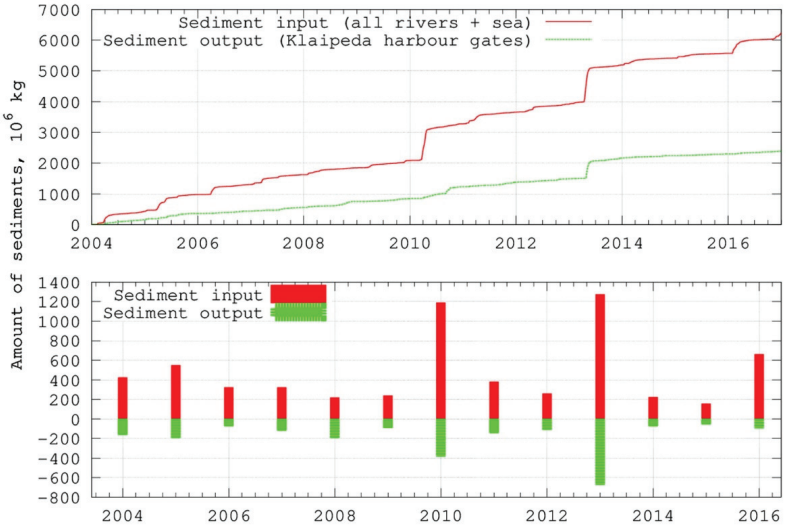

Figure 9. The cumulative amount of sediments coming into the system.

5. Discussion

5.1. In Situ Data and Sediment Rating Curve

The first part of the study, where the sampled suspended sediment data were analyzed, showed that the SSC trends in the rivers and lagoon are different. The highest riverine concentrations are in the winter–spring season when the flood period starts. In the lagoon, the highest TSS (20–57 mg L^{-1}) and SSC values were found in the summer–autumn season, together with the algal bloom or when the cyanobacteria were dominant. This is in agreement with other Curonian Lagoon studies, where the TSS were measured for the ice-free season [60,63], and the highest concentrations were found by [64] with the maximum TSS of 304 mg L^{-1} (in the article called particulate matter) during the summer–autumn season, due to high plankton concentrations. In most of the analyzed studies for the Baltic Sea lagoons and other regions, only the TSS values were measured. Similar trends with lower values in winter (TSS = 5–10 mg L^{-1}) and higher in summer (TSS = 20–35 mg L^{-1}) were found in the similar Vistula and Szczecin lagoons [13,65]. In comparison with the biggest lagoon in the world—the Patos Lagoon in Brazil—where the freshwater and wind are the main drivers, the TSS values variy from 50 until 150 mg L^{-1} (in the article called as Suspended Particulate Matter, g m^{-3}) with the recorded maximum of 1000 mg L^{-1} [66]. In the Patos Lagoon, a strong interannual variability of TSS was found, with the highest concentrations in austral spring and summer and the lowest in autumn and winter.

The closest permanent monitoring station in the Nemunas River is about 90 km from the model boundary, where only the TSS values are measured a few times per season. According to Bukaveckas et al. [60], there was no relationship found between TSS and river discharge in this station. Therefore, the one-year sampling campaign was organized to collect samples close to the model boundary. The developed sediment rating curve for 2015 was used for all the simulation period to estimate the Nemunas River suspended load according to the water discharges. The sediment curve is a useful tool for SSC prediction [67], but it should be used with care since different years can have different sediment supply rates depending on natural or human-caused changes in the watershed. In this study, there were no other data available; therefore, a sediment rating curve based on one-year data was used for the longer simulation periods.

A moderate relationship was found between the measured SSC and Nemunas River discharge. The SSC values predicted by the sediment rating curve during the flood period were lower than the measured values. With respect to the specific features of the Nemunas River, the lower SSC for the high river discharges can cause only minor uncertainties for the model results. Firstly, during the floods, especially large ones, in the delta region, the flow velocities hardly decreases because of the water overflow to the valley [68]. Secondly, it is known that during a flood, big amounts of sediments (about 35% of the suspended sediment input) are deposited in the delta meadows, due to favorable conditions for deposition, and do not reach the Curonian Lagoon [69]. The applied sediment transport model does not take into account the flooded areas and sedimentation in the meadows; as a result, the lower SSC values on the model river boundary should be in good agreement with the possible amounts of sediment that enter the Curonian Lagoon.

5.2. An Introduced Formula for Settling Velocity

In the second part of the study, a numerical model for the Curonian Lagoon was applied to understand the sediment transport mechanisms. First, simulations that were carried out for sediment model calibration show that in warm season, the riverine sediment loads were not sufficient to reproduce the measured SSC values in the lagoon waters. This suggests that the biological components in such complex lagoons like the Curonian Lagoon could be vital for the sediment dynamics and need to be analyzed in more details. The authors of [60] showed that settling velocities for the total suspended sediments in the Curonian Lagoon are very low when positively buoyant cyanobacteria are present. Pilkaitytė and Razinkovas [62] showed a strong relationship between cyanobacteria biomass and water temperature, while the authors of [70] found a moderately strong relationship between Chl-*a* concentrations and water temperature. These studies were a starting point for the development of a new formula for settling velocity. It is important to mention that the water temperature is not the only driver forcing cyanobacteria blooms, and only a moderately strong relationship was found. However, there were no other parameters in the sediment transport model that could be used to compute settling velocities. With the newly introduced formula for settling velocity, the measured and modeled SSC values were in better agreement than before. However, more adequate observations are necessary for settling velocities, especially for the cyanobacterial bloom period in late summer and at the beginning of autumn, especial in the areas with cohesive sediments where the developed model underestimates the measured values (Station S1). In addition, the organic material in suspensions is not the only factor that can affect the suspended sediment concentration and sediment dynamics in the system. For example, the benthic vegetation can influence the bed roughness and bottom sediment erodibility [58,71], which was not considered in this study.

5.3. Analysis of Model Calibration and Validation Results

After the calibration of the sediment transport model for the Curonian Lagoon with the new settling velocity, the S1 station showed lower than 50% model performance quality index that can be explained with the wider knowledge of the entire system. According to seasonal maps of the water currents in Umgiesser et al. [23], the S1 station has a minor influence of the Nemunas River, indicating that other source of the input material should be taken into account. Stronger currents on the western coasts of the lagoon can cause coastline erosion and increase the SSC values. The Curonian Spit is covered with sandy dunes open to aeolian processes, where part of the sand can be blown into the lagoon waters [20]. According to Galkus and Jokšas [17], 37% of the total sediment input (lithogenous income material) can enter the Curonian Lagoon from other sources such as precipitation, shore erosion, aeolian processes, waste waters, etc. All of these processes are not carefully estimated in this region and cannot be taken into account by the sediment transport model; as a result, it may cause model discrepancies. Overall, the applied model showed correct SSC fluctuations in station S1 according to different hydrodynamic conditions, with higher SSC values during the flood period,

and the summer–autumn season when the possible cyanobacteria bloom is present and when higher waves are dominant.

Despite the uncertainties in the S1 station, the model calibration results in the S2 station and validation results show satisfactory agreement between modeled and measured values, where 60% and 72% of the measured values, respectively, fall into the double relative discrepancy interval. Station S2 is located exactly on the way of the river water flow, while validation stations are spread in the northern site of the lagoon with different sedimentation properties.

In general, the model performance showed correct behavior of the SSC values; that is, the main property of the models in the sediment transport research stated in the [59]. There is a big variety of sediment modeling studies where values lower than 50% are accepted during the model calibration or validation processes because of the complexity of the study area and observation errors [6,45,59].

5.4. Factors Controlling Suspended Sediment Distribution

The analysis of the 12-year simulation results (scenario LONG) shows a strong seasonality in the distribution of the suspended sediments. The lowest SSC values were in the winter due to no waves under the ice. In spring, the influence of rivers was evident. The highest concentrations were on the river mouths because of the big amount of sediments transported during the flood period. The Nemunas River entering the lagoon in the central part of the lagoon divides the system into two parts. The northern part, strongly influenced by the river discharge and transport directed northward, had higher SSC values compared with the more stagnant southern part. The southern part depends on meteorological conditions [21,23] and can have considerably varying concentration values depending on the wind speed and direction within different years, with averaged concentration in the water column from about 5 mg L^{-1} in the years 2011 and 2015, until 25–35 mg L^{-1} in 2009 and 2010. In summer, the suspended sediment concentration gradient was formed from east to west due to the water circulation and low river discharges. In this season, the main factor influencing water column mixing and exchange between the southern and the northern part of the lagoon was the wind force [23]. The autumn season showed the biggest part of the lagoon with concentrations >25 mg L^{-1}. This can be explained as the result of high water temperatures in September and lower settling velocities introduced into the model.

Two factors can cause higher concentrations in the southern and eastern parts of the lagoon in autumn season. First, compared with spring and summer, stronger wind events are observed in autumn (see Figure 3C) that cause resuspension. Secondly, the higher water temperature in September decreases the particle settling velocity that leads to higher concentrations in the water column.

5.4.1. Impact of Ice Cover

Additionally, the 3-year short-term simulations were used to investigate the impact of ice cover and strong wind to the sediment distribution and transport running the model with and without ice cover data. The reproduction of ice cover by the model for the winter period reproduced the sheltering of the water from wind and changed the hydrodynamic conditions, described also by [13,23], that influenced the sediment transport in the whole lagoon and changed suspended sediment concentrations. To evaluate the influence of ice cover, the model results from two simulations were used (CAL and NoICE) for the period from 15 January 2014 until 7 March 2014. This was the period when the lagoon was covered in ice. The simulation where ice cover was taken into account gave an averaged SSC value for all of the Curonian Lagoon of 1.50 ± 1.79 mg L^{-1}. Without ice cover, this value increased to 2.8 ± 2.7 mg L^{-1}. A significant increase (>10 mg L^{-1}) appeared when the strong wind events were present in the region. A one-day event with the southeasterly winds and wind speeds of more than 10 m s^{-1} is shown in Figure 10. The absence of ice cover produced much higher bottom shear stress values that caused a bigger suspended sediment concentration in the water column.

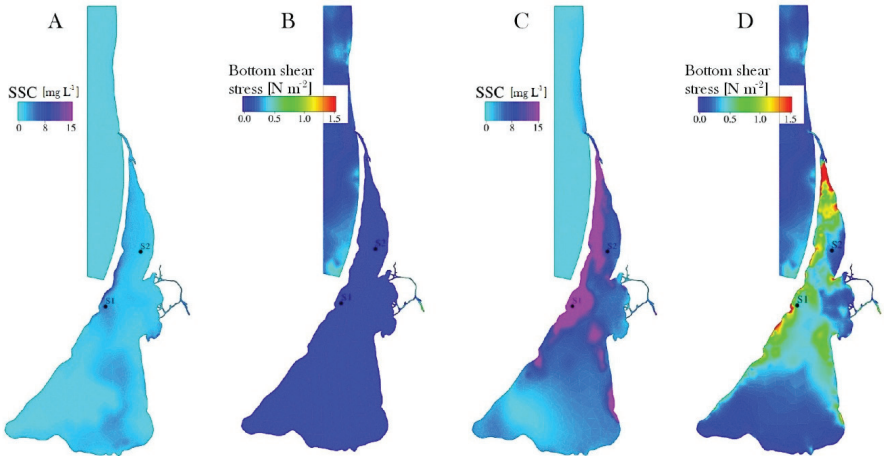

Figure 10. One-day (1 February 2014) event of the influence of ice cover on the sediment transport simulation (wind speed 10 m s^{-1}, SE direction). (**A**) SSC with ice; (**B**) bottom shear stress with ice; (**C**) SSC without ice; (**D**) bottom shear stress without ice.

The time series of SSC in the water column for stations S1 and S2 with and without ice cover are presented in Figure 11. In the deeper muddy station S1, the influence of ice cover was visible only with wind speeds higher than 10 m s^{-1} and wind blowing from the east, south-east, or south directions. In the shallower station S2 with sandy sediments, the influence of the ice cover was visible with winds blowing from south-west to north-west, already with wind speeds of more than 6 m s^{-1}. There were no northerly winds in the analyzed season.

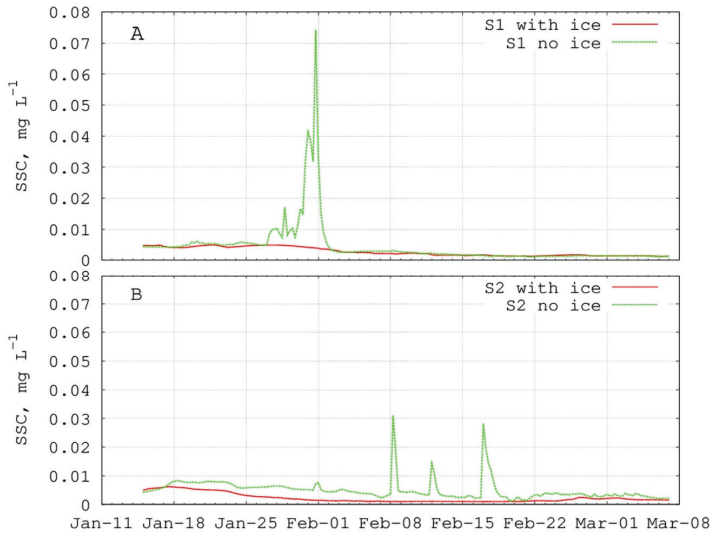

Figure 11. Simulated suspended sediment concentration with and without ice cover at monitoring station S1 (**A**) and S2 (**B**) during the first part of 2014.

This demonstrates that ice cover plays a crucial role for sediment transport as well. The authors of [23] already showed that incorporation of ice coverage data into the model gives much better results in terms of salinity and water renewal time. The use of satellite ice cover data gave us the possibility to analyze the performance of the system in a longer time window and with higher detail. Ice cover sheltered wind forcing over the lagoon surface and stopped the sediment resuspension due to waves induced by the strong winds, which are very common in winter period (Figure 3C,D). The ice cover decreases water exchange between the north and the south of the lagoon, and less fresh water from the Nemunas goes to the south [23]. These factors decreased the suspended sediment concentration in the water column in the winter compared to the concentrations simulated without ice cover. Analysis of 13 years of ice cover data did not show a clear trend for the ice cover presence in the lagoon (Figure 3B). Nevertheless, taking into account the climate change scenarios that predict a decreasing number of days with ice cover in the future [72], higher SSC values in the winter season could be expected due to the wind wave action on resuspension. Therefore, it is expected that the Curonian Lagoon will decrease its capacity to retain sediments in the future. However, it also has to be considered that an increase of the Nemunas sediment load for winter is forecasted in a climate change perspective (emission scenarios RCP4.5 and RCP8.5 [73]), with a probable associated enhancement of the winter sediment load into the lagoon.

5.4.2. Impact of Stormy Wind

The wind effect on the sediment dynamics in the lagoon was investigated for the whole CAL simulation period (3 years). The analysis of strong storm events shows that big amounts of sediments can be washed out of the system in a short period and the time to recover is from few days to seasons. A single storm event on 6 December 2013 with SW winds and wind speed higher than 20 m s^{-1} was analyzed in more detail (Figure 12), which shows that in a one or two days, a great amount of sediments can be resuspended, and part of these sediments can be washed out of the system, forming erosion zones in the lagoon.

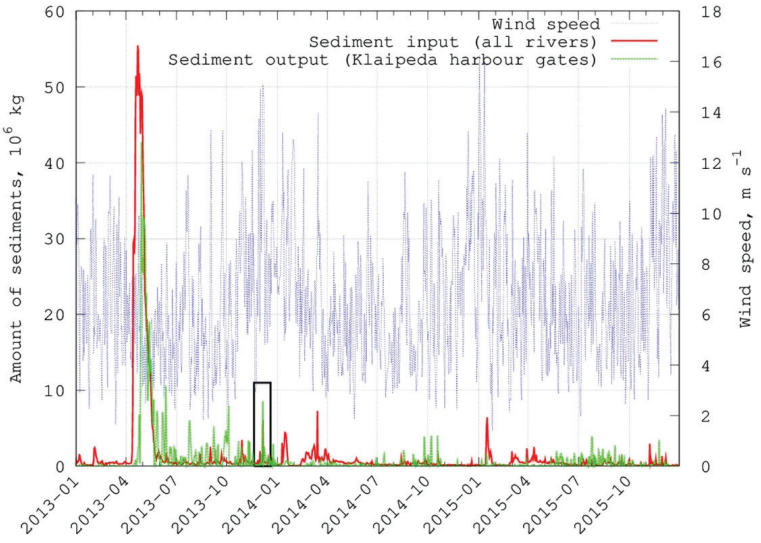

Figure 12. Time series of sediment input and output from the Curonian Lagoon to the sea. Black rectangle indicates the discussed storm event.

The model simulates the sediment fluxes through the given sections, thus it was possible to estimate the sediment input and output to the system (see Section 4.3). An amount of 11.4×10^6 kg was transported outward through the harbor gates in two days (6th and 7th). Taking into account the sediment input on these days, after a storm, the loss of 4.7×10^6 kg of sediments was calculated and big erosion zones in the south-eastern side and central part of the lagoon were formed. This was 8% of all sediment output and 3% of total input in 2015, but only 0.7% of the total output and 0.4% of input in 2013. 2015 and 2013 are the years with minimum and maximum input in the period of 2004–2016. respectively. Comparing these numbers with the average daily sediment riverine input (about $1.10 \times 10^5 \pm 8.6 \times 10^4$ kg day^{-1}), 42 days would be necessary to refill the basin.

The results show that strong storm events are important factors in analyzing the distribution of the suspended sediments and can have a strong influence for the sediment budget calculation or analysis of erosion-accumulation zones in the region, especially if the short period is analyzed. The effect of the strong wind events on sediment erosion in coastal lagoons has received a lot of research attention in the past years (e.g., [74] and references therein), possibly due to climate change forecast on increasing storminess [75]. High wind speeds lead to increased bed shear stress values in function of waves and currents that causes suspension of the sediments.

5.5. Erosion-Accumulation Zones in the Curonian Lagoon

The erosion accumulation zones were in good agreement with [21], where the southern part with a resident time of more than 120 days was classified as an accumulation zone. The northern part, characterized by strong riverine influence, was limited for accumulation of suspended matter and acted as a transitional zone. According to [8], the wind wave impact in the lagoon counteracts the accumulation of suspended material transported by the Nemunas River in the north, which thereby maintains the deeper regions in this lagoon.

The averaged accumulation rate in the southern part was about 0.5 mm year^{-1}, and the averaged erosion rate in the north was about 0.23 mm year^{-1}. When analyzing results in smaller areas, higher erosion and accumulation rates can be found, e.g., in the Nemunas Delta and in the Klaipeda Strait with accumulation rates of about 7 mm year^{-1}. Pustelnikovas [37] measured the accumulation rates in five points (four point in the western site and one close to the Matrosovka River), and it was concluded that the accumulation is 3.2 mm year^{-1} or 3.4 mm year^{-1} in the deeper areas. The measurements were done in the areas where muddy sediments, rich with organic particles, are dominant. The developed model did not include organic particles, and as a result, the estimated sedimentation rates for total suspended material in the southern part should be higher than the ones modeled for inorganic particles only.

5.6. Model Results for Sediment Budget Calculation

The sediment budget for the Curonian Lagoon was calculated through the difference between incoming and outgoing sediments. The estimated averaged annual sediment input to the system, which consisted of riverine input and the input from the sea, was $4.844 \times 10^8 \pm 3.790 \times 10^8$ kg year^{-1}. The annual output to the sea was $1.858 \times 10^8 \pm 1.782 \times 10^8$ kg year^{-1} and $2.986 \times 10^8 \pm 2.381 \times 10^8$ kg year^{-1} stayed in the lagoon in suspensions or on the bottom. It is clear that the Curonian Lagoon acts as a sink for the sediments and differs from similar lagoons in the Baltic area, where the Vistula lagoon is losing sediments [76] and the Szczecin lagoon is transporting sediments to the sea [65]. The sediment budget for the Curonian Lagoon, calculated by other studies, was in range with our study. The total budget calculated by [18] was $\pm 4.542 \times 10^8$ kg year^{-1} and by [17] $\pm 4.508 \times 10^8$ kg year^{-1}. The biggest disagreement in these studies was between the amounts of sediment that exit to the sea and accumulate in the lagoon. In Pustelnikovas research [18], it was calculated that the lagoon accumulates 3.372×10^8 kg year^{-1} and in [17], the accumulation of 1.328×10^8 kg year^{-1} was found. The different amounts of accumulated sediments can be explained by our study, which shows that the budget for different years can vary by more than 5 times. We found strong correlation between incoming and outgoing annual amounts of sediment.

It is important to mention that in the model, at the open sea boundary, the suspended sediment concentration was set to 0 because of the absence of data. This can decrease the simulated sediment input to the Klaipėda Strait area and influence the sediment budget. However, the sediment transport model could be a valuable tool for optimizing the dredging activities in the Klaipeda Strait and harbor. For such specific tasks, the numerical model could be applied with higher resolution in order to reproduce, within the use of the unstructured mesh, both the sediment transport in the lagoon and the small-scale dynamics around the artificial structures of the harbor area. In conclusion, the simulations that have been carried out to study the sediment transport mechanisms in the Curonian Lagoon gave satisfactory results and the possibility to get a holistic view of the system. This was the first study where the sediment transport model was applied for the Curonian Lagoon, but more observations and studies are still necessary to understand the sediment dynamics in such a complex system with rich in organic material and high riverine inflow.

Author Contributions: Conceptualization: J.M., C.F., and G.U.; methodology: J.M., C.F., and G.U.; software: J.M., C.F., and G.U.; calibration: J.M. and C.F.; validation: J.M.; formal analysis: J.M.; investigation: J.M., C.F., and G.U.; data curation: J.M., P.Z., D.V., and R.I.; writing—original draft preparation: J.M.; writing—review and editing: J.M., C.F., G.U., P.Z., D.V., and R.I.; visualization: J.M.; supervision: G.U. and C.F.; funding acquisition: G.U.

Funding: Part of this study was funded by the European Social Fund under the Global Grant measure (CISOCUR project VP1-3.1-ŠMM-07-K-02-086) and EcoServe (project No 09.3.3-LMT-K-712-01-0178) under grant agreement with the Research Council of Lithuania (LMTLT). The major part of the work was supported by the Doctorate Study programme in Ecology and Environmental Sciences, Klaipėda University (for J.M). Sampling activities and data collection for the year 2014–2016 were supported by the 7BP INFORM project (Contract No. 606865), a project funded by Lithuanian Research Council (Contract No. VAT- MIP-040/2014), and the Lithuanian EPA project (No. 28TP-2015-19SUT-15P-13).

Acknowledgments: We thank Mindaugas Zilius, Jolita Petkuviene, and Irma Vybernaite-Lubiene for assistance during the field campaigns and laboratory activities. This work was also inspired by the activities of the scientific community that is building the ESFRI DANUBIUS Research Infrastructure—The International Centre for Advanced Studies on River-Sea Systems (http://www.danubius-ri.eu/).

Conflicts of Interest: The authors declare no conflicts of interest.

References

1. Ji, Z.-G. *Hydrodynamics and Water Quality*; John Wiley & Sons, Inc.: Hoboken, NJ, USA, 2008; ISBN 978-1-11-887715-9.
2. Eisenreich, S.J.; Bernasconi, C. *Climate Change and the European Water Dimension*; EU Report No. 21553; Joint Research Center of European Commission: Ispra, Italy, 2005.
3. Maicu, F.; De Pascalis, F.; Ferrarin, C.; Umgiesser, G. Hydrodynamics of the Po River-Delta-Sea System. *J. Geophys. Res. Ocean.* **2018**, *123*, 6349–6372. [CrossRef]
4. Maselli, V.; Trincardi, F. Man made deltas. *Sci. Rep.* **2013**, *3*, 1926. [CrossRef]
5. Syvitski, J.P.M.; Kettner, A. Sediment flux and the anthropocene. *Philos. Trans. R. Soc. A Math. Phys. Eng. Sci.* **2011**, *369*, 957–975. [CrossRef] [PubMed]
6. Escobar, C.A.; Velásquez-Montoya, L. Modeling the sediment dynamics in the gulf of Urabá colombian Caribbean sea. *Ocean Eng.* **2017**, *147*, 476–487. [CrossRef]
7. Ji, Z.G.; Jin, K.R. Impacts of wind waves on sediment transport in a large, shallow lake. *Lakes Reserv. Res. Manag.* **2014**, *19*, 118–129. [CrossRef]
8. Chubarenko, B.; Lund-Hansen, L.C.; Beloshitskii, A. Comparative analyses of potential wind-wave impact on bottom sediments in the Vistula and Curonian lagoons. *Baltica* **2002**, *15*, 30–39.
9. Teeter, A.M.; Johnson, B.H.; Berger, C.; Stelling, G.; Scheffner, N.W.; Garcia, M.H.; Parchure, T.M. Hydrodynamic and sediment transport modeling with emphasis on shallow-water, vegetated areas (lakes, reservoirs, estuaries and lagoons). *Hydrobiologia* **2001**, *444*, 1–23. [CrossRef]
10. Kataržytė, M.; Mėžinė, J.; Vaičiūtė, D.; Liaugaudaitė, S.; Mukauskaitė, K.; Umgiesser, G.; Schernewski, G. Fecal contamination in shallow temperate estuarine lagoon: Source of the pollution and environmental factors. *Mar. Pollut. Bull.* **2018**, *133*, 762–772. [CrossRef]
11. Zilius, M.; De Wit, R.; Bartoli, M. Response of sedimentary processes to cyanobacteria loading. *J. Limnol.* **2016**, *75*, 236–247. [CrossRef]

12. De Swart, H.E.; Zimmerman, J.T.F. Morphodynamics of Tidal Inlet Systems. *Annu. Rev. Fluid Mech.* **2009**, *41*, 203–229. [CrossRef]
13. Chubarenko, B.; Chechko, V.; Kileso, A.; Krek, E.; Topchaya, V. Hydrological and sedimentation conditions in a non-tidal lagoon during ice coverage – The example of Vistula Lagoon in the Baltic Sea. *Estuar. Coast. Shelf Sci.* **2019**, *216*, 38–53. [CrossRef]
14. Chechko, V.A.; Topchaya, V.Y.; Chubarenko, B.V.; Pilipchuk, V.A. Distribution and composition of suspended matter in water and snow cover in Kaliningrad Bay. *Water Resour.* **2016**, *43*, 33–41. [CrossRef]
15. Chechko, V.A.; Blazchishin, A.I. Bottom deposits of the Vistula lagoon of the Baltic Sea. *Baltica* **2002**, *15*, 13–22.
16. Galkus, A. Vandens cirkuliacija ir erdvine drumstumo dinamika vasara Kuršių marių ir Baltijos jūros Lietuvos akvatorijose [Summer water circulation and spatial turbidity dynamics in the Lithuanian waters of Curonian lagoon and Baltic Sea]. *Geogr. Metrašt.* **2003**, *36*, 3–16.
17. Galkus, A.; Jokšas, K. *Nuosėdinė Medžiaga Tranzitinėje Akvasistemoje [Sedimentary Material in the Transitional Aquasystem]*; Institute of Geography: Vilnius, Lithuania, 1997; ISBN 9986909775.
18. Pustelnikovas, O. *Geochemistry of Sediments of the Curonian Lagoon (Baltic Sea)*; Institute of Geography: Vilnius, Lithuania, 1998; ISBN 978-9-98-690976-7.
19. Pustelnikovas, O. Transport and accumulation of sediment and contaminants in the Lagoon of Kuršiu{ogonek}marios (Lithuania) and Baltic Sea. *Neth. J. Aquat. Ecol.* **1994**, *28*, 405–411. [CrossRef]
20. Trimonis, E.; Gulbinskas, S.; Kuzavinis, M. The Curonian Lagoon bottom sediments in the Lithuanian water area. *Baltica* **2003**, *16*, 13–20.
21. Ferrarin, C.; Razinkovas, A.; Gulbinskas, S.; Umgiesser, G.; Bliudžiute, L. Hydraulic regime-based zonation scheme of the Curonian Lagoon. *Hydrobiologia* **2008**, *611*, 133–146. [CrossRef]
22. Zemlys, P.; Ferrarin, C.; Umgiesser, G.; Gulbinskas, S.; Bellafiore, D. Investigation of saline water intrusions into the Curonian Lagoon (Lithuania) and two-layer flow in the Klaipeda Strait using finite element hydrodynamic model. *Ocean Sci.* **2013**, *9*, 573–584. [CrossRef]
23. Umgiesser, G.; Zemlys, P.; Erturk, A.; Razinkovas-Baziukas, A.; Mėžinė, J.; Ferrarin, C. Seasonal renewal time variability in the Curonian Lagoon caused by atmospheric and hydrographical forcing. *Ocean Sci.* **2016**, *12*, 391–402. [CrossRef]
24. Ferrarin, C. *A Sediment Transport Model for the Lagoon of Venice*; Universiteta Ca'Foscari: Venezia, Italia, 2007.
25. Kriaučiūnienė, J.; Gailiušis, B.; Rimavičiūtė, E. Modelling of shoreface nourishment in the Lithuanian nearshore of the Baltic Sea. *Geologija* **2006**, *53*, 28–37.
26. Kriaučiūnienė, J.; Gailiušis, B. Changes of Sediment Transport Induced by Reconstruction of Kalipėda seaport Entrance Channel. *Environ. Res. Eng. Manag.* **2004**, *2*, 3–9.
27. Žaromskis, R. *Okeanai, Jūros ir Estuarijos [Oceans, Seas, Estuaries]*; Debesija: Vilnius, Lithuania, 1996; ISBN 9986652022.
28. Zilius, M.; Vybernaite-Lubiene, I.; Vaiciute, D.; Petkuviene, J.; Zemlys, P.; Liskow, I.; Voss, M.; Bartoli, M.; Bukaveckas, P.A. The influence of cyanobacteria blooms on the attenuation of nitrogen throughputs in a Baltic coastal lagoon. *Biogeochemistry* **2018**, *141*, 143–165. [CrossRef]
29. Pilkaityte, R.; Razinkovas, A. Seasonal changes in phytoplankton composition and nutrient limitation in a shallow Baltic lagoon. *Boreal Environ. Res.* **2007**, *12*, 551–559.
30. Gasiūnaitė, Z.R.; Daunys, D.; Olenin, S.; Razinkovas, A. The Curonian Lagoon. In *Ecology of Baltic Coastal Waters*; Schiewer, U., Ed.; Springer: Berlin/Heidelberg, Germany, 2008; pp. 197–215. ISBN 978-3-54-073524-3.
31. Gelumbauskaitė, L.Ž.; Grigelis, A.; Cato, I.; Repečka, M.; Kjellin, B. Bottom Topography and Sediment Maps of the Central Baltic Sea: Scale 1: 500,000. A Short Description. *LGT Ser. Mar. Geol. Maps No. 1/SGU Ser. Geol. Maps Ba No. 54.* Available online: https://www.dmu.dk/1_Viden/2_Miljoe-tilstand/3_vand/4_Charm/charm_res/data/WP1/Deliverable9/charm_all%20maps.htm (accessed on 20 September 2018).
32. Gulbinskas, S.; Žaromskis, R. *The Curonian Lagoon Map for Fishery M 1:50 000*; Lithuanian Deparment of Fisheries: Vilnius, Lithuania, 2002.
33. Gailiušis, B.; Kovalenkovienė, M.; Jurgelėnaitė, A. Klaipėdos sąsiaurio tėkmės planinės struktūros pokyčių modeliavimas [Water balance of the Curonian Lagoon]. *Energetika* **1992**, *2*, 67–72.
34. Jakimavičius, D. Changes of Water Balance Elements of the Curonian Lagoon and Their Forecast Due to Anthropogenic and Natural Factors. Ph.D.Thesis, Kaunas University of Technology, Kaunas, Lithuania, 2012.

35. Dailidiene, I.; Davuliene, L. Salinity trend and variation in the Baltic Sea near the Lithuanian coast and in the Curonian Lagoon in 1984–2005. *J. Mar. Syst.* **2008**, *74*, 20–29. [CrossRef]
36. Trimonis, E.; Vaikutiene, G.; Gulbinskas, S. Seasonal and spatial variations of sedimentary matter and diatom transport in the Klaipėda Strait (Eastern Baltic). *Baltica* **2010**, *23*, 127–134.
37. Pustelnikovas, O. On the Eastern Baltic environment changes: A case study of the Curonian Lagoon area. *Geologija* **2008**, *50*, 80–87. [CrossRef]
38. Strickland, J.D.H.; Parsons, T. *A Practical Hand Book of Seawater Analysis*, 2nd ed.; Fisheries Research Board of Canada: Ottawa, ON, Canada, 1972; ISBN 978-0-66-011596-2.
39. Jeffrey, S.W.; Humphrey, G.F. New spectrophotometric equations for determining chlorophylls a, b, c1 and c2 in higher plants, algae and natural phytoplankton. *Biochemie und Physiologie der Pflanzen* **1975**, *167*, 191–194. [CrossRef]
40. Parsons, T.R.; Maita, Y.; Lalli, C.M. *A Manual of Chemical and Biological Methods for Seawater Analysis*; Pergamon Press: New York, NY, USA, 1984; ISBN 978-0-08-030287-4.
41. Catherine, A.; Escoffier, N.; Belhocine, A.; Nasri, A.B.; Hamlaoui, S.; Yéprémian, C.; Bernard, C.; Trousselliер, M. On the use of the FluoroProbe ®, a phytoplankton quantification method based on fluorescence excitation spectra for large-scale surveys of lakes and reservoirs. *Water Res.* **2012**, *46*, 1771–1784. [CrossRef]
42. Umgiesser, G.; Ferrarin, C.; Cucco, A.; De Pascalis, F.; Bellafiore, D.; Ghezzo, M.; Bajo, M. Comparative hydrodynamics of 10 Mediterranean lagoons by means of numerical modeling. *J. Geophys. Res. Ocean.* **2014**, *119*, 2212–2226. [CrossRef]
43. Umgiesser, G.; Canu, D.M.; Cucco, A.; Solidoro, C. A finite element model for the Venice Lagoon. Development, set up, calibration and validation. *J. Mar. Syst.* **2004**, *51*, 123–145. [CrossRef]
44. Neumeier, U.; Ferrarin, C.; Amos, C.L.; Umgiesser, G.; Li, M.Z. Sedtrans05: An improved sediment-transport model for continental shelves and coastal waters with a new algorithm for cohesive sediments. *Comput. Geosci.* **2008**, *34*, 1223–1242. [CrossRef]
45. Ferrarin, C.; Cucco, A.; Umgiesser, G.; Bellafiore, D.; Amos, C.L. Modelling fluxes of water and sediment between Venice Lagoon and the sea. *Cont. Shelf Res.* **2010**, *30*, 904–914. [CrossRef]
46. Ferrarin, C.; Umgiesser, G.; Cucco, A.; Hsu, T.W.; Roland, A.; Amos, C.L. Development and validation of a finite element morphological model for shallow water basins. *Coast. Eng.* **2008**, *55*, 716–731. [CrossRef]
47. Ferrarin, C.; Umgiesser, G.; Roland, A.; Bajo, M.; De Pascalis, F.; Ghezzo, M.; Scroccaro, I. Sediment dynamics and budget in a microtidal lagoon—A numerical investigation. *Mar. Geol.* **2016**, *381*, 163–174. [CrossRef]
48. CERC. *Shore Protection Manual: Volume I and II*; U.S. Government Printing Office: Washington, DC, USA, 1984; ISBN 978-8-57-811079-6.
49. Van Ledden, M.; Van Kesteren, W.G.M.; Winterwerp, J.C. A conceptual framework for the erosion behaviour of sand-mud mixtures. *Cont. Shelf Res.* **2004**, *24*, 1–11. [CrossRef]
50. Van Rijn, L. *Principles of Sediment Transport in Rivers, Estuaries and Coastal Seas*; Aqua Publications: Amsterdam, The Netherlands, 1993; ISBN 9080035629.
51. Li, M.Z.; Amos, C.L. SEDTRANS96: The upgraded and better calibrated sediment-transport model for continental shelves. *Comput. Geosci.* **2001**, *27*, 619–645. [CrossRef]
52. Soulsby, R. *Dynamics of Marine Sands: A Manual for Practical Applications*; Thomas Telford Publishing: London, UK, 1997.
53. Funkquist, L. A unified model system for the Baltic Sea. *Elsevier Oceanogr. Ser.* **2003**, *69*, 516–518.
54. Chen, C.L. Power of Flow Resistance in Open Channels; Manning's Formula Revisited. In *Channel Flow Resistance: Centennial of Manning's Formula*; Yen, B.C., Ed.; Water Resources Publications: Littleton, CO, USA, 1992; ISBN 978-1-88-720-180-3.
55. Vaikasas, S. *Nemuno Žemupio Potvynių Tėkmių ir Nešmenų Dinamikos Modeliavimas [Flood Dynamics and Sedimentation-Diffusion Processes in the Lowland of the River Nemunas]*; Technika: Vilnius, Lithuania, 2009; ISBN 978-9-95-528539-7.
56. Idzelytė, R.; Kozlov, I.E.; Umgiesser, G. Remote Sensing of Ice Phenology and Dynamics of Europe's Largest Coastal Lagoon (The Curonian Lagoon). *Remote Sens.* **2019**, *11*, 2059. [CrossRef]
57. Asselman, N.E.M. Fitting and interpretation of sediment rating curves. *J. Hydrol.* **2000**, *234*, 228–248. [CrossRef]

58. Amos, C.L.; Bergamasco, A.; Umgiesser, G.; Cappucci, S.; Cloutier, D.; DeNat, L.; Flindt, M.; Bonardi, M.; Cristante, S. The stability of tidal flats in Venice Lagoon—the results of in-situ measurements using two benthic, annular flumes. *J. Mar. Syst.* **2004**, *51*, 211–241. [CrossRef]
59. Davies, A.G.; Van Rijn, L.C.; Damgaard, J.S.; Van De Graaff, J.; Ribberink, J.S. Intercomparison of research and practical sand transport models. *Coast. Eng.* **2002**, *46*, 1–23. [CrossRef]
60. Bukaveckas, P.A.; Katarzyte, M.; Schlegel, A.; Spuriene, R.; Egerton, T.; Vaiciute, D. Composition and settling properties of suspended particulate matter in estuaries of the Chesapeake Bay and Baltic Sea regions. *J. Soils Sediments* **2019**, *19*, 2580–2593. [CrossRef]
61. Larson, F.; Lubarsky, H.; Gerbersdorf, S.U.; Paterson, D.M. Surface adhesion measurements in aquatic biofilms using magnetic particle induction: MagPI. *Limnol. Oceanogr. Methods* **2009**, *7*, 490–497. [CrossRef]
62. Pilkaityte, R.; Razinkovas, A. Factors controlling phytoplankton blooms in a temperate estuary: Nutrient limitation and physical forcing. *Hydrobiologia* **2006**, *555*, 41–48. [CrossRef]
63. Kari, E.; Kratzer, S.; Beltrán-Abaunza, J.M.; Harvey, E.T.; Vaičiūtė, D. Retrieval of suspended particulate matter from turbidity–model development, validation, and application to MERIS data over the Baltic Sea. *Int. J. Remote Sens.* **2017**, *38*, 1983–2003. [CrossRef]
64. Remeikaite-Nikiene, N.; Lujaniene, G.; Garnaga, G.; Jokšas, K.; Garbaras, A.; Skipityte, R.; Barisevičiute, R.; Šilobritiene, B.; Stankevičius, A. Distribution of trace elements and radionuclides in the Curonian Lagoon and the Baltic Sea. In Proceedings of the 2012 IEEE/OES Baltic International Symposium (BALTIC) on Ocean: Past, Present and Future, Klaipeda, Lithuania, 8–10 May 2012.
65. Leipe, T.; Eidam, J.; Reinhard, L.; Hinrich, M.; Neumann, T.; Osadczuk, A.; Janke, W.; Puff, T.; Blanz, T.; Gingele, F.X.; et al. Das Oderhaff, Beiträge zur Rekonstruktion der holozänen geologischen Entwicklung und antropogenen Beeinflus sung des Oder Ästuars. *Mar. Sci. Rep.* **1998**, *28*, 1–61.
66. Tavora, J.; Fernandes, E.H.L.; Thomas, A.C.; Weatherbee, R.; Schettini, C.A.F. The influence of river discharge and wind on Patos Lagoon, Brazil, Suspended Particulate Matter. *Int. J. Remote Sens.* **2019**, *40*, 4506–4525. [CrossRef]
67. Warrick, J.A. Trend analyses with river sediment rating curves. *Hydrol. Process.* **2015**, *29*, 936–949. [CrossRef]
68. Rimkus, A.; Vaikasas, S. Mathematical Modeling of the Suspended Sediment Dynamics in the Riverbeds and Valleys of Lithuanian Rivers and Their Deltas. In *Water Pollution*; Balkis, N., Ed.; InTech: Rijeka, Croatia, 2012; pp. 105–124. ISBN 978-9-53-307962-2.
69. Vaikasas, S.; Rimkus, A. Hydraulic Modelling of Suspended Sediment Deposition in an Inundated Floodplain of the Nemunas Delta. *Hydrol. Res.* **2003**, *34*, 519–530. [CrossRef]
70. Aleksandrov, S.; Krek, A.; Bubnova, E.; Danchenkov, A. Eutrophication and effects of algal bloom in the south–western part of the Curonian Lagoon alongside the Curonian Spit. *Baltica* **2018**, *31*, 1–12. [CrossRef]
71. Grabowski, R.C.; Droppo, I.G.; Wharton, G. Erodibility of cohesive sediment: The importance of sediment properties. *Earth-Sci. Rev.* **2011**, *105*, 101–120. [CrossRef]
72. BACC II Author Team. *Second Assessment of Climate Change for the Baltic Sea Basin*; Springer: Cham, Swizerland, 2015; ISBN 978-3-31-916005-4.
73. Čerkasova, N. Nemunas River Watershed Input to the Curonian Lagoon: Discharge, Microbiological Pollution, Nutrient and Sediment Loads under Changing Climate. Ph.D. Thesis, Klaipėda University, Klaipėda, Lithuania, 2019.
74. Forsberg, P.L.; Ernstsen, V.B.; Andersen, T.J.; Winter, C.; Becker, M.; Kroon, A. The effect of successive storm events and seagrass coverage on sediment suspension in a coastal lagoon. *Estuar. Coast. Shelf Sci.* **2018**, *212*, 329–340. [CrossRef]
75. Intergovernmental Panel on Climate Change. *Climate Change 2014 Synthesis Report—IPCC*; IPCC: Geneva, Switzerland, 2014; ISBN 978-9-29-169143-2.
76. Chubarenko, B.V.; Chubarenko, I.P. New way of natural geomorphological evolution of the Vistula Lagoon due to crucial artificial influence. In *Geology of the Gdansk Basin, Baltic Sea*; Yantarny Skaz: Kaliningrad, Russia, 2001; pp. 372–375.

PAPER III

Oceanologia (2020) 62, 428—442

Available online at www.sciencedirect.com

ScienceDirect

journal homepage: www.journals.elsevier.com/oceanologia

ORIGINAL RESEARCH ARTICLE

Study of ice cover impact on hydrodynamic processes in the Curonian Lagoon through numerical modeling

Rasa Idzelytė[a,*], Jovita Mėžinė[a], Petras Zemlys[a], Georg Umgiesser[b,a]

[a] *Marine Research Institute, Klaipėda University, Klaipėda, Lithuania*
[b] *CNR — National Research Council of Italy, ISMAR — Institute of Marine Sciences, Venice, Italy*

Received 27 October 2019; accepted 23 April 2020
Available online 18 May 2020

KEYWORDS
Ice cover impact;
Water circulation;
Numerical modelling;
SHYFEM;
Curonian Lagoon

Summary In this study, we present an analysis of the hydrodynamic processes under ice cover in the largest lagoon in Europe — the Curonian Lagoon. By applying a finite element numerical modelling system (SHYFEM) and remote sensing ice cover data, the residual circulation, water fluxes through specific areas of the lagoon, saltwater intrusions, and water residence time (WRT) were investigated. The results, taken over an 11 year period, show that ice cover affects the circulation patterns in the lagoon by forming and shifting different gyre systems. Different circulation patterns are observed throughout all the meteorological seasons of the year. Since ice decreases circulation, water fluxes also decrease, especially in a cross-section in the middle of the lagoon, where the ice-cover suppressed wind-stress has a higher impact on the water movement rather than it has in the north. The presence of ice cover also decreases the salinity of the water in the northern part of the lagoon. In general, the salinity in the water column averaged over different periods is vertically uniform, however, a slight increase of salt concentration can be observed at the bottom layers in the Klaipėda Strait, where the difference of >1 PSU between bottom and top layers shows up on average 130 hours per year. The ice cover also decreases the saltwater intrusions into the lagoon by nearly 14 days per year. The increase of WRT is most prominent after long ice cover periods, away from the river inlets, especially

* Corresponding author at: Marine Research Institute, Klaipėda University, Universiteto ave. 17, 92294, Klaipėda, Lithuania.
E-mail address: rasa.idzelyte@apc.ku.lt (R. Idzelytė).

Peer review under the responsibility of the Institute of Oceanology of the Polish Academy of Sciences.

Production and hosting by Elsevier

https://doi.org/10.1016/j.oceano.2020.04.006

in the southern part of the lagoon, where without the help of the wind action, water takes a longer time to renew than in the northern part.

1. Introduction

Changing ice cover conditions have a strong impact on the hydrodynamics, exchange processes, and overall ecosystem of the water body, including the fisheries and tourism sector. Ice cover formation is controlled by variations in heat exchange and mixing, as well as the heat storage capacity of the water body (Bengtsson, 2012). The initial ice formation can be rather complex with many freezing and break-up events depending on the strength of the heat loss and wind stress at the water surface.

Ice cover affects a water body in several ways. It suppresses the direct wind stress to the water surface and significantly alters the circulation and mixing (Wang et al., 2010). The movement of the water is highly regulated by thermal processes and by the vertical motion of the ice cover (Bengtsson, 2012). Convective mixing is induced when there is enough light penetrating through the ice and by heat exchange with the sediments. The latter is a very slow process capable to last throughout the whole winter (Bengtsson, 1996). Inflowing water from the rivers induce circulation near the inlets, thus it may only have a local effect on the overall circulation (Cushman-Roisin, 2019).

Freshwater bodies connected to the sea by a strait, such as the Curonian Lagoon, are prone to saltwater intrusions (Müller et al., 2018; Zemlys et al., 2013, and references therein). Although it is a natural process, it can likewise be induced by human activity, e.g., dredging in the strait area (Yuan and Zhu, 2015). This process not only alters the ecosystem of the freshwater environment (Cañedo-Argüelles et al., 2019), but also affects the freezing and melting of the ice (Idzelytė et al., 2019). It can be an increasingly more serious issue due to the climate change with increasing air and water temperatures (Jakimavičius et al., 2018; Wolanski et al., 2019), rising sea level (Carrasco et al., 2016), and the escalating number of extreme weather events (Janković and Schultz, 2017; Ummenhofer and Meehl, 2017).

Lagoons are influenced not only by salty marine water but also by freshwater input from the rivers. The average time a water parcel stays in a domain before leaving it is called water residence time (Ambrosetti et al., 2003). Ice highly affects the ability of the water to be renewed by fresh water from the river inlets, thus its residence time tends to increase, affecting the water chemical composition (Vincent, 2009), and thus affecting the time and intensity of algal blooms in early spring (Nguyen et al., 2017; Twiss et al., 2014).

Ice cover not only alters the physical properties of the water body, but it also has ecological repercussions. The magnitude of solar radiation entering the water body is highly diminished by ice and snow cover on top of it. This way, lowered temperature affects all the chemical and biological processes (Hampton et al., 2017; Wotton, 1995). In general, light provides radiation for primary production and in particularly productive water bodies, the limited light penetration causes dissolved oxygen depletion due to increased respiration of aquatic organisms and microbial decomposition (Vincent, 2009). The addition of the oxygenated water and transfer of oxygen from the atmosphere replenish its levels in the water column. Water motion is primarily responsible for reaeration. When the ice cover blocks the wind stress, there is no motion on the surface, thus oxygenated water can only come from the water inflow areas.

As the climate is changing, leading to increased temperatures, the ice cover season duration is shortening in the Curonian Lagoon (Dailidiene, 2007; Idzelytė et al., 2019). This may lead to the increased coastal erosion, because ice on the coast is a natural breakwater, protecting the shore from winter storms, and preventing the deflation of the sand (Jarmalavičius, 2007). On the other hand, when the ice breaks up and starts drifting, ice heap has a great impact on abrasion of the shoreline, which depends on the mass of the ice, direction and speed of the wind, and water currents. The ice drift affects water level fluctuations in the lagoon by damming the rivers, thus significantly increasing flooded land areas and partially or sometimes even completely changing the riverbed. In the north of the Curonian Lagoon floe clutters cause an increase of the overall water level, reducing the outflow to the sea. Moreover, the lagoon would have much higher suspended sediment concentrations in the water column if the ice cover would not be present during the winter season (Mėžinė et al., 2019).

The circulation patterns, saline water intrusions, and water residence time (WRT) in the Curonian Lagoon have been of high study interest. Ferrarin et al. (2008) showed that the main forcing affecting the circulation patterns in the northern part of the lagoon is the Nemunas River discharge and in the southern part, it is largely driven by wind forcing. The study by Zemlys et al. (2013) revealed that saline water intrusions from the Baltic Sea through the Klaipėda Strait into the lagoon are gradually decreasing and become negligible at a 20 km distance to the south of Kiaulės Nugara Island. Additionally, the results showed that the model performance during the winter season was worse, presumably because ice cover was not included in that model set up. This was improved by Umgiesser et al. (2016), producing better results by using the interpolated data of ice observations from four ground stations. Their study of water renewal time demonstrated that, overall, it is changing only slightly, although a notable increase in WRT is observed during long winters. The above-mentioned study used in situ ice observations from a limited number of

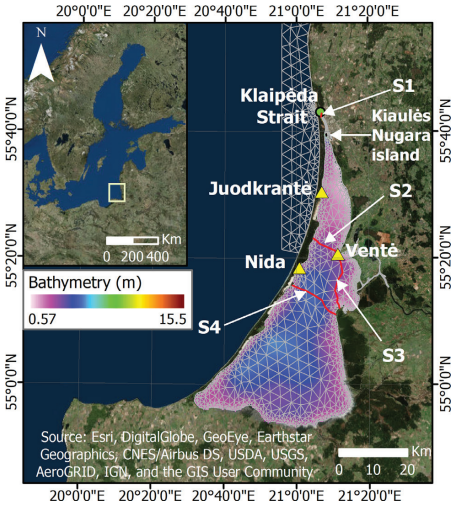

Figure 1 Location of the Curonian Lagoon with respect to the Baltic Sea. The irregular triangular network represents the computational grid, colors throughout the domain indicate the bathymetry of the lagoon, yellow triangles denote ice cover observation stations, the green circle shows a point in Klaipėda Strait for the salinity analysis, and red lines indicate cross-sections for the computation of the fluxes in the Klaipėda Strait (S1), North of Nemunas (S2), Nemunas Delta (S3), and at Lithuanian-Russian border (S4).

stations in the northern part of the lagoon, which were shown by Idzelytė et al. (2019) to not truly represent the real ice cover dynamics in the Curonian Lagoon. Furthermore, only 4 years of ice cover data were available.

With a complete set of ice data for 11 winters, it is now possible to carry out a much more complete study of the ice impact on the hydrodynamic process occurring in the Curonian Lagoon. Therefore, the aim of this paper is to analyze the ice cover effect on the circulation, water exchange capabilities, saltwater intrusions, and water residence time for the period of 2004–2015 using remote sensing ice cover data in the numerical model SHYFEM, simulating the hydrodynamics of the Curonian Lagoon.

2. Material and methods

2.1. Study site

The Curonian Lagoon is located in the southeastern corner of the Baltic Sea (between 54.9°N and 55.9°N) separated from it by a sandy spit, called Curonian Spit and connected to it by the narrow Klaipėda Strait (Figure 1). By occupying an area of around 1584 km^2 (volume 6.3 km^2) (Žaromskis, 1996), it is the largest coastal lagoon in Europe with the northern part belonging to Lithuania, and the larger southern part – to Russia. The Curonian Lagoon is a shallow water body having a mean depth of roughly 3.8 m, the maximum natural depth of 5.8 m in the southern part of the lagoon (Gasiūnaitė et al., 2008) and dredged areas in the Klaipėda Strait up to 15.5 m deep. The southern part is characterized by being freshwater, which is due to the river discharge into the lagoon of approximately 21.8 km^3 yr^{-1}, mainly supplied by the Nemunas River (Dailidiene and Davuliene, 2008; Jakimavičius, 2012). River water is the main water renewal source, especially in the northern part of the lagoon (Umgiesser et al., 2016); however, this area is characterized by a higher salinity due to the Baltic Sea water intrusions, which are determined by the water level difference of the Baltic Sea and the Curonian Lagoon. Saline water inflows along the western shoreline where the influence of Nemunas discharge is weaker (Zemlys et al., 2013). The variability of circulation patterns depends mainly on seasonal changes in hydrographic forcing and on the dominant wind regimes (Umgiesser et al., 2016). The latter are responsible also for the internal mixing and redistribution of the water masses.

Every year the Curonian Lagoon is covered by ice, however, the duration of the ice cover season is displaying a tendency to decrease with the lagoon becoming ice-free sooner. The variability of the ice cover extent throughout the season highly depends on the air temperature. If it is very low for a longer period, then a thick ice cover is able to form, which is capable to withstand positive air temperature events. However, if the negative air temperature is not very low or unstable throughout the ice season, a lot of break-up and refreezing can occur. Historical ice observation data (Baušys, 1978) show that a 10–70 cm ice thickness used to form in the lagoon, but it is steadily decreasing and is projected to be 13–15 cm or thinner by the end of the century due to the climate change (Jakimavičius et al., 2019). There is a significant trend in the final melt onset dates, denoting that ice is starting to melt sooner. Firstly, ice starts breaking in the northern part of the lagoon due to the turbid nature of this area – inflowing saline Baltic Sea water and outflow from the Nemunas River. The southern more limnic part of the lagoon is covered by ice longer than in other areas and melting there is affected more by higher temperatures and wind. Typically, ice cover starts to retreat from the western shoreline to the eastern part of the lagoon due to the prevailing westerly winds during wintertime (Idzelytė et al., 2019).

2.2. Data

For the ice cover data, we used Synthetic Aperture Radar (SAR) images received from three remote sensing missions: Envisat ASAR, RADARSAT-2, and Sentinel-1A and 1B, as well as data from spectroradiometer MODIS. Overall, 11 winter periods from 2004 to 2015 were analyzed and a total of 511 images were processed, with a frequency of 2–5 images per week. The ice polygons were manually digitized from satellite images using ArcGIS software (more about data processing techniques and results see Idzelytė et al., 2019), converted to points in the numerical model grid, and interpolated to fill in the gaps between the dates of received satellite images. The satellite data were validated with ground observations taken once per day in three coastal stations in Juodkrantė, Nida, and Ventė. Ice observation data

was provided by the Marine Research Department of the Environment Protection Agency of Lithuania. Both datasets (satellite images and ground observations) agree quite well, giving a correlation coefficient of 0.92. Some inconsistencies arise in defining the freeze onset in the lagoon, due to the temporal resolution of satellite images being not high enough to capture the fast ice formation. Nonetheless, during the melting period when ice is drifting and break-up occurs far away from the coastal stations, it is firstly detected in satellite images, likewise, the last observation of ice in the lagoon. Therefore, in most cases, satellite data are superior with respect to in situ observations for defining the key stages of ice cover formation and decay.

There are five open boundaries defined in the study domain — one for the Baltic Sea, and other four for the discharging rivers: Nemunas, Minija, Matrosovka, and Deima. Salinity, temperature and water level data at the open sea boundary for the period of 2004—2006 were obtained from the forecasts of operational hydrodynamic model MIKE21 provided by the Danish Hydraulic Institute, for the period of 2007—2009 and 2014—2016 from forecasts of the operational hydrodynamic model HIROMB (High Resolution Operational Model for the Baltic Sea) provided by the Swedish Meteorological and Hydrological Institute, and for the period of 2010—2013 from the forecasts of MOM (Modular Ocean Model) provided by Leibniz Institute for Baltic Sea Research in Warnemünde, Germany. Lithuanian Hydrometeorological Service (LHS) under the Ministry of Environment provided the daily river discharge data.

Meteorological forcings for the period of 2009—2010 were obtained from the forecasts of operational numerical weather prediction model HIRLAM (High Resolution Limited Area Model) provided by LHS, and for the rest of the years data obtained from ECMWF (European Centre for Medium-Range Weather Forecasts) were used.

2.3. Hydrodynamic model

The open source hydrodynamic finite element model for shallow water bodies SHYFEM was used to simulate ice cover effect on circulation, saltwater intrusions from the Baltic Sea, water residence time in the lagoon, and mass fluxes through sections shown in Figure 1. The model was developed at ISMAR-CNR (Institute of Marine Sciences — National Research Council, http://www.ismar.cnr.it/shyfem) and has been already successfully applied for studying hydrodynamic processes of numerous lagoons in Europe (De Pascalis et al., 2011; Ferrarin et al., 2010a, 2010b, 2013; Molinaroli et al., 2014), as well as the Curonian lagoon for which the calibration and validation of the model was done (Ertürk et al., 2015; Ferrarin et al., 2008; Zemlys et al., 2008, 2013). The results obtained by Umgiesser et al. (2016) showed that the model with a simple ice module gave much better results compared to the reference (ice-free) simulation.

SHYFEM consists of several modules: hydrodynamic, transport and diffusion, sediment transport, wave, and an ecological module. It is based on an unstructured grid, which makes it suitable for application to lagoons, coastal seas, estuaries, and lakes with complicated geometry and bathymetry. This model is able to provide 2D as well as 3D simulations; for this study we used a 3D set-up. The equations are integrated in time using a semi-implicit discretization scheme and spatial discretization is achieved using a partially modified finite element method. For salinity and temperature computations, a transport diffusion model is used that takes into account the heat fluxes from the atmosphere and input from rivers. The water residence time computation is done by transforming the near exponential decay of a conservative tracer with a logarithm application to a straight line that then can be used for estimating the WRT through linear regression (Cucco and Umgiesser, 2006).

The ice cover data in the model is represented by a number with values between 0 and 1, where marginal value 0 denotes the absence of ice and value 1 denotes water surface completely covered by ice. The presence of ice was accounted for in the model by weighting the wind drag coefficient by the fractional ice value. This is done to scale the momentum input through the surface by the area free of ice. For the areas having ice concentration equivalent to 1, the momentum transfer to the sea is completely suppressed. This study does not consider ice-ocean stress (Umgiesser et al., 2016). More explanation about the model and its equations can be found in Bellafiore and Umgiesser (2010), Ferrarin et al. (2017), Maicu et al. (2018), and Umgiesser et al. (2004).

2.4. Modelling set up and scenarios

The computational grid of the study area consists of 1309 nodes and 2027 triangular elements (Figure 1). The resolution is much finer in the Klaipeda Strait. For the vertical discretization, 10 sigma layers have been used. A part of the Baltic Sea in front of the lagoon is also included into the numerical grid, preventing the disturbances for computations of the exchanges through the Klaipeda Strait area. The Baltic Sea and Klaipėda Strait were considered ice-free for all simulations since naturally there is no landlocked ice due to intensive shipping, higher depths, and inflowing warmer water from the Baltic Sea.

Three types of simulations have been carried out: 1) ice cover artificially switched off in the model (hereafter no-ice); 2) with ice cover data obtained from the satellite observations (hereafter real ice); 3) an additional set of simulation run where the lagoon is completely covered by ice during the ice cover season, including the Klaipėda Strait area (hereafter idealized ice). The comparison of the ice and idealized ice season simulations allows a better understanding of the role of ice cover in the hydrodynamic processes in the Curonian Lagoon.

The simulation period was from 2004-01-01 to 2015-12-31. Only 11 years were analyzed as the simulation of the year 2004 was used for the model spin-up. For the analysis of ice cover impact on the velocity and direction of the water currents, water fluxes, salinity, and water residence time, the simulation results were averaged over the meteorological seasons of the year: winter (December, January, February), spring (March, April, May), summer (June, July, August), and autumn (September, October, November), as well as over the ice cover seasons, each of them having different durations (different beginning and ending dates of the ice season).

The average differences of simulation results obtained with ice switched on and switched off in the model (real

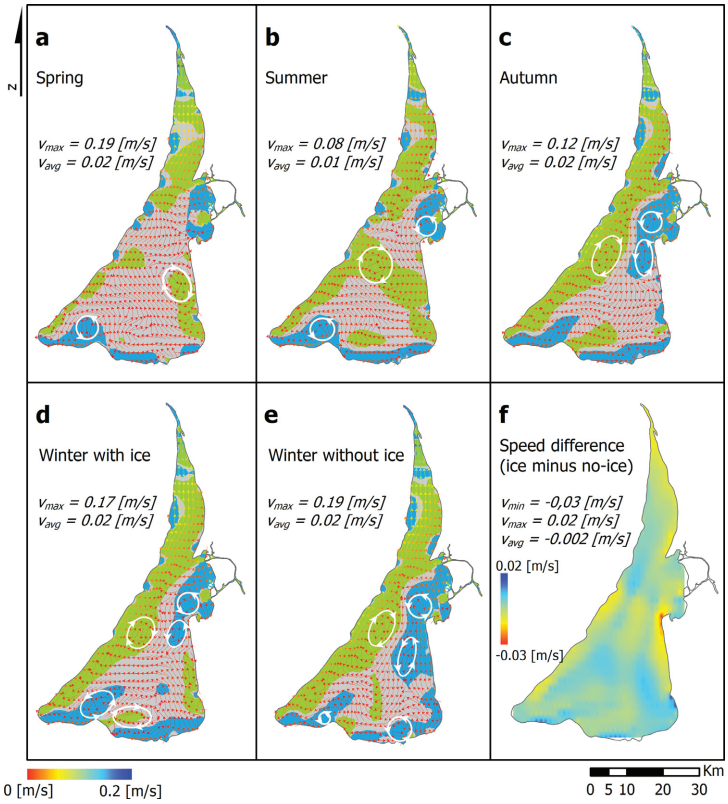

Figure 2 Water circulation (vectors are colored by the current speed in m/s) averaged over the whole simulation period of simulations with ice data in: (a) spring, (b) summer, (c) autumn, and winter seasons (d), without ice in winter (e), and the current speed difference of these winter computations (ice minus no-ice, f). White circles with arrows show gyre systems and their direction, colors in the map show positive (blue), negative (green), and irrotational (gray) vorticity, and numbers indicate the maximum (v_{max}) and average (v_{avg}) velocity of the residual currents.

ice minus no-ice and idealized ice minus no-ice) were calculated to analyze the impact of the ice cover to the above-mentioned hydrodynamic properties of the lagoon. This was done for the averaged ice cover seasons. The salinity time series difference between the bottom and top layers of the water column in Klaipėda Strait (green circle in Figure 1) were analyzed to identify the number of hours per year of salt concentration exceeding the threshold of 1 and 3 PSU. The vertically averaged salinity time series in Juodkrantė were analyzed to count the number of days when the salt concentration exceeds the 2 PSU threshold.

Simulation results of 2004–2015 period were also used for computing the water residence time (WRT) switching its calculation on in the model for the different periods: 1) for the ice-free part of the year and the ice cover season (WRT_{ice}^{real} for the real ice cover and WRT_{ice}^{ideal} for the idealized ice cover season); 2) for every meteorological season of the year defined above (WRT_{season}). All calculations were done twice – considering ice cover data and without it. The water residence time for the winter season (WRT_{winter}) was compared with WRT_{ice}^{real} and the results from Umgiesser et al. (2016). Since the northern and southern part of the Curonian Lagoon has different hydrodynamic properties, WRT was computed separately for both of these areas, as well as for the total lagoon area.

3. Results

3.1. Circulation

The behavior of water motion can be inferred through the analysis of the residual currents, which are currents averaged over a longer period, in our study, averaged over every meteorological season of the year (Figure 2). Residual currents indicate the mean flow of the water, even if much

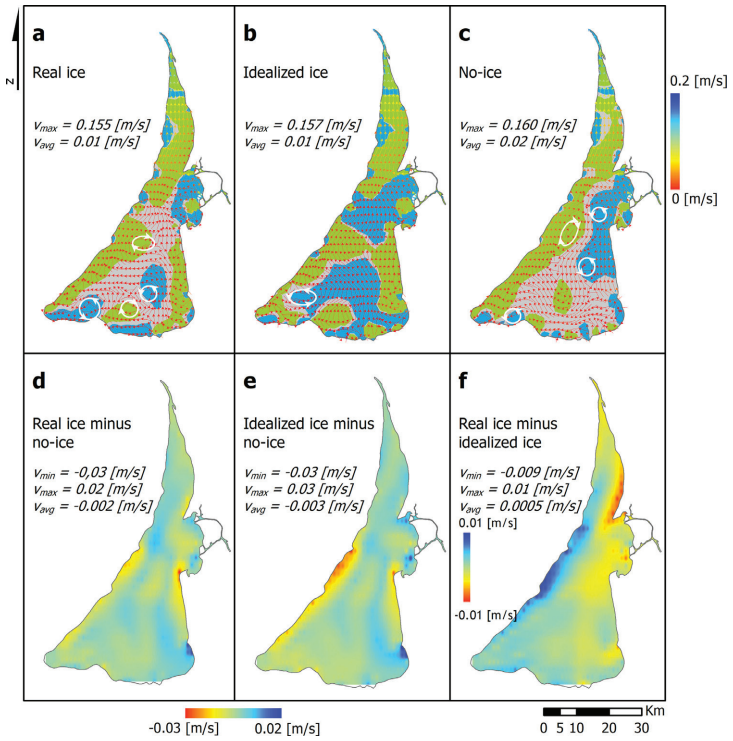

Figure 3 Water circulation (vectors are colored by the current speed in m/s) averaged over ice cover season in simulation with (a) real ice cover, (b) idealized ice cover, and (c) no-ice season set-up, as well as the current speed difference in m/s between simulations: (d) real ice cover minus no-ice, (e) idealized ice cover minus no-ice, and (f) real minus idealized ice cover. White circles with arrows in a, b, and c show gyre systems and their direction, colors in these maps show positive (blue), negative (green) and irrotational (gray) vorticity, and numbers indicate the minimum (v_{min}), maximum (v_{max}), and average (v_{avg}) velocity of the residual currents.

higher and lower instantaneous values can be detected. In the Curonian Lagoon, we can observe a strong flow from the Nemunas River northward to the Klaipėda Strait, having the highest speed throughout the year. During spring season (Figure 2a) in the southern part of the lagoon a two gyre circulation system is observed, one — anticlockwise in the southwestern corner of the lagoon, and the second — clockwise along the eastern shoreline. In summer, the latter one shifts towards the middle part of the lagoon and a third anticlockwise gyre system forms in the Nemunas Delta area (Figure 2b). In summer the current speed is much slower than in spring, with a slightly more pronounced flow along the western shoreline. In autumn (Figure 2c), the current speed slightly increases and the gyre in the southwestern part of the lagoon is not as apparent as during the previous seasons. In addition to this, another anticlockwise gyre system is observed to form in the middle of the lagoon, near the eastern shore. During the winter season under the ice cover (Figure 2d) the same gyre systems remain in the central part of the lagoon and in Nemunas Delta, however, the anticlockwise gyre in the southwestern part of the lagoon becomes more apparent and another clockwise system can be observed to form next to it. The water flow along the western part of the lagoon slightly decreases during winter and it becomes more chaotic near the eastern shoreline, where ice cover stays the longest.

The difference of the simulation results of winter circulation with and without the ice cover (Figure 2f) was computed to investigate how ice cover affects the velocity of the residual currents during the winter season. The results show that circulation under the ice cover becomes weaker by up to 0.03 m/s. Water during the winter season flows slower along the perimeter of the lagoon, especially near the eastern shoreline. As mentioned above, in the simulation with ice cover one can observe a more chaotic water movement along the southeastern shoreline (Figure 2d), compared to simulation results when the ice cover was omitted (Figure 2e). Additionally, there is a difference in gyre systems in the southern part of the lagoon, being more pronounced under ice cover.

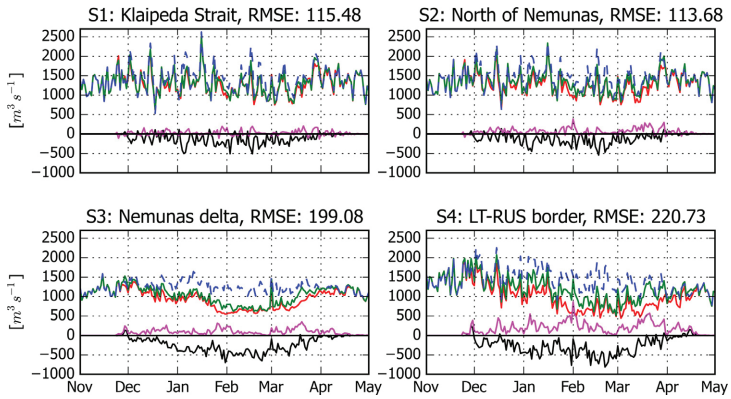

Figure 4 Average water fluxes through cross-sections at Klaipėda Strait (S1), north of Nemunas (S2), Nemunas delta (S3), and Lithuanian-Russian border (S4). The location of each cross-section is shown in Figure 1. Green solid lines indicate water fluxes of simulation with real ice, blue dashed lines – simulation without ice, the black solid line denotes the difference of these simulations (real ice minus no-ice), the red solid line shows the results of simulation with idealized ice, and the magenta solid line indicates the real ice and idealized ice simulation difference (real ice minus idealized ice). Negative values denote higher southward fluxes in the simulation without ice.

Concerning the average residual currents during the real ice cover season (Figure 3a), two gyre systems in the southern part of the lagoon, which are similar to the results averaged over the winter season, can be found (Figure 2d). However, there is a third gyre next to it and only one gyre in the middle of the lagoon during the real ice cover season. For the idealized ice cover (Figure 3b), when the lagoon is completely covered by ice throughout the whole ice season duration, only one gyre forms in the southwestern part of the lagoon. The distribution of the gyre systems in the simulation without ice (averaged over the ice season duration, Figure 3c) is similar to the results averaged over the winter season (Figure 2e), with only one gyre missing near the southern shoreline. The difference of current speed in simulations with real ice and without it (Figure 3d) is similar to the one averaged over the winter season (Figure 2f). The difference of idealized ice cover and no-ice seasons is more pronounced near the western shoreline (Figure 3e). In the idealized case, when the lagoon is completely covered by ice water flows slower along the western shoreline and it is slightly stronger along the eastern shoreline in the northern part of the lagoon, compared to the flow during the real ice cover season (Figure 3f).

By looking at the residual currents of each ice cover season separately (not shown here), it can be seen that in the southern part of the lagoon, the current speed noticeably decreases. This is due to this area being sheltered from the wind by ice cover for a longer period compared to the northern part. When the ice cover is more variable, meaning that it decomposes and refreezes several times throughout the season, it leads to slightly higher current speeds. During each ice-cover season, in the Klaipėda Strait area and approximately 5 km southward from Kiaulės Nugara island, the current speed is always higher compared to the rest of the lagoon. However, if this area is fully covered by ice for a longer period, then the current speed slightly decreases.

3.2. Fluxes

For the computation of the fluxes, four cross-sections were set – in Klaipėda Strait, north of Nemunas River, Nemunas delta, and along Lithuanian-Russian border (red lines in Figure 1). Although the water fluxes through each of the specified sections are rather the same (fluctuating around 1000–1500 $m^3\ s^{-1}$), one can clearly see the difference between simulations with ice and without it. The results show that the ice cover has a higher impact on the water fluxes in the Nemunas delta area (S3 in Figure 4) and through the borderline of the two countries (S4). The difference between simulation results with and without ice is nearly twice as high in these sections than it is in Klaipėda Strait and north of Nemunas sections. The difference is only observed during the ice cover season.

The comparison of idealized ice (fully ice covered lagoon during the ice cover season) and real ice season (ice cover from remote sensing data) simulation results shows that the prolonged full ice cover (idealized ice) has the greatest impact only in middle of the lagoon (at the cross-section along the Lithuanian-Russian border). The changes of the fluxes in the rest of the sections are much smaller.

3.3. Saltwater intrusions

Throughout the meteorological seasons of the year (Figure 5), higher salinity concentration is always observed in the northern part of the lagoon. It is especially prominent in autumn (Figure 5c), while the lowest concentration is observed in spring (D_{max} in Figure 5a). For the spatial average of the salinity over the whole lagoon area, one can see that during winter it is lower under the ice than it would be if the ice cover would not be present (D_{avg} in Figure 5d and e, respectively). The difference between

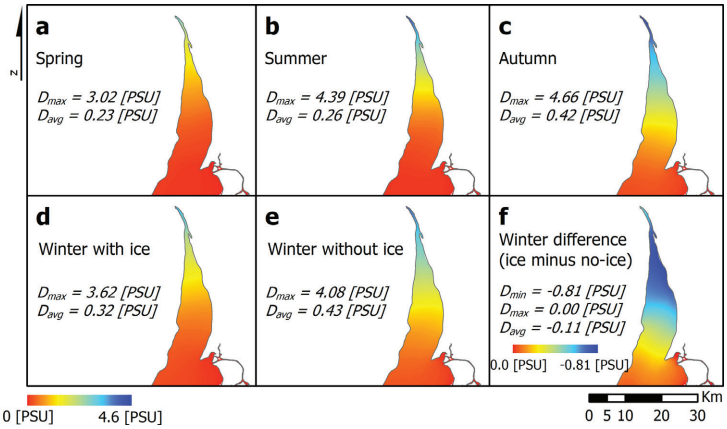

Figure 5 Distribution of salinity in the northern part of the Curonian Lagoon averaged over the whole simulation period of computations with ice data in (a) spring, (b) summer, (c) autumn, and (d) winter seasons, (e) without ice in winter, and the salinity difference of the winter simulations (ice minus no-ice, f). The numbers indicate the maximum (D_{max}) and average (D_{avg}) value of the salinity over the total lagoon area.

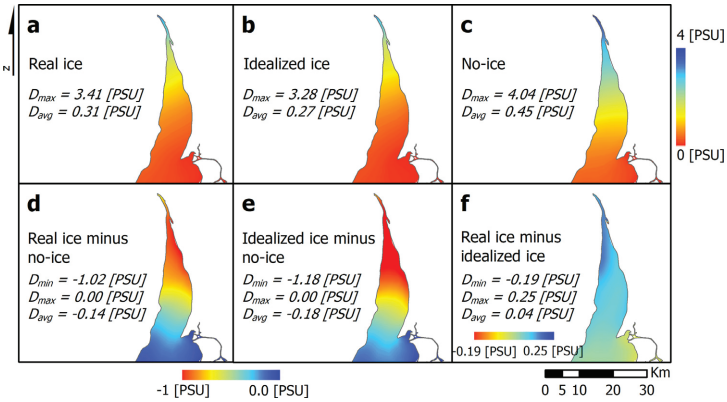

Figure 6 Salinity averaged over ice cover season in simulation with (a) real ice cover, (b) idealized ice cover, and (c) no-ice season set-up, as well as the difference between the simulations: (d) real ice cover minus no-ice, (e) idealized ice cover minus no-ice, and (f) real minus idealized ice cover. The numbers indicate the minimum (D_{min}), maximum (D_{max}), and average (D_{avg}) of salinity over the total lagoon area.

simulations considering ice and no-ice (ice minus no-ice) is negligible in the southern part of the lagoon, but in the north the salinity can be lower by up to 0.81 PSU under the ice cover (Figure 5f) than it would have been if the ice had not been present during the winter season.

The duration of the ice covering the northern part of the lagoon does not have a high impact on salinity when comparing the real and idealized ice seasons (Figure 6a, b, and f). The spatially averaged salinity of the differences between simulations with real ice cover and without it (real ice minus no-ice, Figure 6d) shows that during the real ice cover season salinity can decrease by up to 1.02 PSU, which is higher than the value averaged over the winter season (Figure 5f). During the idealized ice-cover season (Figure 6e), when the lagoon is completely shut off from the atmosphere by ice, salinity under the ice can decrease by up to 1.18 PSU, compared to a situation where ice cover is not present. It is the highest difference compared with values averaged over winter and real and idealized ice cover season, indicating that the presence of the ice and the duration of its full cover

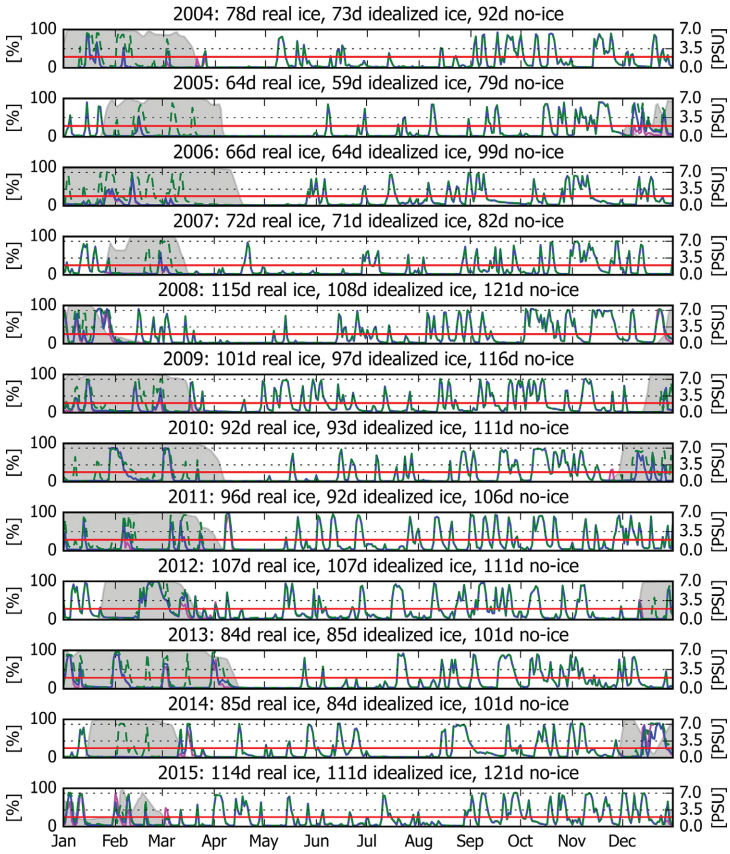

Figure 7 Vertically averaged salinity time series in Juodkrantė. Graph title indicates the year of plotted values, as well as the number of days when the salinity exceeds the threshold of 2 PSU (red solid line) when computations are done using real (real ice, blue solid line) and idealized (idealized ice, magenta solid line) ice cover data, as well as without ice (no-ice, dashed green line). Grey areas show the percentage of ice covering the lagoon, the duration of every ice cover season can be seen in Figure 8.

decreases the intensity of saline water intrusions from the Baltic Sea through the Klaipėda Strait further into the Curonian Lagoon.

The difference of salinity between the bottom and top layers of the water column in the Klaipėda Strait area (green point in Figure 1) shows a high variability throughout the years. In Table 1, the number of hours when this difference exceeds 1 PSU and 3 PSU are shown. The average number of hours is seen to be much higher when the salinity difference exceeds 1 PSU threshold in simulation with ice cover.

In Juodkrantė salinity surpasses the 2 PSU threshold nearly 90 days on average per year when the ice cover is switched-on in the model (Figure 7), this is 13.9 days less on average than in the model results of the simulation without the ice, and the difference between idealized ice cover season and no-ice simulation results is 16.3 days, clearly denoting that the highest impact is observed when the lagoon is fully covered by ice. In Klaipėda Strait salinity is exceeding the 2 PSU threshold on average for 237 days per year, when real ice cover data is used in the model, which is 10.5 days less than the records of model computations without ice. Further in the lagoon, in Nida and Ventė, differences are much lower — less than 1 and 3 days per year, respectively.

3.4. Water residence time

The average WRT values for the specified areas (north, south, and whole lagoon domain) are shown in Table 2. These values indicate that in the northern part of the lagoon the WRT is around 55 days, and in the southern — 150 days, considering the real ice cover conditions (WRT_{ice}^{real}), which are very similar to the ones averaged over the meteorological winter season (WRT_{winter}^{real}). The difference

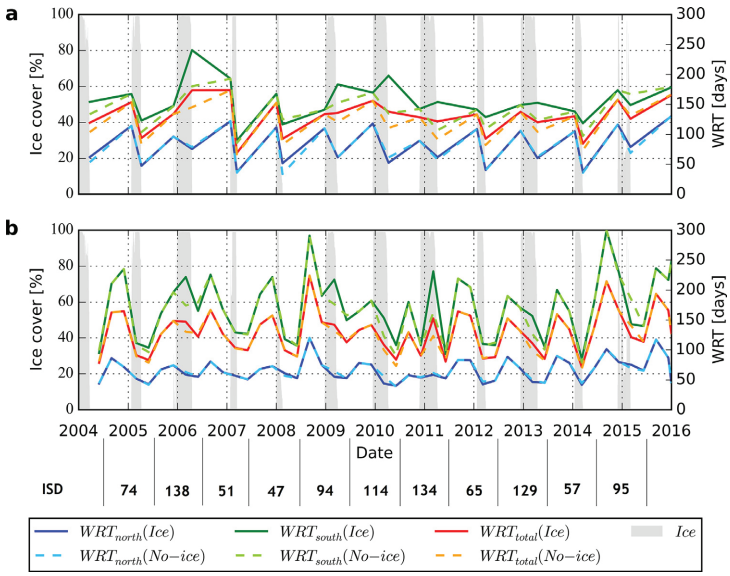

Figure 8 Water residence time in the northern (WRT_{north}), southern (WRT_{south}) parts, and in the whole lagoon area (WRT_{total}) computed with and without the real ice cover: (a) for the ice-free period of the year and the real ice-cover season, (b) seasonally every 3 months. Grey columns indicate ice cover percentage over the lagoon. At the bottom of the graph, the ice season duration (ISD) in days is shown. Please note that in panel (a) only two values per year were available due to the way the WRT was computed. In figure b four values per year were computed.

Table 1 The number of hours per year when salinity difference between bottom and top layers of the water column in the Klaipėda Strait exceeds the threshold of 1 and 3 PSU in simulations with ice and without ice.

Year	Number of hours with salinity [PSU] above threshold			
	>1 with ice	>1 without ice	>3 with ice	>3 without ice
2005	170	138	24	15
2006	190	107	20	12
2007	135	134	18	18
2008	116	114	8	7
2009	112	122	17	27
2010	156	119	12	7
2011	42	32	1	1
2012	75	90	0	12
2013	85	83	9	11
2014	202	172	15	22
2015	149	145	33	27
Mean	**130**	**114**	**14**	**14**

between WRT values in the simulations with and without real ice cover (WRT^{real}_{winter} and WRT^{no-ice}_{ice}) is around 1.5 days in the northern part and around 24 days in the southern part. Results of simulation with the idealized ice cover (WRT^{ideal}_{ice}) show that in the southern part of the lagoon the WRT increases by around 40 and 63 days compared with WRT^{ideal}_{ice} and WRT^{no-ice}_{ice}, respectively. However, in the northern part of the lagoon WRT^{ideal}_{ice} is lower.

The differences of the results averaged over the meteorological winter season (WRT^{real}_{winter} and WRT^{no-ice}_{winter}) are slightly higher in the northern part, due to the variability of the ice season duration (ISD) in this area, and the difference in the southern part is slightly smaller, compared to WRT^{real}_{ice} and WRT^{no-ice}_{ice}.

ISD and different WRT computation periods show a high correlation (from 0.71 to 0.84), denoting a significant ice cover effect on water residence time. However, when considering water residence during the meteorological winter season (WRT^{real}_{winter}), there is no correlation with ISD in the northern part of the lagoon, as mentioned, due to the fact that the ice is more dynamic in this area during the winter season.

The 11-year average water residence time in the Curonian Lagoon (averaged over all meteorological seasons, WRT^{real}_{season}) is around 130 days when the ice cover is switched on in the model, which is a ~1.5 days longer compared to the theoretical period without ice (WRT^{no-ice}_{season}). Higher WRT values can be found in the southern part of the lagoon. In the north, the difference between ice and no-ice simulations is rather small.

The variability of the WRT computation periods can be seen in Figure 8, where the difference between simulation

Table 2 Averaged water residence time (WRT) computed for the northern (WRT_{north}), southern (WRT_{south}) parts and for the total (WRT_{total}) lagoon area as well as correlation between the ice season duration (ISD) and WRT during the ice cover and winter seasons computed in simulations with real ice cover. Subscript indicates different WRT computation periods (ice – ice cover season, winter – December, January, February, and season – every meteorological season), superscript indicates the model set-up type (real – satellite ice cover data, ideal – idealized ice cover data, no-ice – without ice), all described in Section 2.4.

Simulation	WRT_{north} [days]	WRT_{south} [days]	WRT_{total} [days]
WRT_{ice}^{real}	55.48±13.72	150.54±41.10	113.79±28.68
WRT_{ice}^{ideal}	50.01±13.16	190.10±97.92	124.22±43.85
WRT_{ice}^{no-ice}	53.09±14.53	126.52±28.79	99.67±23.97
WRT_{ice}^{real} *correlation with ISD:*	*0.71*	*0.79*	*0.84*
WRT_{winter}^{real}	53.81±9.94	152.47±50.16	112.15±26.33
WRT_{winter}^{no-ice}	56.44±7.60	135.62±33.91	106.43±22.20
WRT_{winter}^{real} *correlation with ISD:*	*0.09*	*0.79*	*0.75*
WRT_{season}^{real}	66.66±18.93	170.53±52.67	129.96±36.09
WRT_{season}^{no-ice}	67.24±18.39	166.60±52.07	128.58±36.49

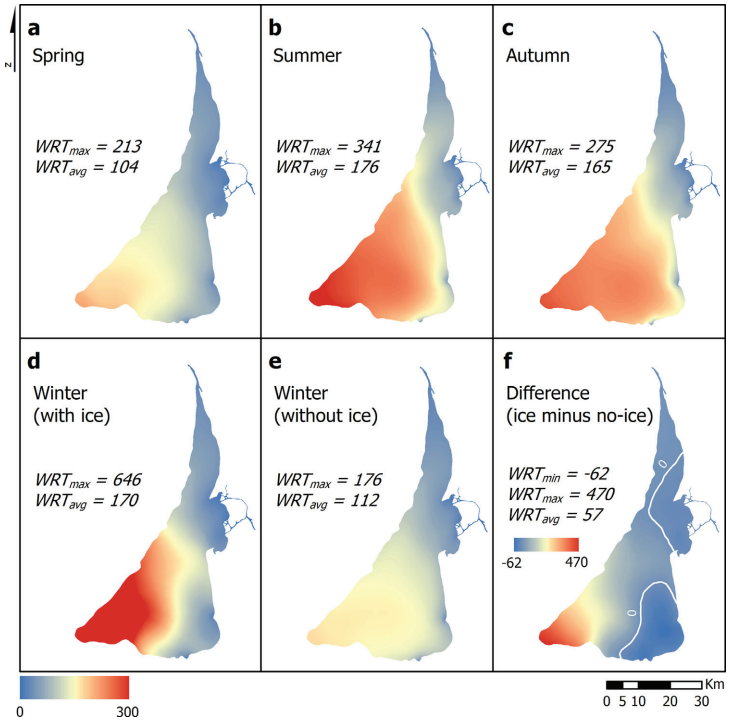

Figure 9 Seasonal water residence time maps (in days) averaged over the whole simulation period of computations with ice data (*WRTseason real*) in (a) spring, (b) summer, (c) autumn, (d) winter, and (e) without ice in winter, as well as the difference of winter simulations (ice minus no-ice, f). Contour lines in the difference map indicate the zero value (no difference) and numbers indicate the maximum (WRT_{max}) and average (WRT_{avg}) water residence time.

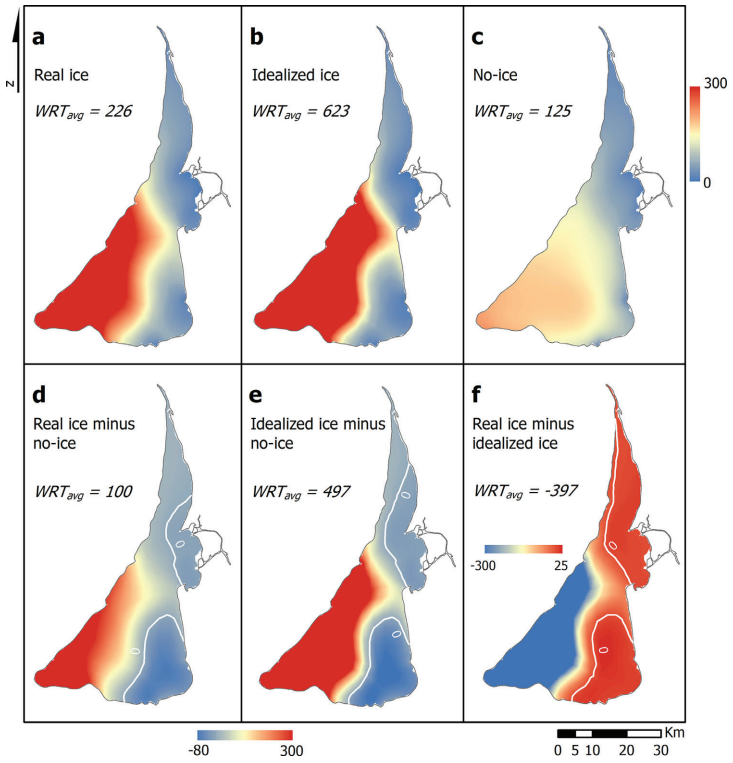

Figure 10 Water residence time distribution in days averaged over the all ice cover seasons in simulation with (a) real ice cover, (b) idealized ice cover, and (c) no-ice season set-up, as well as the difference between the simulations: (d) real ice cover minus no-ice, (e) idealized ice cover minus no-ice, and (f) real minus idealized ice cover. Contour lines indicate the zero value (no difference). The numbers indicate the spatial average (WRT_{avg}) of water residence time.

with and without ice is higher after the long and severe winters, e.g., in 2006, 2009, 2010, 2011 and 2013, when the ice season duration was the longest over the analyzed period (on average 122 days). Again, the higher difference is visible in the southern part of the lagoon, where the ice cover is less dynamic compared to the northern part.

The water residence time throughout the seasons of the year is displayed in Figure 9 (a–d). The values slightly differ throughout the ice-free season, being highest in summer, when the wind and water inflow from the rivers decrease. However, the same overall pattern is observed – high WRT values in the southern part of the lagoon and especially in the southwestern corner. During winter (Figure 9d) in the model runs with real ice the water residence time values are observed to be much higher in the southwestern corner of the lagoon (Figure 9f) than in the reference simulation without ice (Figure 9e), which is much more similar to the spring WRT distribution (Figure 9a). The residence time of nearly 2 years during the winter season means that if the ice conditions had been prolonged to two years, then the water circulation in 2 years would have renewed only 1/e of the initial concentration.

The simulation results of idealized ice cover (Figure 10b) show that the prolonged full ice cover has a much higher impact on the WRT in the southwestern corner of the lagoon compared with the simulation with real ice cover data (Figure 10a). In this area, there are no inflowing rivers, and therefore there are no additional sources of fresh water. Overall, ice affects WRT over the majority of the lagoon area. In the southeastern corner and in Nemunas Delta, where the main river outlets are situated, simulation without ice (Figure 10d and e) shows higher values, meaning that under the ice water is renewing faster than it would be if ice were not present. This difference in the northern part stretches further along the eastern shoreline compared to the no-ice simulations with the idealized ice cover (Figure 10e) than compared to the simulation with the real ice cover (Figure 10d).

4. Discussion and conclusions

The most important drivers of the hydrodynamic processes, when no ice is covering the Curonian Lagoon, is a combination of wind force and Nemunas discharge. However, when ice is present, only the Nemunas River discharge is primarily responsible for accelerating the water masses. Throughout the seasons of the year, we can observe different circulation patterns in the lagoon. In spring, a two-gyre system is observed in the southern part of the lagoon, of which one of them during summer shifts further to the center of the lagoon and another system is observed to form in Nemunas Delta, however, with much lower current speed. The increased wind conditions in autumn force one additional gyre to form near the delta area. However, the highest number of gyre systems are observed during the winter period, when the water surface is sheltered by the ice cover from the wind forcing. The rotation of the gyre systems in and near the Nemunas Delta (along the southeastern shoreline) is anticlockwise, the gyre in the central part of the lagoon is clockwise, and in the southwestern part of the lagoon it is anticlockwise. During the winter season, another clockwise gyre in the south can be observed. These results do not precisely match with the previous study of Umgiesser et al. (2016), because of the ice cover data used, which previously was interpolated from four ground observation stations and available for only for 4 years. In our study, we have used ice data from satellite images, which covered the whole 11-year simulation period.

The comparison of circulation during the real and idealized ice cover seasons reveals that the prolonged full ice cover can diminish the development of gyres in the lagoon. Ice does not only alter the structure of the circulation of the water masses, but also the speed of the currents. When ice cover decomposes and refreezes several times throughout the winter season, it leads to slightly higher current speeds, due to the wind-stress on the ice-free water surface. In the Klaipėda Strait area and approximately 5 km southward from it, the current speed is always higher compared to the rest of the lagoon, however, if this area is fully covered by ice for longer, then this difference slightly decreases.

Since the circulation decreases under the ice cover, there is less exchange between different parts of the lagoon. Therefore, all the water fluxes through the specified four cross-sections are affected by the presence of the ice cover. However, there is a lower impact observed in the northern part of the lagoon contrary to the southern part. It is noticeable that, in the northern part, the fluxes stay nearly the same, just wind is making them fluctuate. In the Klaipėda Strait area, the exchanges are mainly driven by water level fluctuations in the Baltic Sea and are much less wind-driven. However, the situation in the cross-section of Nemunas Delta and along Lithuanian-Russian border is different. Water exits the Nemunas Delta more steadily, without cycling between the delta and the lagoon and less water is diverted to the south, because, during the ice cover season, wind-driven circulation is inhibited and the prolonged full ice cover has the biggest impact on fluxes through the Lithuanian-Russian border.

In the southern part of the lagoon, salinity is small and negligible throughout the year. In the northern part, the concentration is higher, but highly depending on the season. The lowest salinity concentration is observed during spring and the highest during the autumn season when the westerly winds increase allowing for the Baltic Sea water to inflow into the Curonian Lagoon. During the period when ice is covering the lagoon, salinity decreases by up to around 1 PSU. Overall, the highest differences between the results of simulations with ice and without it are observed in the northern part of the lagoon where salinity decreases during the ice cover season, reducing the saltwater intrusion events. For instance, in Juodkrantė (approximately 20 km southward from Klaipėda Strait) saltwater intrusions (overpassing 2 PSU threshold) can be found on average around 90 days per year, which is on average nearly 14 days less when the ice cover was not considered in the model simulations. The simulation results of idealized ice cover show that this difference is even higher – 16.3 days. Thus, we can conclude that when there is ice, it markedly decreases the frequency of saltwater intrusions into the Curonian Lagoon.

The water column is uniform, however, in Klaipėda Strait a slight salt concentration increase is observed in the bottom layers. The difference of bottom and top layers of the water column can exceed the 1 PSU threshold for 130 hours per year on average, which is 16 hours more than it would be if the ice would not be covering the lagoon. Zemlys et al. (2013) have already shown that in the Klaipėda Strait area strong salinity gradients create conditions for three types of water flow: one-directional freshwater outflow to the Baltic Sea, one-directional saline water inflow into the Curonian Lagoon, and two-directional flow with a lagoon water outflow in the surface layers and saline water intrusion in the bottom. However, in their study ice cover was not taken into account, Umgiesser et al. (2016) later did this, showing the more accurate results for salinity validation; yet, they concluded that a high-resolution model used in Zemlys et al. (2013) does a better job in describing salinity variations, even if the ice cover is not included. Since in our study we wanted to present the long-term analysis of model simulation results, we also used a coarser resolution model grid, thus in the future, for a fully updated analysis of salinity variations in the Klaipėda Strait area, including the ice cover data in the model computations, a finer grid should be used.

Ice cover and its duration likewise affect the water residence time (WRT) in the Curonian Lagoon. When ice is present, it takes longer for the water to be renewed. This is especially evident after the long ice cover seasons (e.g., in 2006, 2009, 2010, 2011, and 2013) in the southern part of the lagoon. WRT computations during the ice cover season (WRT_{ice}^{real}), show a high correlation with ice season duration (from 0.71 to 0.84), however, when computing it only during the winter season (WRT_{winter}^{real}) there is no correlation in the northern part of the lagoon. This is due to the fact that the ice season duration in this area is shorter than in the southern part and the computation of WRT during the winter season is limited to only three months (Dec, Jan, Feb), while ice can be observed to start forming, often only in the middle of January and can last much longer than February.

The increased WRT under the ice is true for analyzing water residence in the whole area of the Curonian Lagoon (north, south, and the whole domain) for the real ice cover conditions (WRT_{ice}^{real}). However, computations for the meteorological winter season (WRT_{winter}^{real}) show that it is not the same in the northern part of the lagoon, where simulation results with no ice cover show longer WRT than simulation results with ice. However, the difference is quite small (just 4%), and probably does not exceed the uncertainty of the evaluation of WRT by the model. Comparing the real and idealized ice cover simulation results shows that prolonged full ice cover can lead to an increase of WRT in the southern part of the lagoon. However, in the north, it decreases due to the cutting-off the exchanges between the northern and southern part. Therefore, more water from the Nemunas River stays in the north and does not mix with water in the southern areas. This mechanism contributes to a decrease of WRTs in the northern part.

Our computed WRT values slightly differ from those described in Umgiesser et al. (2016), supposedly as a result of satellite ice cover data used in the model representing more realistic ice distribution with respect to the data interpolated from the observations from coastal stations. The melt-off occurrences during the ice cover season observed in satellite images have a small, but noticeable impact on the WRT by slightly increasing it in the norther part, and decreasing the WRT in the southern part compared to the previous study results with ice.

WRT throughout the seasons is varying. During the ice-free period, the longest time required for water to renew is in summer, due to the decreased wind speed and river water input. The pattern in summer and spring are similar, with the highest WRT being in the southern part of the lagoon. During the winter period, the WRT increases much more in the southwestern corner of the lagoon, which is far away from the rivers inflowing the lagoon, hence the water renewal is very slow. The model results with the idealized ice cover (lagoon fully covered by ice during the entire ice cover season) show that it has a much higher impact to the WRT in the southwestern part of the lagoon. Water near the river outlets — in the southeastern corner of the lagoon and in Nemunas Delta, tends to renew faster under the ice cover and the prolonged full ice cover in the northern part stretches this area further along the eastern shoreline. If ice would not be present during the ice cover season, then the WRT distribution would be much more similar to the situation during the spring.

To conclude, with this study we show how the ice data derived from satellite observations improve the representation of the real conditions of the circulation, saltwater intrusions, and water residence time in the Curonian Lagoon. Currently, an ice model is still not yet integrated in the modelling system SHYFEM, which will be done and will be presented in future publications.

References

Ambrosetti, W., Barbanti, L., Sala, N., 2003. Residence time and physical processes in lakes. J. Limnol. 62, 1–15.

Baušys, J., 1978. Ledo Režimas. In: Rainys, A. (Ed.), Kuršių Marios II. Mokslas, Vilnius, Lithuania, 34–49.

Bellafiore, D., Umgiesser, G., 2010. Hydrodynamic coastal processes in the North Adriatic investigated with a 3D finite element model. Ocean Dyn. 60, 255–273, https://doi.org/10.1007/s10236-009-0254-x.

Bengtsson, L., 2012. Ice Covered Lakes. In: Bengtsson, L., Herschy, R.W., Fairbridge, R.W. (Eds.), Encyclopedia of Lakes and Reservoirs. Springer, Netherlands, Dordrecht, 357–360.

Bengtsson, L., 1996. Mixing in ice-covered lakes. Hydrobiologia 322, 91–97, https://doi.org/10.1007/BF00031811.

Cañedo-Argüelles, M., Kefford, B., Schäfer, R., 2019. Salt in freshwaters: Causes, effects and prospects - Introduction to the theme issue. Philos. Trans. R. Soc. B Biol. Sci. 374, art. no. 20180002, 6 pp., https://doi.org/10.1098/rstb.2018.0002.

Carrasco, A.R., Ferreira, O., Roelvink, D., 2016. Coastal lagoons and rising sea level: A review. Earth-Science Rev. 154, 356–368, https://doi.org/10.1016/j.earscirev.2015.11.007.

Cushman-Roisin, B., 2019. Environmental Fluid Mechanics. John Wiley & Sons Ltd, New York, 406 pp.

Dailidiene, I., 2007. Hidroklimatinių sąlygų kaitos ypatumai Baltijos jūros Lietuvos priekrantėje ir Kuršių mariose. Klaipėda University.

Dailidiene, I., Davuliene, L., 2008. Salinity trend and variation in the Baltic Sea near the Lithuanian coast and in the Curonian Lagoon in 1984-2005. J. Marine Syst. 74, 20–29, https://doi.org/10.1016/j.jmarsys.2008.01.014.

De Pascalis, F., Pérez-Ruzafa, A., Gilabert, J., Marcos, C., Umgiesser, G., 2011. Climate change response of the Mar Menor coastal lagoon (Spain) using a hydrodynamic finite element model. Estuar. Coast. Shelf Sci. 114, 118–129, https://doi.org/10.1016/j.ecss.2011.12.002.

Ertürk, A., Razinkovas, A., Zemlys, P., Pilkaitytė, R., Gasiunaitė, Z., 2015. Linking NPZD and Foodweb Models of an Estuarine Lagoon Ecosystem. Comput. Sci. Tech. 3, 350–412, https://doi.org/10.15181/csat.v3i1.1093.

Ferrarin, C., Cucco, A., Umgiesser, G., Bellafiore, D., Amos, C.L., 2010a. Modelling fluxes of water and sediment between Venice Lagoon and the sea. Cont. Shelf Res. 30, 904–914, https://doi.org/10.1016/j.csr.2009.08.014.

Ferrarin, C., Maicu, F., Umgiesser, G., 2017. The effect of lagoons on Adriatic Sea tidal dynamics. Ocean Model. 119, 57–71, https://doi.org/10.1016/j.ocemod.2017.09.009.

Ferrarin, C., Razinkovas, A., Gulbinskas, S., Umgiesser, G., Bliudžiute, L., 2008. Hydraulic regime-based zonation scheme of the Curonian Lagoon. Hydrobiologia 611, 133–146, https://doi.org/10.1007/s10750-008-9454-5.

Ferrarin, C., Umgiesser, G., Bajo, M., Bellafiore, D., De Pascalis, F., Ghezzo, M., Mattassi, G., Scroccaro, I., 2010b. Hydraulic zonation of the lagoons of Marano and Grado, Italy. A modelling approach. Estuar. Coast. Shelf Sci. 87, 561–572, https://doi.org/10.1016/j.ecss.2010.02.012.

Ferrarin, C., Zaggia, L., Paschini, E., Scirocco, T., Lorenzetti, G., Bajo, M., Penna, P., Francavilla, M., D'Adamo, R., Guerzoni, S., 2013. Hydrological Regime and Renewal Capacity of the Microtidal Lesina Lagoon. Estuar. Coast. 37, 79–93, https://doi.org/10.1007/s12237-013-9660-x.

Gasiūnaitė, Z.R., Daunys, D., Olenin, S., Razinkovas, A., 2008. The Curonian Lagoon. In: Schiewer, U. (Ed.), Ecology of Baltic Coastal Waters. Springer, Berlin/Heidelberg, 197–215.

Hampton, S.E., Galloway, A.W.E., Powers, S.M., Ozersky, T., Woo, K.H., Batt, R.D., Labou, S.G., O'Reilly, C.M., Sharma, S., Lottig, N.R., Stanley, E.H., North, R.L., Stockwell, J.D., Adrian, R., Weyhenmeyer, G.A., Arvola, L., Baulch, H.M., Bertani, I., Bowman, L.L., Carey, C.C., Catalan, J., Colom-Montero, W., Domine, L.M., Felip, M., Granados, I., Gries, C., Grossart, H.P., Haberman, J., Haldna, M., Hayden, B., Higgins, S.N., Jolley, J.C., Kahilainen, K.K., Kaup, E., Kehoe, M.J., MacIntyre, S., Mackay, A.W., Mariash, H.L., McKay, R.M., Nixdorf, B., Nõges, P., Nõges, T., Palmer, M., Pierson, D.C.,

Post, D.M., Pruett, M.J., Rautio, M., Read, J.S., Roberts, S.L., Rücker, J., Sadro, S., Silow, E.A., Smith, D.E., Sterner, R.W., Swann, G.E.A., Timofeyev, M.A., Toro, M., Twiss, M.R., Vogt, R.J., Watson, S.B., Whiteford, E.J., Xenopoulos, M.A., 2017. Ecology under lake ice. Ecol. Lett. 20, 98—111, https://doi.org/10.1111/ele.12699.

Idzelytė, R., Kozlov, I.E., Umgiesser, G., 2019. Remote Sensing of Ice Phenology and Dynamics of Europe's Largest Coastal Lagoon (The Curonian Lagoon). Remote Sens 11 (17), art. no. 2059, 27 pp., https://doi.org/10.3390/rs11172059.

Jakimavičius, D., 2012. Changes of water balance elements of the Curonian Lagoon and their forecast due to anthropogenic and natural factors. Kaunas University of Technology.

Jakimavičius, D., Kriaučiūnienė, J., Šarauskienė, D., 2018. Impact of climate change on the Curonian Lagoon water balance components, salinity and water temperature in the 21st century. Oceanologia 60 (3), 378—389, https://doi.org/10.1016/j.oceano.2018.02.003.

Jakimavičius, D., Šarauskienė, D., Kriaučiūnienė, J., 2019. Influence of climate change on the ice conditions of the Curonian Lagoon. Oceanologia 62 (2), 164—172, https://doi.org/10.1016/J.OCEANO.2019.10.003.

Janković, V., Schultz, D.M., 2017. Atmosfear: Communicating the effects of climate change on extreme weather. Weather. Clim. Soc. 9, 27—37, https://doi.org/10.1175/WCAS-D-16-0030.1.

Jarmalavičius, D., 2007. Jūrinis krantas. In: Bukantis, A., Šinkūnas, P., Taločkaitė, E. (Eds.), Klimato Kaita: Prisitaikymas Prie Jos Poveikio Lietuvos Pajūryje. Vilniaus Universiteto Leidykla, Vilnius, 25—31.

Maicu, F., De Pascalis, F., Ferrarin, C., Umgiesser, G., 2018. Hydrodynamics of the Po River-Delta-Sea System. J. Geophys. Res. 123, 6349—6372, https://doi.org/10.1029/2017JC013601.

Mėžinė, J., Ferrarin, C., Vaičiūtė, D., Idzelytė, R., Zemlys, P., Umgiesser, G., 2019. Sediment Transport Mechanisms in a Lagoon with High River Discharge and Sediment Loading. Water 11 (10), art. no. 1970, 24 pp., https://doi.org/10.3390/w11101970.

Molinaroli, E., Sarretta, A., Ferrarin, C., Masiero, E., Specchiulli, A., Guerzoni, S., 2014. Sediment grain size and hydrodynamics in Mediterranean coastal lagoons: Integrated classification of abiotic parameters. J. Earth Syst. Sci. 123, 1097—1114, https://doi.org/10.1007/s12040-014-0445-9.

Müller, S., Jessen, S., Duque, C., Sebök, E., Neilson, B., Engesgaard, P., 2018. Assessing seasonal flow dynamics at a lagoon saltwater—freshwater interface using a dual tracer approach. J. Hydrol. Reg. Stud. 17, 24—35, https://doi.org/10.1016/j.ejrh.2018.03.005.

Nguyen, T.D., Hawley, N., Phanikumar, M.S., 2017. Ice cover, winter circulation, and exchange in Saginaw Bay and Lake Huron. Limnol. Oceanogr. 62, 376—393, https://doi.org/10.1002/lno.10431.

Twiss, M.R., Smith, D.E., Cafferty, E.M., Carrick, H.J., 2014. Phytoplankton growth dynamics in offshore Lake Erie during midwinter. J. Great Lakes Res. 40, 449—454, https://doi.org/10.1016/j.jglr.2014.03.010.

Umgiesser, G., Canu, D.M., Cucco, A., Solidoro, C., 2004. A finite element model for the Venice Lagoon. Development, set up, calibration and validation. J. Marine Syst. 51, 123—145, https://doi.org/10.1016/j.jmarsys.2004.05.009.

Umgiesser, G., Zemlys, P., Erturk, A., Razinkovas-Baziukas, A., Mezine, J., Ferrarin, C., 2016. Seasonal renewal time variability in the Curonian Lagoon caused by atmospheric and hydrographical forcing. Ocean Sci. 12, 391—402, https://doi.org/10.5194/os-12-391-2016.

Ummenhofer, C.C., Meehl, G.A., 2017. Extreme weather and climate events with ecological relevance: A review. Philos. Trans. R. Soc. B Biol. Sci. 372, https://doi.org/10.1098/rstb.2016.0135.

Vincent, W.F., 2009. Effects of Climate Change on Lakes. In: Encyclopedia of Inland Waters. Acad. Press, Elsevier, 55—60.

Wang, J., Haoguo, H., Schwab, D., Leshkevich, G., Beletsky, D., Hawley, N., Clites, A., 2010. Development of the Great Lakes Ice-circulation Model (GLIM): Application to Lake Erie in 2003—2004. J. Great Lakes Res. 36, 425—436, https://doi.org/10.1016/j.jglr.2010.04.002.

Wolanski, E., Day, J.W., Elliott, M., Ramesh, R., 2019. Coasts and Estuaries. Elsevier, Amsterdam, 726 pp.

Wotton, R.S., 1995. Temperature, Organic Matter and the Sustainability of Aquatic Systems. Freshw. Forum 5, 39—47.

Yuan, R., Zhu, J., 2015. The Effects of Dredging on Tidal Range and Saltwater Intrusion in the Pearl River Estuary. J. Coast. Res. 316, 1357—1362, https://doi.org/10.2112/jcoastres-d-14-00224.1.

Žaromskis, R., 1996. Oceans, Seas, Estuaries. Debesija. Vilnius, 293 pp., (in Lithuanian).

Zemlys, P., Ertürk, A., Razinkovas, A., 2008. 2D finite element ecological model for the Curonian lagoon. Hydrobiologia 611, 167—179, https://doi.org/10.1007/s10750-008-9452-7.

Zemlys, P., Ferrarin, C., Umgiesser, G., Gulbinskas, S., Bellafiore, D., 2013. Investigation of saline water intrusions into the Curonian Lagoon (Lithuania) and two-layer flow in the Klaipeda Strait using finite element hydrodynamic model. Ocean Sci. 9, 573—584, https://doi.org/10.5194/os-9-573-2013.

PAPER IV

BOREAL ENVIRONMENT RESEARCH 26: 61–77
ISSN 1797-2469 (online)

Helsinki 29 April 2021

Application of an ice thermodynamic model to a shallow freshwater lagoon

Rasa Idzelytė[1)*] and Georg Umgiesser[2)1)]

[1)] *Marine Research Institute, Klaipėda University, Universiteto ave. 17, 92294, Klaipėda, Lithuania (*corresponding author's e-mail: rasa.idzelyte@apc.ku.lt)*
[2)] *CNR — National Research Council of Italy, ISMAR — Institute of Marine Sciences, Castello 2737/f, 30122, Venice, Italy*

Received 3 Sep. 2020, final version received 26 Mar. 2021, accepted 29 Mar. 2021

Idzelytė R. & Umgiesser G. 2021: Application of an ice thermodynamic model to a shallow freshwater lagoon. *Boreal Env. Res.* 26: 61–77.

In this study, we apply an ice thermodynamic model to a shallow freshwater lagoon in the south-eastern part of the Baltic Sea — the Curonian Lagoon. The model results were compared with the measurement data from three near-shore stations during the period of 2004–2017. The simulation data showed the model to be capable of replicating ice thickness dynamics rather well (mean R = 0.92, RMSE = 6 cm). Although the model overestimated the number of ice days (NID) on average by one month (ranging from 3 to 40 days), the overall pattern was very similar to observations (R = 0.95). We further assessed the ice thickness and NID projections in the near (2021–2040) and far (2081–2100) future under two climate change scenarios (RCP4.5 and RCP8.5). The results showed that the mean (max) ice thickness could decrease by 10–49% (6–34%) in the near and 41–75% (22–55%) in the far future under RCP4.5, and by 2–52% (2–30%) in the near and 75–88% (50–71%) in the far future under RCP8.5 compared to the baseline period of 1986–2005. The NID will shorten by 9–19% (9–22%) in the near and 15–36% (46–57%) in the far future under RCP4.5 (RCP8.5) scenarios, compared with the baseline period.

Introduction

Many places in the world are experiencing extreme events of precipitation or droughts, rising water level and air temperature, changing ice phenology (Fallis 2018, IPCC 2019). The latter, ice, is an important and early indicator of climate change for which accurate sea ice cover observations are needed. As it is already evident in the polar regions (Stroeve *et al.* 2012, Yadav *et al.* 2020), the reduction of the Arctic sea ice can accelerate global warming in the long run (Wunderling *et al.* 2020), and weather extremes in the northern hemisphere (Börgel *et al.* 2020, Simon *et al.* 2020).

Sea ice has been of high interest for studies in the Baltic Sea region, where its systematic observations started in the 19th century (Jevrejeva *et al.* 2004). During that period, navigation was the main motivation for sea ice observations; whilst nowadays, the interest in climate change impact is increasing (HELCOM 2013). Although the maximum sea ice extent, thickness, season duration and its severity in the Baltic Sea has a large interannual variability, the decreasing trend of it has accelerated since the 1980s (Vihma and Haapala

Editor in charge of this article: Kai Myrberg

2009, Haapala *et al.* 2015) and future modelling projections under different climate change scenarios reveal that this pattern will persist (Luomaranta *et al.* 2014). These changes are largely determined by the atmospheric circulation processes in the North Atlantic, such as North Atlantic Oscillation (Girjatowicz 2005, Yu Karpechko *et al.* 2015, Kļaviņš *et al.* 2016, Idzelytė *et al.* 2019). It is clear that climate change will modify ice characteristics in the future and numerical modelling can evaluate the magnitude of it.

The importance of ice in the polar regions to the global climate, e.g., oceanic and atmospheric circulation (Vihma 2014, Pedersen *et al.* 2016), has led to a progressive large-scale modelling of the sea ice. Global climate models are capable of reproducing the observed present and past climate variations and are suitable for making plausible projections of its future changes by taking into account different climate change scenarios (Randall *et al.* 2007). As global modelling results often do not describe adequately small scales, local scale model applications are needed for better representation of ice parameters.

Freshwater ice phenology is driven by solar radiation, snow accumulation on top of its surface, and mostly by the air temperature (George 2010), which is increasing worldwide (IPCC 2019). The ice season in the northern temperate lakes shortens at a rate of 7 to 17 days per century (EEA 2017), the future projections estimate a similar reduction rate (Sharma *et al.* 2019). Since the formation of sea ice is a very fast process governed mainly by the exchange of heat at the air-water interface and mixing characteristics, along with the overall capacity of the water body to store the heat (Martin and McCutcheon 1999), the smaller and shallower domains tend to freeze faster, due to a much smaller water volume underneath the ice cover.

Although real knowledge comes from studying ice in situ, it is often expensive, complicated, and in many cases dangerous to do winter field sampling campaigns. Numerical modelling is a good tool for assessing the changing processes in the water body. It not only helps filling in the gaps in observational data, but also projects future states of the studied object, e.g., the formation and evolution of ice (Peng *et al.* 2020). Three processes have to be taken into account to model the ice cover: thermodynamic processes, dynamic processes, and the processes that couple these two components (Chassignet and Verron 1998, Hunke *et al.* 2011). Modelling studies of Baltic Sea ice are extensive (Vihma and Haapala 2009), ranging from simulations of thermodynamic ice growth in the fast ice zones along the coast (Tedesco *et al.* 2009) to ridging in the drift zones needing combination of both thermodynamic and dynamic processes (Leppäranta and Myrberg 2009, Herman *et al.* 2011, Pemberton *et al.* 2017, Jakacki and Meler 2019).

Since many of the physical and ecological processes depend on ice thickness, in this paper we focus on ice thermodynamics only, disregarding the variability of ice thickness due to the dynamic processes of ice rafting and ridging. The Curonian Lagoon (Fig. 1) is a large but shallow freshwater body (greatest natural depth: 5.8 m, mean depth: 3.8 m, area: ~1600 km^2) in the southeastern part of the Baltic Sea, connected to it by a narrow strait. The lagoon is influenced by freshwater input from the rivers (mainly from the Nemunas River) and saline water from the sea. During strong northerly winds, the saltwater intrusion events affect the northern part of the lagoon (Zemlys *et al.* 2013). The increase of salinity, shorter water residence time compared to the rest of the lagoon (Umgiesser *et al.* 2016, Idzelytė *et al.* 2020), and the overall turbid characteristics of this area lead to a shorter ice cover season (Idzelytė *et al.* 2019).

In this study, to complement the recent statistical models (Jakimavičius *et al.* 2019) with new methods, we present a case study of deterministic ice thermodynamic model application for the simulation of ice cover thickness in the Curonian Lagoon. Although the numerical description of this lagoon is attracting more interest, this study is a new approach on estimating ice thickness. We evaluated the suitability of calibrated and validated model for other modelling studies and applications for this freshwater environment. Further, since the recreational activities, e.g., ice fishing, during the ice cover season in the Curonian Lagoon are of high relevance, we apply the model to investigate the ice cover response to different climate change scenarios and compare with already present knowledge regarding the Curonian Lagoon and the Baltic Sea region.

Material and methods

Ice in the Curonian Lagoon

Historical ice thickness data (Baukšys 1978) show that during the beginning of the second half of the 20th century, every winter, a 10–70 cm thick ice cover formed in the lagoon. The ice measurements in the lagoon have been taken every season since then, however, comparing with the magnitude of sea ice research in the Baltic Sea, the investigation of ice cover (thickness, extent, duration, and their dynamics) in the Curonian Lagoon (CL) has not been undertaken properly. Only in recent years has this type of research emerged, e.g., a study of remote sensing data evaluating the variability of ice cover extent, phenology, and season dynamics (Idzelytė *et al.* 2019). It revealed that in many cases the satellite data perform better compared to the conventional in situ measurements for defining the ice cover phenology. Furthermore, the spatially detailed data of ice season duration allowed indication of locations where the ice remains the longest/shortest. Likewise, it revealed that the overall ice duration is closely linked to the air temperature. However, this study did not assess ice thickness. Another study by Kozlov *et al.* (2020) revealed that satellite products of ice thickness perform rather well for the periods of gradual ice growth, although in case of rapid growth it is underestimated by 20–50%.

Two other studies were based on statistical methods. The first investigated the dependency of ice cover formation on changes in air temperature, water surface temperature, and salinity by comparing multivariate linear regression and regression kriging methods, of which latter showed better performance (Rukšėnienė *et al.* 2015). However, here, the correlation of the results with observational data was very low, and ice thickness was not addressed separately. The second study looked at future projections of different ice indices, including thickness, using statistical methods and regression analysis in the scope of different climate change scenarios (Jakimavičius *et al*. 2019), called representative concentration pathways (RCPs). Those are greenhouse gas concentration trajectories adopted by the Intergovernmental Panel on Climate Change (IPCC)

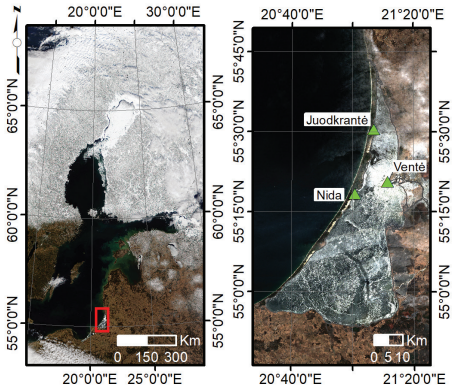

Fig 1. Location of the Curonian Lagoon (right) with respect to the Baltic Sea (left). Green triangles indicate the location of coastal ice observation stations. Image of the Baltic Sea provided by the MODIS Rapid Response team (taken from https://visibleearth.nasa.gov/), image of the Curonian Lagoon acquired from the Copernicus Sentinel-2B mission (taken from https://scihub.copernicus.eu/).

and identified by their approximate total radiative forcing in year 2100 relative to year 1750: 2.6 W m^{-2} for RCP2.6 (limits the increase of global mean temperature to 2°C, called mitigation scenario), 4.5 W m^{-2} for RCP4.5 (stabilizes radiative forcing at 4.5 W m^{-2} in the year 2100 without ever exceeding it, called stabilization scenario), and 8.5 W m^{-2} for RCP8.5 (continuously growing greenhouse gas emissions, called "business as usual" scenario) (IPCC, 2013). Jakimavičius *et al.* (2019) concluded that the annual mean ice thickness in the CL by the end of this century could decline to 13 cm (under RCP 2.6), or 9 cm (under RCP4.5), or even form only once every five years reaching 4–11 cm thickness (under RCP8.5). Statistical models perform very well if the predictors do not change, although if they would, the model cannot project the studied parameters accurately, thus in this article we explore the deterministic ice thermodynamic model results.

Data

The input data required for model calibration consists of cloud cover, downward shortwave radiation, precipitation rate, specific humidity,

air temperature, and wind speed. We obtained these data for the period of 2004–2017 from ERA5 — the fifth generation ECMWF (European Centre for Medium-Range Weather Forecasts) reanalysis for the global climate and weather hourly data on single levels, available in the Climate Data Store developed by the Copernicus Climate Change Service (C3S) at the ECMWF (Hersbach *et al.* 2018).

We validated the model output data with snow and ice thickness observation data in three coastal stations (Nida, Juodkrantė, and Ventė; Fig. 1) provided by Marine Research Department of the Environment Protection Agency (MRD of EPA) of Lithuania. The observation data covered the whole study period in Nida and Ventė, however in Juodkrantė ice observation program was discontinued in 2012.

For the analysis of climate change impact on ice thickness, we acquired the meteorological data from CORDEX (Coordinated Regional Downscaling Experiment) scenarios for Europe from the Rossby Centre regional climate model (RCA4), which consisted of five sets of simulations (downscaling) driven by the following five global climate models: EC-Earth (ICHEC), CNRM-CM5 (CNRM), IPSL-CM5A-MR (IPSL), HadGEM2-ES (MOHC), and MPI-ESM-LR (MPI). These datasets spanned a period from 1970 to 2100, divided in two parts, one from 1970 to 2005 (baseline, BS), and one from 2006 to 2100 (future), according to two Representative Concentration Pathway (RCP) scenarios: RCP4.5 — stabilization scenario, and RCP8.5 — "business as usual" scenario (IPCC 2013).

MRD of EPA of Lithuania provided the air temperature measurement data in all three stations (Nida, Juodkrantė, and Ventė; Fig. 1), and Lithuanian Hydrometeorological Service provided the precipitation measurement data, however measurements were taken only in Nida.

Ice thermodynamic model

Here, we used the improved version of the enhanced sea-ice thermodynamic model ESIM2 by Tedesco *et al.* (2010). The first version of this 0D model was already applied for studying landfast sea ice in four different areas of the Baltic Sea (Tedesco *et al.* 2009). This application showed that model is capable to adequately represent the growth, decay, and overall seasonal changes of the ice, meteoric ice (h_{mi}, consisting of snow ice and superimposed ice), and snow thickness.

The prognostic variables of ESIM2 are three layers of snow and three layers of ice (Fig. 2, Table 1). Snow thickness (h_s) in the model consists of new fallen snow ($(h_s)_n$), "bucket snow" ($(h_s)_{bk}$) — initial snowfall collected in a virtual bucked, which after fully filled is emptied, and snow is compacted ($(h_s)_{cp}$). Ice layers consist of snow ice (h_{si}), superimposed ice (h_{ss}), and sea ice (h_i). The model initiates snow ice formation every time the ice draft exceeded the thickness of the ice. If the melted snow is in contact with the layer of ice, then it refreezes and superimposed ice forms. Finally, sea ice is divided into two layers: biologically active ($(h_i)_{bio}$) and biologically inactive ($(h_i)_{abio}$). The latter two were added for the model to be capable of simulating salinity evolution in sea ice and to be compatible with the biogeochemical flux model (Tedesco *et al.* 2010). Since the Curonian Lagoon is considered mainly freshwater, salinity is set to be constant and equal to zero (Table 1).

The model also simulates temperature at the surface and at the interface of each snow and ice layer. Melting is initiated every time when the surface temperature is at the melting point, while the rate of it depends on the net heat flux balance between the surface (sensible, F_{SE}, latent, F_{LA}, shortwave, F_{SW}, and longwave radiation, F_{LW}) and conductive (F_C) fluxes (Fig. 2).The heat flux from water to the bottom of the ice (oceanic heat flux, F_W) in previous model applications (Tedesco *et al.* 2009, 2010) was represented by a constant value, for our study, we incorporated a bulk formulation by Omstedt and Wettlaufer (1992):

$$F_W = \rho_w C_p C_h \Delta U (T_\infty - T_F), \quad (1)$$

where C_p is specific heat of water, C_h — heat transfer coefficient, ΔU is the relative velocity between the ice drift and the current at a reference level (we consider it to be constant and equal to 0.05 m s^{-1}), T_∞ — mixed layer

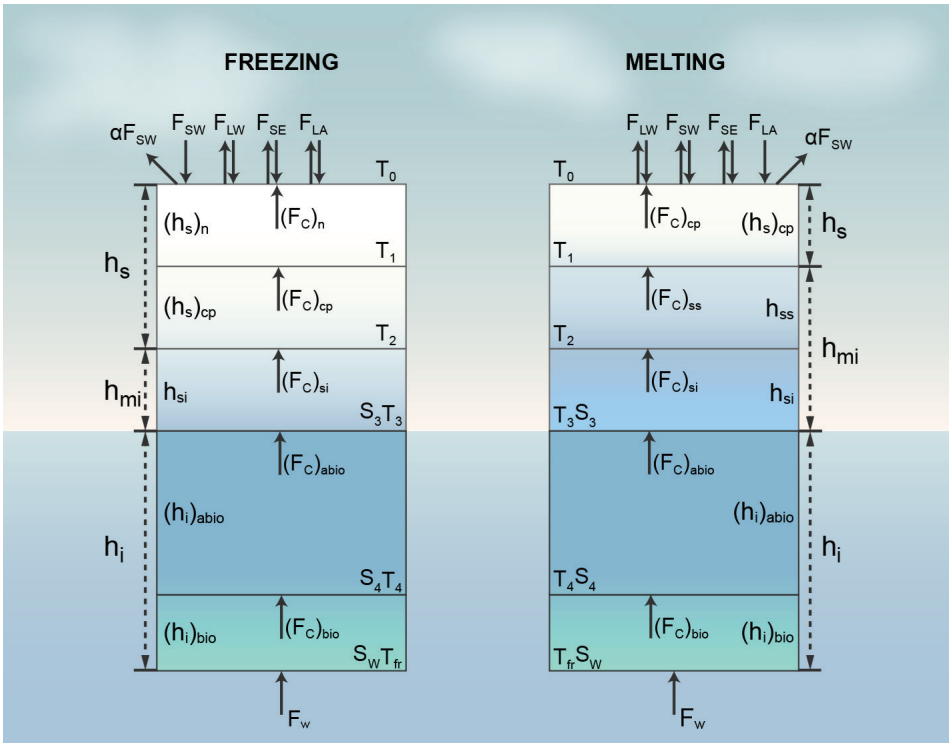

Fig 2. Schematic representation of the ice thermodynamic model structure during the freezing and melting periods (adapted from Tedesco 2009).

temperature, and T_F — freezing temperature. Since the Curonian Lagoon is shallow and has a well-mixed water column, the water temperature beneath the ice is mostly equal to the freezing temperature throughout the ice cover season, which results in $F_W \approx 0$ W m^{-2}.

In order to properly simulate the ice freeze onset and melt-off, the ice thermodynamic model is coupled with a slab ocean model, which is an approximation of the ocean mixed layer. During ice-free periods, this slab ocean model computes a temperature of the mixed

Table 1. Ice thermodynamic model parameters that differ from Tedesco et al. (2009; 2010).

Parameter	Value	Unit
Mixed layer depth, h_{mix}	1.5	m
Water density, ρ_w	1000	kg m^{-3}
Water salinity, S_w	0.0	g/kg
Snow precipitation density, $(\rho_s)_{prec}$	300	kg m^{-3}
Density of cold new snow, $(\rho_s)_y$	300	kg m^{-3}
Density of warm new snow, $(\rho_s)_y$	350	kg m^{-3}
Density of cold "bucket" snow, $(\rho_s)_{bk}$	350	kg m^{-3}
Density of warm "bucket" snow, $(\rho_s)_{bk}$	400	kg m^{-3}
Density of cold compacted snow, $(\rho_s)_{cp}$	350	kg m^{-3}
Density of warm compacted snow, $(\rho_s)_{cp}$	400	kg m^{-3}

layer based on the depth and surface energy fluxes.

Simulations' set-up and scenarios

We carried out several simulations for the model calibration and sensitivity using different snow density values. However in this study, only two types of simulations are presented: 1) with the original model set-up as described in Tedesco *et al.* (2010) (hereafter $\mathrm{Pres_{Orig}}$), and 2) with increased densities of all snow types by 50 kg m^{-3} (hereafter $\mathrm{Pres}_{\rho s}$) (Table 2). We ran the ice model for each of the three stations (Fig. 1) for the period of 2004–2017, with a one-hour model time step, and selected the best model set-up by evaluating the root-mean-square error (RMSE) and Pearson correlation coefficient (R) between measured and observed values of the ice thickness.

We also compared freeze onset (FO) and melt-off (MO) dates derived from coastal observations ($\mathrm{FO_O}$ and $\mathrm{MO_O}$) with the ones of the ice model, by computing the difference in days. The latter we analysed in two parts: 1) the date of first (last) ice, $\mathrm{FO_M}$ ($\mathrm{MO_M}$), and 2) the date of first (last) ice before (after) the continuous ice cover, $\mathrm{FO_{M_{corr}}}$ ($\mathrm{MO_{M_{corr}}}$), this way eliminating the sporadic very thin ice formation events before and after the continuous ice season. Additionally, we compared the total number of ice days (NID), denoting the exact period that ice was observed in the coastal stations and computed by the model.

To investigate the sensitivity of ice model to the air temperature and precipitation rate, we set-up a test case of one ice season in Nida during 2011–2012 when the model gave the best results compared with observation data. For this, we ran the ice thermodynamic model increasing air temperature by 2°, 4°, and 6°C, and decreasing it by 1° and 2°C, as well as increasing and decreasing the precipitation rate by 50% and 100% at every time step. The mean snow and ice thickness were computed for the Nov.–Apr. period, as well as the maximum thickness and number of ice and snow days.

To compute the climate change impact on ice thickness, we used input data from five climate models: CNRM, ICHEC, IPSL, MOHC, and MPI averaged over three points in the lagoon (Nida, Juodkrantė, and Ventė; Fig. 1). For the climate change simulations, we shortened the baseline period starting from 1986 (as suggested in IPCC, 2019) and divided the future period in two sections for near and far future for both RCP scenarios (Table 2).

Since air temperature and precipitation data from the ERA5 and climate models have bias comparing to the observations, we corrected it. The air temperature was corrected (T_{BC}) by simply adding the difference between the observed, T_{O}, and modelled average air temperature, $\overline{T}_{\mathrm{M}}$, respectively (Lenderink *et al.* 2007):

$$T_{\mathrm{BC}}(t) = T_{\mathrm{M}}(t) + \left(\overline{T}_{\mathrm{O}} - \overline{T}_{\mathrm{M}}\right). \quad (2)$$

Precipitation ($\mathrm{PR_{BC}}$) was corrected by multiplying the ratio between the observed ($\mathrm{PR_O}$) and modelled ($\mathrm{PR_M}$) values:

$$\mathrm{PR_{BC}}(t) = \mathrm{PR_M}(t)\frac{\overline{\mathrm{PR_O}}}{\overline{\mathrm{PR_M}}}, \quad (3)$$

Table 2. Summary of the simulations.

Name	Period	Description
$\mathrm{Pres_{Orig}}$	2004–2017	Present-day period with original model set-up as described in Tedesco et al. (2010)
$\mathrm{Pres}_{\rho s}$	2004–2017	Present-day period with increased densities of all snow types by 50 kg m^{-3}
BS	1986–2005	Baseline period
$\mathrm{RCP4.5_{near}}$	2021–2040	RCP4.5 scenario in the near future
$\mathrm{RCP4.5_{far}}$	2081–2100	RCP4.5 scenario in the far future
$\mathrm{RCP8.5_{near}}$	2021–2040	RCP8.5 scenario in the near future
$\mathrm{RCP8.5_{far}}$	2081–2100	RCP8.5 scenario in the far future

$\overline{T}_O$, $\overline{T}_M$, $\overline{PR}_O$, and $\overline{PR}_M$ were computed for the period of Nov.–Apr. of 1993–2005, for which the observation data were available. The bias correction was applied for both — baseline and future datasets. The scenario runs were corrected based on the bias from the corresponding baseline period datasets.

We compared the future projections with the BS by computing the average and maximum ice thickness and number of ice days for the period of Nov.–Apr. of each winter season. The future change was evaluated by computing a percentage of change from the baseline period. The trend significance of the ice thickness during the baseline (1986–2005) and the whole future period (2006–2100) under RCP4.5 and RCP8.5 scenarios was evaluated using the Mann-Kendall test at a 0.05 significance level with a 95% confidence level (Kendall and Gibbons 1990). We evaluated the decrease rate by taking the slope parameter from linear regression equation generated for the same periods.

Results

Model calibration and validation

We calibrated the model by testing several density values of all snow types. The statistics of the results (Table 3) showed that the model achieved the best results when using increased densities of all snow types by 50 kg m^{-3}, $Pres_{\rho s}$, in contrast to the original model set-up described in Tedesco *et al.* (2010). This was especially true for the station in Nida, for which both the air temperature and precipitation ERA5 data were corrected with the measurements, thus the ice model gave higher correlation coefficient values not only for the ice, but for snow thickness as well.

The comparison of ice model results and observations from the coastal stations (Fig. 3) showed that the model largely underestimated snow thickness in all three stations. Although, the overall snow growth pattern in Ventė is moderate, in Nida and Juodkrantė the correlation is strong. Nonetheless, the model described the ice thickness formation and evolution very well (Fig. 4), and in all three stations correlation with the measurement data is high (R is 0.92, 0.96 and 0.89 in Nida, Juodkrantė, and Ventė, respectively).

The average difference of freeze onset dates (Table 4) revealed that in the model initial ice formation (FO_M) started very early, which was not recorded in the coastal stations (FO_O). There usually were very short freezing events with ice thickness in a matter of millimetres, this way leading to a very large initial freeze onset difference. The model data fit the observations much better with eliminated sporadic freezing events in the beginning of the ice season ($FO_{M\,corr}$). The same was with melt-off dates (Table 4); here in many cases, the model still indicated ice presence, although it was already not visible in the coastal stations.

The model overestimated the total number of ice days (NID) in all three stations (Fig. 4) by more than one month in Nida and Juodkrantė, and 19 days in Ventė. Nonetheless, the overall pattern of NID was very similar to that of coastal observations, having a very strong correlation (three station mean R = 0.95). The elimination of short thin ice formation events in the beginning and occasionally at the end of the ice season revealed an even higher correlation with the observed ice duration (three station mean R = 0.98), while the RMSE decreased by 10 days.

Table 3. Calibration statistics of ice and snow thickness. Model set-up types ($Pres_{Orig}$ and $Pres_{\rho s}$) are described in the section Simulations' set-up and scenarios. RMSE values are in meters.

		Nida		Juodkrantė		Ventė	
		$Pres_{Orig}$	$Pres_{\rho s}$	$Pres_{Orig}$	$Pres_{\rho s}$	$Pres_{Orig}$	$Pres_{\rho s}$
Ice	*R*	0.89	0.92	0.95	0.96	0.87	0.89
	RMSE	0.08	0.07	0.06	0.04	0.06	0.06
Snow	*R*	0.69	0.73	0.62	0.63	0.56	0.56
	RMSE	0.05	0.05	0.07	0.07	0.04	0.04

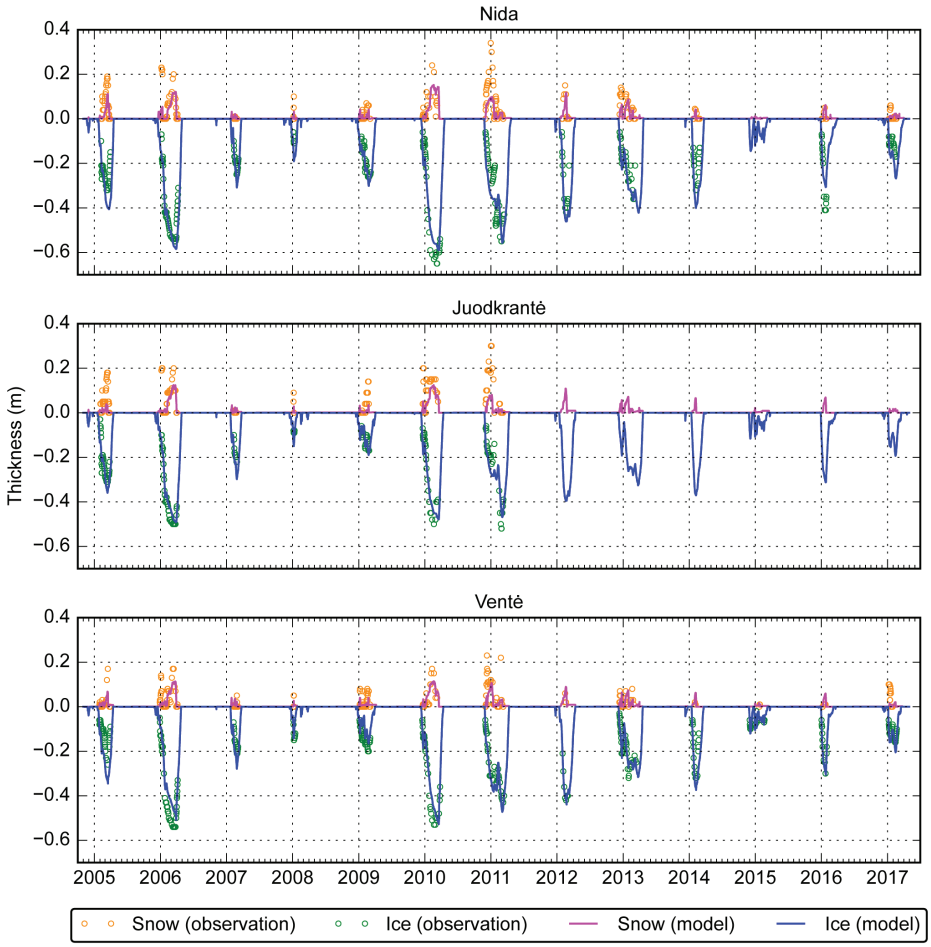

Fig 3. Observations and modelled snow and ice cover thickness in three coastal stations: Nida, Juodkrantė, and Ventė in 2004–2017. Snow and ice thickness layers are grouped together in two groups: snow — positive ordinate, and ice — negative ordinate.

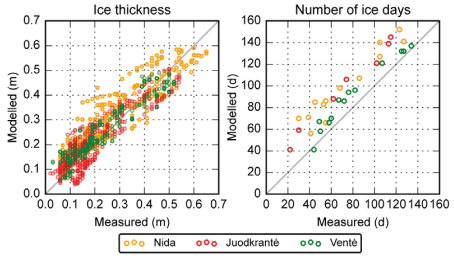

Fig 4. Scatterplots of measured and modelled ice thickness and a number of ice days in Nida, Juodkrantė, and Ventė for the period 2004–2017.

Sensitivity to air temperature and precipitation rate

During the 2011–2012 winter season in Nida, the model produced very good ice ($R = 0.94$) and snow ($R = 0.90$) thickness results, allowing to test the model sensitivity to air temperature and precipitation rate changes in a controlled environment. The results using increased air temperature showed that the average ice thickness decreased by 2 cm/°C, while the maximum ice thickness decreased by 3 cm/°C (Fig. 5). Higher

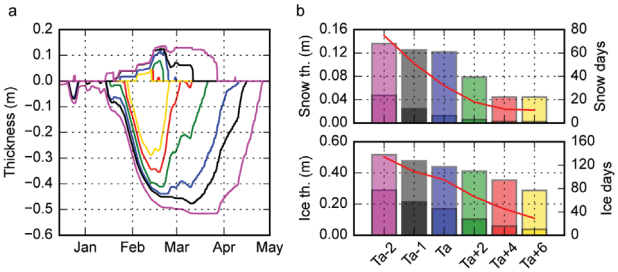

Fig 5. Ice and snow thickness sensitivity due to varying air temperature: in (**a**) Nida during 2011–2012, computed using measured air temperature (Ta, blue), increased by 2°C (Ta+2, green), 4°C (Ta+4, red), and 6°C (Ta+6, yellow), and decreased by 1°C (Ta–1, black) and 2°C (Ta–2, purple); and (**b**) Ice (upper panel) and snow thickness (lower panel) of each air temperature change. Light colour indicates maximum and dark colour average thickness (labelled at the left axis). Also inserted is the red line, labelled on the right, indicating the number of ice and snow days. Average values were computed for a five-month period (Dec. 2011–May 2012).

air temperatures did not have a considerable impact on the average snow thickness, although the maximum of it decreased by 1 cm/°C. The number of ice days decreased by 11 days/°C and snow days by 4 days/°C. The decreasing temperature results showed that the average ice thickness increased by 6 cm/°C, while the maximum ice thickness increased by 4 cm/°C. The maximum snow thickness increased only by 1 cm/°C, while the average by 2 cm/°C. The overall number of ice days increased by 28 and snow by 22 days/°C.

The model is less sensitive to the changes in precipitation rate compared to air temperature. Decreased precipitation rate led to likewise decreased snow thickness (Fig. 6), although while increased rate did not have major effects on the maximum snow thickness and number of days, it increased the average thickness. A precipitation rate decrease of 50% led to 4 cm higher maximum ice thickness, and to 5 cm higher when there was no precipitation. Increased precipitation rate by 50% (100%) led to a maximum ice thickness decrease by 2 cm (3 cm). The increased precipitation rate did not have major effects on overall number of snow days, while number of ice days slightly decreased. The decreased precipitation rate likewise reduces the number of snow days, although the number of ice days stayed the same.

Climate change

The average Nov.–Apr. air temperature during the 1993–2005 period was higher in all climate model datasets by ~1.3°C compared with the measurements, apart from CNRM, which had the most similar air temperature data — the difference being only ~0.16°C. The average Nov.–Apr. air temperature during the baseline period of CNRM, ICHEC, and IPSL climate

Table 4. The difference of freeze onset (melt-off) dates between observation, FO_O (MO_O), and modelling, FO_M (MO_M) and $FO_{M_{corr}}$ ($MO_{M_{corr}}$), data in three coastal stations. Dash indicates subtraction. Negative numbers indicate that ice thermodynamic model produced ice data longer than it was recorded in the coastal stations.

	Nida			Juodkrantė			Ventė		
	mean	min	max	mean	min	max	mean	min	max
FO_O–FO_M	27	1	81	28	1	66	17	1	63
FO_O–$FO_{M_{corr}}$	4	0	13	5	1	12	3	0	9
MO_O–MO_M	–21	–39	–12	–20	–31	–9	–10	–19	–5
MO_O–$MO_{M_{corr}}$	–20	–39	–6	–15	–25	–3	–10	–19	–5

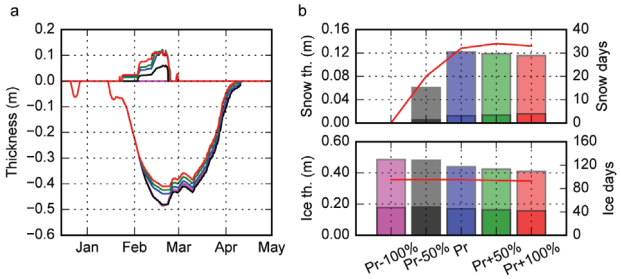

Fig 6. Ice and snow thickness sensitivity due to varying precipitation rate: in (**a**) Nida during 2011–2012, computed using measured precipitation rate (Pr, blue), increased by 50% (Pr+50, green), 100% (Pr+100, red), and decreased by 50%°C (Pr–50, black) and 100% (Pr–100, purple); and (**b**) Ice (upper panel) and snow thickness (lower panel) of each precipitation rate change. Light colour indicates maximum and dark colour average thickness (labelled at the left axis). Also inserted is the red line, labelled on the right, indicating the number of ice and snow days. Average values were computed for five-month period (Dec. 2011–May 2012).

model data was lower compared to the present-day period, while for MOHC and MPI it was higher (Fig. 7), which all became lower compared to the present-day period after the bias correction, and the model produced better results. The precipitation rate was close to the observations, apart from ICHEC and IPSL datasets, having slightly larger values.

The mean ice thickness (averaged over Nov.–Apr.) in the near future, derived using ICHEC, IPSL, and MOHC model data showed a large decrease compared to the baseline period (Table 5), while the model that fit the observations the best (CNRM) showed a mean ice thickness decrease by 10.4–12.7%. The highest change was in the far future, when mean ice thickness decreased by 41–75% under RCP4.5$_{far}$ and 75–88% under RCP8.5$_{far}$. The maximum ice thickness is likely to steadily decrease throughout the century (Fig. 8). In the near future it is not likely to change drastically, by 6–34% under RCP4.5$_{near}$ and 2–30% under RCP8.5$_{near}$,

Table 5. Percentage of a decrease of mean and maximum ice thickness and number of ice days (NID) in the near (2021–2040) and far (2081–2100) future compared to the baseline period (1986–2005) under different climate change scenarios of data from five climate models: ICHEC, CNRM, IPSL, MOHC, and MPI.

	CNRM	ICHEC	IPSL	MOHC	MPI
Mean					
RCP4.5$_{near}$	10.4	39.3	49.0	33.9	27.1
RCP8.5$_{near}$	12.7	52.4	36.5	31.3	1.7
RCP4.5$_{far}$	68.6	59.7	74.5	54.2	40.7
RCP8.5$_{far}$	85.9	88.2	87.8	85.8	75.4
Max					
RCP4.5$_{near}$	6.3	13.9	33.7	24.9	13.6
RCP8.5$_{near}$	2.8	29.6	17.6	13.5	1.8
RCP4.5$_{far}$	45.5	30.9	55.2	40.7	22.3
RCP8.5$_{far}$	60.3	60.2	71.4	64.0	50.3
NID					
RCP4.5$_{near}$	8.5	12.4	19.3	16.2	17.7
RCP8.5$_{near}$	8.7	21.9	11.5	18.3	17.6
RCP4.5$_{far}$	35.5	34.7	29.9	31.4	15.5
RCP8.5$_{far}$	55.7	60.2	67.0	57.3	46.0

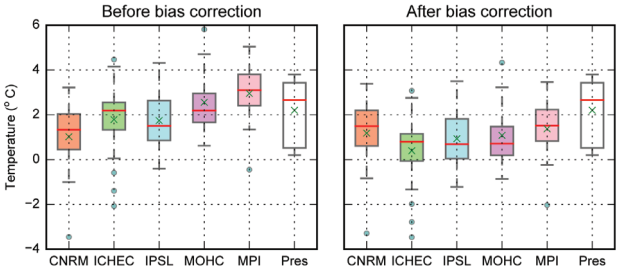

Fig 7. Average Nov–Apr. air temperature during the baseline (1986–2005) period of data from five climate models: ICHEC, CNRM, IPSL, MOHC, and MPI, compared with the present-day period (Pres, 2004–2017). Circles denote the outliers, red line indicate the median, and green "*x*" is the mean. Please note that the bias correction was done using the available observation data for the period of 1993–2005.

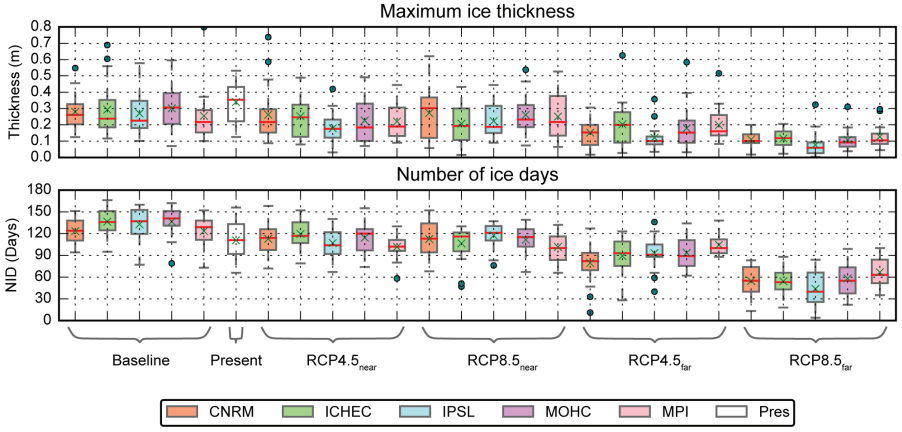

Fig 8. Maximum ice thickness and number of ice days during the baseline (1986–2006), present (2004–2017), near (2021–2040) and far (2081–2100) future periods under RCP4.5 and RCP8.5 scenarios using data from five climate models: ICHEC, CNRM, IPSL, MOHC, and MPI. Circles denote the outliers, red line indicate the median, and green "*x*" is the mean.

although in the far future it could decrease by 22–55% and 50–71% under RCP4.5$_{far}$ and RCP8.5$_{far}$ respectively (Table 5).

The ice thickness distribution (Fig. 9) shows that the five-model mean/max ice thickness was 9/20 cm during the baseline period. In the near future mean thickness could decrease to 6 cm under both RCP scenarios, and the maximum thickness could decrease to 15 cm under RCP4.5$_{near}$ and 16 cm under RCP8.5$_{near}$. In the far future, mean/max ice thickness could reach 4/9 cm under RCP4.5$_{far}$ and 1/4cm under RCP8.5$_{far}$.

The mean and maximum ice thickness from all the models over the 2006–2100 period display statistically significant decreasing trend ($p < 0.05$), while the trends during the baseline period were not significant. During the baseline period mean/max ice thickness was decreasing with 0.30–0.91/0.63–1.32 cm year^{-1}, while MOHC and MPI showed an increasing rate of 0.09/0.36 and 0.34/0.79 cm year^{-1}, respectively (Table 6). The decreasing tendency of mean/max ice thickness varied from 0.04–0.07/0.11–0.18 cm year^{-1} under RCP4.5 and 0.05–0.12/0.11–0.30 cm year^{-1} under RCP8.5 climate change scenarios.

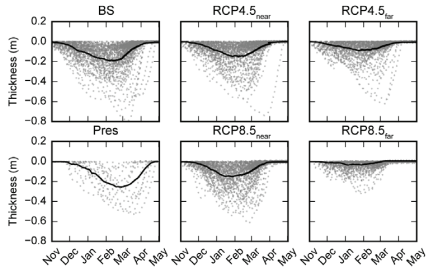

Fig 9. Ice thickness during the baseline (BS, 1986–2005), present (Pres, 2004–2017), and near (2021–2040) and far (2081–2100) future periods under RCP4.5 and RCP8.5 scenarios using data from five climate models: ICHEC, CNRM, IPSL, MOHC, and MPI. Black line is the average thickness of all models.

The decreasing number of ice days (NID) pattern is similar to that of maximum ice thickness (Fig. 8). Since the ice model overestimates the NID, it is more suitable to evaluate its change by computing a percentage compared to the baseline period. The NID can be expected to decrease by 9–19% under RCP4.5$_{near}$ and 9–22% under RCP8.5$_{near}$ (Table 5). The highest difference is computed using the data of ICHEC under RCP8.5$_{near}$, while the model that fit the observations the best (CNRM) showed a shortening NID by ~8.6% in the near future. In the far future the NID can be expected to shorten by 16–36% under RCP4.5$_{far}$ compared with the baseline run, while the highest change can be seen under RCP8.5$_{far}$, ranging from 46% to 67% less ice days.

In all climate model cases, the NID displayed a statistically significant decreasing trend ($p < 0.05$) for the period of 2006–2100, while during the baseline period it was not significant, apart from ICHEC ($p = 0.01$). During the baseline period the NID was decreasing with 0.55–2.39 days year^{-1}, while MPI showed an increasing rate of 0.22 days year^{-1} (Table 6). The decrease ranged from 0.17 to 0.53 days year^{-1} under RCP4.5, and 0.66–1.07 days year^{-1} under RCP8.5 scenario.

Discussion

In this paper, we presented a deterministic numerical modelling application for the ice thickness projections in the shallow freshwater lagoon, the Curonian Lagoon (CL). Our chosen ice thermodynamic model (by Tedesco *et al.*

Table 6. The decrease rate of mean and maximum ice thickness (cm year^{-1}), and number of ice days (NID, days year^{-1}) during the baseline period (BS, 1986–2005) and under RCP4.5 and RCP8.5 climate change scenarios of data from five climate models: ICHEC, CNRM, IPSL, MOHC, and MPI, over the period of 2006–2100.

	CNRM	ICHEC	IPSL	MOHC	MPI
Mean					
BS	–0.30	–0.91	–0.41	0.09	0.34
RCP4.5	–0.07	–0.06	–0.04	–0.07	–0.06
RCP8.5	–0.12	–0.05	–0.06	–0.08	–0.10
Max					
BS	–0.63	–1.32	–1.06	0.36	0.79
RCP4.5	–0.18	–0.13	–0.12	–0.15	–0.11
RCP8.5	–0.30	–0.11	–0.19	–0.23	–0.24
NID					
BS	–0.49	–2.39	–1.22	–0.55	0.22
RCP4.5	–0.53	–0.51	–0.36	–0.47	–0.17
RCP8.5	–0.92	–0.73	–1.07	–0.79	–0.66

2009, Tedesco *et al.* 2010) showed being suitable for ice thickness projections in a freshwater environment. We calibrated the ice thermodynamic model by testing various classes of snow density values, of which the best results gave the higher density model set-up. Higher snow density leads to higher heat conductivity of snow, resulting in an increased ice thickness (Zhao *et al.* 2019). The ice growth and melt patterns as well as thickness were simulated rather accurately in all three stations in the CL (mean RMSE = 0.06 m, R = 0.92). The average snow thickness correlation with the observations was strong in Nida and Juodkrantė, while in Ventė it was moderate. The model's ability to adequately simulate snow thickness highly depends on the meteorological forcing data. Model runs using local weather observations produced much better results.

Since snow is a very good insulator, the model sensitivity tests showed that thicker snow cover leads to slower ice growth, thus the bias in the snow thickness can lead to the bias of maximum ice thickness. However, precipitation rate is highly dependent on the air temperature. Overall ice parameters and air temperature have a linear relationship — decreasing air temperature extends the number of ice and snow days due to prolonged freezing period, likewise increasing the average ice and snow thickness.

Overall, the model represents the total ice thickness very well, and the number of simulated ice layers appears to be enough. Some other studies (Cheng *et al.* 2008, Lecomte *et al.* 2011) suggest that the increased vertical resolution of the model, e.g., by up to 15–20 layers, can improve the results. However, the same study of Cheng *et al.* (2008), stated that the accuracy of model forcing was much more important than the vertical resolution.

The number of ice days was highly overestimated by the model (on average by one month, ranging from 3 to 40 days), while the correlation with the observations was very strong (mean R = 0.95). The computation of common ice season duration from the freeze-up and melt-off dates, did not give good results compared to the observation data, due to short and very thin ice freezing events early in the beginning and sometimes at the end of the continuous ice cover, which were not recorded in the coastal observations. Eliminating these sporadic freezing events in the model data lead to the ice season duration values being much closer to that of observation data (mean R = 0.98, compared to R = 0.78 of uncorrected ice seasons).

The application of global climate model (GCM) projections in ice thermodynamic model revealed that global scale climate data have a very coarse resolution considering the small size of the Curonian Lagoon, and are not entirely suitable for such small-scale applications. Due to the higher air temperature the ice model during the baseline period mostly underestimated ice thickness compared to the present-day period (computed using observation data), thus GCM require downscaling and bias correction to fit the local climate. The downscaling approach is also often carried out for the modelling studies of larger domains, such as the Baltic Sea (Wibig *et al.* 2015), denoting the importance and benefits of high-resolution forcing data (Hermans *et al.* 2020).

The mean ice thickness in the CL could be expected to decrease by ~30% in the near future, having similar results under both RCP scenarios. By the end of the century, the average ice thickness will undergo drastic changes compared with the baseline period, decreasing by on average 60% under RCP4.5 and 85% under RCP8.5 scenarios. The maximum ice thickness can be expected to decrease by 40% in $RCP4.5_{far}$ and 60% in $RCP8.5_{far}$, while only 13–18% in the near future.

Our results correspond with another study of ice thickness projections using statistical methods by Jakimavičius *et al.* (2019), which showed that in the far future ($RCP4.5_{far}$), the average ice thickness will decline by 53% compared to the reference period of 1986–2005. However, they project that for $RCP8.5_{far}$, ice will form once every five years reaching 4–11 cm thickness, while in our projections the ice will form every year but the mean/max ice thickness would be only ~1/4cm. Although, this difference between our study and Jakimavičius *et al.* (2019), could also be due to different averaging periods (we averaged over Nov.–Apr. period) since the averaging period in their study is not specified.

The ice thickness around the Baltic Sea coastal areas does not show any consistent

trend in the baseline observations (Jevrejeva *et al.* 2004, Haapala *et al.* 2015). In the far future under RCP8.5, the area outside the Bay of Bothnia could be ice free and the mean annual maximum ice thickness is projected to decrease with a rate of 0.1–0.34 cm year^{-1} and 0.08–0.76 cm year^{-1} under RCP4.5 and RCP8.5, respectively, with higher values northward (Luomaranta *et al.* 2014). In our study, we project a decrease of maximum ice thickness with a rate of 0.11–0.18 cm year^{-1} under RCP4.5 and 0.11–0.30 cm year^{-1} under RCP8.5.

The NID can be expected to decrease by ~15% (five-model mean) in the near future under both RCP scenarios compared to the baseline data. Whilst in the far future this change could increase up to 30% under RCP4.5 and even 57% under RCP8.5. Translated to days this is decreasing from the average 130 days during the baseline period to 110 days in the near future and 92 days in RCP4.5$_{\text{far}}$ and 56 days in RCP8.5$_{\text{far}}$. However, since ice model overestimated the NID during the present-day period, these values are likely be lower.

The study of Jakimavičius *et al.* (2019) proposed that ice season would last 35–45 days and 3–34 days in the near and far future, respectively. Their study showed that ice duration is on average 55 days during the reference period (1986–2005), ranging from 17 to 87 days. However, the study of Idzelytė *et al.* (2019) showed that during 2002–2003 the ice season duration in the Curonian Lagoon was 123 days based on observation data, which is longer than the specified range of Jakimavičius *et al.* (2019). Jakimavičius *et al.* (2019) also used data from the station in Klaipėda Strait, where the ice usually does not form or is very thin and not land locked, due to the more saline water and intensive shipping. Therefore, it could be implied that the inclusion of data from the strait lead to underestimated values.

In the Baltic Sea, it is expected that the length of the ice season can decrease by 1–2 months in the northern parts and 2–3 months in the central parts (HELCOM 2007). Based on the baseline observations, the decrease is observed from east to west, and from the inner waters towards the sea areas (Haapala *et al.* 2015). In the small sheltered areas in the southern Baltic, e.g., Vistula lagoon, the duration of ice phenomenon is constantly decreasing, however with large irregularities (Majewski 2011). The decrease rate of NID during baseline period in our study is 0.88 days year^{-1} (five-model mean), which is higher than that reported in the study of Jakimavičius *et al.* (0.2 days year^{-1}), along the Lithuanian Baltic Sea coast (0.64 days year^{-1}; Dailidienė *et al.* 2012), along the Latvian coast and in the Gulf of Riga (~0.3 days year^{-1}) (Kļaviņš *et al.* 2016), the eastern Gulf of Finland (0.6 days year^{-1}; Ronkainen 2013), or in the lakes of northern Poland (0.54 days year^{-1}; Bartosiewicz *et al.* 2020).

Although with our study we do not project the ice cover to completely disappear from the Curonian Lagoon, the whole phenology will evidently undergo drastic changes to a shortened ice season duration and loss of thickness. These changes will affect the underwater environment by changes in the hydrodynamic (Idzelytė *et al.* 2020) and ecological (Potyutko 2018) regimes, the living conditions of the residents in coastal areas by decreasing the flooding events caused by ice jams, as well as disappearing winter recreational activities. The applied ice thermodynamic model still requires work to fit the overall observed ice season duration, e.g., inclusion of the varying speed of under-ice currents, mixed layer temperature, salinity data, likewise adjusting the freezing temperature, with possible additional experiments, such as application of a first-order analysis using simple analytic methods (Karetnikov *et al.* 2017). However, the ice thickness corresponded very well to the measurements and could be used as a guideline for future investigations.

Acknowledgements: The preparation of this paper was partially funded by European Social Fund (project no: 09.3.3-LMT-K-712-01-0178) under grant agreement with the Research Council of Lithuania (LMTLT).

References

Bartosiewicz M., Ptak M., Woolway R.I., Sojka M. 2020. On thinning ice: Effects of atmospheric warming, changes in wind speed and rainfall on ice conditions in temperate lakes (Northern Poland). *J. Hydrol.*: 125724, doi:

j.jhydrol.2020.125724.

Baukšys J. 1978. Ledo režimas [Ice regime]. In: Rainys A. (ed.), *Kuršių marios* [*The Curonian Lagoon]*, Vilnius, pp. 34–49. [In Lithuanian].

Börgel F., Frauen C., Neumann T. & Meier H.E.M. 2020. The Atlantic Multidecadal Oscillation controls the impact of the North Atlantic Oscillation on North European climate. *Environ. Res. Lett.* 15: 104025, doi: 10.1088/1748-9326/aba925.

Chassignet E. & Verron J. 1998. *Ocean Modeling and Parameterization*. Springer, Netherlands.

Cheng, B., Z. Zhang, T. Vihma, M. Johansson, L. Bian, Z. Li, and H. Wu (2008), Model experiments on snow and ice thermodynamics in the Arctic Ocean with CHINARE 2003 data. *J. Geophys. Res.* 113: C09020, doi:10.1029/2007JC004654.

Dailidienė I., Davulienė L., Kelpšaitė L., Razinkovas A. 2012. Analysis of the Climate Change in Lithuanian Coastal Areas of the Baltic Sea. *J. Coast. Res*. 28, 557–569, doi: 10.2112/JCOASTRES-D-10-00077.1.

EEA. 2017. *Climate change, impacts and vulnerability in Europe 2016. An indicator-based report*. Luxembourg, Publications Office of the European Union.

Fallis A.G. 2018. Global Warming of 1.5°C. An IPCC Special Report on the impacts of global warming of 1.5°C above pre-industrial levels and related global greenhouse gas emission pathways, in the context of strengthening the global response to the threat of climate change. *J. Chem. Inf. Model*. 53(9): 3–25.

George G. 2010. *The Impact of Climate Change on European Lakes*. Springer Netherlands.

Girjatowicz J.P. 2005. The Relationships Between the North Atlantic Oscillation and Southern Baltic Coast Ice Conditions. *J. Coast. Res.* 212: 281–291, doi: 10.2112/03-0073.1.

Haapala J.J., Ronkainen I., Schmelzer N. & Sztobryn M. 2015. Recent Change – Sea Ice. In: The BACC II Author Team (eds.), *Second Assessment of Climate Change for the Baltic Sea Basin, Regional Climate Studies*, Springer International Publishing, Cham, pp. 145–153.

HELCOM 2007. Climate Change in the Baltic Sea Area –- HELCOM Thematic Assessment in 2007. *Balt. Sea Environ. Proc.* No. 111, 54.

HELCOM, 2013 Climate change in the Baltic Sea Area: HELCOM thematic assessment in 2013. *Balt. Sea Environ. Proc.* No. 137.

Herman A., Jedrasik J. & Kowalewski M. 2011. Numerical modelling of thermodynamics and dynamics of sea ice in the Baltic Sea. *Ocean Sci*. 7: 257–276, doi: 10.5194/os-7-257-2011.

Hermans T.H.J., Tinker J., Palmer M.D., Katsman C.A., Vermeersen B.L.A. & Slangen A.B.A. 2020. Improving sea-level projections on the Northwestern European shelf using dynamical downscaling. *Clim. Dyn.* 54: 1987–2011, doi:10.1007/s00382-019-05104-5.

Hersbach H., Bell B., Berrisford P., Biavati G., Horányi A., Muñoz Sabater J., Nicolas J., Peubey C., Radu R., Rozum I., Schepers D., Simmons A., Soci C., Dee D., Thépaut J-N. 2018. ERA5 hourly data on single levels from 1979 to present. Copernicus Climate Change Service (C3S) Climate Data Store (CDS). (Accessed on < 15-Nov-2020 >), doi: 10.24381/cds.adbb2d47.

Hunke E.C., Lipscomb W.H. & Turner A.K. 2011. Sea-ice models for climate study: Retrospective and new directions. *J. Glaciol.* 56: 1162–1172, doi: 10.3189/002214311796406095.

Idzelytė R., Kozlov I.E. & Umgiesser G. 2019. Remote Sensing of Ice Phenology and Dynamics of Europe's Largest Coastal Lagoon (The Curonian Lagoon). *Remote Sens.* 11, 2059, doi: 10.3390/rs11172059.

Idzelytė R., Mėžinė J., Zemlys P. & Umgiesser, G. 2020. Study of ice cover impact on hydrodynamic processes in the Curonian Lagoon through numerical modeling. *Oceanologia*, 62: 428–442 doi: 10.1016/j.oceano.2020.04.006.

IPCC. 2013. *Climate Change 2013: The Physical Science Basis. Contribution of Working Group I to the Fifth Assessment Report of the Intergovernmental Panel on Climate Change.* Stocker T.F., Qin D., Plattner G.K., Tignor M., Allen S.K., Boschung J., Nauels A., Xia Y., Bex V. & Midgley P.M. (eds.), Cambridge University Press, Cambridge, United Kingdom and New York, NY, USA, 1535 pp.

IPCC. 2019. Technical Summary. In: Pörtner H.O., Roberts D.C., Masson-Delmotte V., Zhai P., Poloczanska E., Mintenbeck K., Tignor M., Alegría A., Nicolai M., Okem A., Petzold J., Rama B. & Weye N.M. (eds.), *IPCC Special Report on the Ocean and Cryosphere in a Changing Climate*. [In press.].

Jakacki J. & Meler, S. 2019. An evaluation and implementation of the regional coupled ice-ocean model of the Baltic Sea. *Ocean Dyn.* 69: 1–19, doi: 10.1007/s10236-018-1219-8.

Jakimavičius D., Šarauskienė D. & Kriaučiūnienė J. 2019. Influence of climate change on the ice conditions of the Curonian Lagoon. *Oceanologia* 62: 164–172, doi: 10.1016/j.oceano.2019.10.003.

Jevrejeva S., Drabkin V.V., Kostjukov J., Lebedev AA., Leppäranta M., Mironov Y.U., Schmelzer N. & Sztobryn M. 2004. Baltic Sea ice seasons in the twentieth century. *Clim. Res.* 25: 217–227, doi: 10.3354/cr025217.Kendall M.G. & Gibbons J.D. 1990. *Rank Correlation Methods*. Edward Arnold, London, UK.

Karetnikov S., Leppäranta M. & Montonen A. 2017. A time series of over 100 years of ice seasons on Lake Ladoga. *J. Great Lakes Res.*, *43*(6), 979–988, doi: 10.1016/j.jglr.2017.08.010.

Kendall M.G. & Gibbons J.D. 1990. *Rank Correlation Methods*. Edward Arnold, London, UK.

Kļaviņš M., Avotniece Z. & Rodinovs V. 2016. Dynamics and Impacting Factors of Ice Regimes in Latvia Inland and Coastal Waters. *Proc. Latv. Acad. Sci. Sect. B. Nat. Exact, Appl. Sci.* 70: 400–408, doi: 10.1515/prolas-2016-0059.

Kozlov I.E., Krek E.V., Kostianoy A.G. & Dailidienė I. 2020. Remote Sensing of Ice Conditions in the Southeastern Baltic Sea and in the Curonian Lagoon and Validation of SAR-Based Ice Thickness Products. *Remote Sens.* 12: 3754, doi: 10.3390/rs12223754.

Lecomte, O., Fichefet, T., Vancoppenolle, M., Nicolaus, M.,

2011. A new snow thermodynamic scheme for large-scale sea-ice models. Ann. Glaciol. 52, 337–346, doi: 10.3189/172756411795931453.

Lenderink G., Buishand A. & Van Deursen W. 2007. Estimates of future discharges of the river Rhine using two scenario methodologies: Direct versus delta approach. *Hydrol. Earth Syst. Sci.* 11: 1145–1159, doi: 10.5194/hess-11-1145-2007.

Leppäranta M. & Myrberg K. 2009. *Physical Oceanography of the Baltic Sea*. Springer-Praxis, Chichester.

Luomaranta A., Ruosteenoja K., Jylhä K., Gregow H, Haapala J. & Laaksonen A. 2014. Multimodel estimates of the changes in the Baltic Sea ice cover during the present century. *Tellus A*. 66: 22617, doi: 10.3402/tellusa.v66.22617.

Majewski W. 2011. Ice Phenomena on the Lower Vistula. *Geophysica* 47: 57–67.

Martin J. & McCutcheon S. 1999. *Hydrodynamics and Transport for Water Quality Modeling*. Boca Raton, CRC Press.

Omstedt A. & Wettlaufer J.S. 1992. Ice growth and oceanic heat flux: Models and measurements. *J. Geophys. Res. Ocean.* 97: 9383–9390, doi: 10.1029/92JC00815.

Pedersen R.A., Cvijanovic I., Langen P.L. & Vinther B.M. 2016. The Impact of Regional Arctic Sea Ice Loss on Atmospheric Circulation and the NAO. *J. Clim.* 29: 889–902, doi: 10.1175/JCLI-D-15-0315.1

Pemberton P., Löptien U., Hordoir R., Höglund A., Schimanke S., Axell L. & Haapala J. 2017. Sea-ice evaluation of NEMO-Nordic 1.0: a NEMO-LIM3.6-based ocean-sea-ice model setup for the North Sea and Baltic Sea. *Geosci. Model Dev*. 10: 3105–3123, doi: 10.5194/gmd-10-3105-2017.

Peng G., Matthews J.L., Wang M., Vose R. & Sun, L. 2020. What Do Global Climate Models Tell Us about Future Arctic Sea Ice Coverage Changes? *Climate* 8, 15, doi: 10.3390/cli8010015.

Potyutko, O.M. 2018. Impact of Seasonal Ice on the Structure of the Dreissena polymorpha (Pallas, 1771) Beds in the Swash-Ice Zone of the Curonian Lagoon and the Peculiarities of Formation of the Zebra-Mussel Bed. *Inland Water Biol* 11**:** 337–343, doi: 10.1134/S199508291803015X.

Randall D.A., Wood R.A., Bony S., Colman R., Fichefet T., Fyfe J., Kattsov V., Pitman A., Shukla J., Srinivasan J., Stouffer R.J., Sumi A., Taylor K.E. 2007. Cilmate Models and Their Evaluation. In: Solomon S., Qin D., Manning M., Chen Z., Marquis M., Averyt K.B., Tignor M., Miller H.L. (eds.), *Climate Change 2007: The Physical Science Basis. Contribution of Working Group I to the Fourth Assessment Report of the Intergovernmental Panel on Climate Change*, Cambridge University Press, Cambridge, United Kingdom and New York, NY, USA.

Ronkainen I. 2013. *Long-Term Changes in Baltic Sea Ice Conditions*. University of Helsinki, Finland. [Master's Thesis].

Rukšėnienė V., Dailidienė I., Myrberg K. & Dučinskas K. 2015. Simple approach for statistical modelling of ice phenomena in the curonian lagoon, the south-eastern Baltic Sea. *Baltica* 28: 11–18, doi: 10.5200/baltica.2015.28.02

Sharma S., Blagrave K., Magnuson J.J., O'Reilly C.M., Oliver S., Batt R.D., Magee M.R., Straile D., Weyhenmeyer G.A., Winslow L. & Woolway R.I. 2019. Widespread loss of lake ice around the Northern Hemisphere in a warming world. *Nat. Clim. Chang.* 9, 227–231, doi: 10.1038/s41558-018-0393-5.

Simon A., Frankignoul C., Gastineau G., & Kwon Y. 2020. An Observational Estimate of the Direct Response of the Cold-Season Atmospheric Circulation to the Arctic Sea Ice Loss. *J. Clim. 33*: 3863–3882, doi: 10.1175/jcli-d-19-0687.1.

Stroeve J.C., Serreze M.C., Holland M.M., Kay J.E., Malanik J. & Barrett A.P. 2012. The Arctic's rapidly shrinking sea ice cover: a research synthesis. *Clim. Change* 110: 1005–1027, doi: 10.1007/s10584-011-0101-1.

Tedesco L. 2009. *Modelling coupled physical-biogeochemical processes in ice-covered oceans*. University of Bologna, Italy. [PhD Thesis].

Tedesco L., Vichi M., Haapala J. & Stipa T. 2009. An enhanced sea-ice thermodynamic model applied to the Baltic Sea. *Boreal Environ. Res.* 14: 68–80.

Tedesco L., Vichi M., Haapala J. & Stipa T. 2010. A dynamic Biologically Active Layer for numerical studies of the sea ice ecosystem. *Ocean Model.* 35: 89–104, doi: 10.1016/j.ocemod.2010.06.008.

Umgiesser G., Zemlys P., Erturk A., Razinkovas-Baziukas A., Mezine J. & Ferrarin C. 2016. Seasonal renewal time variability in the Curonian Lagoon caused by atmospheric and hydrographical forcing. *Ocean Sci.* 12: 391–402, doi: 10.5194/os-12-391-2016.

Vihma T. 2014. Effects of Arctic Sea Ice Decline on Weather and Climate: A Review. *Surv. Geophys.* 35: 1175–1214, doi: 10.1007/s10712-014-9284-0.

Vihma T. & Haapala J. 2009. Geophysics of sea ice in the Baltic Sea: A review. *Prog. Oceanogr.* 80: 129–148, doi: 10.1016/j.pocean.2009.02.002.

Wibig J., Maraun D., Benestad R., Kjellström E., Lorenz P. & Christensen O.B. 2015. Projected Change –- Models and Methodology. In: The BACC II Author Team (eds.), *Second Assessment of Climate Change for the Baltic Sea Basin. Regional Climate Studies*, Springer, Cham, doi: 10.1007/978-3-319-16006-1_10.

Wunderling N., Willeit M., Donges J.F. & Winkelmann R. 2020. Global warming due to loss of large ice masses and Arctic summer sea ice. *Nat. Commun.* 11: 5177, doi: 10.1038/s41467-020-18934-3.

Yadav J., Kumar A. & Mohan R. 2020. Dramatic decline of Arctic sea ice linked to global warming. *Nat Hazards.* 103: 2617–2621, doi: 10.1007/s11069-020-04064-y.

Yu Karpechko A., Peterson K.A., Scaife A.A., Vainio J. & Gregow H. 2015. Skilful seasonal predictions of Baltic Sea ice cover. *Environ. Res. Lett.* 10, 044007, doi: 10.1088/1748-9326/10/4/044007.

Zemlys P., Ferrarin C., Umgiesser G., Gulbinskas S. & Bellafiore D. 2013. Investigation of saline water intrusions into the Curonian Lagoon (Lithuania) and two-layer flow in the Klaipeda Strait using finite element hydro-

dynamic model. *Ocean Sci.* 9: 573–584, doi: 10.5194/os-9-573-2013.

Zhao, J., Cheng, B., Vihma, T., Yang, Q., Hui, F., Zhao, B., Hao, G., Shen, H., Zhang, L., 2019. Observation and thermodynamic modeling of the influence of snow cover on landfast sea ice thickness in Prydz Bay, East Antarctica. Cold Reg. Sci. Technol. 168, 102869. https://doi.org/10.1016/j.coldregions.2019.102869.

Klaipėdos universiteto leidykla

Rasa Idzelytė
ASSESSMENT AND IMPACT OF ICE COVER AND FUTURE PROJECTIONS FOR THE BALTIC CURONIAN LAGOON
Doctoral dissertation

KURŠIŲ MARIŲ LEDO DANGOS VERTINIMAS, POVEIKIS IR ATEITIES PROGNOZĖS
Daktaro disertacija

Klaipėda, 2021

SL 1335. 2021 07 13. Apimtis 13,69 sąl. sp. l. Tiražas 17 egz.
Klaipėdos universiteto leidykla, Herkaus Manto g. 84, 92294 Klaipėda
Tel. (8 46) 398 891, el. paštas: leidykla@ku.lt, interneto adresas: http://www.ku.lt/leidykla/
Spausdino UAB „Druka“, Mainų g. 5, 94101 Klaipėda